UNIVERSITI TEKNOLOGI MARA

ANN-BASED PREDICTIVE MODELING OF MULTIBAND ABSORPTION PROPERTIES FOR ECO-FRIENDLY MICROWAVE ABSORBERS

AZIZAH BINTI AHMAD

PhD

March 2026

UNIVERSITI TEKNOLOGI MARA

ANN-BASED PREDICTIVE MODELING OF MULTIBAND ABSORPTION PROPERTIES FOR ECO-FRIENDLY MICROWAVE ABSORBERS

AZIZAH BINTI AHMAD

Thesis submitted in fulfilment
of the requirements for the degree of
Doctor of Philosophy
(Electrical Engineering)

Faculty of Electrical Engineering

March 2026

CONFIRMATION BY PANEL OF EXAMINERS

I certify that a Panel of Examiners has met on 5th December 2025 to conduct the final examination of Azizah binti Ahmad on her Doctor of Philosophy thesis entitled "ANN-Based Predictive Modelling of Multiband Absorption Properties for Eco-Friendly Microwave Absorbers" in accordance with Universiti Teknologi MARA Act 1976 (Akta 173). The Panel of Examiners recommends that the student be awarded the relevant degree. The Panel of Examiners was as follows:

Ismail Musirin, PhD
Professor
Faculty of Electrical Engineering
Universiti Teknologi MARA
(Chairman)

Roslina Mohamad, PhD
Associate Professor
Faculty of Electrical Engineering
Universiti Teknologi MARA
(Internal Examiner)

Deepak Ghodgaonkar, PhD
Professor
Dhirubhai Ambani Institute of Information and Communication Technology
Dhirubhai Ambani University, India
(External Examiner)

PROFESSOR DR HJH ZURAEDA IBRAHIM
Dean
Institute of Postgraduates Studies
Universiti Teknologi MARA
Date : 12 March 2026

AUTHOR'S DECLARATION

I declare that the work in this thesis was carried out in accordance with the regulations of Universiti Teknologi MARA. It is original and is the results of my own work, unless otherwise indicated or acknowledged as referenced work. This thesis has not been submitted to any other academic institution or non-academic institution for any degree or qualification.

I, hereby, acknowledge that I have been supplied with the Academic Rules and Regulations for Post Graduate, Universiti Teknologi MARA, regulating the conduct of my study and research.

Name of Student	Azizah Binti Ahmad
Student ID. No.	2023566333
Programme	Doctor of Philosophy (Electrical Engineering) - CEEE950
Faculty	Electrical Engineering
Thesis Title	ANN-Based Predictive Modelling of Multiband Absorption Properties for Eco-Friendly Microwave Absorbers
Signature of Student	
Date	12 March 2026

ABSTRACT

The rapid advancement of Industry 4.0 technologies and widespread adoption of 5G communication systems have heightened public concerns about the potential health risks associated with electromagnetic radiation. To mitigate these risks, eco-friendly microwave absorbers have emerged as a promising solution, effectively reducing radiation exposure. However, predicting the absorption performance remains challenging due to their complex and nonlinear interaction with electromagnetic waves. This research proposes a two-stage modelling approach to classify the absorption performance of eco-friendly single-slot pyramidal microwave absorbers. A dataset of 1206 experimental measurement were pre-processed using boxplot analysis for outlier detection and removal, followed by Min-Max normalization to standardize input ranges. After pre-processing, a refined dataset of 1156 samples were used for modelling. In the first stage, linear regression and artificial neural network (ANN) regression models were developed to analyse the relationship between input frequency and absorption behaviour across three single-slot size categories: small, medium and big. While linear regression served as a baseline, the ANN regression achieved superior accuracy and better adaptability in capturing nonlinear patterns. In the second stage, Multilayer perceptron (MLP) networks classified absorption performance using Levenberg-Marquardt (LM), Resilient Backpropagation (RBP) and Scaled-Conjugate Gradient (SCG) algorithms. The RBP algorithm outperformed LM and SCG, achieving 100% classification accuracy for the S-band and the lowest mean squared error (MSE), demonstrating its robustness. All models were developed in MATLAB R2021a and evaluated using accuracy, precision, sensitivity, specificity, MSE and confusion matrix. The results showed that the RBP algorithm consistently outperformed the others, particularly for the S-band, achieving perfect classification accuracy along with the lowest MSE. The study confirms that the integration of data cleaning, normalization, regression and ANN-based classification forms a reliable and effective process for modelling eco-friendly microwave absorber performance. This framework advances radio frequency (RF) absorber research and provides foundation for AI-driven innovations in sustainable electromagnetic interference (EMI) mitigation.

ACKNOWLEDGEMENT

Firstly, I wish to thank God for giving me the opportunity to embark on my PhD and for completing this long and challenging journey successfully.

I am deeply grateful to my supervisor, Prof. Ir. Ts. Dr. Hj. Mohd Nasir bin Taib, for his unwavering support, expert guidance and dedication throughout every stage of this research. I would also like to extend my heartfelt appreciation to my co-supervisors, Dr. Hj. Hasnain Bin Abdullah@Idris, PM. Ir. Ts. Dr. Nurlaila Binti Ismail and PM. Dr. Ahmad Ihsan Bin Mohd Yassin, for their invaluable advice, inspiring mentorship, and enthusiastic encouragement. It has been an honour to have such distinguished and supportive advisors, and I am truly fortunate to be able to seek their wisdom, not only for my PhD but also for my future career endeavours.

Special thanks are also due to my colleagues from the Green Material Microwave Absorbers Research Group (GMMARG) and the Advanced Signal Processing Research Group (ASPRG), as well as to my friends, for their generous support, stimulating discussions and for sharing both technical insights and encouragement throughout this journey. Your contributions have been vital to the progress of this work.

Lastly, and most importantly, I dedicate this thesis to my beloved husband, children, parents and siblings. Your unwavering love, patience, and encouragement have been my greatest source of strength. I am truly blessed to have your support, and I share this achievement with all of you. Alhamdulillah.

TABLE OF CONTENTS

LIST OF TABLES

LIST OF FIGURES

LIST OF SYMBOLS

Symbols

s_r	Relative permittivity
Exp	Exponential
g	Gradient Vector
H	Hessian Matrix
I	Identity Matrix
J	Jacobian Matrix
R^2	Coefficient of Determination
w	Weights
Z	Absorber impedance
\x	Relative permeability

LIST OF ABBREVIATIONS

Abbreviations

ANN	Artificial Neural Network
CST	Computer Simulation Technology
EMI	Electromagnetic Interference
FN	False Negative
FP	False Positives
LM	Levenberg-Marquardt
MLP	Multilayer Perceptron
MSE	Mean Squared Error
RF	Radio Frequency
RBP	Resilient Backpropagation
RMSE	Root Mean Squared Error
SCG	Scaled Conjugate Gradient
TN	True Negative
TP	True Positive

LIST OF NOMENCLATURE

Term	Description
Absorption Performance	Ability of a Material to Attenuate Incident Electromagnetic Waves
Early Stopping	Training Termination Method to Prevent Overfitting in ANN
Hidden Layer	Intermediate ANN layer Between Input and Output Layers
Loss Function	Mathematical Function Used to Quantify Prediction Error
Multiband	Operation Or Analysis Across Multiple Frequency Bands
Nonlinear Modelling	Modelling Approach That Captures Nonlinear Relationships Between Variables.
Overfitting	Condition Where a Model Fits Training Data Well but Performs Poorly on New Data

CHAPTER 1
INTRODUCTION

1.1 Research Background

The increasing demand for effective electromagnetic interference (EMI) shielding and reflection reduction in radio frequency (RF) applications has spurred significant interest in eco-friendly microwave absorbers. This study investigates the application of artificial neural networks (ANN) to accurately model the absorption performance of environmental-friendly microwave absorbers specifically designed for radio frequency (RF) applications. Eco-friendly microwave absorbers are innovative materials designed to address the problem of electromagnetic interference (EMI) and the reflections in the microwave range [1]. These materials are produced from agricultural waste materials such as rice husks, sawdust or coconut fibre, making it a more sustainable and environmentally friendly option than conventional absorbent materials that often contain heavy metals or harmful chemicals. The use of agricultural waste not only reduces manufacturing costs, but also leverages renewable resources, further reducing environmental impact.

These eco-friendly microwave absorbers function by absorbing electromagnetic energy and converting it to heat, which is then dissipated in other harmless forms. This process effectively minimizes electromagnetic interference that can disrupt the performance of sensitive electronic and communication equipment. By reducing microwave reflections, these materials help improve the efficiency of radio frequency (RF) systems, which are important in applications such as wireless communications, radar and navigation systems.

Despite advancements, accurately predicting the multiband absorption properties of microwave absorber using conventional methodologies remains a significant challenge, due to the complex interplay between material characteristics and microwave interactions. Previous studies have explored various approaches to modelling microwave absorbers, such as analytical formulations, numerical simulations, and experimental characterization [2]-[4]. However, these approaches may have drawbacks such as high computational complexity, resource-intensive requirements, and limited predictive accuracy.

1.2 Research Motivation

In light of this situation, the introduction of ANNs offers a fresh approach to overcome these issues by leveraging machine learning to learn complicated patterns from data and generate accurate predictions. Recent literature shows a growing interest in using artificial neural networks (ANN) to model microwave absorbers. Researchers have investigated various ANN architectures including feedforward networks, convolutional networks and recurrent networks to gain a more accurate understanding and prediction of microwave absorption behaviour. In addition, they have explored the use of various materials as absorbing medium from composite materials to nanomaterials, with the aim of improving the efficiency and performance of microwave absorbers [5]-[7].

The training algorithms used in their research are also very diverse including supervised learning algorithms, unsupervised learning and reinforcement learning. Optimization methodologies such as genetic algorithms, particle swarm-based optimization and Monte Carlo methods have been used to improve the performance of ANN models and obtain the best parameters for absorbent materials.

However, a notable gap in the current research landscape is the absence of studies specifically focused on modelling the absorption properties of eco-friendly microwave absorbers that utilize agricultural waste as a coating material. This indicates an important gap in the field of research that needs to be filled, given the great potential of agricultural waste in developing more environmentally sustainable and effective microwave absorbers, potentially offering unique absorption characteristics. Leveraging ANN to model the performance of these materials could lead to novel discoveries and advancements in microwave absorbers technology, while simultaneously promoting environmental sustainability. Consequently, further research in this field not only has the potential to improve the performance of RF technology but also take advantage of renewable resources and reducing agricultural waste.

Before proceeding further in the research, it is essential to emphasize the significance and relevance of studying ANN-Based Predictive Modelling of Multiband Absorption Properties for Eco-friendly Microwave Absorbers. As the increasing demand for effective solutions to reduce electromagnetic interference (EMI) in line with advances in telecommunication systems (wireless communication, 5G), radar systems, and electronic warfare, the development of precise and dependable microwave

absorbers becomes crucial. This research has the potential to significantly advance microwave absorber technologies by utilizing Artificial Neural Networks (ANNs). ANNs offer a flexible and data-driven framework for modelling these complex systems paving the way for the design of next-generation microwave absorbers that are optimized for diverse RF applications. Furthermore, the knowledge acquired from this work can guide future research paths, support efforts to establish industry standards, and promote the use of ANN-based approaches in Microwave absorbers and RF technologies.

1.3 Problem Statement

With the rapid evolution of Industry 4.0, such as the widespread deployment of 5G communication systems, there has been concern among people, especially in terms of the radiation effects on human health [8], [9]. Several studies have indicated various adverse effects on human health, such as headaches, the potential risk of cell damage, brain tumour and cancer due to prolonged electromagnetic wave exposure [10]—[12]. Consequently, establishing environments with safe levels of electromagnetic radiation levels requires the development of highly effective microwave absorbing materials capable of mitigating electromagnetic interference (EMI).

In parallel with technological advancements, the development of microwave absorbers using biomass materials presents a promising avenue for mitigating the effects of electromagnetic radiation [13]—[15]. An interesting property of agricultural waste as a coating material is its ability to greatly absorb microwaves, making it a prospective material for use in microwave absorbers. Accurately predicting the absorption performance of biomass microwave absorbers is a challenging task due to the complexity of the material and its interaction with microwaves [13], [14], [16]. Existing modelling and experimental approaches often involve high computational cost, limited generalization capability indicating that there is a need for efficient predictions of good accuracy.

Artificial neural networks (ANNs) have been used to solve complex nonlinear modelling problems because of their capacity to be trained on a large set of data and the capability to model intricate input-output relationships [17]—[19]. Although their capability has been proved, most of the reported investigations addressed the conventional absorber materials and there have been obviously less reports on the ANN-

based prediction or classification modelling for eco-friendly microwave absorbers from agricultural waste. In addition, the comparative studies of various ANN training algorithms for absorption performance classification at multiband frequencies remain insufficiently explored [5], [20], [21]. This lack of focused modelling studies on eco-friendly microwave absorbers represents a clear research gap that motivates the present study, which aims to employ ANN-based predictive and classification models to enhance absorption performance assessment while supporting sustainable EMI mitigation solutions.

1.4 Research Objectives

The main aim of this study is to propose a new technique using Artificial Neural Network (ANN) with selected training algorithms for predictive modelling and classification of the absorption performance of Eco-Friendly Microwave Absorbers. In order to fullfil this aim, the research is guided by the following objectives:

a) To develop predictive regression models using Linear Regression and Artificial Neural Networks (ANN) to quantify the relationship between input frequency and absorption characteristics across small, medium and big slot configurations of Eco-Friendly Microwave Absorbers.
b) To develop an ANN-based classification model using a Multilayer Perceptron (MLP) with Levenberg Marquardt (LM), Resilient Backpropagation (RBP), and Scaled Conjugate Gradient (SCG) training algorithms for classifying the absorption performance of Eco-Friendly Microwave Absorbers.
c) To evaluate model performance of the proposed technique using statistical metrics (R^2, MSE), classification metrics (accuracy, precision, sensitivity) and confusion matrix analysis, ensuring robustness across L-band, S-band, C-band and X-band frequencies of the Eco-Friendly Microwave Absorbers.
d) To validate the ANN model's superiority over conventional regression methods in predicting absorber performance while maintaining computational efficiency.

1.5 Significance of Study

The proposed research contributes to both scientific and industrial advancements in electromagnetic (EM) wave mitigation through three key innovations.

First, is the AI-driven design paradigm which establishes the first ANN-based framework for modelling eco-friendly microwave absorbers derived from agricultural waste, bridging the gap between sustainable materials and machine learning in EM applications. This also enables data-driven optimization of absorber geometry (slot sizes) and material composition without costly trial-and-error prototyping. Unlike earlier studies that primarily focused on different material analyses, this research extends toward a comprehensive predictive modelling framework that combines regression, prediction and classification across multiple frequency bands. Second, the trained ANN model will enable simulation and helps in further investigations on how absorber behaves under various scenarios, eliminating the need for physical prototyping and testing whilst saving time and resources. It will provide risk mitigation so that potential issues and limitations of the absorber can be identified and addressed during the simulation phase. Third, the proposed ANN model sets a precedent for AI-driven microwave material design, with potential applications in 5G infrastructure shielding, aerospace radar-absorbing structures and sustainable anechoic chamber linings.

1.6 Thesis Scope

The scopes of the study are:

1. The data on the absorption performance of microwave absorbers will be taken from the experimental measurements using the NRL Arch Free, which have been done by previous researcher [22].
2. Linear Regression will be used to investigate the relationship between two variables and Multilayer Perceptron (MLP) will be used as a classifier to classify the absorption performance of Biomass Microwave Absorbers. The MLP training algorithms will be limited to Levenberg Marquardt (LM), Resilient Backpropagation (RBP), and Scaled Conjugate Gradient (SCG).
3. The proposed work will be developed using MATLAB version R2021a.

1.7 Thesis Outline

This thesis consists of five chapters, which are outlined below:

Chapter 1 presents the background of eco-friendly microwave absorbers, the problem statement, research objectives, scope, and the significance of the study. Additionally, it outlines the overall structure of the thesis.

Chapter 2 presents a comprehensive literature review, covering the absorption performance of eco-friendly microwave absorbers and the materials used. The chapter also discusses relevant data processing techniques, including min-max normalization and other data transformation methods. Boxplot analysis is introduced as a visualization tool to assess the distribution of absorption performance across different frequency bands. Furthermore, intelligent modelling techniques such as Linear Regression and Artificial Neural Networks (ANN) are introduced, along with their associated algorithms and performance measures for both regression and classification tasks.

Chapter 3 describes the research methodology implemented for the study. It details the process of data collection, the application and comparison of pre-processing techniques (including min-max normalization), and the implementation of boxplot analysis to explore the data. The chapter then covers the development of both regression and classification models using ANN, including the training and validation procedures for the ANN model, focusing on the three selected algorithms which are Levenberg-marquardt (LM), Resilient Backpropagation (RBP), and Scale-Conjugate Gradient (SCG).

Chapter 4 presents the results and discussion. It includes a statistical analysis of the absorption performance based on pre-processing techniques and boxplot visualizations. This is followed by the results of both Linear Regression and ANN Regression Models. The chapter then provides the classification results using the ANN models, discussing the performance of the three algorithms (LM, RBP and SCG). A critical analysis of the model accuracy, precision and other relevant metrics is also provided.

Chapter 5 concludes the thesis by summarizing the findings and contributions of the research. It also offers recommendations for future research, particularly in the development of predictive models for eco-friendly microwave absorbers and their application in multiband absorption studies.

CHAPTER 2
LITERATURE REVIEW

2.1 Introduction

This chapter is divided into eight sections and provides a detailed review of the relevant literature. It starts with an overview of the content and organization of the chapters. Section 2.2 focuses on microwave absorbers, discussing their types, applications and key parameters for evaluating absorption performance, including reflection loss, absorption efficiency and bandwidth. This section also explores the concept of multiband absorption and its applications across various frequency ranges.

In Section 2.3, eco-friendly microwave absorbers are reviewed, highlighting the importance of sustainable materials. A focus is on biomass-based absorbers such as coconut shell activated carbon, with a detailed analysis of their performance based on material properties, structural influences and frequency response. Section 2.4 then discusses data pre-processing techniques including boxplot analysis for outlier detection and removal, as well as min-max normalization which are critical steps in preparing data for subsequent modelling.

Section 2.5 examines predictive modelling techniques utilized in microwave absorber research, specifically linear regression and artificial neural network (ANN) regression. Following this, Section 2.6 provides a theoretical background on intelligent computational techniques, focusing on the multilayer perceptron (MLP), ANN and three widely used training algorithms for ANN: Scaled Conjugate Gradient (SCG), Levenberg-Marquardt (LM) and Resilient Back Propagation (RBP).

Performance measurement methods are presented in Section 2.7, detailing accuracy metrics, statistical validation approaches and comparisons with existing literature benchmarks. Finally, Section 2.8 concludes the chapter by summarizing the key findings and identifying gaps in the literature, setting the stage for further research.

2.2 Microwave Absorbers

Microwave absorbers typically include a functional filler responsible for energy attenuation and a matrix that holds and supports the filler within the structure. The filler

determines the absorption behaviour and frequency response of the material, whereas the matrix contributes additional benefits including structural flexibility, durability under varying weather conditions and thermal resistance [23]. The measurement of various absorption materials involves the evaluation of their electrical permittivity and magnetic permeability. Microwave absorbers contain dielectric substances. When a microwave interacts with certain materials, the wave weakens and loses energy because it is converted into heat [24], [25]. The energy loss is determined by the frequency of the waves as well as the material's dielectric constant. Various absorption materials can have varying effects on permittivity and permeability over different frequency ranges. Electromagnetic absorbers are applied to suppress reflected electromagnetic waves generated by the surfaces of anechoic chamber walls. Absorbers are the crucial component of an anechoic chamber. Absorbers are designed to absorb electromagnetic energy in order to create a non-reflective environment. Shielded anechoic chambers are commonly employed to create RF isolated testing areas that mimic a free-space testing environment for the purpose of assessing antennas [26]. There has been a rise in the need for different types of electromagnetic wave absorbers, especially for testing instruments or systems without being impacted by wave reflections.

There are different types of microwave absorbers such as urethane pyramids, twisted urethane pyramids, slope absorbers, path absorbers, and hybrid absorbers consisting of a combination of dielectric and magnetic materials [27]. In anechoic chambers, pyramidal and wedge absorber structures are typically placed to form a continuous wall that attenuates stray signals caused by chamber confinement [28]. Pyramidal absorbers have been designed to create a smooth and progressive transition from air to the absorber at the interface. Pyramidal absorbers exhibit a variety of operating frequencies that are contingent upon their dimensions. These absorbers offer optimal performance and are typically employed in anechoic chambers.

In order to create an eco-friendly microwave absorber, the researchers concentrated on agricultural products and agricultural waste materials with high carbon content [22]. Carbon is a very absorptive substance for microwaves. Agricultural waste materials, such as coconut shells, sugar cane, rice husks, egg shells, wood waste, and empty palm oil bunches, have been discovered to possess a higher carbon content [29]. This results in a significant dielectric constant and high dielectric loss, indicating that the material absorbs microwave radiation exceptionally well, which provides further evidence that the material possesses wave-absorbing properties [30]. Figure 2.1 shows

the design of a single slot at different sizes on a biomass hollow pyramidal microwave absorber that has been developed by the previous researcher [22]. Figure 2.1(a) illustrates the small slot configuration, where the slot opening occupies a minimal area on the absorber surface. Figure 2.1(b) presents the medium slot configuration with an increased slot dimension compared to the small slot, while Figure 2.1(c) shows the big configuration, which features the largest slot opening among the three designs.

(a) (b) (c)

Figure 2.1 Design of Single Slot Configurations on a Biomass Hollow Pyramidal Microwave Absorbers: (a) Small Slot (b) Medium Slot (c) Big Slot [22]

2.2.1 Type of Microwave Absorber Applications

Mcrowave absorbers play a vital role in suppressing unwanted electromagnetic reflections and improving energy absorption efficiency across a diverse use cases. These absorbers are typically categorized based on their structural design, material composition and frequency response characteristics. Among the various types, pyramidal absorbers, hybrid absorbers and multilayer absorbers are particularly significant in research focused on improving microwave absorption performance. Their unique properties and customized configurations enable optimized absorption across different frequency bands making them highly suitable for advanced technologies aimed at suppressing electromagnetic interference (EMI), minimizing radar cross-section (RCS) and enhancing wireless communication reliability.

2.2.1.1 Pyramidal Absorbers

Pyramidal absorbers are widely used in anechoic chambers and electromagnetic shielding applications due to their ability to efficiently absorb electromagnetic waves over a broad frequency range [31]. Their unique tapered structure facilitates a gradual

impedance transition, reducing reflections and enhancing absorption efficiency. As incident waves interact with the pyramidal structure, multiple reflections and re-reflections occur along the parallel pyramid sides leading to progressive energy dissipation [32]. This mechanism enables low reflectivity and high absorption performance across various angles and frequency ranges. In conventional pyramidal absorbers, the size of the pyramid is typically greater than the wavelength of the incident wave ensuring that wave reflections remain confined within the structure. As the wave undergoes multiple reflections a portion of its energy is absorbed during each interaction, while the remaining energy continues to propagate toward the absorber base where further attenuation occurs. The controlled reflection and transmission process ultimately minimizes reflected waves ensuring effective microwave absorption. Figure 2.2 illustrates the propagation of an incident wave through a pyramidal absorber, demonstrating the iterative absorption mechanism [32].

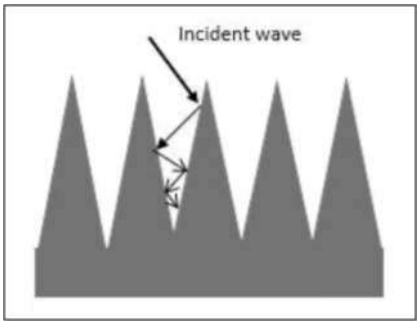

Figure 2.2 Propagation of Incident Wave Passing Through Pyramidal Absorber [32]

Despite their excellent performance, conventional pyramidal absorbers have certain limitations including thickness, material weight and environmental impact due to the use of synthetic materials. To address these challenges, biomass-based pyramidal absorbers have emerged as an eco-friendly alternative, offering comparable absorption efficiency while utilizing sustainable materials [33]. These absorbers integrate biodegradable composites that reduce environmental footprint without compromising microwave absorption performance. Among the innovative designs, biomass hollow pyramidal microwave absorbers with rectangular slot arrays have gained significant attention for their ability to further enhance absorption properties. These absorbers combine the structural advantages of hollow pyramidal shapes with an engineered slot array design, optimizing impedance matching and wave trapping mechanisms. Studies

have shown that slot arrays in pyramidal absorbers can effectively tune absorption bandwidth and improve wave attenuation, making them a promising advancement in sustainable electromagnetic shielding solutions [33].

Pyramidal absorbers are commonly installed in anechoic chambers where they are placed on back walls, side walls, floors and ceilings to minimize unwanted reflections. Various commercial pyramidal absorbers are available in the market, each using different material compositions and coating techniques to optimize performance. For example, the FIP-18PCL pyramidal absorber from ETS-Lindgren is coated with a conductive polyimide resin film which provides high-temperature resistance and durability [34], [35]. In contrast, the TDK ICT 030 from TDK Solution Inc. incorporates carbon-based and non-flammable materials, prioritizing fire resistance and long-term stability [34], [36]. Meanwhile, Ecco orb absorbers utilize urethane foam as the base material, with a carbon coating on the pyramid surface to enhance electromagnetic wave absorption [36]. Most commercial pyramidal absorbers are coated with blue latex paint to improve light reflectance and maintain anechoic chamber aesthetics [34]-[36]. Figure 2.3 presents examples of commercial pyramidal absorbers from ETS-Lindgren, TDK Solution Inc., and Emerson & Cuming [34]-[36].

*m-UHOOH**

Figure 2.3 Examples of Commercial Pyramidal Mcrowave Absorber [34]-[36]

Additionally, various shape modifications have been introduced to enhance the absorption characteristics of pyramidal absorbers. Some commercially available variations include straight square pyramidal, twisted pyramidal, hollow pyramidal and truncated pyramidal designs. These modifications are customized to optimize absorption efficiency, impedance matching and space constraints ensuring effective performance across diverse frequency ranges [31][32][33].

2.2.1.2 Multilayer Absorbers

Multilayer microwave absorbers are increasingly important due to their ability to enhance broadband absorption performance. By strategically layering materials with varying electromagnetic properties, multilayer absorbers can significantly improve impedance matching and energy dissipation leading to excellent absorption efficiency [37]. The narrowband of bandwidth condition can be extended to wider bandwidth by adding more than one layer into the microwave absorber design are illustrated in Figure 2.4. The multilayer configuration allows for more gradual transition of impedance, minimizing reflections and optimizing wave attenuation across a wider frequency range. Zhang et al. [37] demonstrated that single layer absorbers often exhibit narrow absorption bandwidths, a limitation that can be effectively addressed through multilayer structures. By optimizing the electromagnetic properties of each layer, multilayer absorbers achieve improved broadband absorption. Similarly, Assal et al. [38] confirmed that applying impedance gradient principles in multilayer designs enhances overall absorption efficiency by reducing reflections and facilitating progressive wave attenuation.

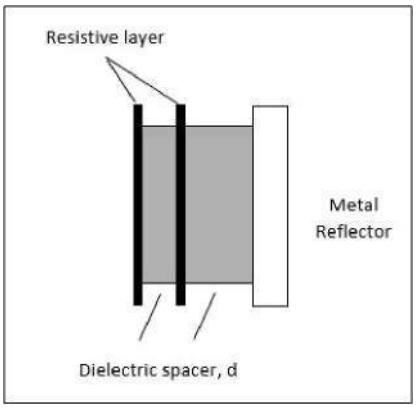

Figure 2.4 Multilayer Absorber Design [39]

2.2.1.3 Hybrid Absorbers

Hybrid absorbers incorporate two types of pyramidal designs: fully pyramidal and tapered pyramidal structures. The fully pyramidal design is typically composed of polyurethane-based foam embedded with carbon or ferrite powders making it suitable for electromagnetic compatibility (EMC) test chambers. These absorbers are generally

paired with low frequency ferrite tiles and a low density dielectric layer to enhance their performance across higher frequency ranges [40].

On the other hand, the truncated pyramid variant features suppressed pyramidal tops, designed to optimize space utilization in compact environments and minimize tip breakage. These absorbers exhibit superior performance at higher frequencies. Figure 2.5 illustrates an example of a commercially available hybrid absorber.

Figure 2.5 Hybrid Absorber Design [41]

In addition to material-based hybridization, hybrid absorbers are also widely recognized in terms of their structural and geometric design. Tapered pyramidal absorbers represent a well-established hybrid approach that combines absorber geometry with graded electromagnetic properties along the pyramid height. The gradual tapering profile provides impedance matching between free scape and the absorber material, thereby reducing reflections over a wide frequency range. Such tapered pyramidal structures are commonly employed in anechoic chambers and broadband EMI mitigation applications due to their proven multiband absorption capability[40], [41] .

2.2.1.4 Slot Arrays in Hollow Pyramidal Absorbers

Slot arrays have been extensively investigated as an effective approach for enhancing microwave absorption by modifying impedance characteristics, improving energy dissipation and broadening the absorption bandwidth. When integrated into Hollow pyramidal absorbers, slot arrays introduce additional impedance transitions facilitating multiple wave interactions and thereby increasing absorption efficiency. The strategic placement of slots within the pyramidal structure alters electromagnetic wave

propagation effectively trapping and dissipating energy through multiple internal reflections.

The influence of slot arrays on microwave absorption has been extensively studied in the context of biomass hollow pyramidal absorbers. Research conducted by [42] demonstrated that incorporating multi-slot arrays significantly enhances absorption efficiency. Their findings revealed that maximum absorption levels reached -30.62 dB with horizontal slots and -46.78 dB with vertical configurations, highlighting the critical role of slot orientation in optimizing absorption performance [42]. Additionally, their study showed that incorporating slotted designs improved the initial absorption performance from -10.3 dB to -11.8 dB, establishing a direct correlation between absorber design, slot configuration and overall performance enhancement [42].

Further investigations have emphasized the adaptability of rectangular slot arrays particularly in optimizing absorption across broad frequency range from 1 GHz to 12 GHz. By exploring various slot sizes in hollow pyramidal absorbers, researchers highlighted how the unique geometry of the hollow pyramidal structure facilitates multiple internal reflections which contribute to improved reflection loss characteristics [43]. Their work confirmed that optimizing slot dimensions can lead to further enhancements in absorption efficiency, reinforcing the importance of precise slot design in absorber performance [43].

The impact of slot arrays is also closely linked to the thickness and material properties of the absorber layers. Integrating slot patterns within multi absorber structures has been shown to extend operational bandwidth, optimizing absorption at both low and high frequency ranges. Computational studies and simulations performed using CST microwave Studio have further validated these observations demonstrating the tuneable nature of slot array configurations in improving the overall absorption characteristics of hollow pyramidal absorbers.

Moreover, an exploration into various slot array angles reveals additional performance benefits. The angular adjustment of slot arrays has been shown to influence absorption capabilities under different incident angles of electromagnetic wave [44]. This research emphasizes the practical considerations of these absorbers, demonstrating compliance with industrial standards while maintaining high performance metrics across defined microwave frequency ranges [44].

Additionally, slot arrays offer a sustainable approach for developing high performance eco-friendly microwave absorbers, particularly when implemented with

biomass-based materials. The combination of biomass-derived substrates and engineered slot arrays in multi hollow pyramidal absorbers has been identified as an effective strategy for optimizing impedance matching and enhancing absorptions absorption characteristics. This design presents a viable alternative to conventional synthetic absorbers offering potential applications in electromagnetic shielding and radar technologies. However, further experimental validation is necessary to assess the real-world effectiveness of slot-enhanced biomass absorbers under different incident angles and polarization conditions.

2.2.2 Key Parameters for Evaluating Absorption Performance

The evaluation of absorption performance for biomass hollow pyramidal microwave absorbers relies on several key parameters that determine their efficiency and effectiveness. These parameters include geometric design, material composition, impedance matching, dielectric properties (such as loss tangent) and reflection loss metrics, all of which contribute to the theoretical foundation necessary for modelling absorption behaviour and optimizing absorber design.

2.2.2.1 Geometric Design and Structural Characteristics

The geometric configuration of an absorber, particularly in a hollow pyramidal structure significantly influence its absorption performance. The pyramidal shape facilitates multiple internal reflections, allowing electromagnetic waves to be progressively attenuated and dissipated within the structure, thereby enhancing wave absorption [42][45]. The integration of slot arrays, such as rectangular or triangular slots, modifies electromagnetic field interactions, optimizing impedance matching and expanding the effective absorption bandwidth [42], [44]. Furthermore, hierarchical porous structures contribute to reduced surface reflection and improved absorption by enhancing the impedance transition between free space and the absorber material [46], [47].

2.2.2.2 Material Composition

The choice of material is a critical factor in determining absorption performance. Biomass-derived carbon materials such as rice husks, bamboo, POFA and kenaf exhibit high dielectric permittivity and conductivity making them suitable for microwave absorption applications [13]—[16], [48]-[50]. Additionally, doped carbon materials such as nitrogen-doped and sulfur-doped carbon, enhance dielectric loss mechanism which improve absorption by effectively converting electromagnetic energy into heat [51], [52]. The absorption effectiveness of these materials is often quantified using reflection loss (RL) measurements, where absorbers achieving RL values below -10 dB shows 90% absorption efficiency, while values below -20 dB indicate 99% absorption capability [16], [31], [53].

2.2.2.3 Impedance Matching

Impedance matching is a fundamental parameter that ensures minimal reflection of incident waves, thereby improving absorption efficiency. An absorber achieves optimal impedance matching when its impedance closely aligns with the free space impedance (Z_0 = 377 fl), allowing smooth wave transmission into the absorber rather than reflection at the interface [12]. The intrinsic impedance of an absorber material, which governs this matching condition can be expressed using the relative permeability and relative permittivity as in Equation (2.1) [47]:

$$Z= \qquad (2.1)$$

Where:

Z = Absorber impedance

[^Relative permeability

s_r=Relative permittivity

In hollow carbon-based absorbers, designed material compositions and structural modifications are crucial for ensuring impedance continuity [47]. Slot arrays

also serve as an effective method for tuning impedance, optimizing absorption efficiency across a broader frequency spectrum.

2.2.2.4 Dielectric Loss and Energy Dissipation

Dielectric loss is an essential mechanism for electromagnetic wave absorption, as it determines the absorber's ability to convert electromagnetic energy into heat. This behaviour is commonly quantified by the loss tangent (tan 8) which represents the ratio of the imaginary part to the real part of the material's complex permittivity. A higher loss tangent indicates greater dielectric energy dissipation and consequently improved absorption efficiency. Inbiomass-based absorber materials, hierarchical structures often promote interfacial polarization which enhances charge carrier mobility and further amplifies energy dissipation through dielectric relaxation processes [52], [54].

2.2.2.5 Reflection Loss and Absorption Bandwidth

Reflection Loss (RL) is a primary metric for evaluating absorber performance. It is defined as the logarithmic ratio of reflected wave magnitude *(E_r)* to the incident wave magnitude (£"j), as expressed in Equation (2.2) [30]:

$$RL\ (dB)=201og\ \frac{"^{r}}{E,} \qquad (22)$$

Where:

E_r= Reflected wave magnitude

E,= Incident wave magnitude

Lower RL values indicate higher absorption efficiency, typically classified as : If the RL < -10 dB the efficiency of absorption is about 90% and if RL< -20 dB the efficiency absorption is 99%.

Another parameter is the absorption bandwidth, which defines the frequency range over which the absorber maintains a high absorption rate. This can be expressed as in Equation (2.3):

$$Af=f_2-fi \quad \textbf{(2.3)}$$

Where:

Af = absorption bandwidth

fjand f_2= Lower and upper frequency limits where RL < -10 dB

The integration of slot arrays and multilayer designs allows for an extension of absorption bandwidth making absorbers more suitable for broadband application such as electromagnetic interference (EMI) shielding and radar cross-section (RCS) reduction [55].

2.2.2.6 Free Space Arch Measurement Method

The Free Space Arch Method is a widely adopted technique for evaluating the reflection loss and absorption bandwidth of microwave absorbers. This non-contact measurement method enables precise characterization of absorber performance over a broad frequency range. The setup involves positioning the absorber between a pair of transmitting and receiving antennas in a free space environment, ensuring minimal interference from external reflections. Figure 2.6 shows the IEEE standard measurement NRL arch reflectivity test configuration, where a transmitting antenna illuminates the absorber sample and the reflected signal is captured by a receiving antenna positioned at a defined angle. The arched arrangement helps approximate plane-wave incidence conditions and reduces edge diffraction effects, allowing accurate measurement of reflection loss across the frequency band of interest [56].

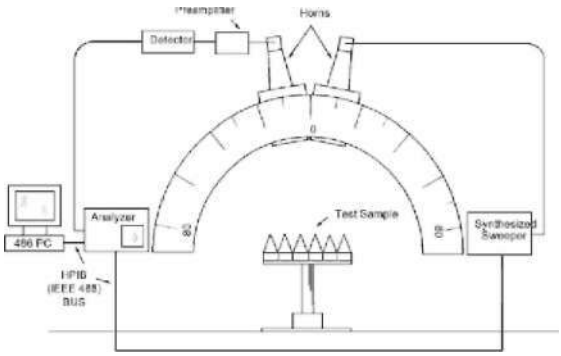

Figure 2.6 The IEEE Standard Measurement NRL Arch Reflectivity Test [56]

In previous studies, free-space measurements have been extensively used to validate the absorption performance of biomass based pyramidal absorbers with slot arrays [30], [31], [33], [42], [43], [53], [57], [58]. This method allows for the measurement of reflection loss, impedance matching and frequency response characteristics ensuring that absorbers meet performance requirements before practical deployment. While this study primarily focuses on modelling pre-existing data rather than conducting experimental validations, the Free Space Arch Method serves as the foundational technique for the dataset used in this research.

2.2.3 Experimental and Simulated Data for Absorption Performance

The evaluation of absorption performance in biomass hollow pyramidal microwave absorbers is crucial for understanding their effectiveness in minimizing electromagnetic interference (EMI) and optimizing wave absorption efficiency. Both experimental and simulated data serve as critical tools in characterizing the absorption behaviour of these materials, particularly in terms of reflection loss, impedance matching and absorption bandwidth. Since this study focuses on modelling pre-existing datasets rather than conducting new experimental validation, an overview of prior research on biomass-based microwave absorbers is necessary to establish the foundation for the dataset utilized in this work. By analysing experimental findings from existing studies and validating them through computational simulations, this research ensures that the data-driven models employed accurately reflect real-world absorption characteristics.

Experimental evaluations of biomass-based hollow pyramidal microwave absorbers have demonstrated their capability to achieve high absorption efficiency across different frequency ranges. A study by [42] investigated biomass hollow pyramidal absorbers, showing that geometric factors and impedance matching properties significantly influence absorption performance [42]. Reflection loss values as low as -41.97 dB in the 7-13 GHz range were achieved with optimized structures, whereas poor impedance matching resulted in lower absorption efficiency [59]. Further studies have examined the effect of slot array configurations, showing that rectangular slot designs improve broadband absorption, achieving reflection loss below -10 dB from 1 GHz to 12 GHz [43].

To complement experimental findings, simulation techniques have been widely utilized to predict and optimize the absorption behaviour of biomass hollow pyramidal absorbers. CST Microwave Studio is commonly used for 3D electromagnetic simulations allowing researchers to analyse reflection loss, impedance matching and dielectric properties of various pyramidal absorber designs. Simulations help optimize absorber geometry before fabrication, reducing material costs and ensuring improved performance [54]. Several studies have demonstrated that simulated results closely match experimental data, reinforcing the reliability of computational modelling in absorption performance studies.

Impedance matching plays a critical role in biomass hollow pyramidal absorber design, ensuring minimal reflection and maximum wave absorption. A previous study emphasized that the structural and compositional configuration of biomass materials directly influences impedance matching, which in turn affects microwave absorption performance[60]. In a related study, researchers analysed the dielectric properties of biomass-based absorbers and demonstrated that optimized material processing significantly enhances electromagnetic wave attenuation across various frequency ranges [54].

The dielectric response of biomass hollow pyramidal absorbers has been investigated using various carbonization and activation techniques. Biomass-derived carbon materials have been reported to exhibit superior absorption characteristics due to increased dielectric loss and optimized impedance matching following specific activation treatments [61]. These studies highlight how biomass-based pyramidal absorbers can be engineered to enhance their absorption performance through material selection and processing techniques.

The reviewed experimental and simulated studies provide essential reference points for the modelling of biomass hollow pyramidal absorbers with slot arrays. Since this study is focused on predictive modelling rather than new experimental validation, the dataset used in this research is derived from previously validated experimental and computational results. The integration of both experimental findings and simulation data ensures a reliable foundation for analysing absorption performance trends in biomass-based pyramidal absorbers.

2.3 Eco-Friendly Microwave Absorbers

The increasing demand for sustainable and environmentally friendly materials has driven research toward biomass-based microwave absorbers as an alternative to traditional synthetic absorbers. Conventional microwave absorbers often incorporate metallic or ferrite-based materials, which while effective, can be expensive, non-biodegradable and environmentally hazardous. In contrast, biomass-derived absorbers offer a sustainable solution, utilizing agricultural waste and renewable natural resources to achieve effective electromagnetic wave attenuation. Figure 2.7 illustrates several potential agricultural waste materials used as absorbing media, including empty palm oil bunches, coconut shell, rice husk and kenaf as shown in Figure 2.7 (a) - (d), respectively.

(0 , I)

Figure 2.7 Agricultural Waste Materials: (a) Empty Palm Oil Bunches (b) Coconut Shell (c) Rice Husk (d) Kenaf [44], [47], [48]

Biomass-based absorbers are derived from natural materials such as coconut shell, palm ash, rice husk, bamboo and kenaf, all of which shows favourable dielectric properties due to their naturally occurring carbon content, porous structures and lightweight characteristics [43], [46]-[48]. These properties make biomass absorbers attractive for radar cross-section (RCS) reduction, anechoic chambers, and electromagnetic interference (EMI) shielding. Furthermore, biomass absorbers are biodegradable and reduce reliance on petroleum-based composites, contributing to environmental sustainability.

In addition to their ecological benefits, biomass absorbers offer significant economic advantages. Since they are produced from abundant agricultural byproducts,

they serve as a cost-effective alternative to conventional microwave absorbers which often require complex manufacturing processes and rely on scarce or hazardous elements. Furthermore, advancements in carbonization and activation techniques have led to improved absorption performance ensuring that biomass-based absorbers remain competitive while maintaining their environmental benefits.

The use of biomass materials for microwave absorption applications aligns with global sustainability goals, promoting the use of eco-friendly technologies in engineering and industrial applications. Future research aims to further optimize the material composition, improve large-scale production methods and enhance the long-term durability of biomass absorbers for broader technological adoption.

Based on the literature, eco-friendly microwave absorbers can be broadly categorized into biomass-derived carbon absorbers, natural fibre-based composite and bio-based dielectric fillers. biomass-derived carbon materials such as coconut shell and rice husk have been reported to achieve reflection loss values below -10dB over selected microwave frequency bands, demonstrating their potential for EMI reduction applications [1], [42]. Despite these advantages, biomass-based absorbers may have the disadvantages of moisture sensitivity, material property fluctuation and inferior mechanical durability relative to conventional synthetic absorbers [62]. These issues indicate that it remains a big challenge to develop more improved modelling and optimization strategies for accurately predicting the absorbing performance, thus improving reliability of eco-friendly microwave absorbers.

2.4 Predictive Modelling Techniques

Predictive modelling techniques are important in various fields, enabling analysts and researchers to predict outcomes based on the previous data. These techniques provide valuable perspectives, facilitating decision making processes in the field such as healthcare, finance and engineering. Among the prominent approaches in predictive modelling are Linear Regression and Artificial Neural Network (ANN) Regression. Each technique has a unique strengths and applications making them essential tools for understanding and addressing complex relationships within data. This section reviews these methods for various predictive analysis tasks.

2.4.1 Linear Regression

Linear regression is a commonly employed technique in predictive modelling, primarily valued for its capability to define a linear relationship between dependent and independent variables. This method works under the premise that the correlation between variables can be expressed as a linear equation which is particularly useful in field such as economics and the social sciences [63], [64]. The simplicity of linear regression makes it easy to interpret and implement, making it the preferred choice for many researchers.

Linear regression involves employing a statistical approach to represent the connection between two variables [65]-[67]. It can be both simple and multivariable. A simple linear regression examines the relationship between a single dependent variable and a single independent variable, whereas a multivariable linear regression examines the relationship between a single dependent variable and multiple independent variables, which are denoted as y and x, respectively, in a linear graph [65], [66], [68]-[70]. Theoretically, the dependent variable is the result of the estimation of the independent variables [69]. The mathematical relationship of linear regression is based on a linear equation, which is $y=mx+c$ [67]. The m refers to the slope of the graph and c is the y-intercept of the fitting line.

In the context of multivariable regression analysis, there exists a technique for efficiently selecting the independent variables that can effectively explain the dependent variable [71]. The technique is known as stepwise regression. The primary goal of stepwise regression is to determine which independent variables should be included or excluded from the model [72]. Stepwise regression involves two types of processes: forward selection and backward removal [73]. The initial phase involves employing a forward selection technique. This approach begins with a model that only includes an intercept term and no other variables. The independent variable starts to add into the model one by one when they are only statistically significant [72], [74]. Next, backward elimination is the reverse technique of forward selection which the models start with full variables including intercept [73], [74]. The variables are deleted one by one that is not statistically significant [72].

Several selection criteria have been utilized to prevent the inclusion and exclusion of variables in stepwise regression [74]. The statistical measures used in this study include the F-test, Bayesian information criteria (BIC), Akaike information

criterion (AIC), coefficient of determination R^2, adjusted coefficient of determination R^2adj, and P-value [67], [71], [73], [74]. The F-test and P-value are commonly used in stepwise regression to examine the significance of variables. These tests are conducted using the a value [73], [74]. The standard significance level, denoted by a, in statistics is typically set at 0.05 [74]. However, it is worth noting that several research studies have used values other than 0.05, as indicated by references [67] and [74]. Stepwise regression offers the advantage of saving time and expense by selecting only the significant parameter [73].

The estimation of solar irradiation was conducted using stepwise regression in a study conducted by [72]. The researcher selects four approaches, namely R^2, R^2_adj, RMSE, and F, to ascertain the variables in the model. After evaluating the model, it was determined that three out of the five variables were deemed the most significant. This conclusion was based on the variables having higher values for R^2, R^2_adj, and F, while also having the lowest RMSE. The research study [73] effectively employed stepwise regression. Stepwise regression identifies the independent variables that are most strongly associated with the best natural fibre for automobiles based on the highest values of R^2 and R^2_adj, while using the fewest number of variables. The study from [75] presents a novel method called Expert-in-the-loop Stepwise Regression, which integrates expert knowledge into stepwise forward regression for predicting air pollution levels. The findings demonstrate that leveraging expert knowledge leads to more reliable and precise predictions, especially when dealing with limited data from air pollution monitoring stations. The proposed method not only enhances interpretability but also delivers better predictions compared to traditional approaches.

Although linear regression has been widely applied in various engineering and prediction problems, its application in microwave absorber modelling remains limited due to the strong nonlinear interaction between electromagnetic waves and material properties [76]. As a result, linear regression is generally insufficient for capturing complex absorption behaviour across wide frequency ranges. In this study, linear regression is therefore employed as a baseline predictive model to provide a reference for comparison with more advanced nonlinear approaches, particularly artificial neural networks.

2.5 **Artificial Neural Network** (ANN)

The concept of Artificial Neural Networks (ANNs) was first introduced by McCulloch and Pitts in the 1940s as a computational model inspired by the functioning of biological neurons. Since then, ANNs have become a popular research tool across various disciplines due to their ability to learn from data and make predictions [77]. An ANN is defined as a massively parallel distributed processor comprising simple processing units known as neurons, interconnected through synaptic weights. These synaptic weights allow neurons to store and process the knowledge required by the network [70], [77]-[79]. The network's ability to learn from data and adapt to changing patterns has made it a widely adopted approach in solving complex problems across fields such as engineering, healthcare and finance.

The structure of an ANN mimics the human brain shown in Figure 2.8 applying the biological concept of learning to computational models [70], [77], [80]. Similar to biological neurons, the artificial neuron consists of key components such as dendrites, axons, synapses and a cell body (soma). The nucleus, located within the cell body, holds genetic information and directs the neuron's functions, while the plasma contains the molecular machinery essential for producing materials required by the neuron. The dendrites act as receivers, collecting signals or impulses from other neurons, while the axon functions as a transmitter delivering the processed signal to subsequent neurons in the network.

When a neuron receives signals through its dendrites, the cell body processes the input and generates an output signal that is transmitted through the axon. At the terminal end of the axon, the impulse reaches a synapse where neurotransmitters, chemical messengers are released [77]. These neurotransmitters bridge the gap between neurons, enabling the transmission of signals across the network. This synaptic connection mechanism allows ANNs to process large amounts of data in parallel and adjust their internal parameters (weights) through learning algorithms, thereby improving accuracy of predictions overtime.

The ability of ANNs to model complex, non-linear relationships and learn from data with minimal human intervention makes them a powerful tool in predictive modelling. Their biological inspiration enables them to mimic cognitive functions such as pattern recognition, classification and decision-making which are critical in addressing real-world problems [81]. This concept is commonly illustrated using a

simplified biological neuron model as shown in Figure 2.8. This biological analogy enhances the understanding of ANN structures, providing a foundation for further exploration of training algorithms and performance evaluation methods discussed in subsequent sections.

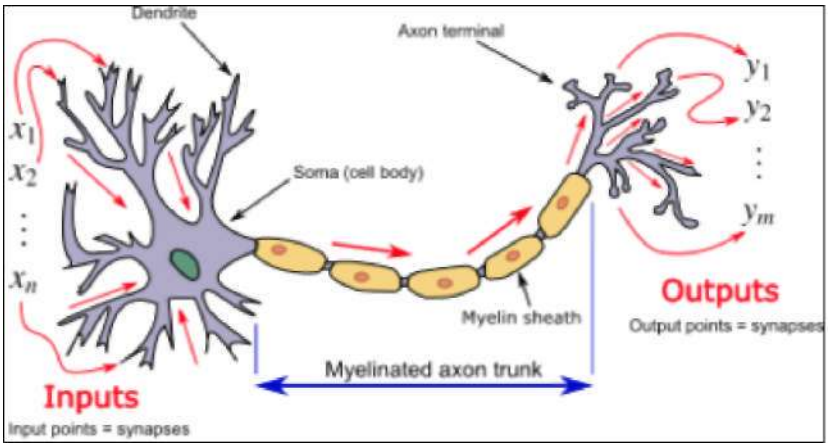

Figure 2.8 Biological Neuron Model [81]

ANNs are generally classified into two main types: feed-forward networks and recurrent networks. The first type, feed-forward networks processes information in a unidirectional manner, with data flowing from the input layer to the output layer without any feedback loops. Examples of feed-forward networks include single-layer perceptrons, multilayer perceptrons and radial basis function networks. These networks are often referred to as static networks because they produce a single set of output values for a given input, without any ongoing interaction or influence from previous outputs [77].

In contrast, recurrent networks incorporate feedback loops, making them dynamic systems that can process sequential data. These networks include models such as competitive networks, Kohonen's Self-Organizing Map (SOM), Hopfield networks and Adaptive Resonance Theory (ART) models, unlike feed-forward networks, recurrent networks continuously adjust their output based on feedback from previous outputs. As a result, these networks are particularly useful in applications where the order or context of the input data matters such as time-series prediction or speech recognition. The feedback paths within recurrent networks allow them to retain information from prior inputs, making them capable of learning temporary patterns and producing dynamic responses each time a new input is presented [77].

The learning model in ANNs can be categorized on three main types: supervised learning, unsupervised learning and hybrid learning [77]. Supervised learning, often referred to as learning with guidance, involves the use of a "teacher" to guide the learning process by providing the network with input-output pairs. The goal of network is to adjust its synaptic weights to produce predictions that closely match the actual output. During supervised learning, the predicted output may initially differ from the actual output. To address this inconsistency, the network applies an error correction rule to update its weight connections, with the aim of reducing the difference between the target output *y* and the predicted output p. In the perceptron learning process, this difference *(y — p)* represents the error term that guides the adjustment of the network weights during training.

A perceptron as illustrated in Figure 2.9, is one of the simplest forms of supervised learning models. It consists of adjustable weights w_m, where m = 0,1,2,...., and input values x_m . During the learning process, the perceptron updates its weights based on the calculated error, thereby improving its prediction accuracy overtime [77]. This iterative process continues until the error is minimized allowing the network to generalize and make accurate predictions when presented with new input data.

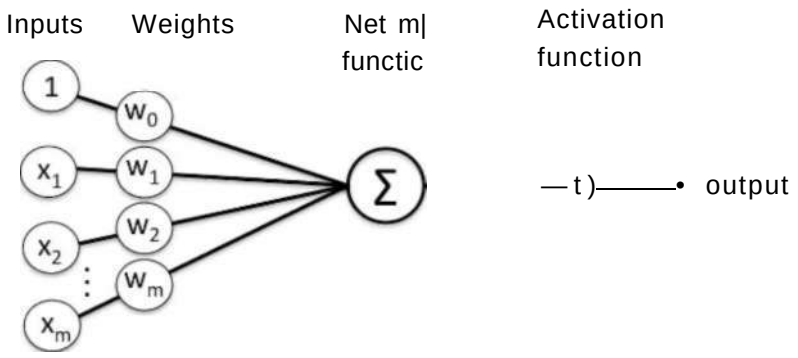

Figure 2.9 A Perceptron [77]

The activation function in Artificial Neural Networks (ANNs) was initially proposed using a binary threshold function as a computational unit, designed to make decisions by producing a binary output based on the weighted sum of its inputs. The relationship between the input and output of a perceptron can be expressed in Equation (2.4), where *v* represents the weighted sum of inputs:

$$V=2_J{}^{W}m^{x}m-\ \text{"} \qquad (^{2}\text{-}^{4})$$

Where w_m denotes the weight applied to each input x_m, and \i represents the bias term. The output of the perceptron is determined by comparing v to a threshold value. The actual output, y is 1 when the weighted sum exceeds the threshold, as expressed in Equation (2.5):

$$y=1 \text{ when } v>0;\ y\ w_m x_m.\ u=1 \qquad (2\text{-}5)$$

Conversely, the output is $y = 0$ when the weighted sum is less than or equal to the threshold as shown in Equation (2.6):

$$y=0 \text{ when } v<0\ ;\ y\ w_m x_m.\ u=0$$

The activation function is a critical component in both the hidden and output layers of artificial neural networks, as it determines the output of a neuron based on its inputs and weights. It applies mathematical operations to decide whether a neuron should be "activated" and contributes to the network's predictive capability. Activation functions introduce non-linearity, allowing neural networks to learn complex patterns that would otherwise be impossible if only linear transformations were used [82], [83]. Without activation functions, neural networks could only model linear relationships, severely limiting their effectiveness in tasks requiring intricate decision boundaries, such as image recognition or natural language processing.

Activation functions transform the summed weighted input from a neuron into an output value that is passed to the next layer or used as the final output [84]. Acting as a gate, they determine whether the input surpassed a critical threshold and should be propagated further. This non-linear transformation enables neural networks to capture intricate patterns and dependencies within the data, enhancing their ability to generalize across different tasks [85].

In the hidden layers, the choice of activation function significantly impacts the network's learning ability and convergence behaviour. Common activation functions include the sigmoid function, hyperbolic tangent (tanh) function and Rectified Linear Unit (ReLU) [86], [87]. The sigmoid function, widely used in earlier neural network architectures, squashes input values into a range between 0 and 1, making it particularly useful for probability-based outputs and classification problems [88], [89]. However, it suffers from vanishing gradient issues in deep networks, which can hinder training. The hyperbolic tangent function operates similarly but maps inputs to a range between -1 and 1, often leading to better convergence in some cases [90].

More recently, ReLU and its variants have gained prominence due to their computational efficiently and ability to reduce vanishing gradient issues [91]. Unlike sigmoid and tanh, ReLU outputs the input directly if it is positive but sets it to zero otherwise. This property speeds up training and enhances model performance. Making it a preferred choice in deep learning applications [92] [93]. Furthermore, adaptive activation functions have been introduced allowing networks to dynamically adjust activation behaviour during training for improved flexibility and learning capacity [94], [95].

The output layer's activation function is equally important, as it defines how the final predictions of network are presented. For classification tasks, the softmax function is commonly employed to normalize outputs into probability distributions, enabling multi-class classification [96]. For regression tasks, a linear activation function (such as purelin) is typically used to produce continuous output values ensuring accurate numerical predictions [97], [98]. Additionally, neural networks can incorporate multiple activation functions within different layers to optimize performance. This hybrid approach allows networks to fit the strengths of various activation functions, enabling more effective learning across diverse problem domains [99], [100].

Figure 2.10(a)-(c) illustrates the commonly used activation functions, including purelin, sigmoid and hyperbolic functions. The sigmoid activation function is often used in hidden layers, particularly for binary classification while the purelin function is commonly applied in the output layer for regression and mapping problems due to it linear characteristics [97], [101].

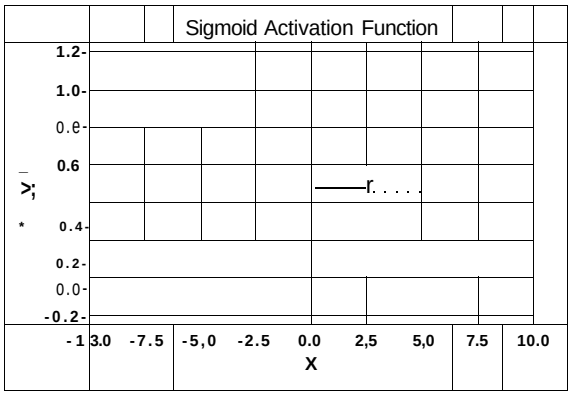

(a) Sigmoid activation function

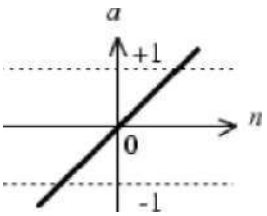

a = purclin(n)

Linear Transfer Function

(b) Purelin activation fimctioii

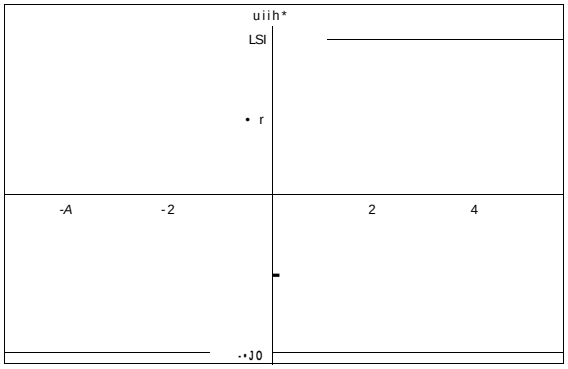

(c) Tangent hyperbolic activation function

Figure 2.10 Type of Activation Functions: (a) Sigmoid Activation Function, (b) Purelin Activation Function, (c) Tangent Hyperbolic Activation Function [100], [101]

The sigmoid function is mathematically defined as shown in Equation (2.7) [102]:

$$F(v(t)> \frac{1}{1+\exp(-v(t))} \tag{2.7}$$

Where v(t) represents the weighted input to the neuron at time t. The sigmoid function maps input values into the range (0,1), making it suitable for classification problems where probabilistic interpretation is required. For the MATLAB implementation in this study, the tangent-sigmoid (tansig) and purelin (linear) transfer functions were employed [103]. These functions are defined as follows:

The tangent-sigmoid (tansig) activation function is given in Equation (2.9):

$$\text{tansig}(v(t)) = \frac{e^{v(t)} - e^{-v(t)}}{e^{v(t)} + e^{-v(t)}} \quad \textbf{(2.8)}$$

This function maps input values into the range (-1, 1), making it effective for applications where symmetrical output distribution is desired.

The purelin (linear) activation function is define as shown in Equation (2.10):

$$\text{purelin}(v(t)) = v(t) \quad (2.9)$$

The purelin function is often used in the output layer for regression tasks, as it allows unrestricted linear mapping of input values without saturation effects.

Among various artificial neural network architectures, the multilayer perceptron (MLP) is the most widely used due to its ability to model complex non-linear relationships [77], [104]-[106]. MLP consists of three sequential layers: the input layer, hidden layer(s) and output layer. The input layer receives and transmits raw data without performing any computation, while the hidden layer processes the data using activation functions that introduce non-linearity to enable deep learning. Finally, the output layer generates predictions typically in a linear or non-linear format depending on the nature of the problem. The data flows in a one-way direction, known as forward propagation making MLP a fully connected feedforward network. The architecture of MLP is illustrated in Figure 2.12.

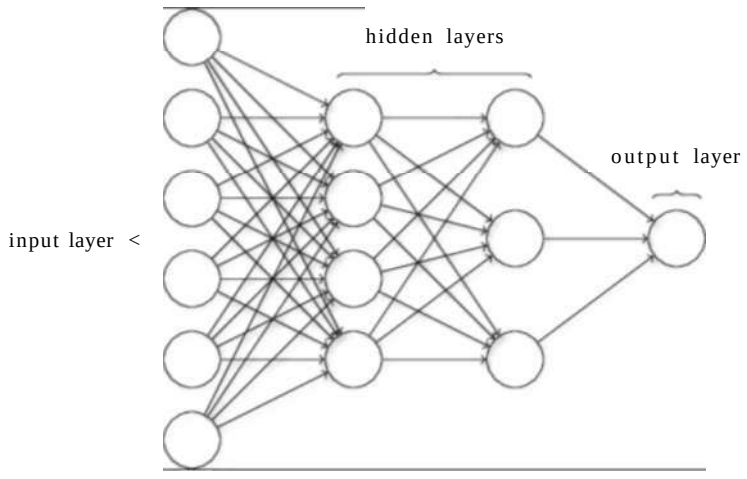

Figure 2.11 A Multilayer Perceptron [101]

To construct an effective MLP network, several structural parameters must be considered, such as the number of iterations, learning rate, number of hidden layers and neurons, total network depth and variations in activation functions [101], [107]. These parameters directly influence the training performance, generalization ability and computational efficiency of the network. Additionally, selecting an appropriate training algorithm is crucial. The most widely used training algorithms for MLP are Levenberg-Marquardt (LM), Resilient Backpropagation (RBP) and Scaled Conjugate Gradient (SCG) [107]. Each algorithm has different characteristics and benefits making it challenging to determine the most optimal one for a given problem. LM is highly effective for a small to medium-sized problems due to its fast convergence, RBP adjusts weight updates adaptively to prevent small gradients changes from slowing down training, while SCG is computationally efficient for large datasets [108], [109].

A fundamental challenge in designing an MLP model is selecting the optimal number of hidden neurons in the hidden layer [110]—[113]. While no universally accepted formula exists, various heuristic and experimental approaches have been proposed in the literature [111], [114]. These methods include stepwise trial-and-error, rule of thumb, simple methods and the sequential orthogonal approach [111], [114]. The stepwise trial-and-error method remains the most widely used technique, where the number of hidden neurons is gradually increased (forward approach) or decrease (backward approach) until the optimal model performance is achieved. Although effective, this method is computationally intensive [114]—[116]. Alternatively, the rule of thumb method suggests that the number of hidden neurons should be within a specific range: between the size of the input and output layers, approximately 2/3 of the input layer size plus the output layer size and less than twice the size of the input layer [[117], [118].

Other heuristic methods include the simple method, where the hidden neuron count follows a pre-defined network structure such as (1 -p-q), meaning it is proportional to the number of input and output nodes. For example, a 2-2-2 architecture maintains equal hidden, input and output neurons [111]. The sequential orthogonal approach is another technique where the number of hidden neurons is systematically adjusted until the minimum neural network error is achieved [111]. However, selecting too few hidden neurons can cause underfitting, limiting the learning of network capacity and resulting in poor performance, while too many hidden neurons can lead to overfitting where the network memorizes training data instead of generalizing patterns [110], [111], [119].

Overfitting also causes slow convergence and increased computational costs making it essential to balance model complexity [118].

To reduce overfitting, Early Stopping (ES) is a commonly used technique [102], [120]-[122]. ES monitors validation error during training and halts the process once the error begins increasing, thereby maintaining the model's generalization ability. This method is regarded as more effective than traditional regularization techniques in preventing overfitting [120], [122]. ES involves splitting the dataset into three subsets: training, validation and testing [18], [104], [120], [122]. The training set is used for weight adjustments, while the validation set prevents overtraining. The validation error initially decreases but starts increasing when the model begins overfitting. Once a rise in validation error persists for a certain number of iterations, training is stopped. Finally, the testing dataset is used exclusively to assess the performance of model on unseen data [18], [102].

MLPs have been extensively used in real-world applications due to their robustness in handling non-linear data. In the essential oil industry, MLPs have been successfully applied to estimate the extraction yield of oregano and valerian essential oils [101], [107]. Studies have demonstrated that the LM training algorithm outperforms others, achieving the lowest prediction error [107]. In pattern recognition, MLPs have been used in image processing tasks such as defect classification in leaves, where they successfully distinguished between defected and non-defected leaves [123]. Additionally, MLPs have been implemented in resume classification, where they outperformed Support Vector Machines (SVM) and k-Nearest Neighbours (k-NN) in word recognition and classification based in job specification [19].

In the medical field, MLPs have been employed for disease prediction, including stroke patient classification. A comparative study trained MLP models using SCG and LM algorithms with different numbers of hidden neurons (ranging from 1 to 50). The findings indicated that increasing the number of hidden neurons improved classification accuracy, reinforcing the importance of optimal neuron selection for complex medical dataset [124]. Beyond healthcare, MLPs have also been utilized in aerodynamics to predict pressure distributions and aerodynamic coefficients. Researchers have successfully incorporated physics-based regularization to improve the reliability of MLP predictions, highlighting the growing trend of integrating domain knowledge into neural network models [125].

Additionally, MLPs have been widely applied in environmental monitoring, particularly in drought forecasting. These models have demonstrated strong predictive performance when trained using advanced optimization techniques such as genetic algorithms and backpropagation [126]. Moreover, the efficiency of MLPs has been significantly enhanced by recent computational advancements. Techniques such as noise injecting during training have been used to improve fault tolerance, allowing models to maintain stable performance despite input variations [127]. The adoption of parallel computing has further reduced the time required for MLP training, making them more applicable in real-time decision-making scenarios [127].

In conclusion, the multilayer perceptron (MLP) remains a fundamental component of neural network-based machine learning due to its ability to model complex relationships in various domains. Its performance depends on several key factors including the selection of hidden neurons, the reduction of overfitting through techniques like Early Stopping and the choice of an appropriate training algorithm. MLPs have been successfully applied in fields such as medicine, environmental science, pattern recognition and aerodynamics demonstrating their adaptability and effectiveness. The continuous refinement of training techniques, network architectures and computational optimizations will further enhance the efficiency and accuracy of MLPs in future applications.

2.5.1 ANN-Based Modelling in Electromagnetic and Microwave Applications

Artificial Neural Networks (ANNs) have been increasingly applied in electromagnetic and microwave related modelling due to their ability to capture complex and nonlinear relationships between input parameters and electromagnetic responses. Previous studies have demonstrated the effectiveness of ANN-based approaches in predicting dielectric properties, microwave absorber performance and electromagnetic interference (EMI) shielding behaviour [5], [20], [21]. These applications highlight the suitability of ANN techniques for modelling frequency dependent electromagnetic characteristics that are difficult to represent using conventional analytical methods.

Existing works primarily focus on composite materials, nanomaterials, metamaterials and conventional absorber structures. For example, Agatonovic et al. demonstrated the capability of feedforward ANN models to predict the reflection

coefficient of pyramidal microwave absorbers with reduced computational complexity compared to full electromagnetic simulations [20]. Najim et al. applied an ANN-based approach to predict optimal layer thickness and material sequencing for a two-layer microwave absorber, demonstrating the effectiveness of ANN in broadband absorption performance optimization [5]. In addition, Arya and Sharma further proposed a hybrid ANN-ML prototype model that integrates material permittivity and permeability to improve microwave absorber design prediction. However, the framework remains conceptual and has not been extended to eco-friendly or biomass-derived absorber materials [21]. Jain et al. compared several machine learning regression techniques for predicting metamaterial microwave absorber performance and demonstrated that data-driven models can significantly reduce computational cost while maintaining high prediction accuracy [76]. Similarly, Dunga et al. employed a machine learning-based framework using a random forest regressor combined with genetic algorithms to predict optimal multilayer absorber configurations, demonstrating the effectiveness of data-driven models in reducing design complexity [128]. More recently, advanced machine-learning and deep-learning techniques have been explored for absorber inverse design and optimisation. Qi et al. proposed a machine learning-based inverse design framework using on MLP- mixer network to map desired electromagnetic response to absorber structures, achieving ultra-wide bandwidth microwave absorption [129]. In addition, variational autoencoders-based approaches have been reported for inverse design and optimization of metamaterial microwave absorbers [6]. However, these methods remain focused on synthetic structures and single band applications rather than eco-friendly absorber materials.

Most studies aim to predict reflection loss, absorption bandwidth, or dielectric parameters using frequency, geometry and material properties as input features. While promising results have been reported, these investigations are largely limited to non-eco-friendly materials and do not address absorbers derived from agricultural or biomass waste. Furthermore, the reviewed studies typically emphasize either regression-based prediction or performance optimisation for specific absorber configurations with limited attention given to systematic modelling across multiple geometries and frequency bands. To the best of the author's knowledge, no prior study has established an ANN-based predictive framework specifically for eco-friendly microwave absorbers derived from agricultural waste materials. This identified gap provides the primary motivation for the present study, which aims to develop an ANN-

based model for multiband absorption performance prediction of eco-friendly microwave absorbers.

Table 2.1 provides a systematic synthesis of ANN-based modelling studies and closely related machine learning approaches reported in electromagnetic and microwave absorber research. The comparison highlights absorber types, materials, modelling inputs and output, learning strategies, key contributions and identified limitations. As summarized in the table, existing studies predominantly focus on conventional, composite or metamaterial absorbers, with no dedicated ANN-based predictive framework reported for eco-friendly microwave absorbers derived from agricultural or biomass waste materials. This consolidated analysis further reinforces the research gap addressed in the present study.

Table 2.1
Summary of ANN-based and Related Machine Learning Modelling Studies in Electromagnetic and Microwave Applications

Author/ Year	Absorber Type	Material/ Structure	Input parameters	Output	ANN/ ML Model	Contribution	Limitation (Research Gap)
Agatonovic et al. (2011)	Pyramidal microwave absorber	Coventional pyramidal absorber	Frequency, incident angle	Reflection coefficient	Feedforward ANN	Demonstrated ANN capability in predicting absorber reflection coefficients with reduced computational complexity compared to EM simulations	Limited to conventional materials; eco-friendly absorbers and systematic multiband modelling not considered
Najim et al. (2016)	Two-layer microwave absorber	Fe-Al hybrid nano-composite	Frequency, material properties, layer configuration	Reflection loss, layer thickness	ANN (MLP-based)	ANN used to predict optimal layer thickness and material sequencing, achieving reduced absorber thickness with broadband absorption	Focus on synthetic nano-composites, not eco-friendly materials, limited to specific multilayer configuration
Arya and Sharma et al. (2021)	Microwave absorber (prototype model)	Generic filler-matrix absorber system	Permittivity, permeability, material type, thickness	Reflection loss, optimal design	Hybrid ANN + ML classifier	Proposed a hybrid AI-ML framework incorporating material electrical and magnetic properties to improve absorber design prediction	Conceptual prototype, lack experiment validation, not applied to eco-friendly or biomass-based absorber materials
Jain et al. (2023)	Metamaterial microwave absorber	FR-4-based metamaterial absorber	Frequency. Geometric parameters	Absorption performance	ML rgressors (DT, KNN, RF, ET, GBM, XGBoost)	Comparative ML study showing effective prediction of metamaterial absorber performance while reducing simulation cost	Emphasizes non-ANN ML models, focuses on metamaterials, not applied to eco-friendly or biomass-based absorbers
Dunga et al. (2025)	Multilayer Microwave absorber	Polymer nanocomposites	Dielectric & magnetic properties, layer thickness	Absorption performance	Random Forest Regressor + GA	ML-based framework for predicting optimal multilayer configurations achieving >98% X-band absorption	Uses non-ANN models, relies on synthetic polymer composites, limited to single-band analysis

Author/ Year	Absorber Type	Material/ Structure	Input parameters	Output	ANN/ ML Model	Contribution	Limitation (Research Gap)
Qi et al. (2025)	Frequency-selective surface absorber	Periodic FSS structure	Desired EM response (frequency, bandwidth)	Absorber topology	MLP- Mixer (deep NN)	Deep learning-based inverse design achieving ultra-wide bandwidth wit experimental validation	Focuses on synthetic structures and inverse topology design, not eco-friendly materials
On et al. (2021)	Metamaterial absorber	Conductive meta-structure	Image-based pattern	Reflection spectrum	VAE + CMA-ES	Deep learning inverse design achieving optimized X-band absorption	Single-band focus, synthetic metamaterials, not applicable to biomass-based absorbers

2.5.2 Data Pre-Processing for ANN Modelling

Data transformation serves as a crucial preprocessing stage in the data mining, enhancing both the quality and suitability of the input data. Among the various preprocessing techniques, outlier detection and normalization play important roles in improving the efficiency and accuracy of data-driven algorithms. For outlier detection, boxplot analysis is widely recognized as a robust method for identifying and removing data points that deviate significantly from the expected range, thereby ensuring the reliability of subsequent analyses [130], [131].

Normalization, particularly min-max normalization, is essential for scaling datasets to a standard range, which benefits neural network-based models by accelerating the training phase and enhancing prediction accuracy [132]—[134]. By focusing on boxplot analysis for outlier detection and min-max normalization for scaling, this review addresses key techniques integral to effective data preprocessing.

2.5.2.1 Boxplot Analysis for Outlier Detection and Removal

Boxplot Analysis was utilized to visualize the distribution, central tendency and variability of the absorption performance data [130], [135], [136]. Commonly referred to as whisker plots, boxplots provide a visual summary of a dataset using five statistical measures: the minimum, first quartile (Ql), median, third quartile (Q3) and maximum. Outliers were determined as data points that lie beyond 1.5 times the interquartile range (IQR) from the respective quartiles [131], [137], [138]. As illustrate in Figure 2.12, the boxplot structure incorporates all five summary statistics.

The first quartile (25^{th} percentile) indicates the value below which 25% of the data fall and lies between the minimum and the median. The median represents the midpoint of the dataset, dividing it into two equal halves. The third quartile (75^{th} percentile) lies between the median and the maximum, identifying the point below which 75% of the data are found. The interquartile range, spanning from Ql to Q3, encompasses the central 50% of the data. Finally, the whiskers extend to values outside the quartiles and help in identifying potential outliers beyond this central range.

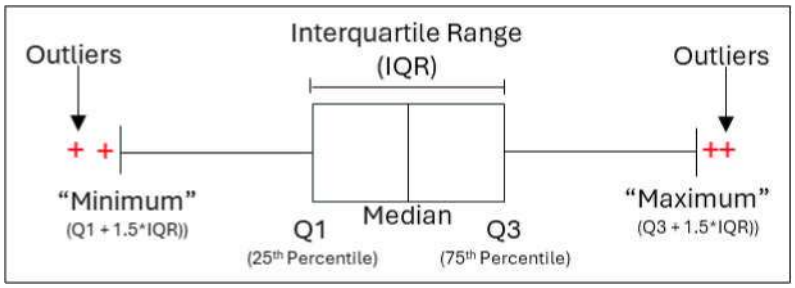

Figure 2.12 Boxplot Structure [135], [137], [139], [140]

The effectiveness of boxplots in identifying outliers has been demonstrated in variety of fields. For example, in biological studies, boxplots have been used to visualize and analyse data distributions, allowing the identification of extreme values that may bias the results [141], [142]. Similarly, in environmental research, boxplots have been used to detect outliers in datasets on the health benefits of green areas, demonstrating the importance of this method in understanding environmental impacts [143], [144]. Furthermore, boxplots have proven to be very useful in clinical studies where the removal or outliers can significantly increase the reliability and accuracy of statistical analyses [145], [146].

The advancements in boxplot methodology in this era, such as the development of functional boxplots, have significantly enhanced the capabilities of outlier detection. This approach combines traditional boxplot techniques with functional data analysis, allowing more robust outlier identification, especially in multivariate datasets [147], [148]. By integrating directional outliers, this method evaluates both of shape and magnitude of data, offering a precise approach to outlier detection that is less sensitive to marginal shape distortions [149], [150]. While advanced methods, such as the two-stage functional boxplot, have demonstrated excellent performance in handling complex and multivariate datasets [147], [151], the traditional boxplot remains a reliable and effective tool for outlier detection and removal in many practical applications, including this study.

Furthermore, boxplots are not only easy to interpret but also facilitate visual identification of outliers, making them the preferred choice in many analytical scenarios [152]. The integration of boxplot functionality into software tool such as R and SPSS has further enhanced their accessibility, enabling researchers across various disciplines to efficiently analyse and visualize data [141], [153].

2.5.2.2 Min-Max Normalization

Min-max normalization is a widely used data preprocessing technique that rescales the features of a dataset to a specific range, typically 0 to 1 [0,1]. Min-max normalization was selected in this study because it preserves the original data distribution while ensuring all input features remain within a bounded range, which is particularly suitable for ANN-bases models that are sensitive to input scaling compared to alternative methods such as Z-score normalization [154], [155]. This method is very useful in machine learning applications, because it can help reduce issues related to varying scales between characteristics, which can significantly impact the performance of various algorithms. The min-max normalization formula is defined as in Equation (2.10) [155]:

$$X' = \frac{X - X_{min}}{X_{max} - X_{min}} \tag{2.10}$$

Where X represents the normalized value, X is the original feature value, X_{min} is the minimum value of the feature, and X_{max} is the maximum value of the feature. In this study, min-max normalization was applied to the input features related to frequency and absorption performance parameters prior to regression and ANN modelling to ensure consistent scaling across all datasets.

This transformation ensures that all features are at a uniform scale, reducing the possibility of numerical instability and improving convergence in training algorithms such as those used in artificial neural networks (ANNs), including multilayer perceptrons (MLPs). This preprocessing step can also improve the interpretability and training efficiency of the model [154]. It is acknowledged that min-max normalization is sensitive to outliers, as extreme values can significantly affect the scaling range, therefore outlier detecting using boxplot analysis was performed prior to normalization to reduce this limitation.

The effectiveness of min-max normalization has been demonstrated in various studies. For example, in intrusion detection systems, min-max normalization combined with other preprocessing techniques achieved a high accuracy of 99.46% in a study using the CSE-CIC-IDS-2018 dataset [156]. Similarly, in breast cancer type classification using KNN, min-max normalization outperformed Z-score normalization

demonstrating it robustness in improving model accuracy [155]. Additionally, studies on groundwater level prediction have highlighted the importance of min-max normalization in providing data consistency and reliability for accurate predictions [157].

2.5.3 Artificial Neural Network (ANN) Regression

Artificial Neural Networks (ANNs) are advanced predictive modelling techniques inspired by the structure and function of the human brain. Consisting of multiple layers of interconnected nodes (neurons), ANNs are highly adept at handling complex, nonlinear relationships and high-dimensional data sets challenges where traditional linear regression often fails [158][159]. The backpropagation algorithm is a common training method for ANNs facilitates learning by adjusting model parameters based on errors, thereby incrementally improving prediction accuracy. This adaptive learning capability makes ANNs highly effective for a variety of regression tasks where the objective is to predict a continuous output value based on one or more input variables.

ANN regression outperforms traditional linear regression in a variety of applications, especially in fields requiring precision and the ability to process complex, non-linear relationships [160]. For example, in medical diagnostics, ANN models have shown excellent performance, effectively managing complex relationships between clinical features and patient outcomes [160]. Similarly, their scalability and ability to handle large datasets with variety of variables make them well suited for applications in finance where they are used for credit scoring and stock price prediction, and also in environmental modelling where they assist in predicting changes based on diverse environmental factors [161]. These examples show the versatility and strength of ANNs in addressing complex real-world problems that exceed the capabilities of simpler models.

Different types of neural networks are commonly applied to regression tasks, with their choice depending on the characteristics of the data and the specific problem requirements. Among these, Feedforward Neural Networks (FNNs) are the most widely used, as they process data in a straightforward, one-way flow from input to output without any feedback or cycles. This structure makes them highly effective for static data where the relationships between variables remain unaffected by prior outputs

[162], [163]. On the other hand, Recurrent Neural Networks (RNNs) are designed for sequential data processing. They include loops that retain information from previous inputs, enabling them to account for dependencies overtime. This feature makes RNNs particularly suitable for tasks such as time-series forecasting and other scenarios where earlier inputs significantly influence future predictions[164].

ANN regression offers significant advantages, especially in tackling challenges that traditional regression methos often struggle to address. One of its standout features is its ability to model non-linear relationships, capturing complex interactions between variables that conventional linear models fail to represent effectively [165]. Another benefit is its scalability, which allows ANN regression to efficiently manage large datasets, making it particularly suitable for applications involving big data [165]. Additionally, ANNs are highly versatile, offering the flexibility to customize their architectures and adjust hyperparameters to suit the unique characteristics of different datasets and problems [166]. This adaptability ensures that ANNs can be adjusted to handle a wide range of input features and deliver output predictions.

While ANN regression models offer numerous advantages, they also present several challenges that need to be carefully managed to ensure their successful implementation. A major limitation is their "black box" nature, which makes it difficult to interpret how specific inputs influence outputs [167]. Unlike linear regression models where the relationship between variables is clearly represented by coefficients, ANNs lacks this level of transparency making them harder to explain and trust in critical decision-making processes [68]. Another significant challenge is the computational demand associated with training ANNs especially deep networks. These models often require substantial processing power and extended training time, which can pose difficulties for researchers or organizations with limited access to high-performance computing resources [168]. This challenge may impact the practicality of deploying ANN models in environments with restricted infrastructure.

Additionally, overfitting remains a common issue in ANN regression, particularly when models are trained on small or imbalanced datasets. Overfitting results in a model that performs well on the training data but struggles to generalize to new unseen data [161]. To address this, strategies such as dropout (which randomly deactivates certain neurons during training) and early stopping (which halts training once performance on validation data stop improving) are commonly used [111][169].

These techniques help enhance the robustness and generalization ability of the model reducing the likelihood of overfitting and improving its performance on real-world data.

The practical applications of ANN regression encompass a wide range of fields and industries due to its flexibility and ability to model complex, non-linear relationships. In healthcare, ANNs regression models are used to predict patient outcomes by analysing historical data and clinical features. These predictive capabilities contribute to personalized treatment plans and early diagnosis of diseases[160]. In finance, ANN regression is applied to estimate stock prices, assess credit risks and identify fraudulent transactions [170]—[173]. By processing a massive number of financial indicators ANN models provide valuable insights that support more informed investment decisions and improved risk management strategies. The engineering field also benefits from ANN regression in tasks such as material modelling and structural analysis [174], [175]. For example, ANN models can predict how materials will behave under different conditions such as stress, temperature and pressure, enabling engineers to optimize designs and improve safety measures in construction and manufacturing^76]. In marketing, ANN regression models are widely used to forecast customer behaviours by analysing past interactions, purchasing patterns and demographic data [177]-[179]. These predictions support the development of targeted advertising campaigns and personalized recommendations, ultimately improving customer engagement and retention.

Although artificial neural networks have been applied to microwave absorber modelling and performance prediction in various contexts, existing studies have primarily focused on synthetic materials, metamaterial structures or conventional absorber designs [20], [76], [180]. To date, the application of ANN regression specifically for modelling the absorption performance of eco-friendly or biomass-derived microwave absorbers remains limited. This gap highlights the need for ANN-based predictive regression frameworks linked to sustainable absorber materials, which motivates the present study.

Overall, ANN regression demonstrates significant versatility and value across various domains. Its ability to handle complex datasets, model intricate relationships and provide highly accurate predictions makes it an essential tool for solving real-world problems in both academic research and industry practices. However, the successful implementation of ANN regression requires careful consideration of its challenges including computational demands, interpretability issues and the risk of overfitting.

With continued advancements in neural network optimization and increasing access to high-performance computing, ANN regression is expected to remain a vital component of predictive analytics and data-driven decision making.

2.5.4 Levenberg-Marquardt (LM)

The error backpropagation algorithm also known as the steepest descent algorithm is one of the most widely used methods for training neural networks [181]—[183]. Introduced by Rumelhart and McClelland in 1986 [182], this method updates network weights iteratively by following the negative gradient to minimize the error function. However, it has a major drawback which is slow convergence. There are two reasons for the slow convergence: the use of large step sizes which can lead to instability and the non-uniform curvature of the error surface which affects learning speed [181]. To address these limitations, the Gauss-Newton algorithm was introduced. This method optimizes the step size for each direction making the learning process faster [181]. However, its effectiveness depends on how well the error function can be approximated using a quadratic model.

The Levenberg-Marquardt (LM) algorithm, developed by Kenneth Levenberg and Donald Marquardt was designed to address the limitations of both the steepest descent and Gauss-Newton methods [181]. LM is a numerical optimization technique used for minimizing nonlinear functions and solving least-squares curve fitting problems [181], [183]. It belongs to the category of second-order gradient methods but avoids the computational burden of explicitly calculating the Hessian matrix [182]. The LM algorithm effectively combines the strengths of its predecessors such are the steepest descent method is stable but slow, while the Gauss-Newton method is faster but less reliable [181], [184]. By combining the benefits of both approaches, LM achieves a balance between speed and stability making it a more robust alternative to Gauss-Newton [181].

In terms of convergence speed, the Gauss-Newton is the fastest followed by LM, while the steepest descent method remains the slowest. Despite its efficiency, the LM algorithm is primarily recommended for neural network training involving small to medium-sized datasets as it can become computationally expensive for larger datasets [181].

The Levenberg-Marquardt (LM) algorithm is derived through four stages: the steepest descent algorithm, Newton's method, the Gauss-Newton algorithm and finally the LM formulation. A detailed derivations of the equations for the steepest descent algorithm, Newton's method and the Gauss-Newton method can be found in [181]. In the context of Artificial Neural Networks (ANNs) implemented in MATLAB R2021a, the performance function is computed based on the Mean Squared Error (MSE), which is defined as in Equation (2.11) [185]:

$$1\ V^{N}\ r \qquad \wedge 2 \tag{2.11}$$

Where:

N is the number of data points

y_t is the target (desired) output

ji is the predicted output

Since the LM algorithm is based on the non-linear least-squares optimization technique, the non-linear least-squares equation is mathematically equivalent to the MSE function as represented in Equation (2.12) [185]:

Rather than explicitly computing second-order derivatives, the Levenberg Marquardt algorithm employs an efficient approximation strategy that balances convergence speed and numerical stability. A key feature of the algorithm is the damping parameter, which regulates the transition between gradient-based learning and second-order optimization behaviour [181]. In the context of microwave absorber modelling, this adaptability is particularly relevant, as absorption behaviour is strongly nonlinear and frequency dependent. The ability of LM to achieve fast convergence while maintaining numerical stability makes it a suitable candidate for modelling multiband absorption performance using moderate sized datasets as considered in this study.

The Levenberg-Marquardt (LM) algorithm is widely recognized as an efficient and effective optimization technique for Artificial Neural Networks (ANNs) [186],

[187]. Its adaptability has made it valuable across various fields, from signal processing to medical diagnostics and fault detection. LM has been effectively used in estimating backscattered echoes in Principle Component Analysis (PCA), Independent Component Analysis (ICA) and Kalman Filtering [183]. The findings indicate that LM produced promising results across all three techniques, demonstrating superior performance in terms of amplitude, bandwidth and frequency resolution. In the field of medical diagnostics, LM has shown remarkable efficiency in disease detection. One study applied LM for breast cancer diagnosis and compared its performance with the backpropagation (BP) algorithm [182]. The results confirmed that LM exhibits significantly faster convergence than BP. Specifically, LM completed training in just 37 iterations, whereas BP required 2,574 iterations to reach a similar level of accuracy [182]. Another comparative study on breast cancer diagnosis evaluated LM against the Scaled Conjugate Gradient (SCG) algorithm [78]. The study concluded that LM not only converged faster but also achieved the highest classification accuracy with a relatively simple neural network architecture. Beyond medical applications, LM has also been successfully employed in fault detection systems. A study comparing LM and BP in diagnosing gear faults revealed that LM converged in just 23 epochs, whereas BP required 1,694 epochs to achieve similar performance [183]. Additionally, another study examined the efficiency of LM, SCG, and Gradient Descent (GD) in diagnosing thyroid disease. The findings demonstrated that LM outperformed the other two algorithms by requiring the lowest number of epochs and the shortest training time [188]. These studies collectively highlight the advantages of LM in both convergence speed and accuracy making it a preferred choice for classification and predictive modelling tasks. Its ability to quickly and efficiently train neural networks has solidified its role as a powerful tool in ANN-based optimization.

The Levenberg-Marquardt (LM) algorithm has been widely used in image classification and pattern recognition due to its efficiency and accuracy [109]. In a study comparing twelve different optimization algorithms, LM outperformed all others in both training and testing phases. The study evaluated various methods including gradient descent (GD), gradient descent with adaptive learning backpropagation (GDA), gradient descent with momentum and adaptive learning backpropagation (GDX), resilient backpropagation (RBP), BFGS Quasi-Newton backpropagation, Bayesian regularization, conjugate gradient methods (including Fletcher-Reeves and Polak-Ribiere updates), scaled conjugate gradient (SCG), LM, and one-step secant

backpropagation. Among all these methods, LM stood out as the most effective, achieving the highest classification accuracy for both training and testing phases. The study concluded that LM is the most reliable algorithm for image classification tasks due to its superior convergence speed and accuracy compared to other optimization techniques [109].

The Levenberg-Marquardt (LM) algorithm has consistently proven to be a powerful tool for predictive modelling across various fields. In a study evaluating diabetes prediction using eight different algorithms, LM outperformed the others by achieving high accuracy with fewer training epochs. Similarly, LM proved highly effective in the classification of agarwood oil into high- and low-quality categories, achieving a 100% classification accuracy across training, validation, and testing datasets while also exhibiting the fastest convergence [117]. Furthermore, LM has been successfully applied in predicting student's GPA, where it achieved the highest predictive accuracy compared to both manual prediction methods and the backpropagation (BP) algorithm [185]. Another study reinforced LM's efficiency in diabetes detection, where it surpassed eight other algorithms in terms of convergence speed and classification accuracy [189].

Additionally, the LM algorithm has also been used in computer network security evaluation. A comparative study between LM and the standard BP algorithm assessed their performance in terms of computational efficiency and generalization capability [190]. The study involved multiple evaluation phases, including data processing, weight determination, training and network evaluation. Results indicated that LM significantly outperformed BP, achieving convergence at just 4 epochs with minimal error in 2.7 seconds, whereas BP required 2000 epochs to reach minimum convergence. These findings highlight LM as a highly efficient and reliable optimization algorithm, making it a preferred choice for classification and prediction modelling tasks.

A recent study compared seven backpropagation (BP) algorithms to evaluate their performance in curve fitting and pattern classification for soil quality assessment [191]. The tested algorithms included Levenberg-Marquardt (LM), Scaled Conjugate Gradient (SCG), One-Step Secant (OSS), Conjugate Gradient methods (Fletcher-Reeves and Polak-Ribiere updates), Gradient Descent, and Gradient Descent with Momentum. The results showed that both SCG and LM achieved lower Mean Squared Error (MSE) values, indicating better accuracy. However, LM stood out by achieving an accuracy of over 90%, making it the best-performing algorithm in the study [191].

Further evidence of LM's effectiveness was highlighted in another study that analyzed curve fitting algorithms in neural networks using the housing dataset [192]. This study compared LM, SCG and Bayesian Regularization, evaluating their performance based on MSE and regression analysis. Although Bayesian Regularization achieved the lowest MSE and the highest regression accuracy, it required significantly longer training time. In contrast, LM delivered high regression accuracy with much faster training times, making it a more practical choice for applications where both speed and precision are crucial.

2.5.5 Resilient Backpropagation (RBP)

The backpropagation (BP) algorithm is one of the most widely used supervised learning methods in neural network systems [193], [194]. It operates by updating the network's weight based on the error function [193]. However, the weights adjustments in the BP algorithm are influenced by the learning rate which presents a fundamental trade-off: a smaller learning rate results in a prolonged training process, whereas a larger learning rate may lead to instability, causing the weight values to deviate significantly from the optimal minimum [194], [195]. One of the key limitations of the BP algorithm is its slow convergence rate which makes it prone to becoming trapped in local minima, especially in large-scale networks. This occurs because small weight updates lead to gradual changes, slowing down the overall convergence process [193]. Moreover, selecting appropriate training parameters for the BP algorithm remains a challenging task, further complicating the learning process and potentially impacting model performance [193].

To overcome the limitations of the BP algorithm, an alternative supervised learning method known as Resilient Backpropagation (RBP) was introduced [195], [196]. Developed by Riedmiller and Braun in 1993 [193], RBP enhances the weight update process by dynamically adjusting the step size based on local gradient information [193], [195]. This mechanism helps to counteract the negative impact of small weight magnitudes in BP and reduces the likelihood of the algorithm becoming trapped in local minima. Unlike traditional BP which depends on the magnitude of the gradient, RBP relies solely on the gradient's sign to determine weight adjustments. This independence from gradient magnitude improves training efficiency and makes RBP more robust for neural network learning tasks [197].

The weight update mechanisms of the Backpropagation (BP) and Resilient Backpropagation (RBP) algorithms differ significantly [197]. In the BP algorithm, weight updates are directly influenced by the magnitude of partial derivatives, whereas RBP updates weights based solely on the sign of the gradient, making it independent of gradient magnitude [197]. Table 2.1 presents a comparative overview of these key differences in weight update mechanisms between BP and RBP.

Table 2.2
Comparison Between BP and RBP Algorithm

Parameters	**Backpropagation Algorithm (BP)**	**Resilient Backpropagation Algorithm (RBP)**
1. Forward pass.	The error at each output level is recorded independently for evaluation	The error is recorded similarly, but the focus is on changes in the gradient's sign rather than its magnitude.
2. Backpropagation and error gradient calculation	Error is computed at each level and derivatives of activation functions are used to calculate the gradient for weight updates.	Only the sign of the gradient is considered, making the update process independent of gradient magnitude.
3. Weight updates	Weights and thresholds are adjusted using scaled gradient descent.	Updates depend only on the gradient's sign, adjusting the step size dynamically for efficient convergence.
4. Learning rate [157]	Uses a fixed learning rate that determines the step size for weight updates.	Employs two learning rate factors: an increasing factor to accelerate learning and a decreasing factor to prevent excessively large step sizes.

In the BP algorithm, weight updates are computed based on the magnitude of partial derivatives as represented in Equation (2.13). However, selecting an appropriate learning rate (e) is critical, if the learning rate is too small, the algorithm requires many iterations to converge, while an excessively high learning rate can lead to oscillations, preventing the model from stabilizing [193].

$$Aw_{mn}(t) = -e \frac{5E}{5w_m,}(t) + uw_{mn}(t-l) \tag{2.13}$$

where:

e is the learning rate

jj. is the momentum parameter

The Resilient Backpropagation (RBP) algorithm refines the weight update process by individually adjusting the step size for each connection based on changes in the gradient's sign. Unlike standard Backpropagation (BP), which relies on the magnitude of the gradient, RBP updates weights independently of gradient size making it more resilient to vanishing or excessively large gradients.

By dynamically adapting weight updates based on gradient sign changes, RBP effectively highlight issues of slow convergence and oscillation commonly encountered in standard BP. This adaptive mechanism enhances the stability and efficiency of the training process, making RBP a more robust alternative for neural network learning.

The Resilient Backpropagation (RBP) algorithm is widely utilized for training neural networks. Its performance is often evaluated in comparison to the traditional Backpropagation (BP) algorithm across various studies. Numerous researchers have demonstrated the effectiveness of the RBP algorithm in their respective domains. For instance, both BP and RBP have been applied in spam classification, where their performance was found to be comparable [195]. However, RBP exhibits superior efficiency due to its faster convergence and higher accuracy compared to BP. Additionally, both algorithms have been employed in estimating blood glucose concentrations in non-invasive monitoring devices [194]. The findings from this study further validate the theoretical advantages of RBP, particularly in terms of convergence speed. The results indicate that RBP requires fewer iterations, achieves convergence in a shorter time, and yields a lower mean squared error (MSE) compared to BP, demonstrating its robustness in real-world applications.

In the context of microwave absorber modelling, where absorption characteristics vary nonlinearly across frequency bands, the gradient sign-based update mechanism of RBP offers improved training stability. This makes RBP a suitable alternative for modelling multiband absorption behaviour, especially when robustness is prioritized over rapid convergence.

Beyond its application in Artificial Neural Networks (ANNs), the Resilient Backpropagation (RBP) algorithm has also been employed for training Radial Basis Function (RBF) networks, particularly in differentiating the surfaces of three-dimensional (3D) objects in range images [196]. Additionally, researchers have evaluated the performance of RBP across eight different machine learning datasets, including arrhythmia, breast cancer, dermatology, diabetes, heart disease, thyroid disease, postoperative patient outcomes and hepatitis. The results demonstrated that

RBP outperformed the Backpropagation (BP) algorithm in terms of convergence time for these classification problems. The efficiency of the RBP algorithm has also been validated in 3D human action recognition, where it achieved the highest accuracy compared to other training methods applied to the datasets [197]. Furthermore, the study highlighted RBP's capability in handling large neural networks reinforcing its effectiveness in complex machine learning tasks.

A recent study evaluated the Resilient Backpropagation (RBP) algorithm alongside the Backpropagation (BP) algorithm in classifying inrush and internal fault currents. The comparison was based on several criteria, including learning iterations, optimal network architecture, convergence time and regression analysis. Among these factors, RBP demonstrated superior performance achieving a lower error rate at fewer epochs, faster convergence time and an impressive 99% classification accuracy, as indicated by high regression values [198]. Furthermore, the fast convergence capability of the RBP algorithm was successfully validated in approximating two-dimensional geometric dilution of precision (2D-GDOP) [199]. Another study employed RBP to classify snack products based on near-infrared spectra, comparing its performance against Partial Least Squares Discriminant Analysis (PLS-DA) and Random Forest (RF) [200]. Among the three methods, RBP outperformed the others, achieving an AUC (Area Under the Curve) value of 0.90, highlighting its effectiveness in classification tasks.

Next, an Artificial Neural Network (ANN) trained with the Resilient Backpropagation (RBP) algorithm has been implemented to simulate the dynamic behaviour of biological systems [201]. The ANN model was evaluated using accuracy factor and bias factor, where the acceptable range for model validation is between 0.87 and 1.43. The results confirmed that the ANN-RBP model met this criterion, demonstrating low Root Mean Square Error (RMSE) and a high coefficient of determination (R^2), further validating its predictive accuracy and reliability. In a recent study [191], an RBP-based neural network was developed to recognize numerical notation in musical instrumentations. The process involved image input, preprocessing, segmentation and pattern recognition using the neural network. The RBP-based model was trained using two different sample sizes: 50 samples and 100 samples. The results showed that accuracy improved with a larger training dataset with the 50-sample model achieving 74.4% accuracy, while the 100-sample model reached 87.9% accuracy. This

study confirmed that increasing the number of training samples enhances the network's accuracy and performance[202].

Additionally, the study compared the execution time of the Backpropagation (BP) and Resilient Backpropagation (RBP) algorithms during training. The results showed that RBP significantly outperformed BP, completing training in less than one minute whereas the BP algorithm required more than one minute. This finding further reinforces that RBP trains faster than the BP algorithm. Furthermore, a Multilayer Perceptron (MLP) neural network using the RBP algorithm has been applied to predict the risk of developing Venous Thromboembolism (VTE) in hospitalized patients [112]. The study implemented an MLP architecture with one input layer consisting of 35 input neurons, three hidden layers with 19, 10 and 5 neurons respectively, and one output neuron, which categorizes five risk levels: low, lower, mild, moderate and high (normalized values). The dataset was divided into training (80%), validation (10%) and testing (10%>) sets. The results demonstrated that the RBP algorithm achieved high accuracy, exceeding 65% overall, with 100%> accuracy for the high-risk category. This study highlights RBP's effectiveness in predicting medical risks with improved classification accuracy.

2.5.6 Scaled Conjugate Gradient (SCG)

The Scaled Conjugate Gradient (SCG) algorithm is a supervised learning method that utilizes second-order derivative information from neural networks to update weights and biases effectively [78], [188]. Developed as an advancement over conventional conjugate gradient (CG) and backpropagation (BP) algorithms, SCG specifically addresses the limitations of slow convergence often encountered in these methods [203]. While BP and standard CG techniques typically require numerous iterations to achieve convergence, SCG overcomes this challenge by eliminating the computationally intensive line search process which is a common drawback in algorithms such as Levenberg Marquardt (LM). This characteristic makes SCG particularly well suited for training large scale neural networks where traditional BP methods often struggle due to high computational costs [109], [117], [203]. Moreover, SCG enhances numerical stability and convergence efficiency by employing different step sizes when computing gradients smaller step sizes for first-order gradients and

comparatively larger ones for second-order gradients, thereby ensuring a more stable and efficient training process [204].

To effectively adjust the step size, the SCG algorithm employs the trust-region technique [204], [205]. This method defines a localized region around the current search point where the approximation function or model function is considered sufficiently accurate in representing the actual cost function being minimized. Within this trust region, the step size is determined by identifying an approximate minimum of the cost function. Compared to the conventional line-search approach which heavily depends on user defined parameters, the trust-region method offers greater robustness and adaptability in optimization [204].

The SCG algorithm was introduced by Moller in 1993 as an enhancement to conventional backpropagation methods by integrating key features from the Levenberg Marquardt algorithm, renowned for its model confidence interval approach with the conjugate gradient (CG) technique [124]. Mathematically, SCG is defined by the Equation (2.14) [124]:

$$s_k = \frac{E' W s k P w \wedge}{°k}(t) + \wedge k P_k \qquad (^{214})$$

where:

s_k represents the Hessian matrix approximation

E is the total error function

E' is the gradient of the error function E

A_k and a_k are scale factors that are dynamically adjusted during training iterations

w_k is the current weight vector

p_k is the search direction at iteration k

The scale factor A_k is adaptively modified at each iteration based on the sign of a_k which directly indicates whether the gradient E' (w_{fc}) remains non-positive. While SCG may require more iterations to converge compared to some alternative optimization methods, its computational efficiency remains high since it eliminates the need for costly line-search procedures. This advantage makes SCG particularly

effective in training large-scale neural networks were reducing per-iteration complexity is crucial for overall performance.

The SCG algorithm has demonstrated it effectiveness in various classification and predictive modelling tasks. A previous study successfully applied SCG to classify agarwood essential oil into high- and low-quality categories, achieving an impressive 100%) accuracy while maintaining the lowest mean squared error (MSE) [206].

Furthermore, SCG has been applied in medical diagnostics, particularly in detecting infant hypothyroidism using cry signals [207]. One of these studies extracted infant cry features using Mel-Frequency Cepstral Coefficients (MFCC) analysis, varying the number of hidden neurons and feature coefficients to optimize performance [207]. The study concluded that the lowest MSE and an accuracy exceeding 88%> were achieved with 15 hidden neurons and 20 feature coefficients. Additionally, SCG has been employed to optimize weight initialization routines, improving the efficiency of artificial neural networks (ANNs) across eight different weight initialization techniques [208].

In another application, the SCG algorithm was compared with other classification methods for recognizing handwritten digits (0-9) [209]. Prior to classification, image processing techniques were applied, and the results demonstrated that the SCG-based method achieved the highest accuracy (98.8%>), outperforming alternative classification techniques. Additionally, a study explored SCG-based neural networks for indoor positioning system classification, comparing its performance with algorithms such as Bayes Net, J48, Naive Bayes, Sequential Minimal Optimization (SMO) and standard neural networks [210]. The proposed SCG-based network employed a dataset split of 90% for training and 10%> for validation, using a four-layer architecture with hidden layers containing 1000, 100, 50, and 25 neurons, respectively. Among all tested methods, the SCG-based approach achieved the highest accuracy (99%>), demonstrating its superior performance in this application.

The Total Body Water (TBW) has been monitored using an artificial neural network (ANN) system designed as a user-friendly and automated device, incorporating the SCG and Levenberg-Marquardt (LM) algorithms [141]. The performance of both algorithms was evaluated based on mean squared error (MSE) values and Pearson's correlation coefficient (r). The findings indicate that the SCG algorithm achieved a lower MSE than the LM algorithm, with an R-value approaching 1, suggesting a strong correlation between predicted and actual values.

The SCG-based neural network has also been applied for predicting Service Level Agreement (SLA) violations, ensuring reliability in real-world scenarios [205]. In this study, 10,000 real-world samples were used, with the dataset split into 70% for training, 15% for validation, and 15% for testing. Two datasets (SI and S2), each containing the same number of samples but differing in the number of SLA violations (1,500 and 4,500, respectively) were analysed. The evaluation was based on accuracy, MSE and the number of epochs required for convergence. The SCG algorithm successfully predicted SLA violations in both datasets, maintaining an MSE below 1 while achieving execution times of less than one second. Additionally, the accuracy for both datasets exceeded 90%, demonstrating SCG's efficiency in SLA violation prediction.

Further demonstrating its versatility, SCG has been applied in power quality assessment for three-phase electrical systems where it was compared against six other backpropagation algorithms [211]. This included conjugate gradient descent, LM, one-step secant, Bayesian regularization, gradient descent with momentum and gradient descent with adaptive learning rate. Performance was assessed based on MSE, the number of neurons used, classification accuracy and required training iterations. The study optimized the network architecture by varying the number of hidden neurons (ranging from 1 to 100) across two hidden layers. The results showed that SCG outperformed all other algorithms, achieving the highest accuracy, the lowest MSE and requiring fewer training iterations and epochs making it a highly efficient choice for power quality analysis.

Additionally, SCG has been employed in digital forensic applications, particularly for digital camera identification through noise extraction [212]. The effectiveness of the SCG-based classifier was evident with classification accuracies exceeding 80%, supporting its suitability for forensic investigations involving digital image authentication.

2.6 Performance Measurement

In this study, the performance of the classifier used for predicting microwave absorption performance is evaluated using key metrics including the confusion matrix, accuracy, precision, sensitivity, specificity, mean squared error (MSE) and the number of epochs. These metrics are selected to evaluate both the classification accuracy of

absorption performance levels and the regression accuracy of continuous absorption related parameters across multiple frequency bands. Classification tasks in machine learning can be categorized into binary classification, multi-class classification, multi-label classification and hierarchical classification [213].

Among these, binary classification is the most commonly used approach. The confusion matrix is a widely adopted evaluation metric for supervised classification problems [213]—[216]. It represents the relationship between actual and predicted class labels where rows indicate actual classes and columns represent predicted classes [214]-[216]. For binary classification as shown in Figure 2.13, the confusion matrix is structured as a 2x2 matrix consisting of four fundamental elements: true positive (TP), true negative (TN), false positive (FP) and false negative (FN) [105], [217]. These elements allow for the calculation of various performance metrics including accuracy, which measures the proportion of correctly classified samples; precision which indicates the proportion of correctly predicted positive cases among all predicted positives; sensitivity (recall) which assesses the model's ability to correctly classify negative instances [216]. In the context of microwave absorber modelling, these classification metrics are used to evaluate the model's ability to correctly categorize absorption performance into predefined group (small, medium and big), which is relevant for practical absorber selection and design decisions. Sensitivity and precision are particularly important, as misclassification may lead to incorrect assessment of absorber effectiveness across different frequency ranges. However, accuracy alone can be misleading, particularly in the presence of an imbalanced dataset [216]. This limitation is especially relevant in absorber performance classification, where certain absorption categories may dominate specific frequency bands.

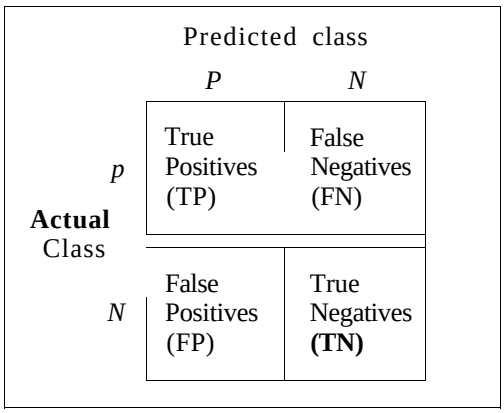

Figure 2.13 The Confusion Matrix [213], [216]

In regression-based neural network modelling, mean squared error (MSE) serves as a fundamental performance metric that quantifies the difference between predicted and actual values [218]. As defined in Equation (2.11), MSE incorporates both bias and variance, reflecting the squared mean error and variance of estimates. A lower MSE value theoretically indicates better model performance by ensuring a closer fit between the predicted and actual values [185]. For microwave absorber predictive modelling, MSE directly reflects the accuracy of predicting continuous absorption characteristics such as reflection loss magnitude across frequency bands. However, MSE is sensitive to large prediction errors and may be influenced by outliers, which necessitates complementary evaluation using additional performance metrics.

Another crucial aspect of performance evaluation in neural networks is the number of epochs, which influences the model's ability to learn from data effectively. In an artificial neural network (ANN), the learning parameters, including weights and biases, are randomly initialized before training begins. These values are iteratively adjusted to minimize error and enhance performance. An epoch refers to a single complete pass over the entire dataset, where weight updates occur continuously to optimize predictions. The choice of the number of epochs plays a critical role in achieving optimal performance, as an insufficient number of epochs may result in underfitting, where the model fails to capture underlying patterns, while excessive epochs may lead to overfitting, where the model memorizes noise and performs poorly on unseen data [120]. The impact of epoch optimization is further elaborated in Section 2.6. In microwave absorber modelling, appropriate epoch selection is crucial to ensure reliable generalization of frequency dependant absorption behaviour without overfitting to specific measurement conditions. Therefore, a combination of classification and regression-based performance metrics is necessary to provide a comprehensive evaluation of predictive modelling accuracy for microwave absorbers.

2.7 Summary

This chapter has systematically reviewed the critical literature supporting the development of artificial neural network (ANN) model for eco-friendly microwave absorber performance prediction. The discussion began with an overview of microwave absorbers, including their classifications and key performance parameters such as reflection loss and bandwidth. The review highlighted the growing importance of

sustainable solutions in electromagnetic interference (EMI) mitigation, especially in the context of increasing demands from modern RF and communication systems. While this study does not directly focus on experimental or simulation procedures, references to previous works have helped establish the baseline understanding of absorption behaviour in conventional and eco-friendly absorber materials.

The literature also highlighted the emergence of environmentally sustainable microwave absorbers, especially those derived from biomass and agricultural waste which offer promising electromagnetic properties while addressing ecological concerns. Despite this growing interest, existing studies remain largely focused on material characterization and experimental validation with limited feature on predictive modelling framework. In addition, data preprocessing methods such as boxplot analysis for outlier detection and removal and min-max normalization were reviewed, showing their importance in ensuring data reliability and consistency prior to modelling.

Next, the chapter examined predictive modelling approaches, including linear regression and artificial neural network (ANN) regression. Linear regression was reviewed as a baseline technique for identifying relationships between variables, while ANN-based approaches demonstrated best capability in modelling complex nonlinear patterns. The review on training algorithms namely Levenberg-Marquardt (LM), Resilient Backpropagation (RBP) and Scaled Conjugate Gradient (SCG) was also presented their respective strengths and limitations in learning nonlinear absorption behaviour. However, the literature reveals a lack of systematic comparison of eco-friendly microwave absorber geometries and slot configurations across multiple frequency bands using integrated ANN-based predictive frameworks.

Lastly, performance measurement techniques were reviewed to support both regression and classification model evaluation, focusing on metrics such as accuracy, loss values and statistical indicators. Collectively, the reviewed literature reveals a significant research gap in the absence of dedicated ANN-based predictive frameworks for eco-friendly, agricultural waste-derived microwave absorbers, especially those that integrate regression and classification analysis across multiband frequencies. These gaps provide strong justification for the proposed study. Accordingly, chapter 3 presents the research methodology adopted to address these limitations and performance evaluation procedures used in this work.

CHAPTER 3
RESEARCH METHODOLOGY

3.1 Introduction

This chapter is organized into seven sections. The first section provides an overview of the general methodology through a flowchart. Section 3.2 covers the data collection process used for the experimental analysis, briefly explaining how the data was collected and highlighting key characteristics of the absorber measurements. Section 3.3 focuses on data pre-processing techniques, including min-max normalization, handling outliers, and boxplot analysis. Section 3.4 and 3.5 discuss the development of the models. Section 3.4 explores the development of both linear regression and artificial neural network (ANN) regression models, detailing the steps involved in their development. Section 3.5 shifts to the development of ANN classification models, providing an overview of ANN techniques and explaining the specific architecture used for classifying absorption performance. In addition, various multilayer-layer perceptron (MLP) training algorithms are presented, including Levenberg-Marquardt (LM), Resilient Backpropagation (RBP), and Scaled Conjugate Gradient (SCG). Section 3.6 explains the methods used for performance evaluation. Finally, Section 3.7 provides a summary of the research methodology.

Figure 3.1 illustrates the overall research methodology. The process begins with data collection, followed by pre-processing techniques that include min-max normalization and outlier detection (via boxplot analysis) with subsequent removal. These pre-processing steps result in refined, eco-friendly microwave absorption performance data, which are then used as inputs for both regression and ANN modelling. The training algorithms employed in the modelling process are Levenberg-Marquardt (LM), Resilient Backpropagation (RBP) and Scaled Conjugate Gradient (SCG). The absorption performance values are trained using these algorithms by optimizing the number of hidden neurons, ranging from 1 to 10. The best ANN architecture is selected based on its ability to meet all performance criteria including means square error (MSE), number of epochs, confusion matrix, accuracy, sensitivity, specificity and precision. If the ANN model fails to meet these requirements, it is retrained to achieve optimal performance.

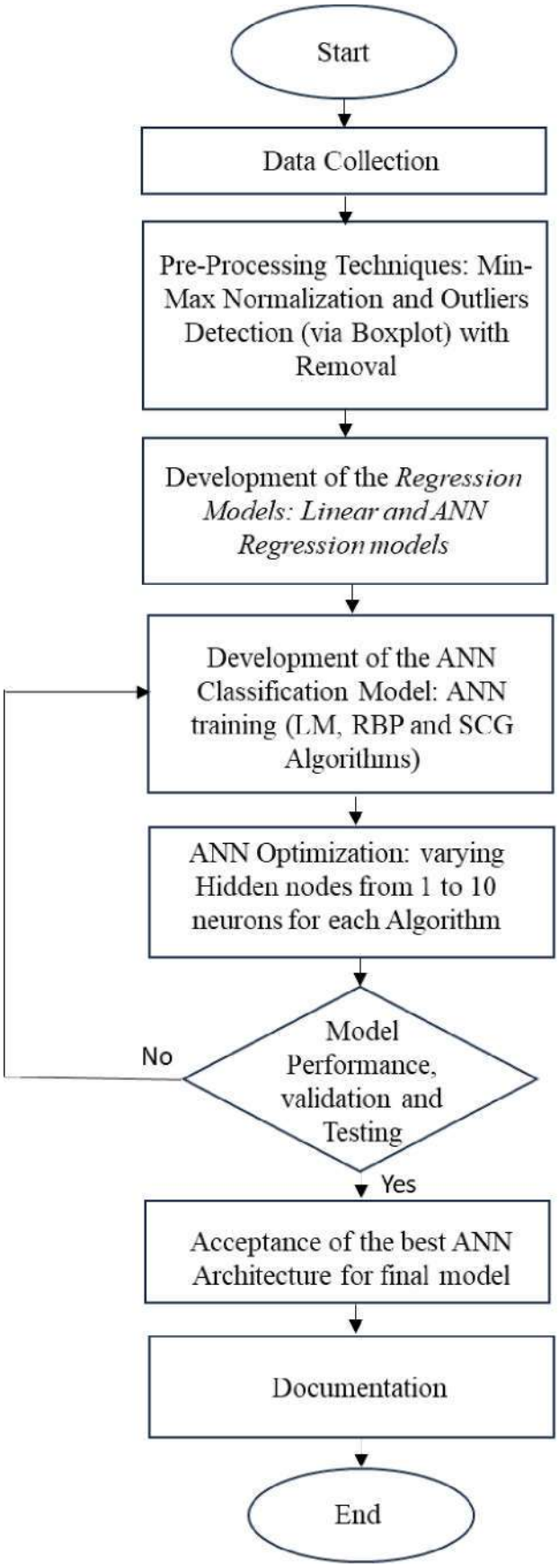

Figure 3.1 General Methodology of the Research

3.2 Data Collection

The data on the absorption performance of microwave absorbers was obtained from experimental measurements conducted by a previous researcher using the NRL Arch Free method, as shown in Figure 3.2 [22]. This dataset consists of 1206 absorption performance values for different single-slot sizes, divided into four Microwave frequency bands, namely L band (1-2GHz), S-band (2-4 GHz), C-band (4-8 GHz) and X-band (8-12 GHz). Experiments were conducted within each frequency band to assess absorption performance across varying slot sizes. Table 3.1 shows the original dataset, which are grouped by frequency band, frequency range and single-slot size. As illustrated in Figure 3.3 (a)-(c), slot size refers to the rectangular slot array positioned at the centre of each vertical side surface of the hollow pyramidal absorber. These opening affects the interaction between incoming electromagnetic wave and the absorber structure, so it significantly influences its absorption properties. The slots are classified into three-dimensional categories: small (3x6 cm), medium (4x8 cm) and big (8x18 cm) [22].

In this study, the eco-friendly hollow pyramidal microwave absorbers were fabricated using cardboard as the substrate structure, chosen due to its low cost, biodegradability and wide availability. The coating layer (absorbing material) was prepared by mixing coconut shell activated carbon, white acrylic paint and water, forming an absorptive slurry that was applied onto the cardboard surface to create the microwave absorbing layer [22], [44]. Coconut shell activated carbon was selected because agricultural carbon wastes are known to exhibit favourable dielectric loss characteristics, making them suitable for energy absorption and sustainability driven applications.

The eco-friendly hollow pyramidal microwave absorbers are categorized into three single-slot sizes: small, medium, and big. The dataset includes one input parameter, which consist of frequency, while the output corresponds to the classification of the single-slot size based and absorption performance on this input. This dataset forms the foundation for developing both regression models and Artificial Neural Network (ANN) classification model in this study, allowing for comprehensive analysis of the relationship between frequency and absorption performance across different frequency bands.

Figure 3.2 The Free Space Arch Measurement Set Up [22]

Table 3.1
Dataset of Eco-Friendly Microwave Absorption Performance

Frequency Band	Frequency Range	Number of Absorption Performance Values		
		Single Slot Size Small	Single Slot Size Medium	Single Slot Size Big
L	1-2 GHz	29	29	29
S	2-4 GHz	57	57	57
C	4-8 GHz	114	114	114
X	8-12 GHz	202	202	202

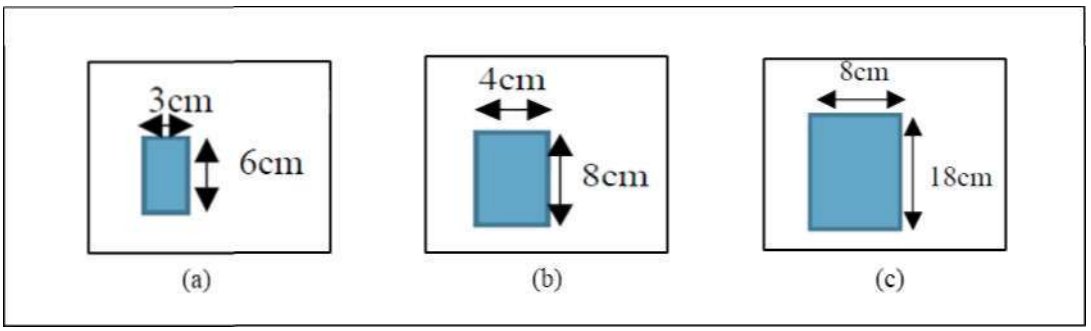

Figure 3.3 Slot Size Dimensional Classification For Hollow Pyramidal Microwave Absorbers : (a) Small - 3x6 cm, (b) Medium - 4x8cm and (c) Big - 8x18 cm [22]

3.3 Data Pre-Processing Techniques

In this research, data pre-processing is an essential step to ensure data quality before model development. The data processing stage involves two main techniques: Boxplot Analysis for Outlier Detection and Removal and Min-Max Normalization for scaling. These techniques are illustrated in Figure 3.4, which outlines the data processing workflow.

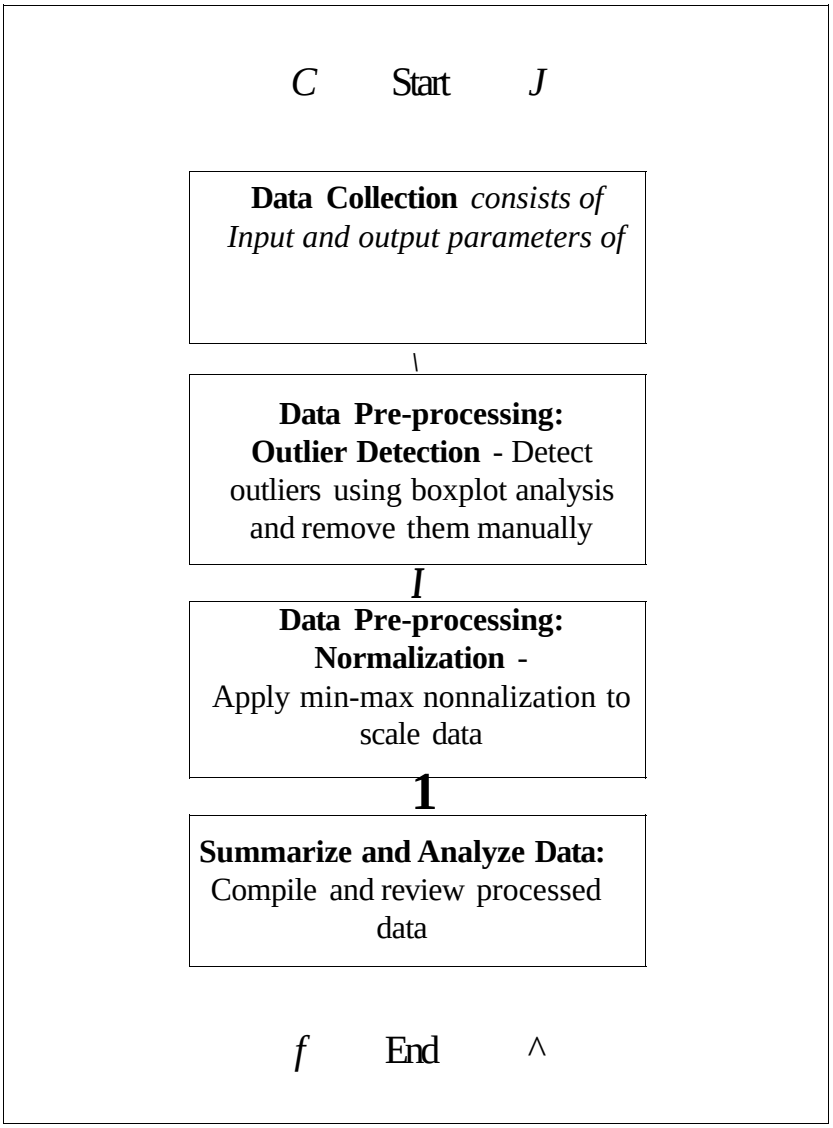

Figure 3.4 Flowchart of Data Processing Techniques

3.3.1 Boxplot Analysis for Outlier Detection and Removal

Boxplot analysis was used to examine the distribution of the dataset and identify any outliers, values that deviate significantly from the main data distribution. Outliers

can distort subsequent analyses and potentially lead to inaccurate model predictions. By visualizing the data through boxplots, these outliers were detected and manually removed, ensuring that only reliable data points contributed to the model training process.

Although more advanced multivariate anomaly-detection tecniques exist, such as mahalanobis distance-based multivariate thresholding [219] and machine-learning outlier screening method like Isolation Forest [220], their applicability is most appropriate for datasets with multiple continuous predictors. However, the dataset in this study contains one continuos input variable (frequency) and output (absorption performance). Acorrdingly, univariate boxplox based IQR filtering is the most suitable technique for identifying distribution-level anomalies, as it evaluates dispersion and extreme variability within each independent frequency band subset [130], [135].

The absorption measurments were grouped according to the frequency bands listed in Table 3.1, for this analysis. Outliers of boxplot are denoted as ' *' figures placed above and below the whiskers. The lower quartile (Ql) represents the 25th percentile of the dataset, the upper quartile (Q3) represents the 75th percentile and the median (Q2) is illustrated by a line inside the box. The length of the whiskers is determined based on the interquartile range (IQR), as calculated in Equation (3.1), while Equation (3.2) and (3.3) define the acceptable lower and upper data limits [130], [140].

$$IQR=Q3-Q1 \tag{3.1}$$

$$\text{Maximum range}=Ql-l.5(IQR) \tag{3.2}$$

$$\text{Minimum range}=Q3+1.5(IQR) \tag{3.3}$$

Observations falling outside these cutoffs were removed to retain only data representative of the central distribution. After the removal process, the dataset was re-evaluated using a second boxplot to confirm the absence of remaining extreme anomalies, to present a consistent and reliable dataset for further regression and ANN modeling approaches.

3.3.2 **Min** - Max Normalization

After removing outliers, min-max normalization was applied to scale the data. Min-max normalization is a widely used technique that scales data to a fixed range,

typically between 0 and 1, as shown in Equation (2.4). This transformation is achieved by adjusting each value based on the minimum and maximum of each feature, ensuring that all variables contribute equally to the model and preventing features with larger numerical ranges from dominating the analysis. This step is particularly important for algorithms like neural networks, which are sensitive to the scale of input data.

This transformation standardizes feature values to a similar scale, improving model performance and accelerating convergence during training. In addition, min-max normalization is particularly effective when the dataset contains no significant outliers, the upper and lower range of features are well-defined, and preserving the original distribution's shape is important. However, if outliers are present, they can distort the scaling process, as extreme values disproportionately affect the range.

In this study, the sensitivity of min-max normalization to outliers was addressed by performing boxplot-based outlier removal prior to normalization. As a result, the dataset used for ANN modelling contained no significant extreme values that could distort the scaling process. Althogh alternative normalization techniques such as z-score standardization and robust scaling were considered, min-max normalization was selected due to its ability to preserve the original data distribution and its compatibility with ANN training, especially in improving covergence stability.

3.4 Development of Regression Models

3.4.1 Linear Regression Model

Figure 3.5 presents the flowchart of the experimental process for developing the linear regression model in this study. The process begins with the loading of absorption performance data [22] into the MATLAB R2021a. This dataset is then structured into independent variables *(X)* and dependent variables *(Y)*. For the linear regression analysis, the dataset was partitioned into training and testing sets using a 70:30 split. The training dataset was used to estimate the regression coefficients, while the testing dataset was employed to evaluate the predictive performance of the model. This split was selected to ensure sufficient data for model fitting while retaining an independent dataset for performance evaluation. The independent variables, represented by *X*, consist of the frequency band values, while the dependent variable *Y* corresponds to the

output, define by the observed absorption performance values of the eco-friendly based pyramidal microwave absorbers.

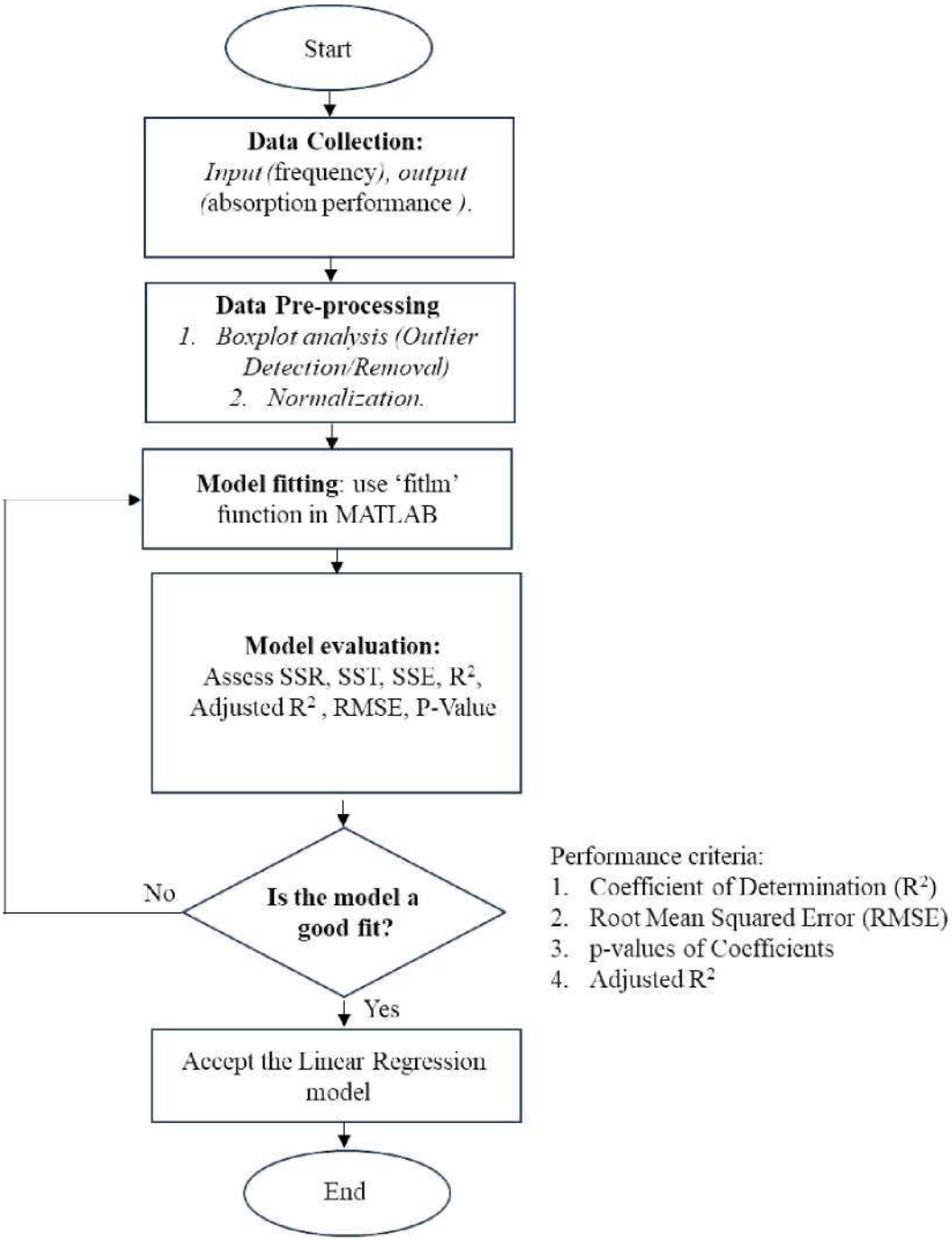

Figure 3.5 Detailed Experiment Procedure for the Linear Regression Model

Table 3.2 presents a sample of the dataset structure used in the linear regression analysis for the X-band, illustrating the independent variable (frequency) and the corresponding observed normalized absorption performance. The linear regression

analysis in this study was performed using the pre-processed dataset after boxplot-based outlier removal and min max normalization.

Table 3.2
Example of Normalized Dataset Structure for Linear Regression Analysis in the X-band

Sample No.	Frequency (GHz) - input X	Normalized Absorption Performance - output Y
1	8.0	0.4876
2	8.1	0.8196
3	8.2	0.8339
4	8.3	0.7671
5	8.4	0.7329

In the next step, a linear regression model is applied to the pre-processed data to establish the relationship between the independent and dependent variables. The linear regression model aims to fit a line to the data, described by the equation $Y = mX + c$, where m is the slope (or coefficient) representing the relationship between X and Y, and c is the intercept.

Once the model is fitted, it undergoes an evaluation phase to measure its accuracy and overall performance. The model's accuracy is assessed using several statistical metrics:

1. Coefficient of Determination (R^2): This indicates the proportion of the variance in the dependent variable that is predictable from the independent variables. A higher R^2 value, approaching 1, suggests a strong fit and a better predictive model. The R^2 is calculated using Equation (3.4) [68], [100]:

$$R^2 = \frac{SSR}{SST} = 1 - \frac{SSE}{SST} \quad (3.4)$$

Where:

- SSR *{Sum of Squared Regression)* is represents the variation explained by the regression model. It is the sum of squared differences between the predicted values and the mean of the observed values.
- SST *{Sum of Squared Total)* is representing the total variation in the dependent variable. It is the sum of squared differences between the observed values and the mean of the observed values.
- SSE *{Sum of Squared Errors)* represents the unexplained variation in the model. It is the sum of squared differences between the observed values and the predicted values.

2. Adjusted Coefficient of Determination (R^2 adjusted): Unlike R^2, the adjusted R^2 accounts for the number of predictors in the model, providing a more accurate measure of the model performance, especially when multiple predictors are involved. The adjusted R2 is calculated using Equation (3.5)[68J:

$$\text{adjusted } R^2 = 1 - \frac{(P-1)}{(P-Q)} \times \frac{SSE}{SST} \qquad (3.5)$$

Where:

- P: The total number of observations in the dataset.
- Q: The number of predictors (independent variables) in the model.

3. Root Mean Squared Error (RMSE): The RMSE measure the standard deviation of the residuals (prediction errors), which are the differences between observed and predicted values. It provides an estimate of the average error in the model predictions, reflecting how spread out the residuals are. A lower RMSE value, approaching 0, indicates that the model has a better fit. The RMSE is calculated using Equation (3.6):

$$RMSE = \frac{s\,\hat{}}{DOF} \qquad <">$$

Where:

- DOF (Degree of Freedom): represents the difference between the total number of observations (P) and the number of predictors (Q) in the model. It is calculated as DOF=P-Q, which adjusts for the number of predictors, ensuring that the RMSE accounts for model complexity.

4. P-values of Coefficients: These values test the statistical significance of each coefficient in the model. Lower p-values (approaching 0) indicate that the coefficients are statistically significant, meaning they contribute meaningfully to predicting the dependent variable.

The model also evaluates term such as Sum of Squared Errors (SSE), Sum of Squared Regression (SSR), and Sum of Squared Total(SST) to understand the variance captured by the regression model. These components contribute to the calculation of R^2, adjusted R^2, and RMSE, ensuring a comprehensive evaluation of model performance.

Once the model is evaluated, a decision-making step determines whether it meets the criteria for a good fit. These criteria include a high R^2, low RMSE, and statistically significant p-values. If the model meets these requirements, it is considered acceptable, and the process move forward to visualization. If the model does not meet the criteria, adjustments are made to the model iteratively, either by modifying the input variables, adjusting the parameters, or refining the model structure. This iterative process continues until a satisfactory model is achieved. The criteria for assessing model performance in this study are as follows:

1. An R^2 or adjusted R^2 value close to 1 indicates that a large proportion of variability in the dependent variable is explained by the model.
2. An RMSE value close to 0 signifies a lower average error between observed and predicted values.
3. p-values less than 0.05 indicate that the coefficients are statistically significant.

This methodology ensures that the linear regression model developed in this study is both accurate and reliable, providing meaningful insights into the relationship between frequency bands and absorption performance of the absorbers.

3.4.2 Artificial Neural Network (ANN) Regression Model

Figure 3.6 presents the flowchart outlining the experimental procedure for developing the ANN regression model in this methodology.

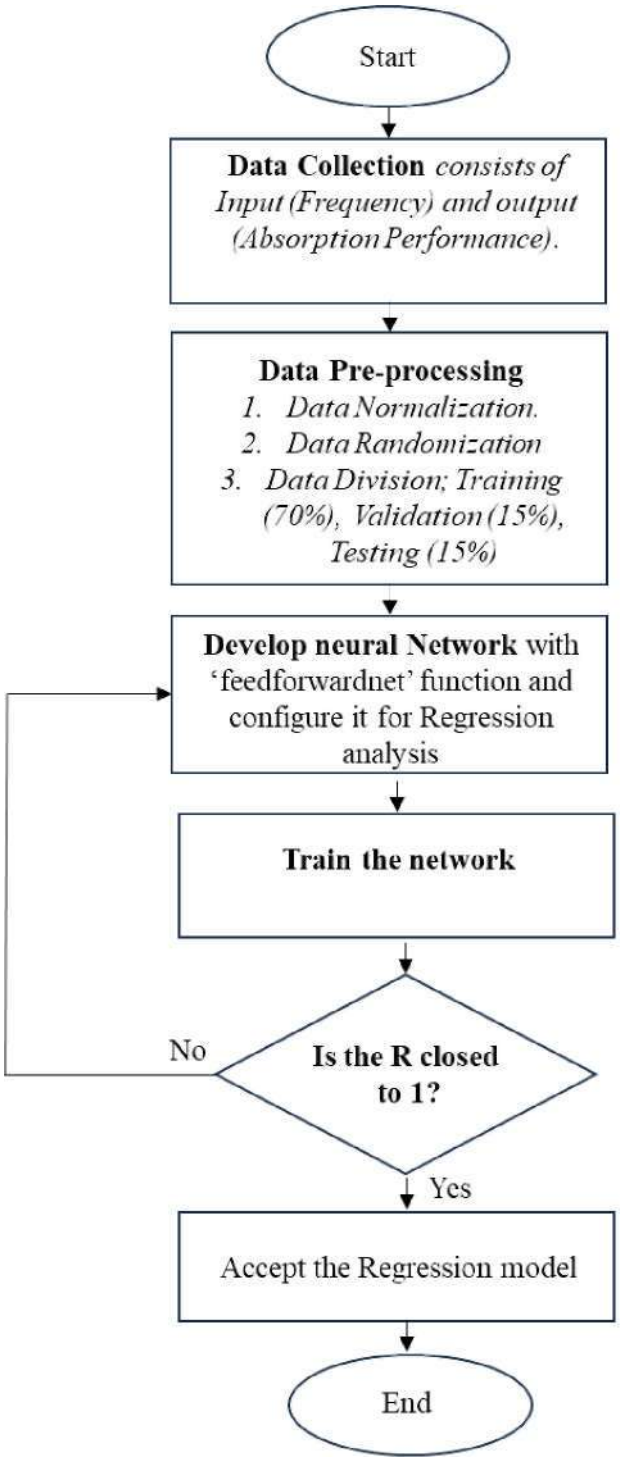

Figure 3.6 Detailed Experiment Procedure for the ANN Regression Model

ANN regression is used in this study to capture the strongly nonlinear relationship between frequency and absorption performance in eco-friendly microwave absorbers, which difficult to model accurately using conventional linear regression techniques. As highlighted in Chapter 2, most existing studies focus on experimental characterization and numerical simulations with relatively limited attention given to data-driven predictive modelling, particularly for biomass-based absorbers. Therefore, the application of ANN regression in this work aims to address this gap by providing a robust predictive framework capable of modelling complex multiband absorption behaviour.

Firstly, the data of absorption performance [22] is loaded into MATLAB R2021a. The data is then organized into independent variables, X (frequency) and dependent variables, Y (absorption values). The ANN model architecture consists of an input layer with one neuron representing frequency, three hidden layers and an output layer with one neuron representing absorption value. The hidden layers employ the rectified linear unit (ReLU) activation function to enhance the learning process, while the output layer uses the sigmoid activation function to produce normalized output values.

Next, a series of data pre-processing steps are applied to prepare the dataset for analysis:

1. Data Normalization: This step standardizes the input features, ensuring they are on a similar scale. Normalization promotes convergence during the training process and prevents any single feature from disproportionately influencing the model.
2. Data Randomization: After normalization, the dataset is randomized to minimize any potential biases from the data collection process, ensuring a more generalized model.
3. Data Division was divided into three subsets comprising a training set (70%), a validation set (15%), and a testing set (15%). This division allows the model to undergo separate phases of learning, generalization monitoring, and independent performance evaluation, thereby ensuring robustness and minimizing the risk of overfitting. As a representative example, the L-band dataset consisted of 78 data samples, which were randomly distributed across the three subsets following the predefined 70:15:15 proportion. This allocation

ensures a fair and unbiased distribution of input-output pairs across all subsets. The corresponding dataset partitioning for the L-band is summarized in Table 3.3.

The same dataset partitioning strategy was consistently applied to the S, C, and X-bands, with the number of samples in each subset adjusted according to the total observations available for each frequency band. The input-output structure of the dataset used in this partitioning follows the normalized format shown in Table 3.2.

Table 3.3
Representative Dataset Partitioning for the L-band Based on a 70:15:15 Training, Validation, and Testing Split

Subset	Number of Samples	Percentage (%)
Training	**54**	69.2
Validation	**12**	**15.4**
Testing	**12**	**15.4**
Total	**78**	**100**

In stage 4, the neural network is developed using the feedforwardnet function in MATLAB, specifically configured for regression analysis. This function creates a feedforward neural network, a type of artificial neural network suitable for modelling continuous outputs due to its acyclic node connections. The configuration process involves several steps:

1. *Defining Network Architecture:* The architecture includes an input layer for frequency (independent variable) and an output layer for absorption performance (dependent variable). Then, the number of neurons in the hidden layers is adjusted through experimentation, testing configurations with varying number of hidden layers (e.g. one, two or three layers) and neuron counts. This approach aims to maximize accuracy while preventing overfitting.
2. *Experimenting with Hidden Layers and Neurons:* The choice of hidden layers and neurons affects the network's capacity to learn complex patterns. Various configurations are tested to balance the model flexibility and generalization capability, incrementally increasing neurons and layers.

3. Selecting Activation Functions:
    - The ReLU activation function, defined in Equation (3.7) [221] was employed in the hidden layers to improve convergence during ANN regression training.

$$f(x)=\max(0,x) \tag{3.7}$$

    - The sigmoid activation function, defined in Equation (3.8) [221] was used in the output layer to produce normalized absorption values consistent with the preprocessing stage.

$$\text{™-}T\text{^} \tag{<38)}$$

$$1+ e^{x}$$

In Equation (3.7) and (3.8), x denotes the net input to the neuron and f(x) represents the corresponding activation output.

4. *Initial Weight and Bias Setup:* Weights and biases are initialized using the default settings in MATLAB's feedforwardnet function, though adjustments may be made to improve convergence speed and avoid local minima.
5. *Hyperparameter Tuning:* Other hyperparameters, such as learning rate, momentum and regularization, are fine-tuned to optimized model performance and reduce issues like overfitting and underfitting.
6. *Evaluation of Configurations:* Each network configuration is evaluated based on the correlation coefficient (R). configurations achieving an R value close to 1 are considered suitable, while those that do not meet this criterion are adjusted by revisiting parameters like hidden layers, neuron count or other parameters.

Through iterative tuning, the optimal neural network architecture is identified, ensuring the ANN regression model generalizes well while maintaining high predictive accuracy.

Next, in stage 5 is train the network, the model is trained on the dataset after defining the network architecture. This stage involves specifying essential parameters and closely monitoring the model's learning process:

1. Configuring Training Parameters
    - Epochs: The number of complete passes through the training dataset. A balanced number of epochs is chosen to allow sufficient learning without overfitting.

- Batch Size: Controls how many samples are processed before the model's weights are updated. Smaller batch sizes yield quicker convergence, while larger sizes offer more stable updates.
- Validation Data: A separate subset of the data is used to validate the model during the training, helping to identify overfitting or underfitting.

2. Monitoring Training Process
   - Metrics such as training loss (error between predictions and actual values in the training set) and validation loss (error on the validation data) are tracked over epochs. This monitoring provides insight into the model's learning and highlights potential issues.
   - Visualization Tools: Training curves illustrate the progress of training and validation loss, identifying patterns that may indicate overfitting (if validation loss increases while training loss decreases) or underfitting (if both remain high).

By tracking these metrics, timely adjustments can be made to the training process, preventing overfitting or underfitting and ensuring the model generalizes effectively.

After training, the model is evaluated on a separate test set to assess its predictive accuracy. Key evaluation metrics include Root Mean Squared Error (RMSE) and Mean Absolute Error (MAE), which measure prediction errors. Additionally, the Correlation Coefficient (R) quantifies how closely the model's predictions align with actual values, with high R values, especially those close to 1, indicating strong predictive accuracy and effective model generalization.

If the evaluation shows that the R value is not sufficiently close to 1, further adjustments are made to improve model performance. These adjustments include the hyperparameter tuning which modifying parameters like learning rate, batch size or regularization parameters, as well as network architecture refinement by adjusting the number of neurons or layers to enhance model accuracy and generalization. This process of training, evaluation and fine-tuning is repeated until a satisfactory R value is achieved, at which point the model is accepted as the final ANN regression model.

This ANN-based regression framework enables accurate prediction of absorption performance across frequency bands, supporting efficient analysis and design of eco-friendly microwave absorbers.

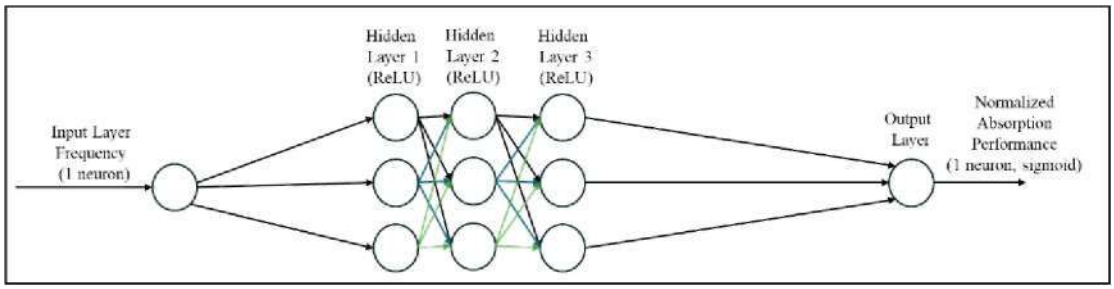

Figure 3.7 Architecture of the ANN Regression Model Used For Absorption Performance Prediction, Consisting of One Input Neuron (Frequency), Three Hidden Layers with ReLu Activation, and One Output with Sigmoid Activation

As illustrated in Figure 3.7, the final ANN regression model employed in this study consists of one input neuron representing frequency, three hidden layers and one output neuron representing normalized absorption performance. ReLU activation functions are applied in the hidden layers to effectively model nonlinear absorption behaviour, while a sigmoid activation function is used at the output layer to generate normalized regression output. The number of hidden layers and neurons was determined through experimental tuning to balance model accuracy and generalization performance, thereby avoiding underfitting and overfitting. This architecture was selected to capture the complex nonlinear relationship between frequency and absorption performance observed in eco-friendly microwave absorbers.

3.5 Artificial Neural Network (ANN) Classification Model Development

3.5.1 ANN-Based Classification Framework

Figure 3.8 presents the flowchart of the experimental setup for MLP training. The process begins by loading the data into MATLAB R2021a, which consists of the input and output data for absorption performance which have been conducted the previous researcher [22]. The next step is data pre-processing, a crucial phase that ensures the data is in a suitable format for the neural network inputs and outputs, thereby highlighting the effects of varying input ranges.

The pre-processing involves several steps, beginning with outlier detection using boxplot analysis, followed by manual removal of the identified outliers. This step ensures that extreme values that could negatively impact model training are eliminated. After outlier removal, the next pre-processing step is normalization using the min-max scaling technique, which scales input features to a range between 0 and 1. This scaling

is particularly important for the eco-friendly absorption dataset, as it ensures consistency across continuous variables and improves the convergence of the neural network training. Following normalization, the data is randomized to prevent any ordering biases that could affect the training process.

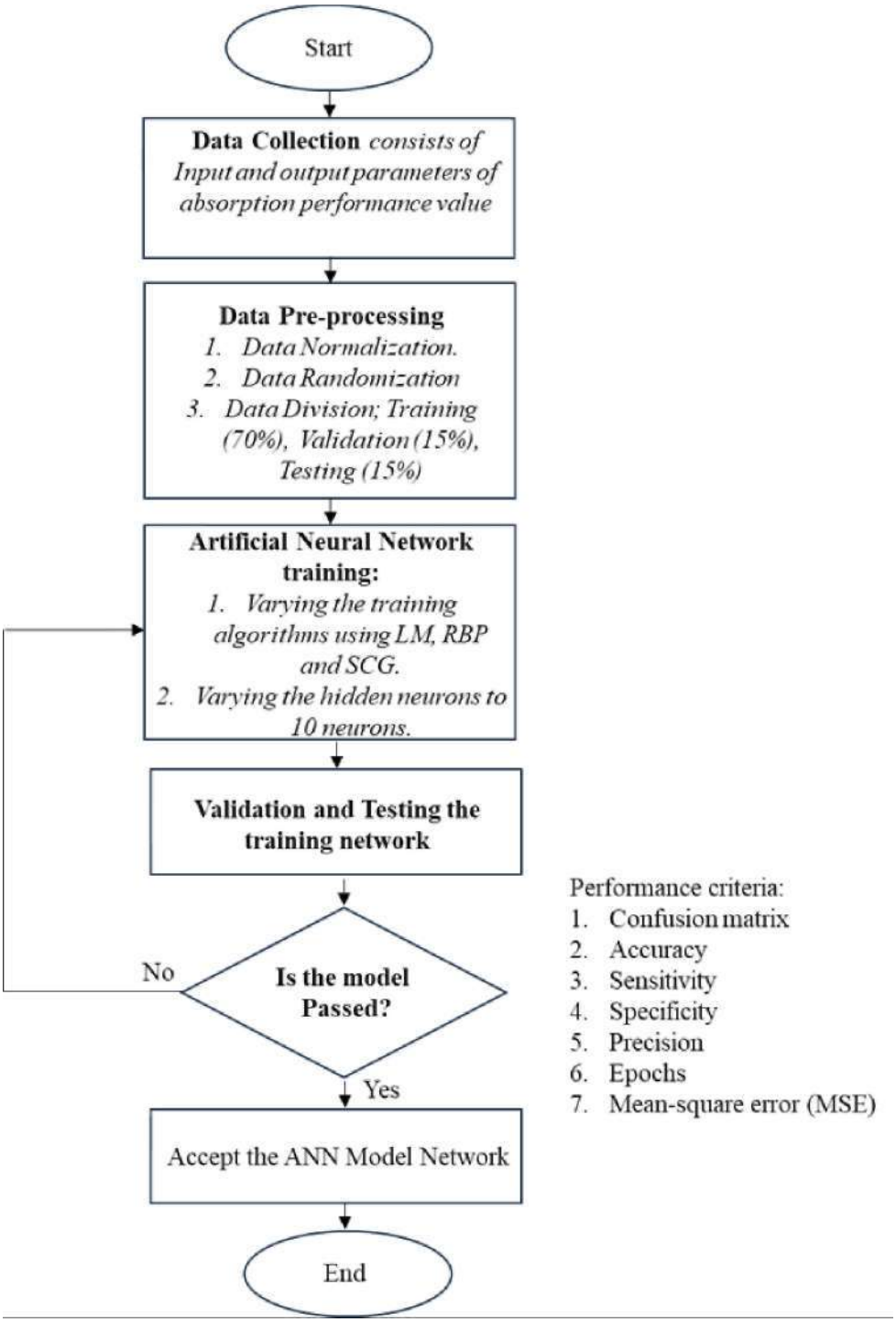

Figure 3.8 Flowchart of the ANN Experiment to Determine Absorption Performance

For ANN-based classification, the preprocessed continuous absorption values were restructured into discrete class labels. Each data sample was assigned to a specific class based on its absorber configuration, resulting in three classification categories corresponding to small, medium and big absorber sizes (Class 1, Class 2 and Class 3 respectively). This restructuring converts the regression output into categorial labels suitable for supervised classification.

Figure 3.9 illustrates a representative ANN classification architecture implemented in MATLAB for this study. The network consists of an input layer, a single hidden layer, and an output layer. The input layer comprises one neuron representing the operating frequency, which serves as the primary input feature for classification. The hidden layer employs a nonlinear activation function and contains 10 neurons in the configuration shown, which represents one of the tested architectures. In practice, the number of hidden neurons was varied from 1 to 10 during experimental tuning to identify the optimal network structure that balances classification accuracy and generalization performance. The output layer consists of three neurons corresponding to the absorber slot size classes. A 3-bit binary encoding scheme is adopted, where each output pattern represents a specific class: small (001), medium (010), and large (100). This architecture enables multi-class classification by mapping frequency-dependent absorption behaviour to discrete absorber size categories.

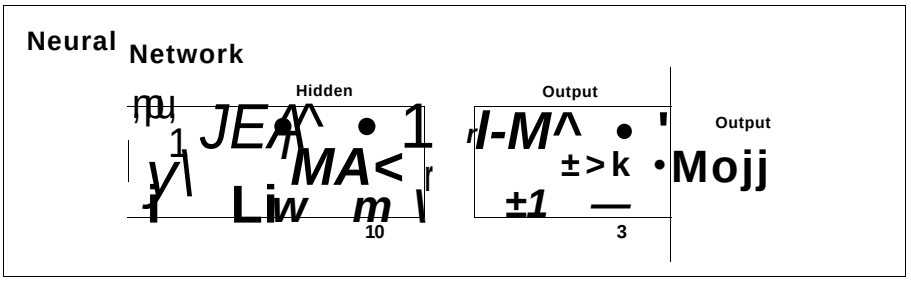

Figure 3.9 Example ANN Classification Architecture Implemented in MATLAB, Consisting of One Input Neuron (Frequency), A Single Hidden Layer with 10 Neurons (Varied From 1-10 During Tuning), and An Output Layer with Three Neurons Representing Small, Medium and Large Slot Size Classes

Once normalized, randomized and labelled, the dataset is divided into three groups: training (70%), validation (15%) and testing (15%), as summarize in Table 3.3. The training set is used to update the network weights, the validation set evaluates the final model's accuracy and generalization to unseen data, and the testing set provides an independent evaluation of classification performance.

The distribution of samples across the three classification categories is examined to assess potential class imbalance. The dataset exhibits a reasonably balanced distribution among the classes; therefore, no additional resampling or class-weighting strategies are required. This ensures that the ANN classifier does not exhibit bias toward any particular class during training.

The dataset is then trained and classified using MLP algorithms. Three learning algorithms are employed, namely Levenberg Marquadt (LM), Resilient Backpropagation (RBP) and Scaled-Conjugate Gradient (SCG). Besides, the number of neurons in hidden layer varies from 1 to 10 for each algorithm, using the Pattern Recognition Network (patternet) function in Matlab R2021a. After training, the model undergoes validation and testing. The results are displayed in the Neural Network Traning tool (nntraintool), which provides performance plots and progress updates. Figure 3.10 illustrates the architecture of the ANN classification model employed in this study, showing the input layer representing frequency, a single hidden layer with ReLu activation (1-10 neurons) and an output layer with three softmax neurons corresponding to small, medium and big absorber classes.

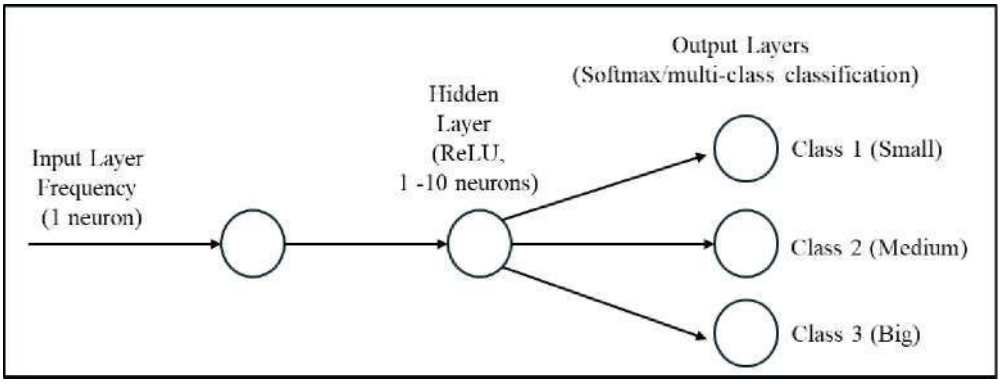

Figure 3.10 Architecture of the ANN Classification Model Employed in This Study, Showing the Input Layer Representing Frequency, A Single Hidden Layer with ReLu Activation (1-10 neurons) and an Output Layer with Three Softmax Neurons Corresponding to Small, Medium and Big Absorber Classes

ANN-based classification is adopted in this study due to its capability to model complex nonlinear relationships between frequency-dependent absorption behaviour and absorber configuration. As discussed in Chapter 2, the absorption characteristics of eco-friendly microwave absorbers exhibit strong nonlinearity across multiband frequency ranges, making them difficult to classify using simple linear or rule-based approaches. The MLP classifier provides flexible decision boundaries and robust

classification performance when handling continuous input data and complex absorption patterns.

The model's performance criteria are evaluated based on several criteria such as confusion matrix, accuracy, sensitivity, specificity, precision, number of epochs and mean-squared error (MSE). A trained model is considered acceptable if it achieves high classification accuracy of at least 85%, demonstrated balanced sensitivity and specificity across all classes and exhibits stable validation performance without signs of overfitting. If the model meets these criteria, it is accepted as the final ANN classification model. If not, the training process is repeated by revisiting the ANN training step, as shown in the Figure 3.8.

3.5.2 Training Algorithm for Multilayer Perceptron (MLP)

3.5.2.1 Implementation ofLevenberg Marquardt (LM)

The Levenberg Marquardt (LM) algorithm is commonly used for training neural networks due to its fast convergence and effectiveness for moderate sized datsets. In this study, the LM algorithm is implemented using the trainlm function in MATLAB to train the ANN classification model.

During training, the algorithm adaptively adjusts the combination coefficient, u, to balance gradient descent and Gauss-Newton optimization. If the training error increases after a weight update, the update is reversed and u is increased to ensure stable convergence. Conversely, if the error decreases, the updated weights are retained and u is reduced to allow finer optimization. This adaptive mechanism enables efficient and robust network training.

The training process is controlled using predefined stopping criteria, including the maximum number of epochs, validation performance monitoring, minimum performance gradient and upper limits on the combination coefficient u. These parameters ensure effective convergence while preventing overfitting or excessive weight adjustments. The network training parameters used for the LM algorithm are presented in Table 3.4.

The training parameters listed in Table 3.4 were selected based on standard MATLAB default settings and commonly adopted practices in ANN-based modelling studies. Parameters such as the maximum number of epochs, validation failure limit and

performance gradient threshold were chosen to ensure sufficient learning while preventing overfitting through early stopping. The initial value of the combination coefficient u, along with its increase and decrease factors, follows the recommended configuration for the Levenberg Marquardt algorithm to balance convergence speed and training stability. Similar parameter settings have been widely reported in previous ANN studies employing LM-based training for nonlinear modelling tasks [18], [222]. These settings were found to provide stable convergence and reliable classification performance in this study.

Table 3.4
Network Training Parameters for the LM Algorithm

Parameter	Value	Description
i. Maximum number of epochs	1000	Specifies the maximum number of iterations allowed during training, ensuring adequate opportunities to converge.
ii. Maximum validation failures	6	Allows early stopping of training if validation performance does not improve over six consecutive epochs.
iii. Minimum performance gradient	1×10^{-7}	Define a minimum gradient threshold for stopping training based on the performance improvement, indicating sufficient accuracy.
iv. Initial u	0.001	Sets the starting value of the combination coefficient, balancing gradient descent and Gauss-Newton.
v. Decrease factor for u	0.1	Reduces u when total error decreases, enabling finer adjustments to the weights.
vi. Increase factor for u	10	Increases u when total error increases, allowing larger adjustments to correct errors.
vii. Maximum factor for u	1×10^{10}	Sets the upper limit for u, stopping the training if exceeded to prevent excessive adjustments.

3.5.2.2 Implementation of Resilient Backpropagation (RBP)

The RBP training algorithm in MATLAB's patternnet function was implemented using the 'trainrp' function. This algorithm updates network weights based solely on the sign of the gradient, making it less sensitive to the magnitude of the gradient and suitable for stable convergence. The learning rate, *e* was set to 0.01 to enhance the efficiency and speed of the network during the training process.

Firstly, the initial weight update A_{mn} is assigned to an initial value of 0.07 (A_{mn} = 0.07). The range for weight update is constrained by a maximum limit, A_{max} = 50.0 and a minimum limit, $A_{m;n}$ = 1 x 10~ . The maximum limit prevents the weights from becoming excessively large, while the minimum limit helps to avoids underflow issues in floating-point calculations [193], [202]. The increasing factor, r|$^{+}$ and decreasing factor, r|~ are defined within the range of 0.5 < r| < 1.2. These factors influence the adjustment of the weights during training. The weight update is reduced by the decreasing factor when overshooting occurs, which happens if the previous update was too large. This decreasing factor, also referred to as 'principle binary search' [216], aids in fine-tuning the adjustments. On the other hand, the increasing factor must be large enough to ensure consistent changes in the weight direction [193]. Existing studies [182] have recommended that values of 0.5 and 1.2 for the increasing and decreasing factors, respectively, yield optimal results. The network training parameters for the RBP algorithm are presented in Table 3.5.

Table 3.5
Network Training Parameters for the RBP Algorithm

Parameter		Value	Description
i.	Maximum number of epochs	1000	Specifies the maximum number of iterations allowed, ensuring sufficient opportunities to convergence.
ii.	Maximum validation checks	6	Allows early stopping of training if validation performance fails to improve over six consecutive epochs.
iii.	Learning rate, e	0.01	Enhances the efficiency and speed of the network during training.
iv.	Initial weight change, A_{mn}	0.07	Sets the starting value for weight updates.
v.	Minimum weight change, A_{min}	1 x 10^{-5}	Ensures updates do not become too small to drive meaningful changes.
vi.	Maximum weight change, A_{max}	50	Prevents excessively large updates that could destabilize training.
vii.	Decreasing factor, *rf*	0.5	Reduces the step size to prevent overshooting minima during training.
viii.	Increasing factor,	1.2	Increases the step size to accelerate convergence when needed.

3.5.2.3 Implementation of Scaled Conjugate Gradient (SCG)

The Scaled Conjugate Gradient (SCG) algorithm is implemented in this study to train the ANN classification model due to its efficiency and ability to avoid time-consuming line searches. The SCG algorithm is implemented using the 'trainsg' function in MATLAB, making it suitable for large-scale optimization problems and stable network training. During training, the SCG algorithm updates the network weights by combining the advantages of conjugate gradient methods with adaptive scaling to ensure stable convergence. The algorithm utilizes predefined parameters to regulate the approximation of second-order information and maintain the positive definiteness of the Hessian matrix, thereby improving optimization efficiency. These mechanisms enable effective weight updates without requiring explicit computation of the Hessian matrix.

The training process is managed with common stopping criteria (e.g. the maximum number of epochs, validation performance monitoring and minimum performance gradient threshold). The criteria as mentioned above lead to a fast convergence of the training, and can also prevent overfitting. The network training parameters of the SCG algorithm are presented in Table 3.6. All parameter values follow the default settings recommended in MATLAB R2021a, which are commonly adopted in ANN-based classification studies.

Table 3.6
Network Training Parameters for the SCG Algorithm

Parameter		Value	Description
i.	Maximum number of epochs	1000	Specifies the maximum number of iterations allowed, ensuring sufficient opportunities for convergence.
ii.	Maximum validation checks	6	Allows early stopping of training if validation performance does not improve over six consecutive epochs.
iii.	Minimum performance gradient	1×10^{-6}	Sets as lower threshold for the performance gradient to prevent stagnation, ensuring that updates continue only if they contribute meaningfully to error reduction.
iv.	change in weight for second derivation, o	5×10^{-5}	Adjusts the weight vector to approximate the second-order derivative of the error function, aiding in efficient calculation of Hessian-vector product.

Parameter		Value	Description
v.	Regularization parameter for Hessian definiteness	5×10^{-7}	Regulates the definitenes of the Hessian matix to maintain stability during optimization.

The training process for all algorithms halts if any of the following conditions are met: (i) the maximum number of epochs which is 1000 is reached; (ii) the maximum allowable time is exceeded; (iii) performance is minimized to the target goal; (iv) the performance gradient falls below the specified minimum gradient (LM = lxlO"^{7}, RBP = lxlO"^{5}, SCG = lxlO"^{6}); or (v) the validation performance fails to improve for more than the maximum allowed validation failures (set to 6), which corresponds to the last observed decrease [102]. Validation checks are crucial for preventing overfitting, setting a higher number of validation checks may risk network instability [218].

3.6 Performance Measurement

The performance of the ANN was evaluated using several criteria, including the confusion matrix, accuracy, sensitivity, precision and mean square error (MSE). The confusion matrix, shown in Table 3.6, provides a detailed breakdown of the model's classification performance such as True Positives *(TP),* False Positives *(FP),* False Negatives *(FN)* and True Negatives (77V). It provides insights into how well the model distinguishes between these categories presenting the number of correct and incorrect classifications.

Table 3.7
The Confusion Matrix

Data Group	Predicted/Classified as Positive	Predicted/Classified as Negative
Positive	True Positives (TP)	False Negatives (FN)
Negative	False Positives (FP)	True Negatives (TN)

The confusion matrix can also be expressed in mathematical form as in Equation (3.9).

$$f^{TP \quad FP}_{LFN \quad TNJ} 1 \qquad (39)$$

TP indicates the number that is accurately classified as positive, while *TN* rpresents the number correctly classified as negative. FP refers to negative samples incorrectly classified as positive, and FN denotes positive samples incorrectly classified as negative. The performance of the ANN classification technique is evaluated by calculating the accuracy, sensitivity, specificity , precision, and mean squared error (MSE), which are defined in equations (3.10) to (3.14), respectively [223]-[225].

Accuracy is a quantitative statistic that evaluates the overall correctness [17] of the classification model:

$$\text{Accuracy} = \frac{TP+TN}{TP+FP+FN+TN} 100 \qquad (3\ 10)$$

Sensitivity is the ability of a classifier to identify positive occurrences among all actual groups of size correctly:

$$\text{Sensitivity} = \frac{TP}{TP+FN} 100 \qquad (3\ 11)$$

Specificity measures the ability of the model to detect negative cases accurately:

$$\text{Specificity} = \frac{TN}{TN+FP} 100 \qquad (3,12)$$

Precision is a measure of how closely the data label aligns with the positive labels assigned by the classifier.

$$\text{Precision} = \frac{TP}{TP+FP} 100 \qquad (3\ 13)$$

Where:

TP = True Positives; TN = True Negatives;

FP = False Positives; FN = False Negatives.

The *Mean-Squared Error (MSE)* evaluates the average squared difference between predicted and actual showing the model's prediction accuracy.

$$MSE = \frac{1}{n}\sum_{i=1}^{n}(y_t - \hat{y}_t)^2$$

Where: y_t = Actual value; y_t = Predicted value; n = number of observations.

Based on the evaluation criteria, the model is assessed for its performance. If the model meets the required performance standards it is accepted as the final MLP model network. If not, the model undergoes further tuning and training iterations until the desired performance is achieved.

3.7 Summary

This chapter presented a comprehensive methodology framework designed to address the research objectives of modelling and characterizing the absorption performance of eco-friendly microwave absorbers using data-driven techniques. The methodological workflow combines data preprocessing, regression analysis, ANN based classification and systematic performance evaluation to ensure both predictive accuracy and practical relevance.

The initial stages of data acquisition and preprocessing establish a reliable foundation for modelling by ensuring data consistency across multiband frequency ranges. Outliers removal by boxplot can enhanced data reliability, on the other hand min-max normalization also makes input and output in standardize way to help ANN training become more stable and effective. These steps are necessary to eliminate measurement uncertainties often found in experimental absorption data.

Regression modelling, implemented through linear regression and ANN regression, directly addresses the objective of capturing the nonlinear relationship between operating frequency and absorption performance. The inclusion of ANN regression enables more accurate modelling of complex frequency dependent absorption behaviour that cannot be sufficiently represented using conventional linear approaches.

In parallel, ANN based classification is employed to translate continuous absorption responses into discrete absorber size categories, supporting decision oriented analysis. This classification framework complements regression by enabling the systematic categorization of absorber configurations (small, medium, and large) based on their frequency-dependent absorption characteristics. The use of multiple ANN

training algorithms (LM, RBP, and SCG) allows a comparative assessment of learning efficiency and generalization capability across frequency bands.

Performance measurement using classification and regression metrics, including accuracy, sensitivity, specificity, precision and mean squared error, provides objective criteria for evaluating model reliability and selecting optimal training strategies. Taken together, the methodology presented in this chapter establishes a robust and reproducible framework for applying ANN based predictive and classification models to eco-friendly microwave absorber analysis. This integrated approach represents a key contribution of the study by extending ANN methodologies to sustainable absorber materials, thereby forming the basis for the results and discussions presented in Chapter 4.

CHAPTER 4
RESULTS AND DISCUSSION

4.1 Introduction

This chapter presents the results and discussion of ANN-based modelling for eco-friendly microwave absorbers across the L, S, C and X frequency bands. The chapter begins by examining the characteristics of the post-processed absorption performance data for different slot sizes. This is followed by an evaluation of regression and classification performance using linear regression and artificial neural network models. The chapter concludes with a summary of key findings and their implications in relation to the research objectives.

4.2 Effects of Data Pre-processing and Data Normalization on Absorption Performance

4.2.1 L-Band

Figure 4.1 illustrates the distribution of L-Band absorption performance data following data refinement. The visualization provides insights into the absorption performance of eco-friendly microwave absorbers based on different single-slot sizes. The dataset comprises three slot sizes which are small (1), medium (2) and big (3). The corresponding statistical characteristics are summarized in Table 4.1, including the quartiles, median, extreme values and the number of retained data points. The refined dataset comprises 24, 25 and 29 data points for the small, medium and big slot sizes, respectively, indicating improved data consistency for subsequent analysis.

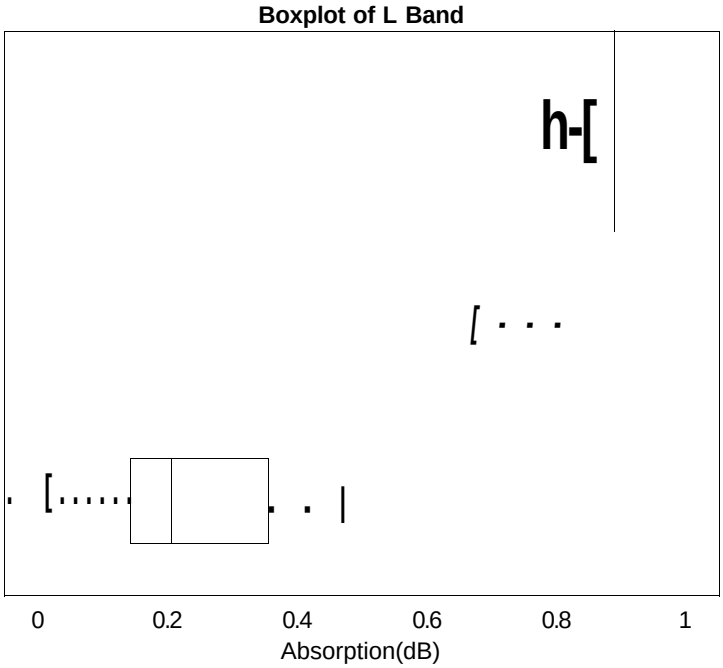

Figure 4.1 Distribution of Post-Processed L-Band Absorption Performance Data for Different Slot Sizes

For the Big slot size (3), the data shows a narrow interquartile range (IQR) from 0.8350 dB to 0.8916 dB, with a median of 0.8618 dB. The maximum and minimum values are 0.9045 dB and 0.7775 dB, respectively. This low variability indicates consistent and reliable absorption performance, making the big slot size a suitable choice for applications that require stability in absorption characteristics.

In contrast, the medium slot size (2) exhibits a wider IQR, ranging from 0.8463 dB to 0.9795 dB, with a median of 0.9338 dB. Although the medium slot size shows a higher absorption potential, its variability is reflected in the maximum and minimum values of 1.000 dB and 0.6717 dB, respectively. While it can achieve higher absorption performance, the lack of consistency suggests that it may not be ideal for applications requiring uniform results.

The small slot size (1) has the widest IQR, ranging from 0.1434 dB to 0.3567 dB, with a low median of 0.2078 dB. Its maximum and minimum values are 0.5199 dB and 0.0000 dB, respectively, showing high variability and the lowest absorption performance among the slot sizes. This makes the small slot size unsuitable for L-Band applications requiring consistent and high absorption. Further redesign or optimization may be necessary to improve its performance.

Table 4.1
Statistical Summary of Boxplot Analysis for L-Band Absorption Data by Slot Size

Single-Slot Size	75^{th} Percentile (Upper Quart)	Median	25^{th} percentile (Lower Quart)	Max	Min	Number of Data Points
1 (Small)	0.3567	0.2078	0.1434	0.5199	0.000	24
2 (Medium)	0.9795	0.9338	0.8463	1.0000	0.6717	25
3 (Big)	0.8916	0.8618	0.8350	0.9045	0.7775	29

In summary, the big slot size demonstrates the most stable and reliable performance, making it the preferred choice for L-Band applications. The medium slot size, while having the highest absorption potential, is less consistent and requires careful consideration for specific applications. In contrast, the small slot size shows the lowest performance and variability, making it less suitable for practical use without further modifications. These results highlight the importance of slot size in optimizing the absorption characteristics of eco-friendly microwave absorbers for the L-band.

4.2.2 S-Band

Figure 4.2 presents distribution of S-Band absorption performance data following data refinement. This analysis provides significant insights into the absorption performance of eco-friendly microwave absorbers across different single-slot sizes. The dataset is categorized into three slot sizes which are small (represented by 1), medium (represented by 2) and big (represented by 3). Table 4.2 summarizes the key statistical values for each slot size, including the quartiles, median, extreme values as well as the number of retained data points.

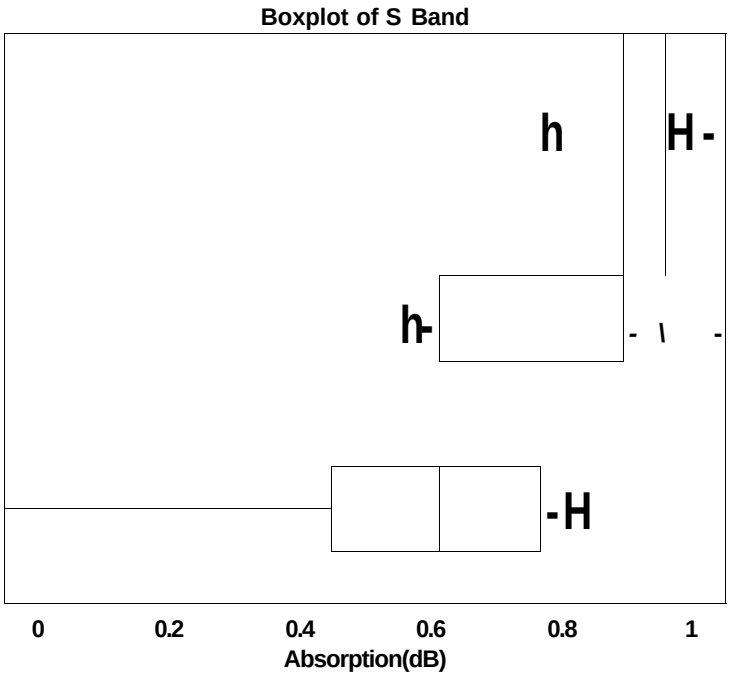

Figure 4.2 Distribution of Post-Processed S-Band Absorption Performance Data for Different Slot Sizes

The Big slot size (3) exhibits a very narrow interquartile range (IQR) from 0.7980 dB to 0.9577 dB, indicating minimal variability in absorption performance. With a median absorption value of 0.8868 dB, this slot size demonstrates consistent and high absorption capabilities. The range between maximum (1.0000 dB) and minimum (0.7698 dB) values further highlights the stability and reliability of the big slot size for achieving effective absorption in the S-Band.

The medium slot size (2) shows a moderately wider IQR, spanning from 0.6236 dB to 0.9024 dB, with a median value of 0.7300 dB, the medium slot size achieves good absorption performance, though it is slightly lower than the big slot size. The broader range between the maximum (0.9900 dB) and minimum (0.5555 dB) values suggests that while effective the medium slot size may be less consistent compared to the big slot size.

The small slot size (1) has the widest IQR, ranging from 0.4490 dB to 0.7755 dB, indicating the highest variability among the three slot sizes. The median absorption value of 0.6053 dB is the lowest, highlighting its relatively weaker absorption performance. Furthermore, the range extends from 0.0000 dB to 0.8489 dB, showcasing significant variability and lower reliability compared to the big and medium slot sizes.

Table 4.2
Statistical Summary of Boxplot Analysis for S-Band Absorption Data by Slot Size

Single-Slot Size	75^{th} Percentile (Upper Quart)	Median	25^{th} percentile (Lower Quart)	Max	Min	Number of Data Points
1 (Small)	0.7755	0.6053	0.4490	0.8489	0.000	47
2 (Medium)	0.9024	0.7300	0.6236	0.9900	0.5555	57
3 (Big)	0.9577	0.8868	0.7980	1.0000	0.7698	57

In summary, the big slot size emerges as the most consistent and effective option for S-Band absorption performance, while the medium slot size provides decent performance but with moderate variability. The small slot size exhibits the highest variability and the least effective absorption, making it less favourable for applications requiring high and stable absorption performance.

4.2.3 C-Band

Figure 4.3 presents the distribution of C-Band absorption performance data following data refinement. The visualization for the C-Band absorption performance provides critical insights into the effectiveness of different single-slot sizes. The dataset comprises three slot sizes which are small (represented by 1), medium (represented by 2) and big (represented by 3) with their statistical characteristics summarized in Table 4.3. The analysis highlights variations in absorption performance and their implications for the design and application of eco-friendly microwave absorbers.

The big slot size (3) shows a moderate interquartile range (IQR) from 0.6865 dB to 0.8840 dB, indicating a moderate level of variability in absorption performance. With a median value of 0.7675 dB, this slot size demonstrates relatively high absorption performance nearing the upper quartile. However, the range between the maximum (1.0000 dB) and minimum (0.4063 dB) values is broad, suggesting that while the big slot size is effective, it lacks consistency in its absorption performance.

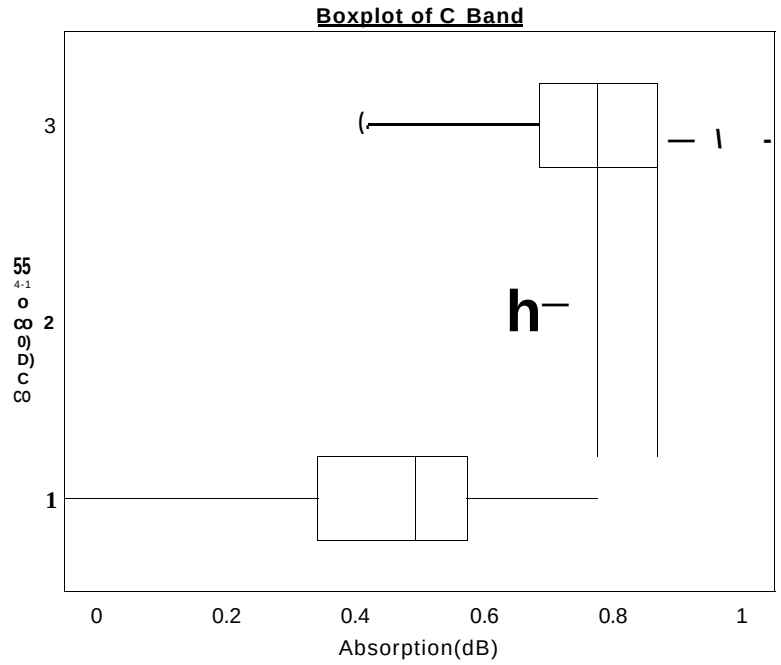

Figure 4.3 Distribution of Post-Processed C-Band Absorption Performance Data for Different Slot Sizes

The medium slot size (2), on the other hand, has a narrower IQR, spanning from 0.7632 dB to 0.8546 dB, reflecting lower variability compared to the big slot size. The median absorption value of 0.7979 dB is slightly higher than that of the big slot size, indicating superior absorption performance. The range between the maximum (0.9831 dB) and minimum (0.6369 dB) values is also narrower, signifying more consistent performance. This makes the medium slot size an excellent candidate for applications requiring stable and reliable absorption in the C-Band.

Conversely, the small slot size (1) demonstrates the widest IQR, ranging from 0.3422 dB to 0.5737 dB, which signifies the highest variability in absorption performance among the three slot sizes. With a median value of 0.4940 dB, the small slot size exhibits the lowest absorption capability. Furthermore, the range extends from 0.0000 dB to 0.8016 dB, reflecting significant variability and inconsistency, making it the least effective slot size for C-Band absorption.

Table 4.3
Statistical Summary of Boxplot Analysis For C-Band Absorption Data by Slot Size

Single-Slot Size	75^{th} Percentile (Upper Quart)	Median	25^{th} percentile (Lower Quart)	Max	Min	Number of Data Points
1 (Small)	0.5737	0.4940	0.3422	0.8016	0.000	111
2 (Medium)	0.8546	0.7979	0.7632	0.9831	0.6369	100
3 (Big)	0.8840	0.7675	0.6865	1.0000	0.4063	112

The findings suggest that the medium slot size offers the most consistent absorption performance with minimal variability and a high median value, making it ideal for applications that demand stable and reliable absorption in the C-Band. The big slot size, while demonstrating strong absorption capabilities, exhibits moderate variability and can be utilized in applications where high absorption is a priority but some variability can be tolerated. However, the small slot size is less effective due to its high variability and low absorption performance, making it unsuitable for applications requiring consistent results. Further evaluation or redesign of the small slot size may be necessary to enhance its absorption performance. This analysis provides valuable insights into the absorption characteristics of different slot sizes in the C-Band, enabling informed decisions for the selection and optimization of eco-friendly microwave absorbers tailored to specific applications.

4.2.4 X-Band

Figure 4.4 presents the distribution of X-Band absorption performance data following data refinement. This analysis provides critical insights into the absorption performance of eco-friendly microwave absorbers across different single-slot sizes. The dataset consists of three slot sizes which are small (represented by 1), medium (represented by 2) and big (represented by 3) with their statistical characteristics summarized in Table 4.4.

The big slot size (3) shows a moderate interquartile range (IQR) from 0.7780 dB to 0.9757 dB, reflecting moderate variability in absorption performance. With a median value of 0.9201 dB, the big slot size demonstrates relatively high and consistent absorption performance, nearing the upper quartile. However, the range between the

maximum (1.0000 dB) and minimum (0.5165 dB) values is relatively broad, indicating strong absorption potential but with some variability.

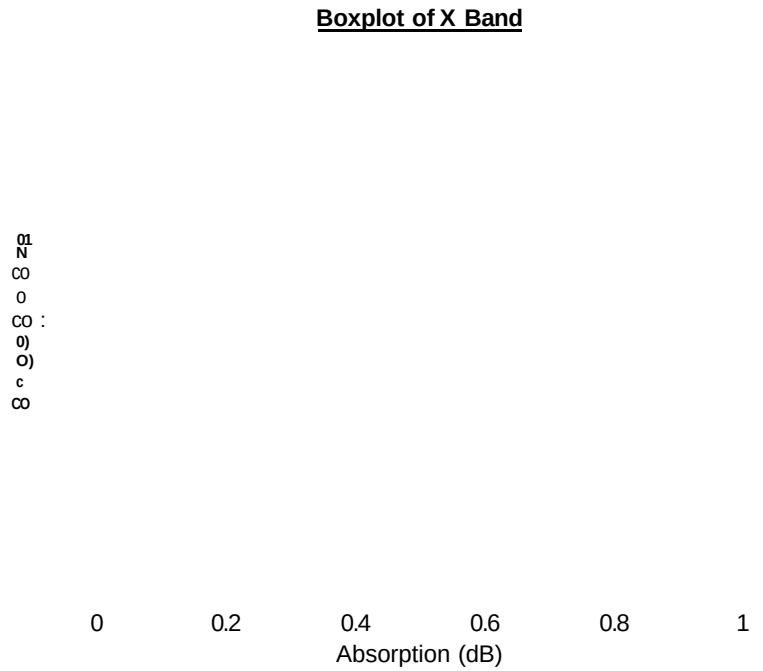

Figure 4.4 Distribution of Post-Processed X-Band Absorption Performance Data for Different Slot Sizes

The medium slot size (2), shows a wider IQR, spanning from 0.5996 dB to 0.8487 dB, indicating higher variability compared to the big slot size. The median absorption value of 0.7390 dB signifies good absorption performance, although it is lower than the big slot size. The broader range between the maximum (0.9975 dB) and minimum (0.2662 dB) values suggests that while effective, the medium slot size exhibits considerable variability, making it less consistent than the big slot size.

The small slot size (1) displays the widest IQR, ranging from 0.4045 dB to 0.7057 dB, which signifies the highest variability among the three slot sizes. With a median absorption value of 0.6098 dB, the small slot size exhibits the lowest absorption capability. Furthermore, the range extends from 0.0000 dB to 0.8459 dB, indicating significant variability and inconsistent absorption performance compared to the big and medium slot sizes.

Table 4.4
Statistical Summary of Boxplot Analysis For X-Band Absorption Data by Slot Size

Single-Slot Size	75^{th} Percentile (Upper Quart)	Median	25^{th} percentile (Lower Quart)	Max	Min	Number of Data Points
1 (Small)	0.7057	0.6098	0.4045	0.8459	0.000	194
2 (Medium)	0.8487	0.7390	0.5996	0.9975	0.2662	198
3 (Big)	0.9757	0.9201	0.7780	1.0000	0.5165	201

The analysis suggests that the big slot size is the most suitable choice for X-Band applications, offering high and consistent absorption performance with minimal variability. The medium slot size, while demonstrating good absorption capability, is less consistent due to its higher variability and may be appropriate for applications where a balance between performance and variability is acceptable. In contrast, the small slot size is the least effective, with the lowest median value and the highest variability, making it less favourable for practical applications without further refinement or redesign.

In conclusion, the big slot size is recommended for applications requiring stable and reliable absorption in the X-band. The medium slot size can be considered for scenarios where its absorption performance is sufficient, and variability can be tolerated. However, the small slot size requires further evaluation and optimization to enhance its performance and reduce variability. This analysis provides valuable insights into the absorption characteristics of different slot sizes in the X-Band, aiding in the informed selection and optimization of microwave absorbers for specific use cases.

4.3 Regression Analysis Across Frequency Bands

Regression analysis is a core statistical method used to model and analyse the relationship between a dependent variable and one or more independent variables. In this study, two types of regression models were employed: Linear regression, which presumes a straight-line correlation among variables and Artificial Neural Network (ANN) regression, a nonlinear modelling technique designed to identify intricate and nonlinear patterns within the data.

The objective of this analysis is to evaluate and compare the predictive performance of these two methods in modelling the relationship between the absorption performance (dependent variable) and the corresponding input features. By examining both linear and non-linear models, this study aims to identify which approach yields the most accurate and robust predictions across the multiband frequency dataset.

In this study, linear and ANN regression models were evaluated under two different analytical perspectives. Specifically, linear regression was applied using a frequency band-based analysis to examine the effect of slot size on absorption performance, while ANN Regression was applied using a slot size-based analysis to evaluate the influence of frequency band on absorption behaviour. This dual approach enables a comprehensive comparison of regression methods in capturing both linear and nonlinear patterns in the data. The most suitable regression method is determined based on performance metrics including Means Squared Error (MSE), coefficient of determination (R^2) and residual analysis across both perspectives.

4.3.1 Linear Regression-Based Analysis

Linear regression is a fundamental statistical technique used to model the relationship between a dependent variable and one or more independent variables. In the context of this research, linear regression was applied to examine the relationship between frequency and the normalized absorption performance using pre-processed data. The following subsections present the regression results for each frequency band.

4.3.1.1 L-Band

Figure 4.5 illustrates the linear regression analysis of the normalized absorption performance the L band frequency range (1-2 GHz). Although the regression line exhibits a positive slope, the data points are widely scattered around the fitted line, indicating a weak linear relationship between frequency and absorption performance. This visual observation suggests that frequency alone is insufficient to describe the absorption behaviour in the L-band using a linear model.

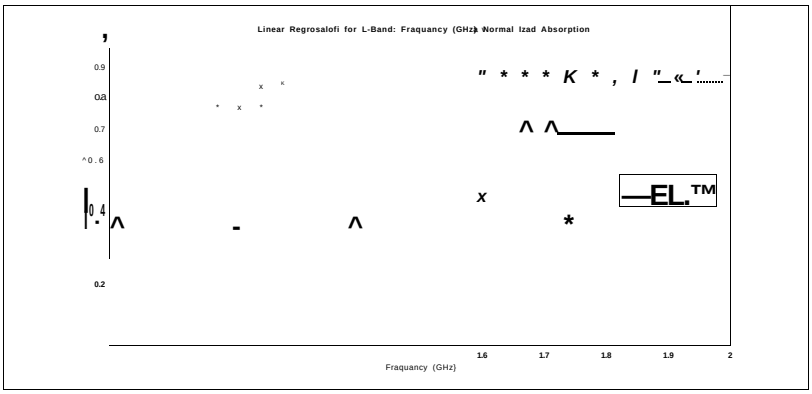

Figure 4.5 Linear Regression Analysis of Normalized Absorption within the L-Band Frequency Range

This observation is quantitatively confirmed by the statistical results summarized in Table 4.5. The regression model yields a low coefficient of determination ($R^2 = 0.0504$), indicating that only 5.04% of the variation in absorption performance is explained by frequency. In addition, the RMSE value of 0.319 reflects a relatively high prediction error for the normalized dataset. Although the model is statistically significant with a p-value of 0.0481, the low R^2 value demonstrates that statistical significance does not correspond to strong predictive capability in this case.

The poor agreement between the regression line and the experimental data highlights the limitation of linear regression for modelling L-band absorption performance, which is influenced by multiple interacting factors such as slot size, absorber geometry and material properties. Consequently, both the visual evidence in Figure 4.5 and the statistical indicators in Table 4.5 confirm that linear regression is inadequate for accurate L-band absorber prediction. This limitation motivates the use of nonlinear modelling approaches, such as artificial neural networks which are better suited to capturing the complex relationships present in the data.

Table 4.5
Summary of Linear Regression Results for L-Band Absorption Data

Metric	Value
Linear Equation	0.2297 + 0.27098x
R-squared (R^2)	0.0504
RMSE	0.319
Number of samples	78
p-value (model)	0.0481

4.3.1.2 S-Band

Figure 4.6 presents the linear regression analysis of the normalized absorption performance within the S band frequency range (2-4 GHz). The fitted regression line shows a negative slope, indicating a general decreasing trend in the normalized absorption values with increasing frequency. However, the data points remain widely scattered around the regression line, suggesting that the linear relationship between frequency and absorption performance is relatively weak. The scattered distribution of data points suggests that absorption performance in the S-band is influenced by multiple interacting parameters, limiting the predictive capability of a simple linear regression model.

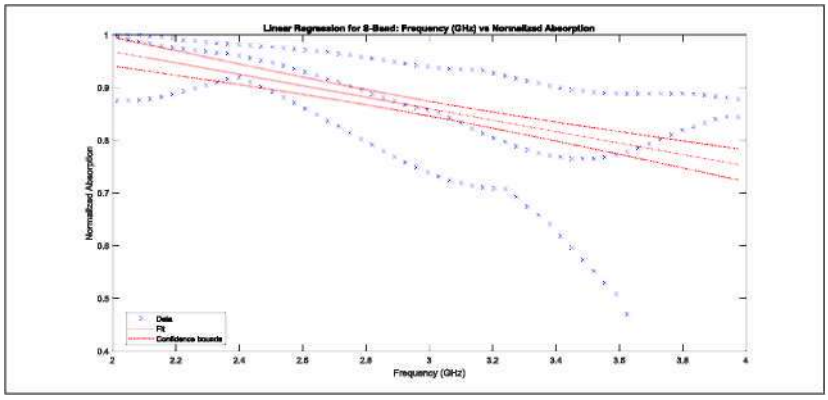

Figure 4.6 Linear Regression Analysis of Normalized Absorption within the S-Band Frequency Range

The statistical results summarized in Table 4.6 support this observation. The regression model achieved an R^2 value of 0.313, indicating that approximately 31.3% of the variation in normalized absorption performance is explained by frequency. While this represents an improvement compared to the L-band case, it still reflects a modest explanatory capability. The RMSE of 0.0896 further indicates moderate prediction accuracy, confirming that substantial variability remains unaccounted for by the linear model. The regression equation obtained for the S-band dataset is given in Table 4.6. Although the model is statistically significant ($p = 1.22 \times 10^{-14}$), the combination of the modest R^2 value and visible data scatter in Figure 4.6 demonstrates the limitation of linear regression for accurately modelling S-band absorption performance. These findings highlight the need for nonlinear modelling approaches, such as artificial neural

networks which are better suited to capturing the complex and multivariate relationships present in the absorber data.

Table 4.6
Summary of Linear Regression Results for S-Band Absorption Data

Metric	**Value**
Linear Equation	1.1853 -0.10844x
R-squared (R^2)	0.313
RMSE	0.0896
Number of samples	161
p-value (model)	1.22 xlO"^{14}

4.3.1.3 C-Band

Figure 4.7 illustrate the linear regression analysis of the normalized absorption performance within the C band frequency range (4-8 GHz). The fitted regression line shows a negative slope; however, the data points are widely dispersed around the regression line, indicating a weak relationship between frequency and absorption performance.

Figure 4.7 Linear Regression Analysis of Normalized Absorption within the C-Band Frequency Range

This observation is quantitatively supported by the statistical results summarized in Table 4.7. The regression model achieved a low coefficient of determination (R^2 = 0.116), indicating that only 11.6% of the variation in normalized

absorption performance is explained by frequency. In addition, the RMSE value of 0.200 reflects a moderate prediction error, confirming that a substantial portion of the variability remains unaccounted for by the linear model. Although the regression is statistically significant with a p-value of 3.33×10^{-10}, the low R^2 value demonstrates that statistical significance does not equate to strong predictive capability. The weak linear relationship observed in both Figure 4.7 and Table 4.7 suggests that absorption behaviour in the C-band is governed by multiple interacting factors beyond frequency alone. These include slot size variation, absorber geometry, and frequency-dependent electromagnetic interactions, which introduce nonlinear effects into the absorption response. Consequently, both the visual evidence and statistical metrics confirm the limitations of linear regression for C-band absorption prediction, thereby motivating the application of nonlinear modelling techniques such as artificial neural networks.

Table 4.7
Summary of Linear Regression Results for C-Band Absorption Data

Metric	**Value**
Linear Equation	y =1.0566-0.0638x
R-squared (R^2)	0.116
RMSE	0.200
Number of samples	323
p-value (model)	3.33×10^{-10}

4.3.1.4 X-Band

Figure 4.8 presents the linear regression analysis of the normalized absorption performance within the X-band frequency range (8-12 GHz). Although the fitted regression line exhibits a negative slope, the absorption data points are widely scattered around the regression line, indicating a weak linear relationship between frequency and absorption performance.

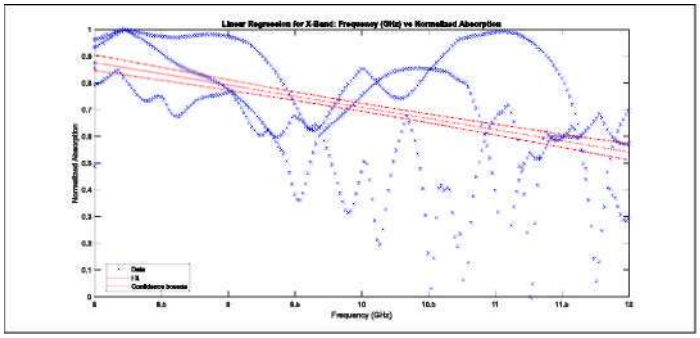

Figure 4.8 Linear Regression Analysis of Normalized Absorption within the X-Band Frequency Range

This observation is supported by the statistical results summarized in Table 4.8. The regression model achieves an R^2 value of 0.213, indicating that only 21.3% of the variation in normalized absorption performance is explained by frequency. In addition, the RMSE value of 0.186 reflects a moderate prediction error, confirming that a substantial portion of the absorption variability is not captured by the linear model. Although the regression is statistically significant ($p = 1.22 \times 10^{-32}$), the relatively low R^2 value demonstrates that statistical significance does not necessarily correspond to strong predictive capability. The weak linear relationship observed in both Figure 4.8 and Table 4.8 suggests that X-band absorption behaviour is influenced by multiple interacting factors beyond frequency alone. At higher frequency ranges, absorption performance becomes increasingly sensitive to slot size variation, geometric resonances, and frequency-dependent electromagnetic interactions, resulting in nonlinear absorption characteristics. Consequently, both the visual evidence and statistical indicators confirm the limitation of linear regression for X-band absorption prediction.

Table 4.8
Summary of Linear Regression Results for X-Band Absorption Data

Metric	**Value**
Linear Equation	y= 1.5434 -0.0835x
R-squared	0.213
RMSE	0.186
Number of samples	594
p-value (model)	1.22 xlO"^{32}

4.3.2 ANN-Based Regression Analysis

To complement the frequency band-based regression analysis presented in Section 4.3.1, the ANN-based regression analysis is further examined by grouping the data according to slot size. The earlier analysis demonstrated that linear regression provides limited predictive capability when absorption data from different slot sizes are combined, indicating that frequency alone is insufficient to describe the absorption behaviour. Since slot size represents a key geometric parameter that strongly influences absorption performance through nonlinear and geometry-dependent effects, grouping the ANN regression by slot size enables these effects to be isolated more clearly. This approach allows the nonlinear modelling capability of ANN to be evaluated more effectively while retaining frequency as an input variable across all bands.

The artificial Neural Network (ANN) models used in this study were developed using MATLAB's 'patternnet' function with one input node, one output node, and a three-hidden-layer architecture. The training algorithm was selected based on the best predictive performance for each slot size category. Depending on the case, one of the following algorithms was used: Levenberg-Marquardt (trainlm), Resilient backpropagation (trainrp) or Scaled Conjugate Gradient (trainscg). The performance function was set to Mean Squared Error (MSE) for all models.

Data division was performed randomly using 'dividerand' method with 70% of the dataset allocated for training, 15% for validation and 15% for testing. The specific neuron configurations, training functions and performance metrics for each slot size category are presented in Sections 4.3.2.1 to 4.3.2.3.

4.3.2.1 Small Slot Size (L, S, C and X Band)

For small slot size category, a total of 388 absorption performance data points were used after data pre-processing, comprising L-band (29), S-band (47), C-band (111) and X-band (201). These cleaned and normalized data points formed the basis for the ANN regression model. The optimal ANN configuration for this dataset employed a three hidden layer architecture with 38, 34 and 27 neurons, respectively. Among the training algorithms evaluated, the Levenberg-Marquardt algorithm (trainlm) achieved the best predictive performance for the small slot size category.

The artificial Neural Network (ANN) demonstrated stable and well-converged learning behaviour. As shown in Figure 4.9, the training process terminated after 47 epochs, indicating convergence of the learning process. The optimal validation performance was achieved at epoch 46, where the lowest validation mean squared error (MSE) of 1.6199 was recorded (Figure 4.10). The training continued for one additional epoch before termination, reflecting stable learning behaviour without signs of overfitting. The final gradient value of 2.5562 indicates that the error surface was sufficiently minimized during training. The absence of validation failures (validation checks =0) confirms that the validation-based early-stopping criterion implemented in MATLAB was not triggered. In this study, early stopping is governed by a validation-based mechanism in which training is terminated if the validation error fails to improve for six consecutive epochs; since no such failures occurred, the training process was allowed to proceed until convergence.

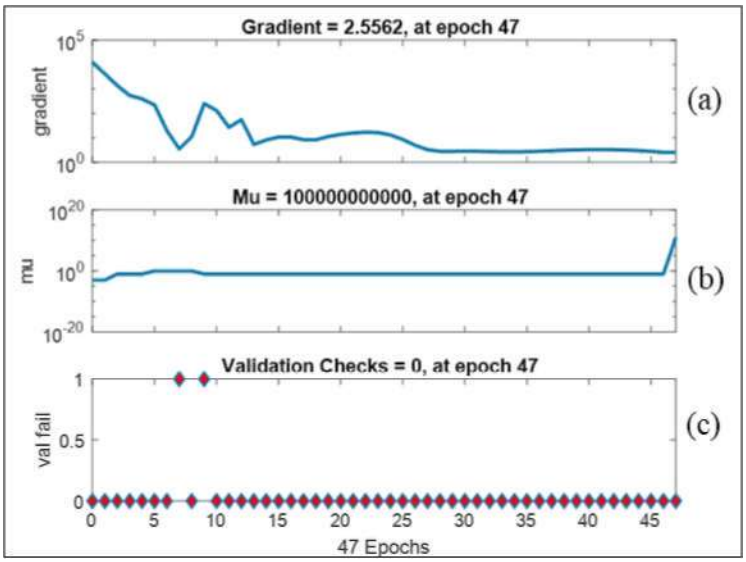

Figure 4.9 ANN Training Convergence Characteristics for the Selected Model: (a) Gradient Variation with epochs; (b) Adaptive Learning Parameter (mu) Versus epochs, and (c) Validation Checks Indicating Best Validation Performance at epoch 47

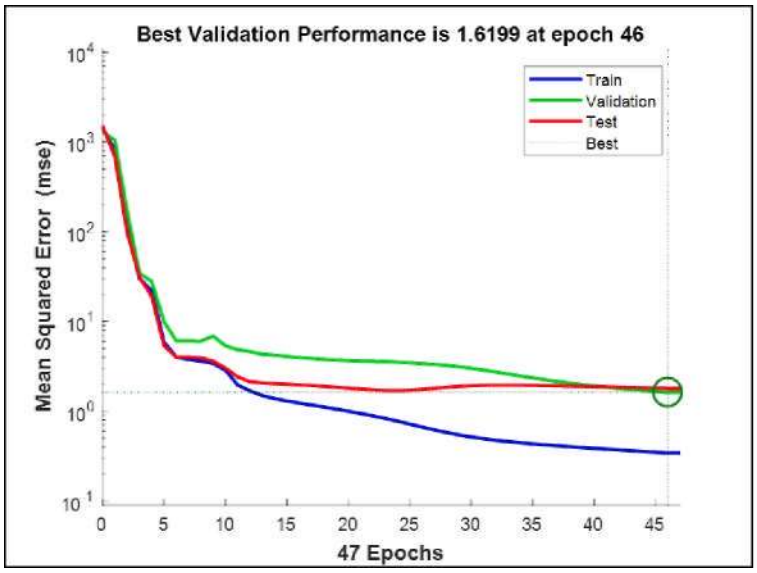

Figure 4.10 Best Validation Performance of the ANN Model showing Mean Squared Error (MSE) Versus epochs For the Training, Validation, and Testing Datasets. The Mnimum Validation MSE of 1.6199 Was Achieved at epoch 46, while the Training Process Terminated After 47 epochs

The regression plots in Figure 4.11 show excellent agreement between predicted outputs and the target values across all dataset partitions. In the regression plots, 'Y' represents the ANN-predicted output and 'T' denotes the target (actual) value. The line Y=T indicates the ideal case of perfect prediction. The correlation coefficients (R-Values) were 0.998 for training, 0.993 for validation, 0.991 for testing and 0.996 overall dataset. The close alignment of the predicted outputs with the target values across the training, validation, testing and overall datasets demonstrates the strong learning capability and generalization performance of the ANN model. These consistently high R-values confirm that the ANN model effectively captured the nonlinear relationship between frequency and absorption performance across the 1-12 GHz range.

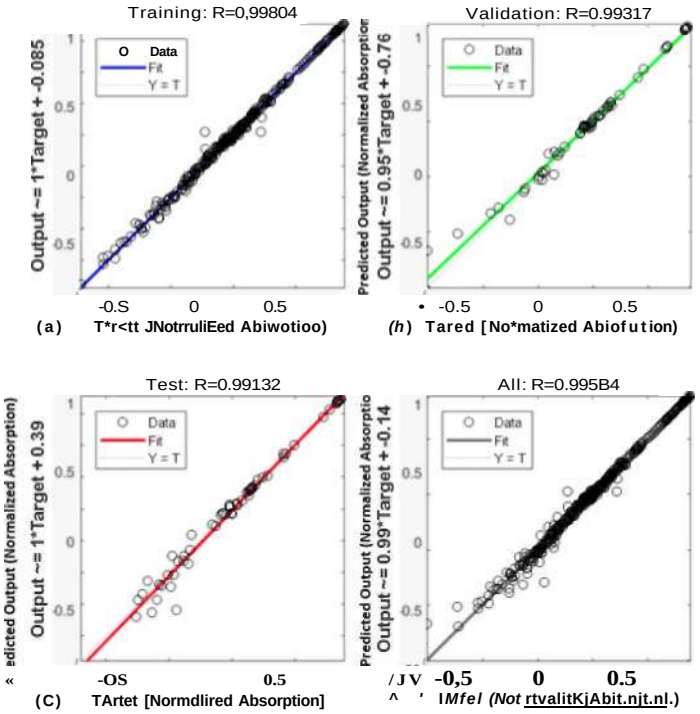

Figure 4.11 Regression Plots of Predicted Output Versus Target Values for the ANN Model Corresponding to The Small Slot Size: (a) Training, (b) Validation, (c) Testing, and (d) Overall Datasets. The Consistently high R-values Across All Datasets Indicate Excellent Predictive Accuracy and Strong Generalization Performance of the Trained ANN Model

Additional validation is presented in Figure 4.12, where the predicted absorption curve closely aligns with the actual measured data indicating strong generalization capability. However, as shown in Figure 4.13, minor discrepancies were observed particularly at certain frequency peaks. These deviations may be attributed to the inherent complexity of absorption behaviour or slight variations in the training data. Despite these small residuals, the overall prediction accuracy remains high demonstrating the robustness and reliability of the ANN model.

A summary of the ANN model's performance metrics for the small slot size is provided in Table 4.9. The consistently high R-values across the training, validation, testing and overall datasets confirm the strong predictive accuracy and generalization capability of the ANN model. In particular, the low validation MSE and near unity output-target relationship indicate that the model effectively captured the nonlinear absorption behaviour across the 1-12 GHz frequency range.

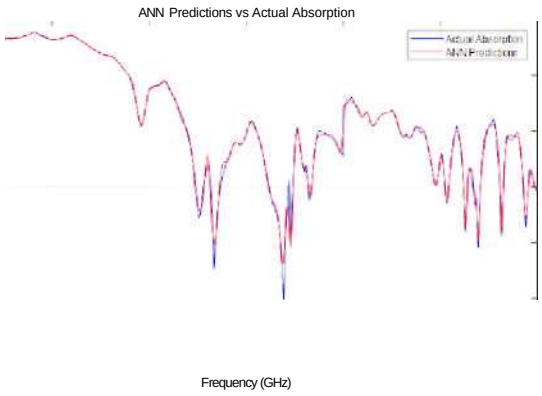

Figure 4.12 Comparison of ANN-Predicted and Actual Absorption Performance for Small Slot Size.

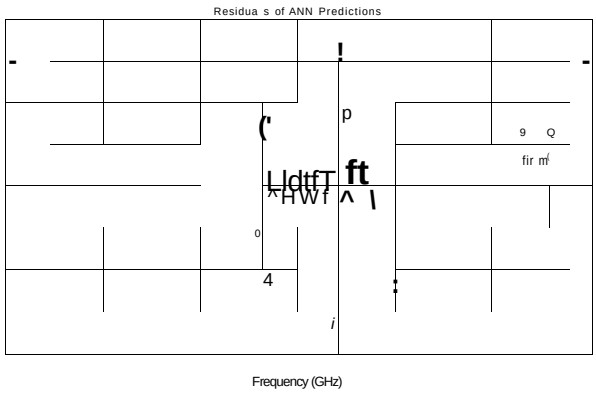

Figure 4.13 Residual Plot of ANN Model Predictions for Small Slot Size.

Table 4.9
Performance Summary of ANN Regression Model for Small Slot Size

Metric	**Training**	**Validation**	**Testing**	**Overall**
R-value	0.99804	0.99317	0.99132	0.99548
Mean Squared Error (MSE)	-	1.6199 (best at epoch 46)	-	-
Output Equation	Output = 1 x Target - 0.085	-	-	Output = 0.99 x Target - 0.14
Epoch Reached	47	47	47	47

*The best validation MSE of 1.6199 was recorded at epoch 46 with the training process successfully converging and stopping at epoch 47 based on early stopping criteria (maximum of 6 validation failures).

4.3.2.2 Medium Slot Size (L, S, C and X Band)

For Medium slot size category, a total of 380 absorption performance data points were used after data pre-processing, comprising L-band (25), S-band (57), C-band (100) and X-band (198). These cleaned and normalized data were used as input to the ANN regression model. The optimal ANN architecture for this dataset employed a three hidden layer configuration with 22, 34 and 29 neurons, respectively. Among the training algorithms evaluated, the Resilient Backpropagation algorithm (trainrp) achieved the best predictive performance for the medium slot size category.

The Artificial Neural Network (ANN) training process for the medium slot size category terminated after 6 epochs due to early stopping triggered by six consecutive validation failures, as shown in Figure 4.14. The final gradient of 0.97234 indicates that the network parameters were updated rapidly during the initial training stages. The minimum validation MSE of 0.0648 occurred during the initial training stage, after which no further improvement was observed, leading to early stopping (Figure 4.15). This behaviour indicates that the ANN reached its optimal generalization capability quickly and that additional training iterations did not enhance performance. Overall, the results suggests that the absorption behaviour for the medium slot size exhibits a relatively smooth and well-conditioned nonlinear relationship that can be captured effectively with a limited number of training iterations.

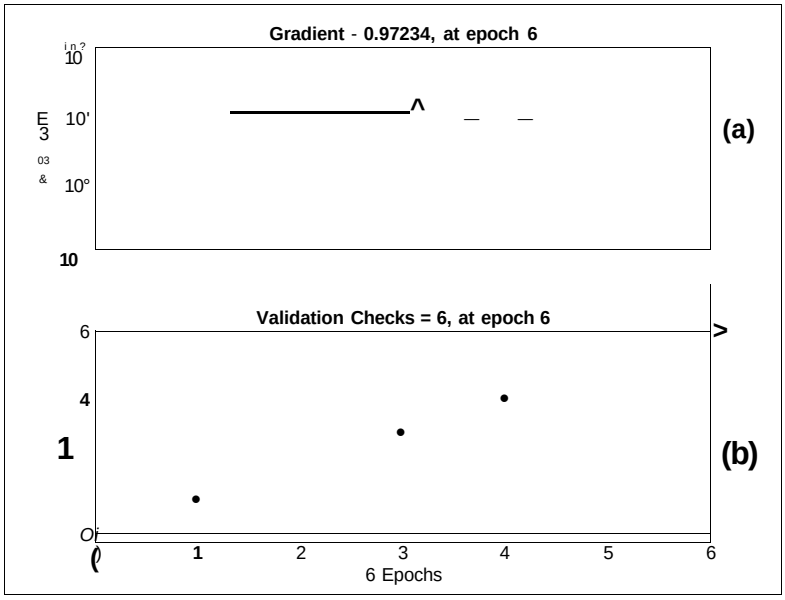

Figure 4.14 ANN Training State For The Medium Slot Size Model: (a) Gradient Variation with Epochs, and (b) Validation Checks Indicating Early Stopping Triggered After Six Consecutive Validation Failures at epoch 6

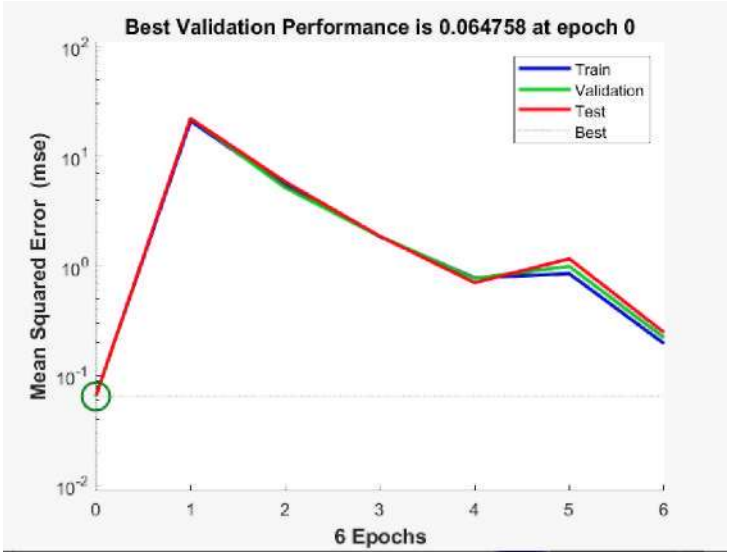

Figure 4.15 Best Validation Performance of the ANN Model for The Medium Slot Size, Showing Mean Squared Error (MSE) Versus Epochs. The Lowest Validation MSE Of 0.0648 Was Observed During the Initial Stage of Training, After Which No Further Improvement in Validation Performance Was Achieved

The regression plots in Figure 4.16 demonstrate excellent agreement between predicted and actual values across all dataset partitions. The correlation coefficients (R-values) were 0.99413 for training, 0.99565 for validation, 0.99474 for testing and 0.99431 overall. These consistently high R-values confirm that the ANN model

successfully captured the nonlinear relationship between frequency and absorption performance across the 1-12 GHz range and generalizes well across unseen data.

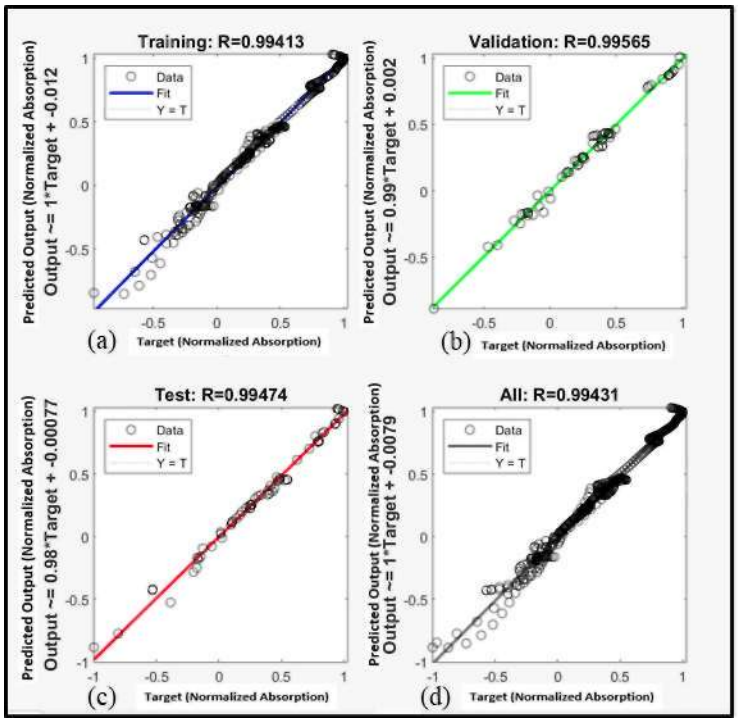

Figure 4.16 Regression Plots of Predicted Output Versus Target Values For the ANN Model Corresponding to the Medium Slot Size: (a) Training, (b) Validation, (c) Testing, and (d) Overall Datasets. All values Are Presented in Normalized Absorption Form. The Consistently High R-values Demonstrate Excellent Predictive Accuracy and Generalization Performance of the ANN Model

Additional validation of the ANN model is illustrated in Figure 4.17, where the predicted absorption curve (red dashed line) closely aligns with the actual measured data (blue solid line) demonstrating strong generalization capability across the 1-12 GHz frequency range. The corresponding residual plot in Figure 4.18 further confirms the model's performance. Although minor discrepancies were observed at certain frequency peaks (particularly above 8GHz), these residuals generally remain within an acceptable range. Such deviations are likely due to the inherent complexity of absorption behaviour or subtle irregularities in the training data.

Despite these localized differences, the overall prediction accuracy remains high, highlighting the robustness and reliability of the ANN model in predicting the absorption characteristics of microwave absorbers for the medium slot size category.

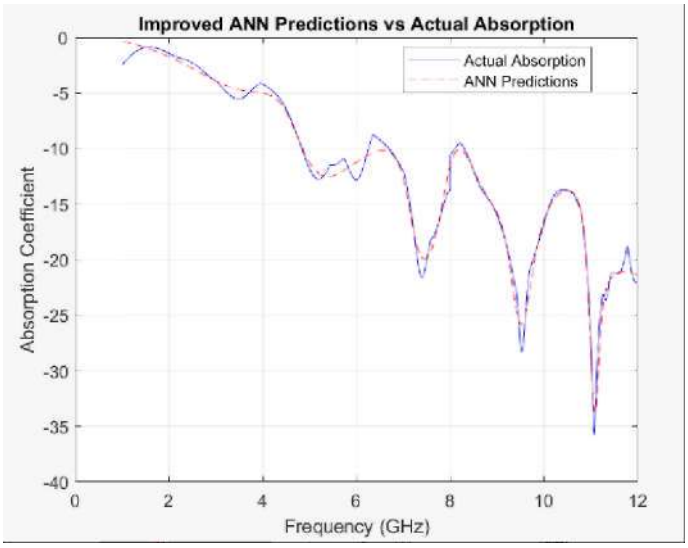

Figure 4.17 Comparison of ANN-Predicted and Actual Absorption Performance for Medium Slot Size

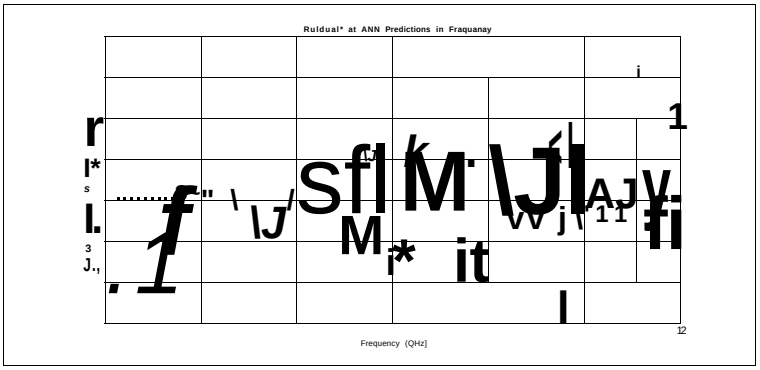

Figure 4.18 Residual Plot of ANN Model Predictions for Medium Slot Size

Table 4.10 provides a concise summary of the ANN regression performance for the medium slot size category. The consistently high R-values across all dataset partitions confirm the strong agreement between predicted and target normalized absorption values observed in the regression plots. The low validation MSE and output equations close to the ideal unity relationship further indicate that the ANN model achieved accurate and stable predictions, reinforcing the robustness of the proposed model.

Table 4.10
Performance Summary of ANN Regression Model for Medium Slot Size

Metric	Training	Validation	Testing	Overall
R-value	0.99413	0.99565	0.99474	0.99431
Mean Squared Error (MSE)	-	0.0648 (best at epoch 0)	-	-
Output Equation	Output = 1 x Target - 0.012	-	-	Output = 1 x Target - 0.0079
Epoch Reached	6	6	6	6

*The lowest validation MSE was observed during the early stage of training, with training terminated at epoch 6 based on the early stopping criteria.

4.3.2.3 Big Slot Size (L,S,CandX Band)

For Big slot size category, a total of 388 absorption performance data points were used after data pre-processing, comprising L-band (24), S-band (57), C-band (112) and X-band (195). These cleaned and normalized data points served as inputto the ANN regression model. The optimal ANN configuration for this dataset employed a three hidden layer architecture with 22, 34 and 30 neurons, respectively. The model achieved its best predictive performance using the Resilient Backpropagation (trainrp) training algorithm.

The Artificial Neural Network (ANN) demonstrated strong learning capability in predicting the absorption performance of the designed microwave absorber. As shown in Figure 4.19, the training process was terminated after 6 epochs due to early stopping triggered by six consecutive validation failures, with a final gradient of 5.549. The lowest validation means squared error (MSE) of 0.0544 was observed at early stage of training (Figure 4.20), after which no further improvement in validation performance was achieved. This behaviour indicates that the ANN reached its optimal generalization capability rapidly, suggesting that the absorption characteristics for the big slot size are governed by a smooth and well-conditioned nonlinear relationship that can be effectively captured with limited training iterations.

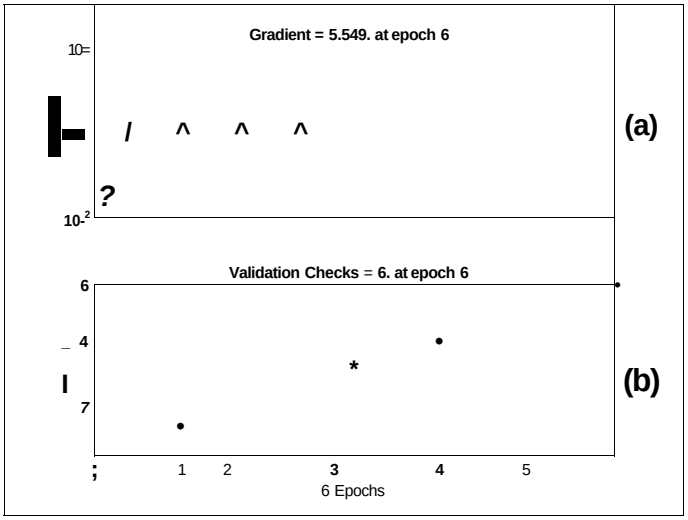

Figure 4.19 ANN Training State For the Big Slot Size Model: (a) Gradient Variation with Epochs, and (b) Validation Checks Indicating Early Stopping Triggered After Six Consecutive Validation Failures at Epoch 6

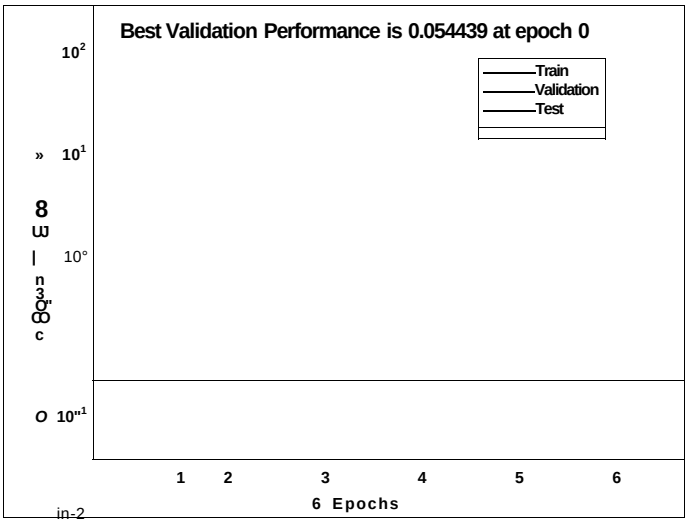

Figure 4.20 Best Validation Performance of the ANN Model for the Big Slot Size, Showing Mean Squared Error (MSE) Versus Epochs. The Lowest Validation MSE of 0.0544 Was Observed During the Early Stage of Training, After Which No Further Improvement Was Achieved

The regression plots in Figure 4.21 demonstrate excellent agreement between predicted and actual values across all dataset partitions. The correlation coefficients (R-values) were 0.99242 for training, 0.99180 for validation, 0.99047 for testing and 0.99197 overall. These consistently high R-values confirm that the ANN model successfully captured the nonlinear relationship between frequency and absorption performance across the 1-12 GHz range and generalizes well across unseen data.

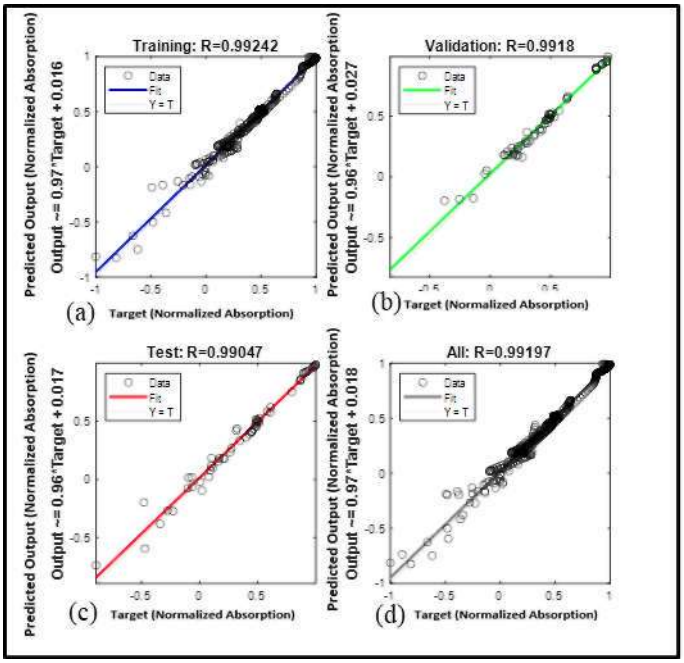

Figure 4.21 Regression Plots of Predicted Output Versus Target Values For the ANN Model Corresponding To The Big Slot Size: (a) Training, (b) Validation, (c) Testing, and (d) Overall Datasets. All Values Are Presented in Normalized Absorption Form. The Consistently High R-values Indicate Strong Predictive Accuracy and Generalization Performance of the ANN Model

Additional validation of the ANN model is illustrated in Figure 4.22, where the predicted absorption curve (red dashed line) closely follows the actual measured data (blue solid line) showing strong generalization capability across the 1-12 GHz frequency range. The corresponding residual plot in Figure 4.23 further confirms the model's performance. Although some discrepancies were observed at specific frequency peaks (particularly above 8GHz), most residuals remain within a tolerable range. These deviations may be attributed to the complex nature of absorption behaviour or slight variations in the training data.

Despite these localized errors, the overall prediction accuracy remains high, highlighting the robustness and reliability of the ANN model in predicting the absorption characteristics of microwave absorbers for the big slot size category.

Table 4.11 provides a concise summary of the ANN regression performance for the big slot size category. The consistently high R-value across all dataset partitions confirm the strong agreement between predicted and target normalized absorption values observed in the regression plots. The low validation MSE and output equations close to a unity relationship further demonstrate the robustness and reliability of the ANN model for predicting absorption performance in the big slot size configuration.

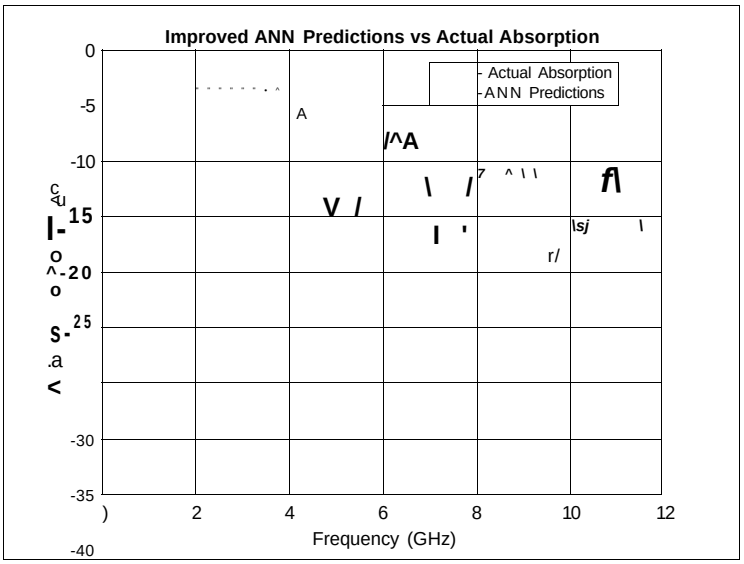

Figure 4.22 (Comparison of ANN-Predicted and Actual Absorption Performance for Big Slot Size

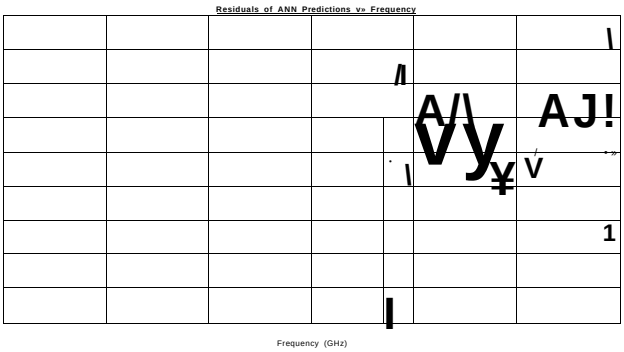

Figure 4.23 Residual Plot of ANN Model Predictions for Big Slot Size

Table 4.11
Performance Summary of ANN Regression Model for Big Slot Size

Metric	Training	Validation	Testing	Overall
R-value	0.99242	0.99180	0.99047	0.99197
Mean Squared Error (MSE)	-	0.0544 (best at epoch 0)	-	-
Output Equation	Output = 0.97 x Target + 0.016	-	-	Output = 0.97 x Target + 0.018
Epoch Reached	6	6	6	6

**The lowest validation MSE was observed during the early stage of training, with training terminated at epoch 6 based on the early stopping criterion.*

4.3.3 Comparative Analysis Between Linear Regression and ANN Models

To evaluate the effectiveness of the proposed ANN model, a comparison was made between the performance of linear regression and ANN-based regression across all frequency bands. The linear regression results demonstrated weak predictive capability, as reflected by low R^2 values and higher RMSE across the L-, S-, C-, and X-band datasets, indicating that frequency alone is insufficient to describe the complex absorption behaviour of the microwave absorbers.

In contrast, the ANN models consistently achieved significantly higher correlation coefficients (R-values exceeding 0.99) and lower prediction errors, demonstrating superior learning and generalization capability. This performance improvement is attributed to the ANN's ability to capture nonlinear relationships arising from complex interactions between frequency, absorber geometry, and material characteristics.

The comparative results clearly indicate that while linear regression provides a basic trend analysis, it fails to adequately model the nonlinear absorption behaviour observed in the experimental data. The ANN-based approach therefore offers a more robust and accurate predictive framework for absorption performance modelling, supporting its selection as the primary modelling tool in this study. A summary comparison between linear regression and ANN-based regression performance is presented in Table 4.12.

Table 4.12
Comparison of Linear Regression and ANN Performance (Overall)

Model	**Typical R/R^2**	**RMSE**	**Capability**
Linear Regression	Low R^2 (<0.3)	High	Linear trend only
ANN Regression	$R>0.99$	Low	Nonlinear modelling

4.4 ANN-Based Classification Performance Across Frequency Bands

Artificial Neural Networks (ANN) were employed to model the nonlinear relationship between frequency and absorption performance for eco-friendly microwave absorbers. Using the ANN architecture, encoding scheme, and data

partitioning strategy described in Chapter 3, the classification performance of three training algorithms: Levenberg Marquardt (LM), Resilient Backpropagation (RBP) and Scaled-Conjugate Gradient (SCG) is evaluated across the L, S, C and X band frequency ranges. The ANN classification task aims to categorize absorber slot sizes into three classes: small, medium and big. The following subsections present a detailed analysis of the ANN classification performance for each frequency band.

4.4.1 ANN-Based Classification Results for L-Band

Following the preprocessing stage, the dataset for the L-band consisted of 78 data points, distributed into three single-slot size categories: small (24), medium (25), and big (29). The dataset was divided into training, validation, and testing subsets following the partitioning strategy described in Chapter 3. This section presents the classification performance of the ANN model for the L-band across different training algorithms.

4.4.1.1 Classification of L-band using the Levenberg-Marquardt (LM) Algorithm

Table 4.13 shows the classification accuracy and mean squared error (MSE) obtained using the Levenberg-Marquardt (LM) algorithm for different hidden neuron configurations in the L-band classification task. Overall, the LM algorithm demonstrates strong and consistent performance across the training, validation and testing datasets. Training accuracy ranges from 70% to 100%, while validation and testing accuracies vary between 81.8% and 100%, indicating reliable generalization behaviour.

The optimal configuration was achieved using five hidden neurons, which not only produced the highest classification accuracy (100% for training, validation and testing) but also recorded the lowest mean squared error (MSE) value of 0.0209. This result confirms the suitability of the LM algorithm for modelling the nonlinear relationship between frequency-dependent absorption characteristics and slot size categories in the L-band.

Table 4.13
Classification Accuracy and MSE Values for the LM Algorithm (L-Band)

Hidden Neuron	Accuracy (%)			MSE Value
	Training	Validation	Testing	
1	70	90.9	81.8	0.1080
2	88	90.9	100	0.1084
3	88	81.8	90.9	0.1364
4	86	100	81.8	0.0752
*5	100	100	100	0.0209
6	82	90.9	81.8	0.0744
7	86	100	90.9	0.1369
8	98.1	100	100	0.0565
9	84	81.8	90.9	0.0506
10	88	90.9	100	0.2402

*Best hidden neuron in LM

To systematically evaluate the classification performance based on slot size, confusion matrix analysis is performed for the optimal LM configuration, as shown in Figure 4.24. The confusion matrices for the training, validation, testing and overall datasets demonstrate that all samples are correctly classified into their respective slot size categories (small, medium and big), with no misclassification observed. This indicates excellent class separability and highlights the robustness of the LM based ANN classifier for L-band absorption data.

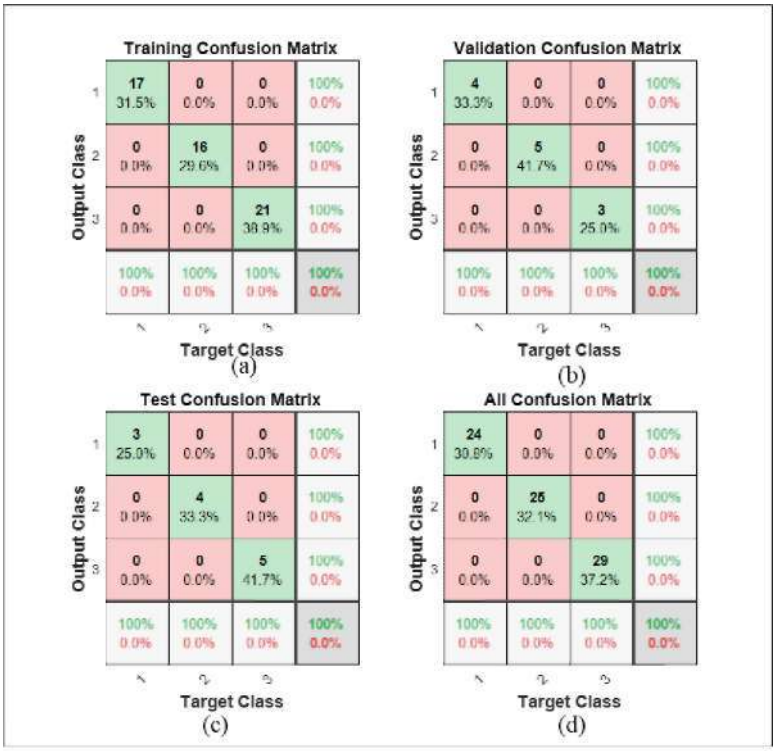

Figure 4.24 Confusion Matrices for L-band Slot Size Classification Using the LM Algorithm: (a) Training, (b) Validation, (c) Testing, (d) Overall

Based on the confusion matrix results, class-specific performance metrics are computed and summarized in Table 4.14. The LM classifier achieves 100% precision, recall and F1-score for all three slot size classes, indicating balanced and unbiased classification performance across categories.

Table 4.14
Class-Wise Classification Performance Metrics for L-Band using the LM Algorithm (5 Hidden Neurons

Slot Size	**Precision (%)**	**Recall (%)**	**F1-Score (%)**
Small	100	100	100
Medium	100	100	100
Big	100	100	100

While Table 4.14 presents the class-wise classification behaviour, the overall performance of the LM-based classifier is summarized in Table 4.15. The model achieves 100% overall accuracy, sensitivity, specificity and precision, confirming its reliability and consistency for L-band slot size classification.

Table 4.15
Overall Classification Performance Metrics for L-Band using the LM Algorithm (5 Hidden Neurons)

Performance Metric	Percentage (%)
Accuracy	100
Sensitivity	100
Specificity	100
Precision	100

Note: Metrics are based on the best hidden neuron configuration (HN=5).

The training convergence behaviour of the LM-based ANN classifier is illustrated in Figure 4.25, which shows the training, validation and testing performance curves plotted against the number of epochs. The mean squared error decreases steadily during training and the validation curve closely follows the training trend, reaching the best validation performance at epoch 25. The absence of divergence between training and validation curves indicates stable learning behaviour and confirms that overfitting does not occur.

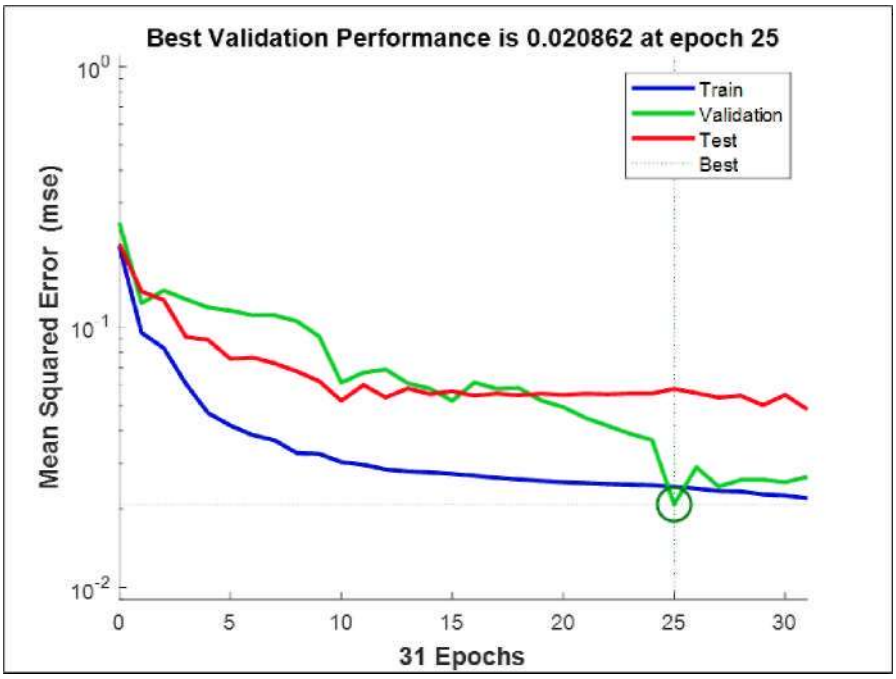

Figure 4.25 Training/ Validation/ Testing vs Epoch

Overall, the LM algorithm demonstrates excellent classification performance for the L-band dataset. The combined analysis of confusion matrices, class specific

performance metrics, and training convergence behaviour confirms that the LM-based ANN classifier provides an accurate, stable and well generalized solution for slot size classification in the L-band.

4.4.1.2 Classification of L-band using the Resilient Backpropagation (RBP) Algorithm

Table 4.16 shows the classification accuracy and mean squared error (MSE) obtained using the Resilient Backpropagation (RBP) algorithm for the L-band dataset across different hidden neuron configurations. Overall, the RBP-based ANN demonstrated reasonable classification capability across the training, validation, and testing datasets, although its performance was consistently lower than that achieved using the Levenberg Marquardt (LM) algorithm. Training accuracy ranged from 62.0% to 92.6%, while validation accuracy varied between 72.7% and 100%. Testing accuracy ranged from 72.7% to 91.7%, indicating moderate generalization capability.

The optimal RBP configuration was achieved using eight hidden neurons which produced the highest training accuracy (92.6%) and the lowest MSE value (0.0721). This configuration was therefore selected for detailed performance evaluation. Compared to LM, the RBP algorithm exhibited slightly higher error values and greater variability across datasets, reflecting its slower convergence characteristics and reduced sensitivity to second-order error information.

Table 4.16
Classification Accuracy and MSE Values for the RBP Algorithm (L-Band)

Hidden Neuron	**Accuracy (%)**			**MSE Value**
	Training	**Validation**	**Testing**	
1	62	100	81.8	0.0350
2	70	90.9	81.8	0.0765
3	86	90.9	72.7	0.0730
4	80	90.9	90.9	0.0953
5	82	90.9	81.8	0.0910
6	84	100	90.9	0.0955

Hidden Neuron	Accuracy (%)			MSE Value
	Training	Validation	Testing	
7	90	72.7	81.8	0.1670
*8	92.6	83.3	91.7	0.0721
9	82	82.8	90.9	0.1360
10	82	81.8	90.9	0.1281

*Best hidden neuron in RBP

Figure 4.26 illustrates the confusion matrices for L-band slot size classification using the RBP algorithm, covering the training, validation, testing and overall datasets. The confusion matrices provide a detailed view of the class-wise prediction behaviour for the three slot size categories (small, medium and big).

Figure 4.26 Confusion Matrices for L-band Slot Size Classification Using the RBP Algorithm: (a) Training, (b) Validation, (c) Testing, (d) Overall

Inspection of the confusion matrices shows that the big slot size class was consistently classified with high accuracy across all datasets. In contrast, most misclassifications occurred between the small and medium slot sizes, particularly in the validation and testing datasets. This indicates partial overlap in the absorption

characteristics of these two slot sizes within the L-band frequency range, which poses a greater challenge for the RBP learning mechanism.

To further quantify classification performance, Table 4.17 summarizes the precision, recall, and F1-score for each slot size based on the optimal configuration with eight hidden neurons. The results indicate excellent classification performance for the big slot size, while minor misclassifications between small and medium slot sizes slightly reduced the precision and recall values, reflecting overlapping absorption characteristics in the L-band.

Table 4.17
Class-Wise Classification Performance Metrics for L-Band using the RBP Algorithm (8 Hidden Neurons)

Slot Size	**Precision (%)**	**Recall (%)**	**F1-Score (%)**
Small	84.0	87.5	85.7
Medium	87.5	84	85.7
Big	100	100	100

An overall summary of classification performance is provided in Table 4.18, which reports the aggregate accuracy, sensitivity, specificity and precision values. The RBP-based ANN achieved an overall classification accuracy of 91.0%, with sensitivity of 90.5%, specificity of 95.6% and precision of 90.5%, confirming reliable but suboptimal classification compared to the LM-based model.

Table 4.18
Overall Classification Performance Metrics for L-Band using the RBP Algorithm (8 Hidden Neurons)

Performance Metric	**Percentage (%)**
Accuracy	91.0
Sensitivity	90.5
Specificity	95.6
Precision	90.5

Note: Metrics are based on the best hidden neuron configuration (HN=8).

The training convergence behaviour of the RBP-based ANN classifier is illustrated in Figure 4.27, which presents the training, validation, and testing mean squared error (MSE) curves plotted against the number of epochs. The MSE decreases steadily during the initial training phase, indicating effective learning of the classification patterns. As training progresses, the error reduction becomes more gradual and stabilizes toward later epochs. initial training phase, indicating effective learning of the classification patterns. As training progresses, the error reduction becomes more gradual and stabilizes toward later epochs. The validation curve generally follows the training trend without significant divergence, suggesting that the model maintains reasonable generalization capability and does not exhibit severe overfitting. However, small fluctuations are observed in the validation MSE near convergence, indicating less stable learning behaviour compared to the LM-based classifier, which achieved faster and smoother convergence. Overall, the convergence characteristics confirm that the RBP algorithm is capable of learning the L-band classification task, although with slower convergence and higher steady-state error relative to the LM algorithm.

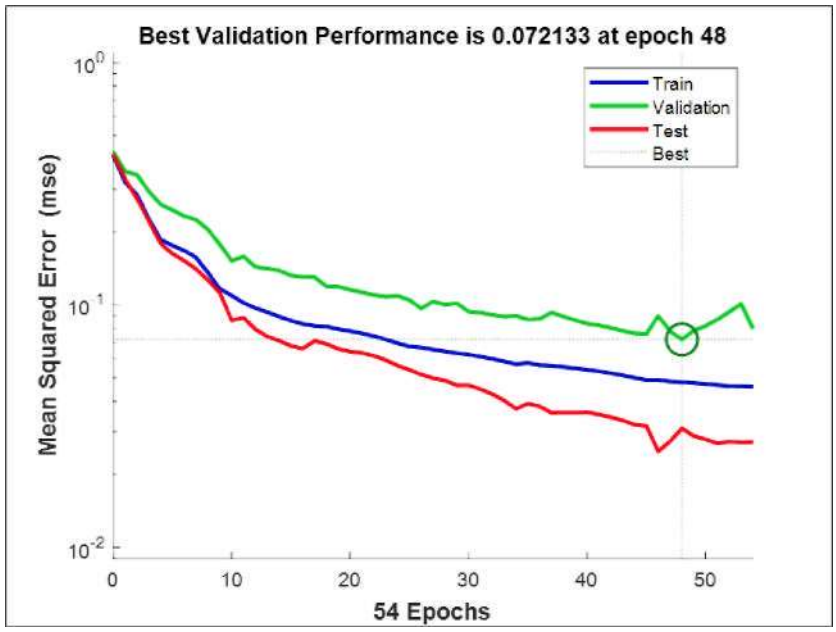

Figure 4.27 Training, Validation, and Testing Mean Squared Error (MSE) Versus Epochs for the RBP-based ANN Classifier (L-band)

In summary, the RBP algorithm demonstrates acceptable classification performance for L-band slot size identification, particularly for the big slot size category, which achieved perfect classification. However, increased misclassification

between the small and medium slot sizes and higher MSE values indicate that the RBP algorithm is less effective than the LM algorithm in modelling the nonlinear absorption behaviour present in the L-band dataset.

4.4.1.3 Classification of L-band Using the Scaled-Conjugate Gradient (SCG) Algorithm

Table 4.19 presents the classification accuracy and mean squared error (MSE) obtained using the Scaled-Conjugate Gradient (SCG) algorithm for the L-band dataset across different hidden neuron configurations. Overall, the SCG-based ANN demonstrated reasonable classification capability across the training, validation, and testing datasets. However, its performance was consistently lower than that achieved using the Levenberg Marquardt (LM) algorithm and Resilient Backpropagation (RBP) algorithms. Training accuracy ranged from 72.0% to 90.7%, while validation accuracy varied between 63.6% and 100%. Testing accuracy ranged from 72.7% to 90.9%, indicating moderate generalization capability.

Table 4.19
Classification Accuracy and MSE Values for SCG Algorithm (L-Band)

Hidden Neuron	**Accuracy (%)**			**MSE Value**
	Training	**Validation**	**Testing**	
1	72	81.8	81.8	0.1068
2	82	63.6	90.9	0.1274
3	86	90.9	72.7	0.0911
4	82	100	90.9	0.1260
5	72	90.9	81.8	0.0860
6	88	72.7	81.8	0.2212
7	82	81.8	72.7	0.1521
8	82	100	81.8	0.0769
9	88	100	81.8	0.1365
*10	90.7	100	83.3	0.1049

*Best hidden neuron in SCG

The optimal SCG configuration was achieved using ten hidden neurons, which produced the highest training accuracy (90.7%) together with an MSE value of 0.0721. This configuration was therefore selected for detailed performance evaluation. Compared to LM and RBP algorithms, the SCG algorithm exhibited higher error values and greater variability across datasets, reflecting its first-order optimization nature and slower convergence characteristics when modelling complex nonlinear relationships.

Figure 4.28 illustrates the confusion matrices for L-band slot size classification using the SCG algorithm, covering the training, validation, testing and overall datasets. The confusion matrices provide a detailed view of the class-wise prediction behaviour for the three slot size categories (small, medium and big).

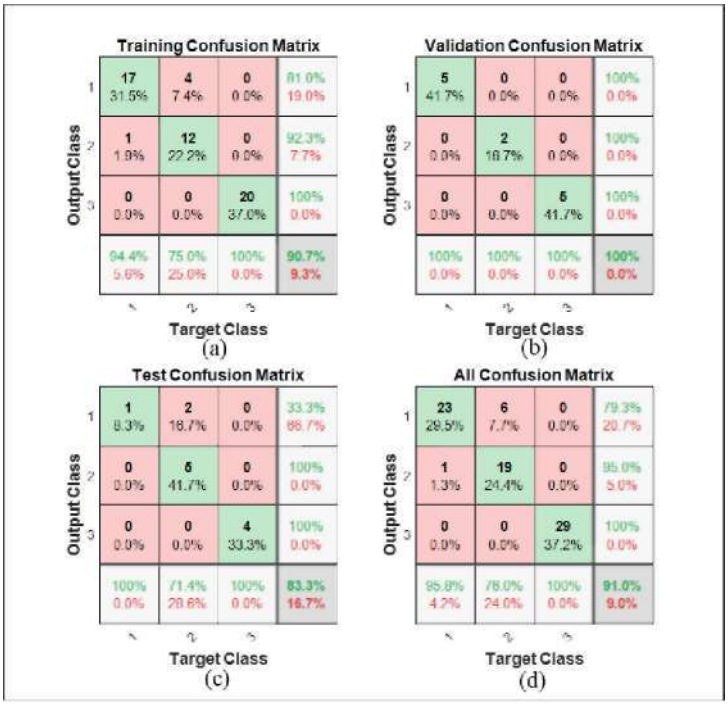

Figure 4.28 Confusion Matrices for L-band Slot Size Classification Using the SCG Algorithm: (a) Training, (b) Validation, (c) Testing, (d) Overall

Inspection of the confusion matrices shows that the big slot size class was consistently classified with perfect accuracy across all datasets. In contrast, most misclassifications occurred between the small and medium slot sizes, particularly in the validation and testing datasets. This behaviour suggests partial overlap in the absorption characteristics of these two slot sizes within the L-band frequency range, which poses a greater challenge for the SCG learning mechanism.

To further quantify classification performance, Table 4.20 summarizes the precision, recall, and F1-score for each slot size based on the optimal SCG configuration with ten hidden neurons. The results indicate excellent classification performance for the big slot size, while minor reductions in precision and recall are observed for the small and medium slot sizes due to mutual misclassification.

Table 4.20
Class-Wise Classification Performance Metrics for L-Band using the SCG Algorithm (10 Hidden Neurons)

Slot Size	**Precision (%)**	**Recall (%)**	**F1-Score (%)**
Small	79.3	95.8	86.8
Medium	95	76	84.4
Big	100	100	100

An overall summary of classification performance is provided in Table 4.21, which reports the aggregate accuracy, sensitivity, specificity and precision values. The SCG-based ANN achieved an overall classification accuracy of 91.0%, with sensitivity of 90.6%, specificity of 95.7% and precision of 91.4%, confirming reliable but suboptimal classification compared to the LM-based model. Although the SCG and RBP algorithms achieved comparable overall classification accuracy for the L-band dataset, the RBP algorithm demonstrated slightly more stable convergence behaviour and lower classification loss, while SCG exhibited marginally higher variability between the small and medium slot size classes. Consequently, both algorithms are effective, but LM remains the most reliable classifier for L-band slot size identification.

Table 4.21
Overall Classification Performance Metrics for L-Band using the SCG Algorithm (10 Hidden Neurons)

Performance Metric	**Percentage (%)**
Accuracy	91.0
Sensitivity	90.6
Specificity	95.7
Precision	91.4

Note: Metrics are based on the best hidden neuron configuration (HN=8).

The training convergence behaviour of the SCG-based ANN classifier is illustrated in Figure 4.29, which presents the training, validation, and testing mean squared error (MSE) curves plotted against the number of epochs. The MSE decreases gradually during the early epochs, indicating effective learning of the classification patterns. As training progresses, the error reduction becomes more gradual and stabilizes, reflecting the slower convergence behaviour typically associated with the SCG algorithm. The absence of strong divergence between training and validation curves suggests that severe overfitting did not occur, although convergence is less efficient compared to the LM-based model.

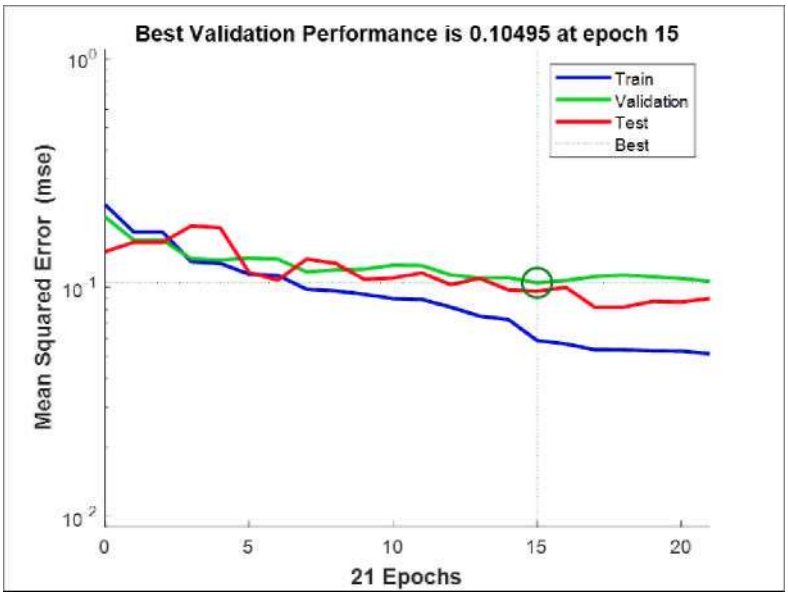

Figure 4.29 Training, Validation, and Testing Mean Squared Error (MSE) Versus Epochs For the SCG-based ANN Classifier (L-band)

In summary, the SCG algorithm demonstrates acceptable classification performance for L-band slot size identification, particularly for the big slot size category, which achieved perfect classification. However, increased misclassification between the small and medium slot sizes together with higher MSE values and slower convergence, indicate that the SCG algorithm is less effective than the LM and RBP algorithms in modelling the nonlinear absorption behaviour present in the L-band dataset.

4.4.1.4 Comparison of the MLP Training Algorithms for L-Band Classification

Table 4.22 summarizes the optimal configurations and overall classification performance of the three MLP training algorithms applied to L-band slot size classification. Among the evaluated algorithms, the Levenberg-Marquardt (LM) algorithm with five hidden neurons outperformed the others, achieving perfect classification accuracy across training, validation and testing datasets, as well as the lowest MSE value. This superior performance can be attributed to LM's efficient convergence and ability to model complex, nonlinear relationships in the dataset.

Table 4.22
Summary of Best Hidden Neuron Configurations for Each MLP Algorithm (L-Band)

Training Algorithm	**Hidden Neuron**	**Accuracy (%)**			**MSE Value**
		Training	**Validation**	**Testing**	
*Levenberg Marquardt (LM)	***5**	**100**	**100**	**100**	0.0209
Resilient Backpropagation (RB)	**8**	92.6	**83.8**	**91.7**	0.0721
Scaled-Conjugate Gradient (SCG)	**10**	90.7	**100**	83.3	0.1049

'Best hidden neuron

The Resilient Backpropagation (RBP) algorithm demonstrates strong performance but with slightly reduced accuracy and higher error compared to LM, reflecting minor misclassifications between slot size categories. In contrast, the Scaled-Conjugate Gradient (SCG) algorithm exhibited the lowest overall accuracy and highest MSE, indicating comparatively weaker generalization capability for the L-band dataset.

To further clarify class-wise behaviour, slot size-based classification performance for each algorithm is presented in Table 4.23, derived from the corresponding confusion matrices.

Table 4.23
Slot Size-Based Classification Performance (Recall) for L-Band using Different ANN Training Algorithms

Slot Size	LM (%)	RBP (%)	SCG (%)
Small	100	87.5	95.8
Medium	100	84	76
Big	100	100	100

Note: Slot-size-based performance is reported using recall (sensitivity), which quantifies the proportion of correctly classified samples for each slot size.

As shown in Table 4.23, all three ANN training algorithms achieved perfect classification performance for the big slot size category, showing that this class is well separated in the feature space. However, performance differences among algorithms are more evident for the small and medium slot sizes. The LM algorithm consistently achieved perfect recall across all slot sizes, demonstrating superior class discrimination capability. The RBP and SCG algorithms showed reduced recall for the small and medium slot sizes, suggesting partial overlap in their absorption characteristics within the L-band frequency range and highlighting the greater robustness of the LM-based classifier.

4.4.1.5 Comprehensive Performance Evaluation of the ANN Classifiers for L-Band

Table 4.24 and Figure 4.30 provide a comparative evaluation of the ANN classifiers based on overall accuracy, precision, sensitivity and specificity. The LM-based classifier achieved 100% across all performance metrics, confirming its robustness and reliability for L-band slot size classification.

Table 4.24
Performance Evaluation of MLP Algorithms for L-Band

Training Algorithm	Hidden Neuron	Accuracy (%)	Sensitivity (%)	Specificity (%)	Precision (%)
*Levenberg Marquardt (LM)	5	100	100	100	100
Resilient Backpropagation (RB)	8	91.0	90.5	95.6	90.5

Training Algorithm	Hidden Neuron	Accuracy (%)	Sensitivity (%)	Specificity (%)	Precision (%)
Scaled-Conjugate Gradient (SCG)	10	91.0	90.6	95.7	91.4

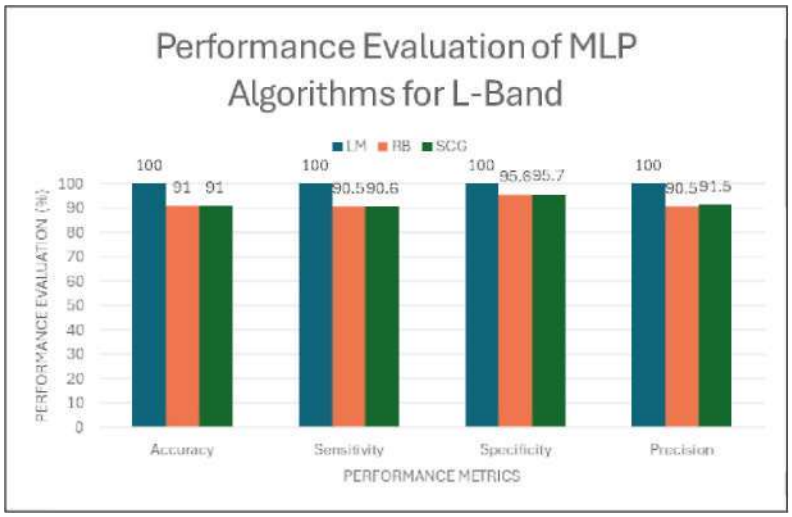

Figure 4.30 Comparative Performance Evaluation of MLP Algorithms for L-Band

Both the RBP and SCG classifiers achieved comparable overall performance, indicating that they are capable of learning the global decision boundaries for L-band slot size classification. While minor differences exist at the class level, as discussed in Section 4.4.1.4, the overall results confirm the superiority and stability of the LM algorithm for this application.

4.4.2 ANN-Based Classification Results for S-Band

Following the preprocessing stage, the dataset for the S-band consisted of 161 data points, distributed into three single-slot size categories: small (47), medium (57), and big (57). The dataset was divided into training, validation, and testing subsets following the partitioning strategy described in Chapter 3. This section presents the classification performance of the ANN model for the S-band across different training algorithms.

4.4.2.1 Classification ofS-band Using the Levenberg-Marquardt (LM) Algorithm

Table 4.25 shows the classification accuracy and mean squared error (MSE) obtained using the Levenberg-Marquardt (LM) algorithm for different hidden neuron configurations in the S-band classification task. The LM algorithm demonstrated strong and consistent performance across all evaluation metrics. During training, classification accuracy ranged from 78.9%> to 100%). For validation set, the accuracy ranged from 65% to 100%), while testing accuracy ranged from 70% to 100%), indicating reliable generalization behaviour.

The optimal configuration was achieved with one hidden neuron, which not only produced the highest classification accuracy (100%> for training, validation and testing) but also recorded the lowest mean squared error (MSE) value of 0.03 92. These findings highlight the LM algorithm's ability to effectively model the nonlinear characteristics of the S-band dataset, enabling precise and reliable classification of absorption performance.

Table 4.25
Classification Accuracy and MSE Values for the LM Algorithm (S-Band)

Hidden Neuron	**Accuracy (%)**			**MSE Value**
	Training	**Validation**	**Testing**	
***1**	100	100	100	0.0392
2	80	65	95	0.0833
3	91.6	80	90	0.0667
4	78.9	95	90	0.0416
5	82.1	85	80	0.0500
6	91.6	95	90	0.0416
7	84.2	85	90	0.0667
8	91.6	85	90	0.0667
9	83.2	80	70	0.0415
10	93.7	95	95	0.0510

*Best hidden neuron in LM

To systematically evaluate the classification performance based on slot size, confusion matrix analysis is performed for the optimal LM configuration, as shown in Figure 4.31. The confusion matrices for the training, validation, testing and overall datasets demonstrate that all samples are correctly classified into their respective slot size categories (small, medium and big), with no misclassification observed. This indicates excellent class separability and highlights the robustness of the LM based ANN classifier for S-band absorption data.

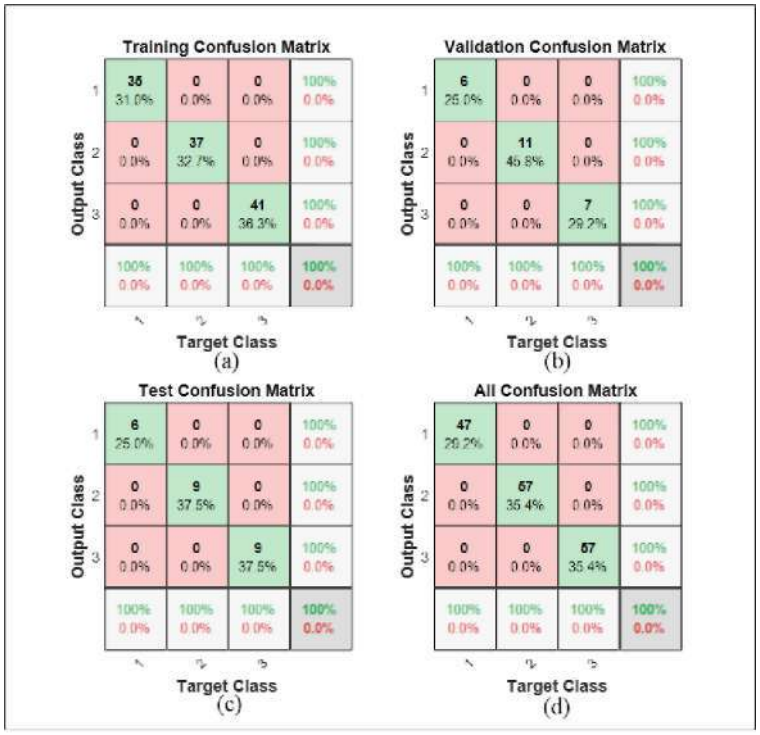

Figure 4.31 Confusion Matrices for S-band Slot Size Classification Using the LM Algorithm: (a) Training, (b) Validation, (c) Testing, (d) Overall

Based on the confusion matrix results, class-specific performance metrics are computed and summarized in Table 4.26. The LM classifier achieves 100% precision, recall and F1-score for all three slot size classes, indicating balanced and unbiased classification performance across categories.

Table 4.26
Class-Wise Classification Performance Metrics for S-Band using the LM Algorithm (1 Hidden Neuron

Slot Size	Precision (%)	Recall (%)	F1-Score (%)
Small	100	100	100
Medium	100	100	100
Big	100	100	100

While Table 4.26 presents the class-wise classification behaviour, the overall performance of the LM-based classifier is summarized in Table 4.27. The model achieves 100% overall accuracy, sensitivity, specificity and precision, confirming its reliability and consistency for S-band slot size classification.

Table 4.27
Overall Classification Performance Metrics for S-Band using the LM Algorithm (1 Hidden Neuron)

Performance Metric	Percentage (%)
Accuracy	100
Sensitivity	100
Specificity	100
Precision	100

Note: Metrics are based on the best hidden neuron configuration (HN=1).

The training convergence behaviour of the LM-based ANN classifier is illustrated in Figure 4.32, which shows the training, validation and testing performance curves plotted against the number of epochs. The mean squared error decreases steadily during training and the validation curve closely follows the training trend, reaching the best validation performance at epoch 13. The absence of divergence between training and validation curves indicates stable learning behaviour and confirms that overfitting does not occur.

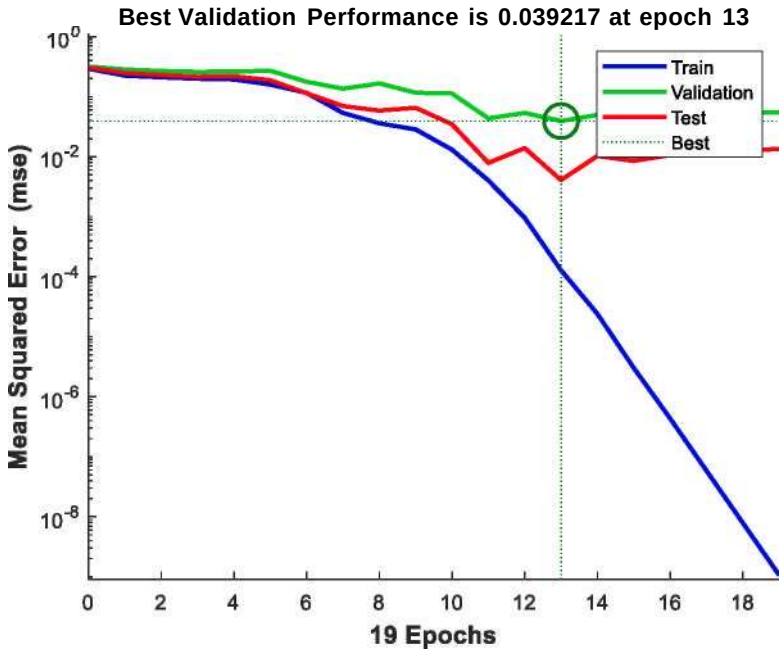

Figure 4.32 Training, validation, and Testing Mean Squared Error (MSE) Versus Epochs For the LM-based ANN Classifier (S-band)

Overall, the LM algorithm demonstrates excellent classification performance for the S-band dataset. Although the combined analysis of confusion matrices, class specific performance metrics for the training convergence behaviour together with the lowest MSE value confirms that the LM-based ANN classifier provides an accurate, stable and well generalized solution for slot size classification in the S-band.

4.4.2.2 Classification of S-band using the Resilient Backpropagation (RBP) Algorithm

Table 4.28 presents the classification results of the training, validation and testing datasets using the Resilient Backpropagation (RBP) algorithm for different hidden neuron configurations in the S-band classification task. Overall, the RBP-based ANN demonstrated strong and consistent classification performance across the training, validation and testing datasets. The training accuracy ranged from 82.1% to100%, validation accuracy varied from 70% to 100% and testing accuracy ranged from 75% to 100%, indicating reliable generalization behaviour.

The optimal configuration was achieved using four hidden neurons, which produced perfect classification accuracy (100%) across all datasets and recorded the lowest mean squared error (MSE) value of 0.0281. This result shows the effectiveness

of the RBP algorithm in modelling the nonlinear absorption characteristics of the S-band dataset and achieving precise slot size classification.

Table 4.28
Classification Accuracy and MSE Values for the RBP Algorithm (S-Band)

Hidden Neuron	**Accuracy (%)**			**MSE Value**
	Training	**Validation**	**Testing**	
1	100	100	100	0.1500
2	100	100	100	0.0583
3	84.2	85	90	0.0500
*4	100	100	100	0.0281
5	89.5	70	100	0.0916
6	100	100	100	0.0583
7	84.2	80	85	0.0583
8	86.3	85	90	0.0416
9	82.1	100	75	0.0333
10	84.2	85	75	0.0583

*Best hidden neuron in RBP

To further examine class-wise prediction behaviour, confusion matrix analysis was performed for the optimal RBP configuration, as shown in Figure 4.33. The confusion matrices for the training, validation, testing and overall datasets indicate that all samples were correctly classified into their respective slot size categories (small, medium, and big), with no misclassification observed. This confirms excellent class separability and robust learning behaviour of the RBP-based ANN classifier for the S-band dataset.

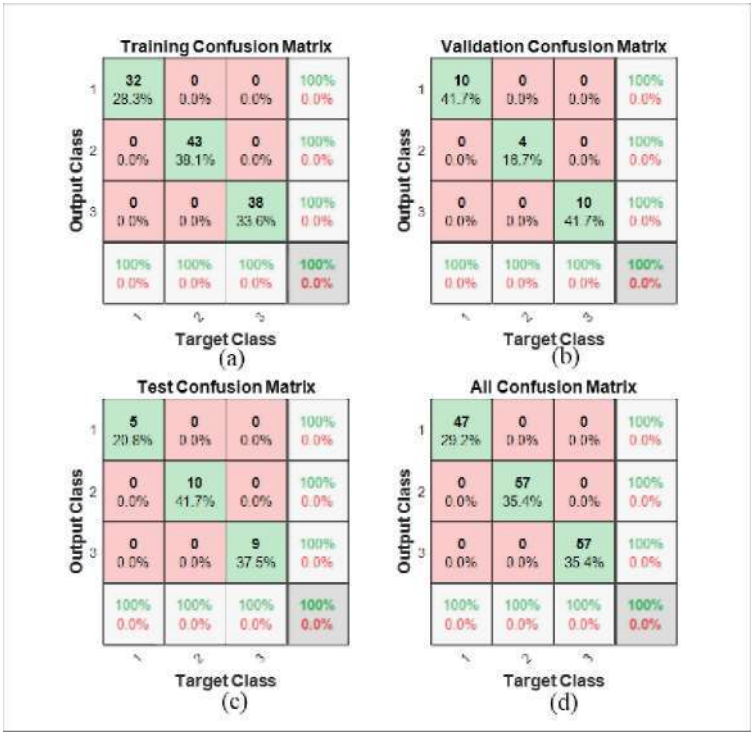

Figure 4.33 Confusion Matrices for S-band Slot Size Classification Using the RBP Algorithm: (a) Training, (b) Validation, (c) Testing, (d) Overall

Based on the confusion matrix results, class-specific performance metrics are computed and summarized in Table 4.29. The RBP classifier achieves 100% precision, recall and F1-score for all three slot size classes, indicating balanced and unbiased classification performance across categories.

Table 4.29
Class-Wise Classification Performance Metrics for S-Band using the RBP Algorithm (4 Hidden Neurons)

Slot Size	**Precision (%)**	**Recall (%)**	**F1-Score (%)**
Small	100	100	100
Medium	100	100	100
Big	100	100	100

While Table 4.29 presents the class-wise classification behaviour, the overall performance of the RBP-based classifier is summarized in Table 4.30. The model achieves 100% overall accuracy, sensitivity, specificity and precision, confirming its reliability and consistency for S-band slot size classification.

Table 4.30
Overall Classification Performance Metrics for S-Band using the RBP Algorithm (4 Hidden Neurons)

Performance Metric	Percentage (%)
Accuracy	100
Sensitivity	100
Specificity	100
Precision	100

Note: Metrics are based on the best hidden neuron configuration (HN=4).

The training convergence behaviour of the RBP-based ANN classifier is illustrated in Figure 4.34, which presents the training, validation, and testing mean squared error (MSE) curves plotted against the number of epochs. The MSE decreases steadily during the initial training phase, indicating effective learning of the classification patterns. As training progresses, the error reduction becomes more gradual and stabilizes toward later epochs. The validation curve generally follows the training trend without significant divergence, suggesting stable generalization behaviour and the absence of severe overfitting. Minor fluctuations near convergence indicate slightly less smooth learning behaviour compared to the LM-based classifier; however, the final convergence remains stable and accurate.

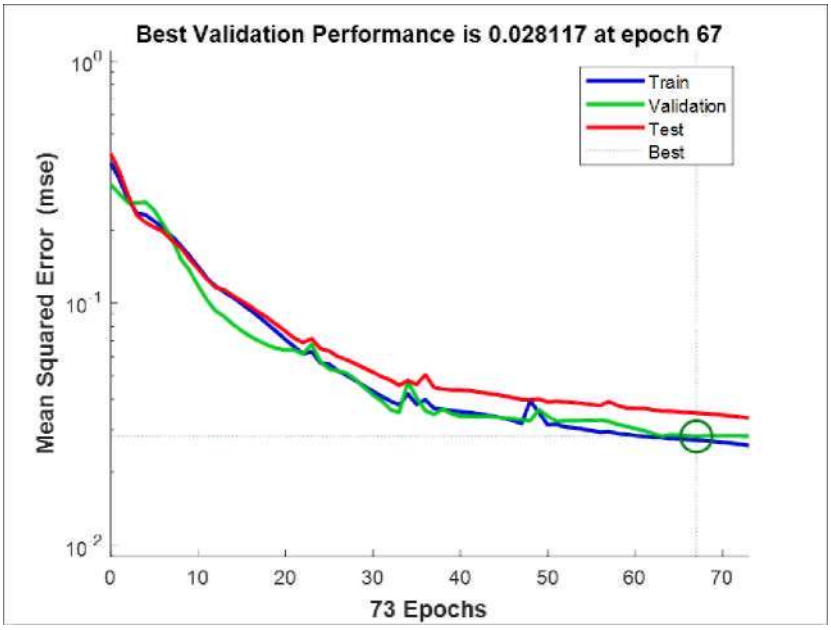

Figure 4.34 Training, Validation, and Testing Mean Squared Error (MSE) Versus Epochs for the RBP-based ANN Classifier (S-band)

Overall, the RBP algorithm demonstrates excellent classification performance for the S-band dataset. The combined analysis of classification accuracy, confusion matrices, class specific performance metrics and training convergence behaviour confirms that the RBP-based ANN classifier provides an accurate, stable and well generalized solution for slot size classification in the S-band frequency range.

4.4.2.3 Classification of S-band using the Scaled-Conjugate Gradient (SCG) Algorithm

Table 4.31 presents the classification results of the training, validation and testing datasets using the Scaled-Conjugate Gradient (SCG) algorithm for different hidden neuron configurations in the S-band classification task. Overall, the SCG-based ANN demonstrated strong and consistent classification performance across the training, validation and testing datasets. The training accuracy ranged from 78.9% to100%, validation accuracy varied from 75% to 100% and testing accuracy ranged from 70% to 100%, indicating reliable generalization behaviour.

The optimal configuration was achieved using three hidden neurons, which produced 100% classification accuracy for the training, validation, and testing datasets and recorded the lowest mean squared error (MSE) value of 0.0436 among the configurations that achieved perfect accuracy. Therefore, this configuration was selected for detailed evaluation.

Table 4.31
Classification Accuracy and MSE Values for SCG Algorithm (S-Band)

Hidden Neuron	**Accuracy (%)**			**MSE Value**
	Training	**Validation**	**Testing**	
1	100	100	100	0.1166
2	100	100	100	0.1000
*3	100	100	100	0.0436
4	90.5	90	100	0.0500
5	78.9	90	90	0.0583
6	88.4	80	80	0.0672

Hidden Neuron	Accuracy (%)			MSE Value
	Training	Validation	Testing	
7	87.4	80	85	0.0667
8	84.2	75	80	0.0500
9	86.3	80	70	0.0750
10	92.6	85	95	0.0724

*Best hidden neuron in SCG

To examine class-wise prediction behaviour, confusion matrix analysis was performed for the optimal SCG configuration, as shown in Figure 4.35. The confusion matrices for the training, validation, testing and overall datasets show a perfectly diagonal pattern, where all samples were correctly classified into their respective slot size categories (small, medium, and big), with no misclassification observed. This confirms excellent class separability for the S-band dataset using the SCG-based classifier.

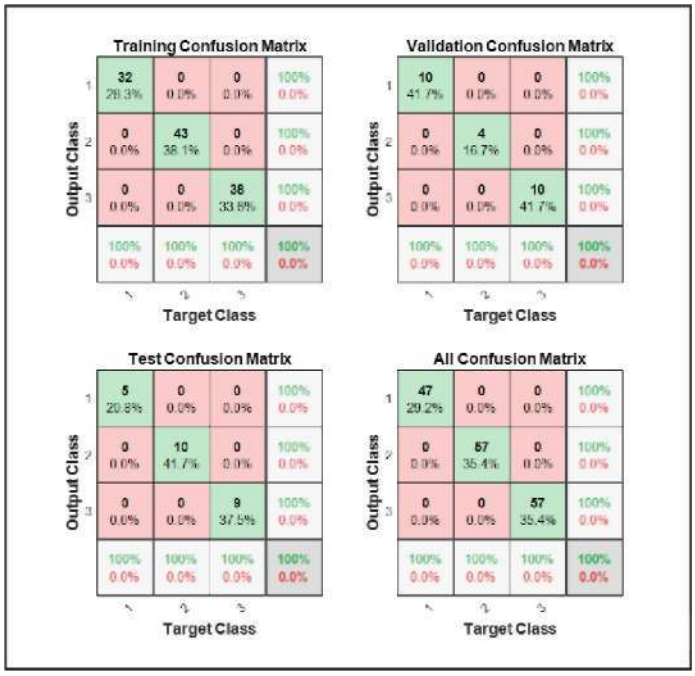

Figure 4.35 Confusion Matrices for S-band Slot Size Classification Using the SCG Algorithm: (a) Training, (b) Validation, (c) Testing, (d) Overall

Based on the confusion matrix results, class-specific performance metrics are computed and summarized in Table 4.32. The SCG classifier achieves 100% precision,

recall and F1-score for all three slot size classes, indicating balanced and unbiased classification performance across classes.

Table 4.32
Class-Wise Classification Performance Metrics for S-Band using the SCG Algorithm (3 Hidden Neurons)

Slot Size	Precision (%)	Recall (%)	F1-Score (%)
Small	100	100	100
Medium	100	100	100
Big	100	100	100

While Table 4.32 presents the class-wise classification behaviour, the overall performance of the RBP-based classifier is summarized in Table 4.33. The model achieves 100% overall accuracy, sensitivity, specificity and precision, confirming its reliability and consistency for S-band slot size classification.

Table 4.33
Overall Classification Performance Metrics for S-Band using the SCG Algorithm (3 Hidden Neurons)

Performance Metric	Percentage (%)
Accuracy	100
Sensitivity	100
Specificity	100
Precision	100

Note: Metrics are based on the best hidden neuron configuration (HN=3).

The training convergence behaviour of the SCG-based ANN classifier is illustrated in Figure 4.36, which presents the training, validation, and testing mean squared error (MSE) curves plotted against the number of epochs. The error decreases progressively during the training, and the validation curve follows the overall trend without strong divergence, showing stable learning and good generalization. The best validation performance is achieved at approximately epoch 44 (out of 49 epochs), after which the curves stabilize, suggesting that overfitting does not occur.

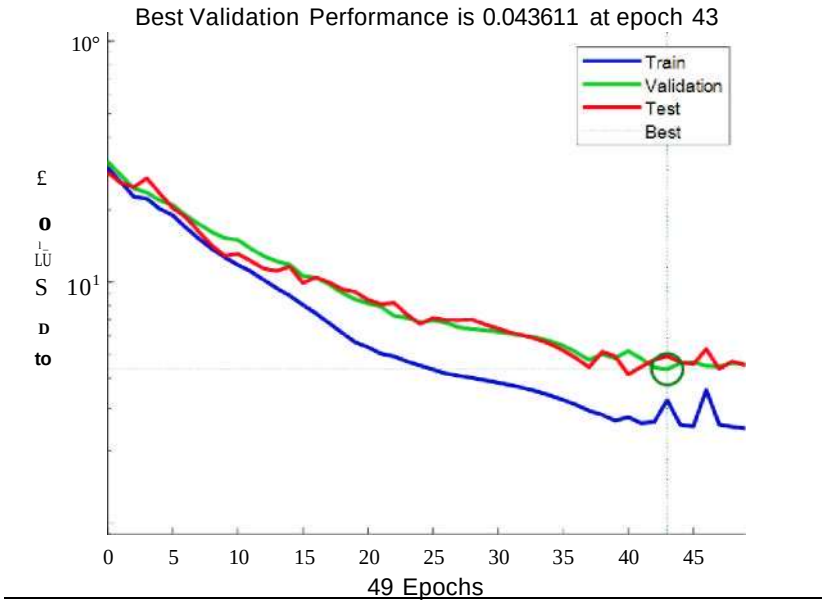

Figure 4.36 Training, Validation, and Testing Mean Squared Error (MSE) Versus Epochs For the SCG-based ANN Classifier (S-band)

Overall, the SCG algorithm demonstrates excellent classification performance for the S-band dataset. The combined analysis of classification accuracy, confusion matrices, class specific performance metrics and training convergence behaviour confirms that the SCG-based ANN classifier also provides an accurate, stable and well generalized solution for slot size classification in the S-band frequency range.

4.4.2.4 Comparison of the MLP Training Algorithms for S-Band Classification

Table 4.34 summarizes the optimal configurations and overall classification performance of the three MLP training algorithms applied to S-band slot size classification. All evaluated algorithms achieved perfect classification accuracy (100%) across the training, validation and testing datasets, indicating that the S-band dataset is highly separable and can be effectively modelled using different MLP training strategies. Among the three algorithms, the Resilient Backpropagation (RBP) algorithm with four hidden neurons recorded the lowest mean squared error (MSE) value of 0.0281, indicating more efficient convergence and reduced prediction error compared to the Levenberg-Marquardt (LM) and Scaled-Conjugate Gradient (SCG) algorithms, which recorded MSE values of 0.0392 and 0.0436, respectively.

Table 4.34
Summary of Best Hidden Neuron Configurations for Each MLP Algorithm (S-Band)

Training Algorithm	Hidden Neuron	Accuracy (%)			MSE Value
		Training	validation	Testing	
Levenberg Marquardt (LM)	1	100	100	100	0.0392
*Resilient Backpropagation (RB)	4	100	100	100	0.0281
Scaled-Conjugate Gradient (SCG)	3	100	100	100	0.0436

*Best hidden neuron

To further clarify class-wise behaviour, slot size-based classification performance for each algorithm is presented in Table 4.35, derived from the corresponding confusion matrices.

Table 4.35
Slot Size-Based Classification Performance (Recall) for S-Band using Different ANN Training Algorithms

Slot Size	LM (%)	RBP (%)	SCG (%)
Small	100	100	100
Medium	100	100	100
Big	100	100	100

Note: Slot-size-based performance is reported using recall (sensitivity), which quantifies the proportion of correctly classified samples for each slot size.

As shown in Table 4.35, all three ANN training algorithms achieved perfect recall across all slot size categories, confirming that the small, medium and big slot sizes are clearly separable in the S-band frequency range. This consistent class-wise performance further demonstrates the robustness of the ANN-based classifiers for S-band slot size identification. While all algorithms performed equally well in terms of classification accuracy, the lower MSE obtained using the RBP algorithm suggests a more efficient learning process and improved numerical stability for this dataset.

4.4.2.5 Comprehensive Performance Evaluation of the ANN Classifiers for S-Band

Table 4.36 and Figure 4.37 present a comparative evaluation of the ANN classifiers based on overall accuracy, precision, sensitivity and specificity. All three MLP training algorithms: Levenberg-Marquardt (LM), Resilient Backpropagation (RBP) and Scaled-Conjugate Gradient (SCG) achieved 100% across all evaluation metrics, indicating excellent and equivalent classification capability for the S-band dataset.

Table 4.36
Performance Evaluation of MLP Algorithms for S-Band

Training Algorithm	**Hidden Neuron**	**Accuracy (%)**	**Precision (%)**	**Sensitivity (%)**	**Specificity (%)**
Levenberg Marquardt (LM)	**1**	100	100	100	100
*Resilient Backpropagation (RB)	**4**	100	100	100	100
Scaled-Conjugate Gradient (SCG)	**3**	100	100	100	100

*Although all algorithms achieved perfect classification performance, the RBP algorithm recorded the lowest MSE value (0.0281), indicating more efficient numerical convergence.

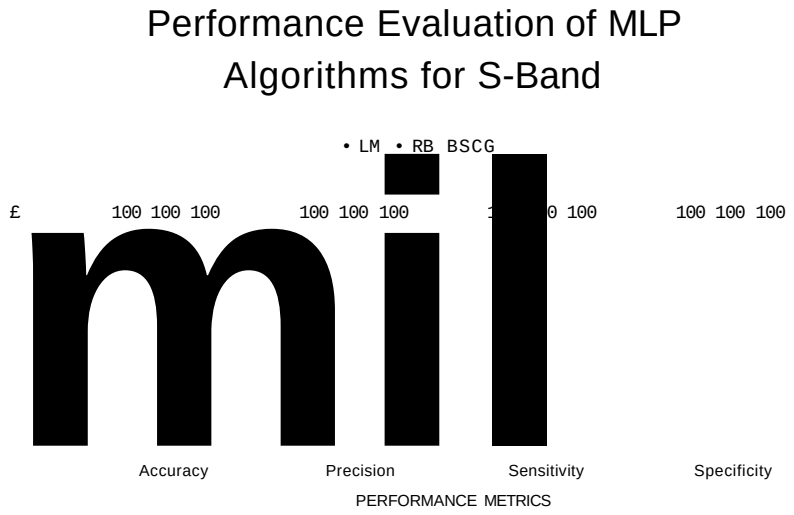

Figure 4.37 Comparative Performance Evaluation of MLP Algorithms for S-Band

Figure illustrates the comparative performance of the MLP algorithms for the S-band, further confirming that all classifiers exhibit identical overall classification effectiveness. Overall, the results demonstrate that the S-band slot size classification problem is highly separable, enabling all three ANN training algorithms to learn the underlying decision boundaries effectively. While classification performance is equivalent across algorithms, differences in MSE values highlight variations in convergence efficiency, with the RBP algorithm providing the most numerically efficient solution for the S-band dataset.

4.4.3 ANN-Based Classification Results for C-Band

Following the preprocessing stage, the dataset for the C-band consisted of 323 data points, distributed into three single-slot size categories: small (111), medium (100), and big (112). The dataset was divided into training, validation, and testing subsets following the partitioning strategy described in Chapter 3. This section presents the classification performance of the ANN model for the C-band across different training algorithms.

4.4.3.1 Classification of C-band using the Levenberg-Marquardt (LM) A Igorithm

Table 4.37 presents the classification accuracy and mean squared error (MSE) obtained using the Levenberg-Marquardt (LM) algorithm for different hidden neuron configurations in the C-band classification task. Overall, the LM-based ANN demonstrates strong and consistent classification performance across the training, validation, and testing datasets. Training accuracy ranges from 81.9% to 100%, validation accuracy from 81.2% to 100%), and testing accuracy from 79.2% to 100%), indicating reliable generalization behaviour across configurations.

The optimal configuration was achieved with eight hidden neurons, which produced perfect classification accuracy (100%>) for training, validation and testing datasets while maintaining a low MSE value of 0.0474. This configuration was therefore selected for further detailed evaluation. These results highlight the effectiveness of the LM algorithm in modelling the nonlinear characteristics of the C-band absorption data and achieving precise slot size classification.

Table 4.37
Classification Accuracy and MSE Values for LM Algorithm (C-Band)

Hidden Neuron	Accuracy (%)			MSE Value
	Training	Validation	Testing	
1	100	100	100	0.1181
2	91.2	89.6	97.9	0.0660
3	92.5	89.6	79.2	0.0590
4	85.9	85.4	87.5	0.0451
5	97.8	97.9	100	0.0556
6	100	100	100	0.0521
7	85.5	89.6	81.2	0.0523
*8	100	100	100	0.0474
9	81.9	81.2	93.8	0.0659
10	99.1	95.8	100	0.0625

*Best hidden neuron in LM

To further evaluate class-wise prediction behaviour, confusion matrix analysis was performed for the optimal LM configuration, as illustrated in Figure 4.38. The confusion matrices for the training, validation, testing and overall datasets show that all samples are correctly classified into their respective slot size categories (small, medium and big), with no misclassification observed. This confirms excellent class separability and robust learning behaviour of the LM based ANN classifier for C-band dataset.

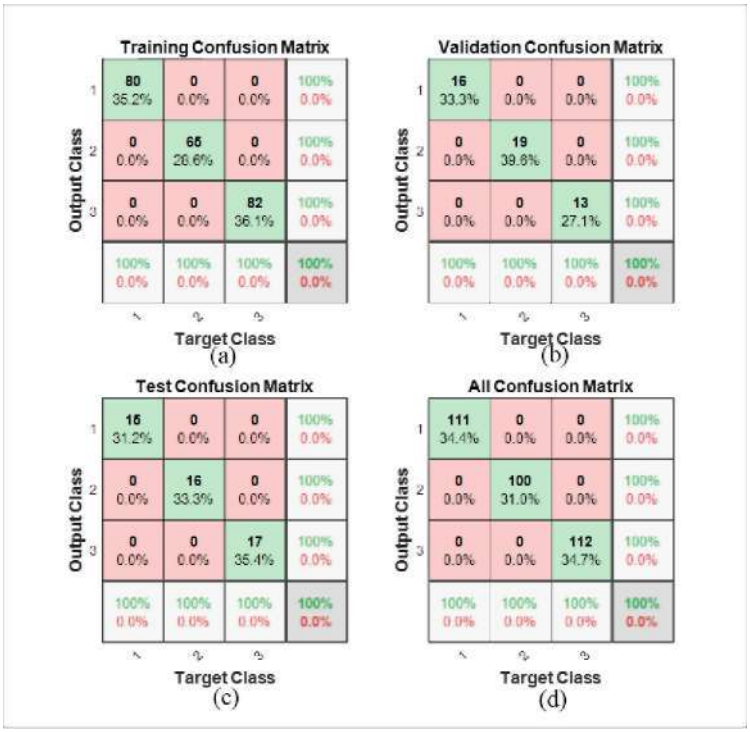

Figure 4.38 Confusion Matrices for C-band Slot Size Classification Using the LM Algorithm: (a) Training, (b) Validation, (c) Testing, (d) Overall

Based on the confusion matrix results, class-specific performance metrics are computed and summarized in Table 4.38. The LM classifier achieves 100% precision, recall and F1-score for all three slot size classes, indicating balanced and unbiased classification performance across categories.

Table 4.38
Class-Wise Classification Performance Metrics for C-Band using the LM Algorithm (8 Hidden Neurons

Slot Size	**Precision (%)**	**Recall (%)**	**F1-Score (%)**
Small	100	100	100
Medium	100	100	100
Big	100	100	100

While Table 4.38 presents the class-wise classification behaviour, the overall performance of the LM-based classifier is summarized in Table 4.39. The model achieves 100% overall accuracy, sensitivity, specificity and precision, confirming its reliability and consistency for C-band slot size classification.

Table 4.39
Overall Classification Performance Metrics for C-Band using the LM Algorithm (8 Hidden Neurons)

Performance Metric	Percentage (%)
Accuracy	100
Sensitivity	100
Specificity	100
Precision	100

Note: Metrics are based on the best hidden neuron configuration (HN=8).

The training convergence behaviour of the LM-based ANN classifier is illustrated in Figure 4.39, which shows the training, validation and testing performance curves plotted against the number of epochs. The mean squared error decreases steadily during training and the validation curve closely follows the training trend, reaching the best validation performance at epoch 25. The absence of divergence between training and validation curves indicates stable learning behaviour and confirms that overfitting does not occur.

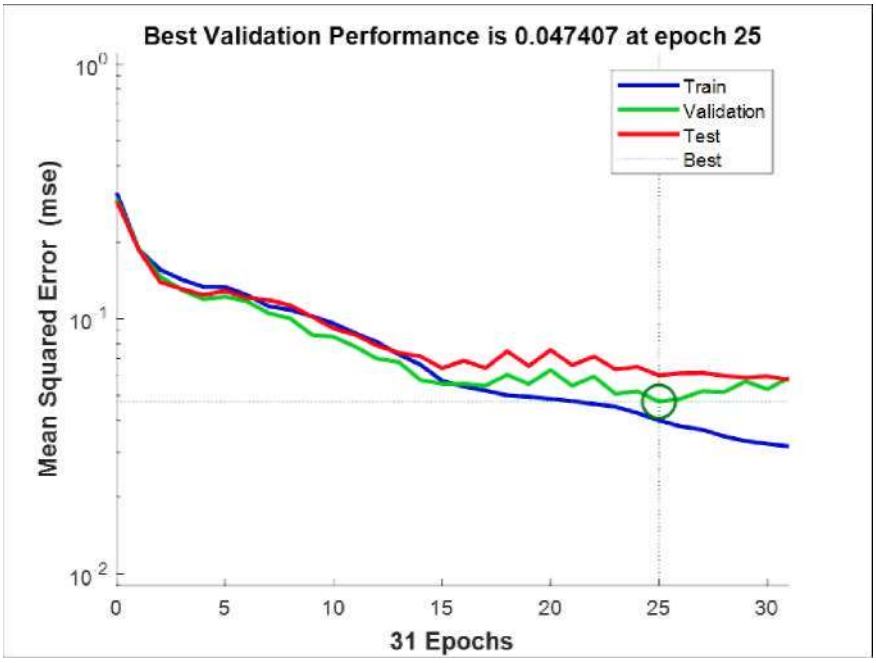

Figure 4.39 Training, Validation, and Testing Mean Squared Error (MSE) Versus Epochs For the LM-based ANN Classifier (C-band)

Overall, the LM algorithm demonstrates excellent classification performance for the C-band dataset. The combined analysis of confusion matrices, class specific performance metrics for the training convergence behaviour together with the lowest MSE value confirms that the LM-based ANN classifier provides an accurate, stable and well generalized solution for slot size classification in the C-band frequency range.

4.4.3.2 Classification of C-band using the Resilient Backpropagation (RBP) Algorithm

Table 4.40 presents the classification results of the training, validation and testing datasets using the Resilient Backpropagation (RBP) algorithm for different hidden neuron configurations in the C-band classification task. Overall, the RBP-based ANN demonstrated strong and consistent classification performance across the training, validation and testing datasets. The training accuracy ranged from 92.1% to100%, validation accuracy varied from 83.3% to 100% and testing accuracy ranged from 91.7% to 100%, indicating reliable generalization behaviour.

The optimal configuration was achieved using four hidden neurons, which produced perfect classification accuracy (100%) across all datasets and recorded the lowest mean squared error (MSE) value of 0.0278. This result shows the effectiveness of the RBP algorithm in modelling the nonlinear absorption characteristics of the C-band dataset and achieving precise slot size classification.

Table 4.40
Classification Accuracy and MSE Values for RBP Algorithm (C-Band)

Hidden Neuron	**Accuracy (%)**			**MSE Value**
	Training	**Validation**	**Testing**	
1	100	100	100	0.0764
2	100	100	100	0.0556
3	100	100	100	0.0660
*4	100	100	100	0.0278
5	100	100	100	0.0556
6	99.6	97.9	100	0.0521

Hidden Neuron	Accuracy (%)			MSE Value
	Training	Validation	Testing	
7	97.8	93.8	95.8	0.0972
8	100	100	100	0.1250
9	100	100	100	0.1458
10	92.1	83.3	91.7	0.0659

*Best hidden neuron in RBP

To further examine class-wise prediction behaviour, confusion matrix analysis was performed for the optimal RBP configuration, as shown in Figure 4.40. The confusion matrices for the training, validation, testing and overall datasets indicate that all samples were correctly classified into their respective slot size categories (small, medium, and big), with no misclassification observed. This confirms excellent class separability and robust learning behaviour of the RBP-based ANN classifier for the C-band dataset.

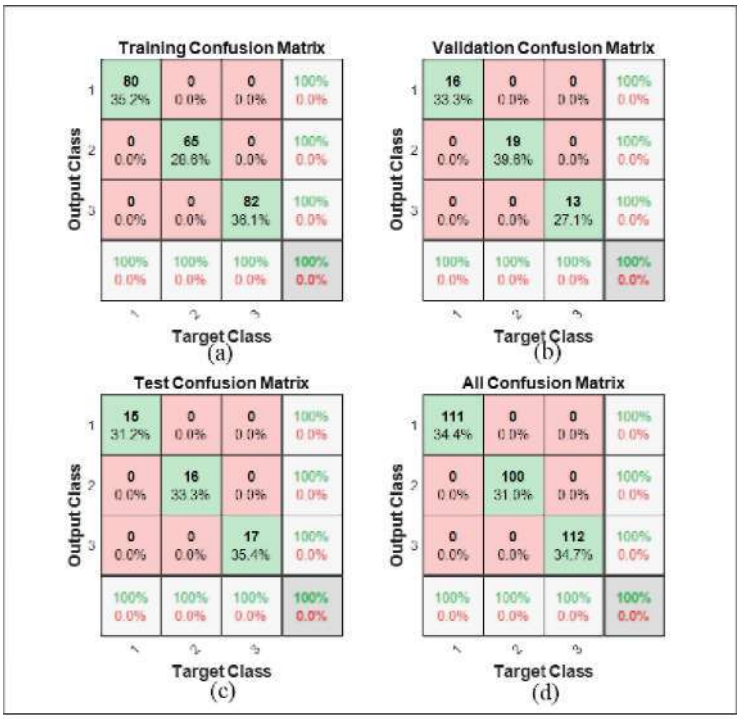

Figure 4.40 Confusion Matrices for C-band slot Size Classification Using the RBP Algorithm: (a) Training, (b) Validation, (c) Testing, (d) Overall

Based on the confusion matrix results, class-specific performance metrics are computed and summarized in Table 4.41. The RBP classifier achieves 100% precision, recall and F1-score for all three slot size classes, indicating balanced and unbiased classification performance across categories.

Table 4.41
Class-Wise Classification Performance Metrics for C-Band using the RBP Algorithm (4 Hidden Neurons)

Slot Size	**Precision (%)**	**Recall (%)**	**F1-Score (%)**
Small	100	100	100
Medium	100	100	100
Big	100	100	100

While Table 4.41 presents the class-wise classification behaviour, the overall performance of the RBP-based classifier is summarized in Table 4.42. The model achieves 100% overall accuracy, sensitivity, specificity and precision, confirming its reliability and consistency for C-band slot size classification.

Table 4.42
Overall Classification Performance Metrics for C-Band using the RBP Algorithm (4 Hidden Neurons)

Performance Metric	**Percentage (%)**
Accuracy	100
Sensitivity	100
Specificity	100
Precision	100

Note: Metrics are based on the best hidden neuron configuration (HN=4).

The training convergence behaviour of the RBP-based ANN classifier is illustrated in Figure 4.41, which presents the training, validation, and testing mean squared error (MSE) curves plotted against the number of epochs. The MSE decreases steadily during the initial training phase, indicating effective learning of the classification patterns. As training progresses, the error reduction becomes more gradual and stabilizes toward later epochs. The validation curve generally follows the

training trend without significant divergence, suggesting stable generalization behaviour and the absence of severe overfitting.

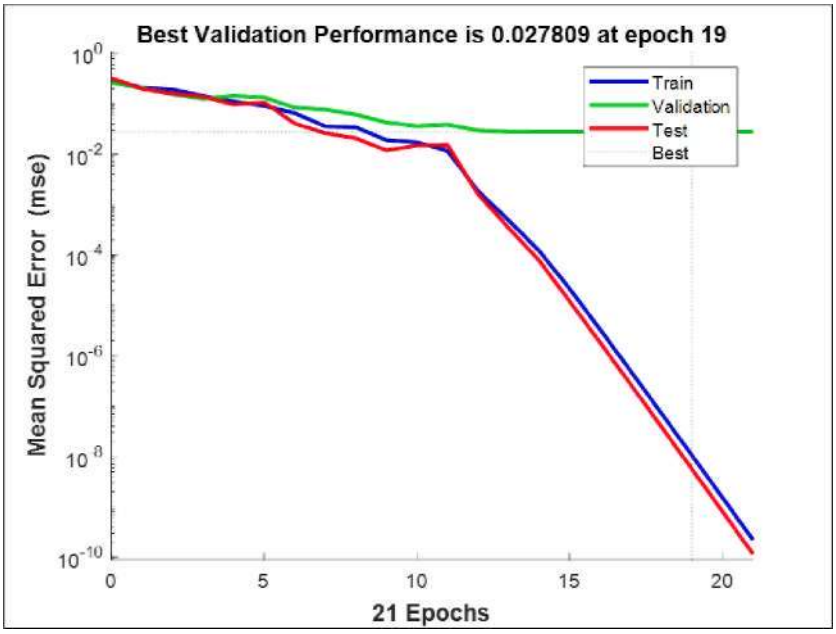

Figure 4.41 Training, validation, and Testing Mean Squared Error (MSE) Versus Epochs For the RBP-based ANN Classifier (C-band)

Overall, the RBP algorithm demonstrates excellent classification performance for the C-band dataset. The combined analysis of classification accuracy, confusion matrices, class specific performance metrics and training convergence behaviour confirms that the RBP-based ANN classifier provides an accurate, stable and well generalized solution for slot size classification in the C-band frequency range.

4.4.3.3 Classification of C-band using the Scaled-Conjugate Gradient (SCG) Algorithm

Table 4.43 presents the classification results for training, validation and testing datasets using the Scaled-Conjugate Gradient (SCG) algorithm. Based on the results, the SCG algorithm demonstrated competitive performance with training accuracy ranging of 86.3% to 100%, validation accuracy between 87.5% and 100% and testing accuracy from 81.2% to 100%, indicating reliable generalization behaviour across different network configurations.

The optimal configuration is achieved using one hidden neuron, which produced 100% classification accuracy for the training, validation, and testing datasets and

records the lowest mean squared error (MSE) among the configurations achieving perfect accuracy, with a value of 0.0987. This configuration was selected for detailed evaluation.

Table 4.43
Classification Accuracy and MSE Values for SCG Algorithm (C-Band)

Hidden Neuron	**Accuracy (%)**			**MSE Value**
	Training	**Validation**	**Testing**	
*1	100	100	100	0.0987
2	89.9	91.7	87.5	0.0521
3	92.5	91.7	91.7	0.0555
4	96.0	95.8	97.9	0.0972
5	93.8	93.8	93.8	0.0486
6	86.8	93.8	85.4	0.0625
7	89.4	91.7	87.5	0.0521
8	86.3	87.5	81.2	0.0625
9	97.4	93.8	89.6	0.0729
10	90.7	89.6	85.4	0.0591

*Best hidden neuron in SCG

To examine class-wise prediction behaviour, confusion matrix analysis was performed for the optimal SCG configuration, as shown in Figure 4.42. The confusion matrices for the training, validation, testing and overall datasets show a perfectly diagonal pattern, where all samples were correctly classified into their respective slot size categories (small, medium, and big), with no misclassification observed. This confirms excellent class separability for the C-band dataset using the SCG-based classifier.

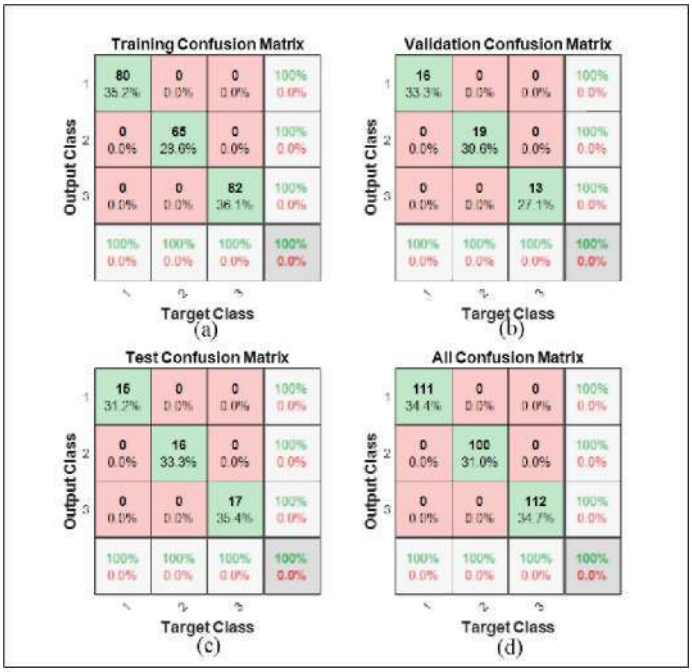

Figure 4.42 Confusion Matrices For C-band Slot Size Classification Using the SCG Algorithm: (a) Training, (b) Validation, (c) Testing, (d) Overall

Based on the confusion matrix results, class-specific performance metrics are computed and summarized in Table 4.44. The SCG classifier achieves 100% precision, recall and F1-score for all three slot size classes, indicating balanced and unbiased classification performance across classes.

Table 4.44
Class-Wise Classification Performance Metrics for C-Band using the SCG Algorithm (1 Hidden Neuron)

Slot Size	**Precision (%)**	**Recall (%)**	**F1-Score (%)**
Small	100	100	100
Medium	100	100	100
Big	100	100	100

While Table 4.44 presents the class-wise classification behaviour, the overall performance of the SCG-based classifier is summarized in Table 4.45. The model achieves 100% overall accuracy, sensitivity, specificity and precision, confirming its reliability and consistency for C-band slot size classification.

Table 4.45
Overall Classification Performance Metrics for C-Band using the SCG Algorithm (1 Hidden Neuron)

Performance Metric	Percentage (%)
Accuracy	100
Sensitivity	100
Specificity	100
Precision	100

Note: Metrics are based on the best hidden neuron configuration (HN=1).

The training convergence behaviour of the SCG-based ANN classifier is illustrated in Figure 4.43, which presents the training, validation, and testing mean squared error (MSE) curves plotted against the number of epochs. The error decreases progressively during the training, and the validation curve follows the overall trend without strong divergence. The best validation performance is achieved at approximately epoch 138 out of 144 epochs, after which the curves stabilize, suggesting that overfitting does not occur.

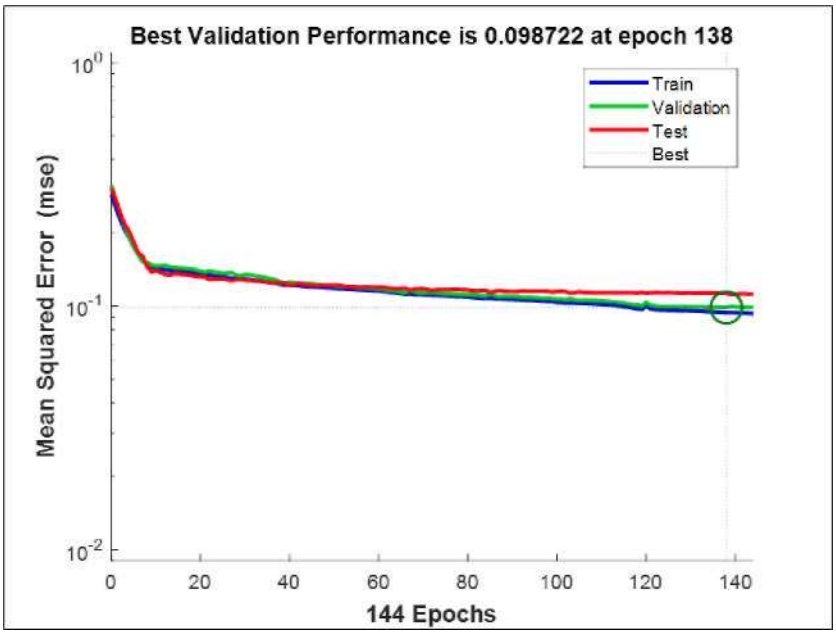

Figure 4.43 Training, Validation, and Testing Mean Squared Error (MSE) Versus Epochs For the SCG-based ANN Classifier (C-band)

Overall, the SCG algorithm demonstrates excellent classification performance for the C-band dataset. The combined analysis of classification accuracy, confusion

matrices, class specific performance metrics and training convergence behaviour confirms that the SCG-based ANN classifier also provides an accurate, stable and well generalized solution for slot size classification in the C-band frequency range.

4.4.3.4 Comparison of the MLP Algorithms for C-Band Classification

Table 4.46 summarizes the optimal configurations and overall classification performance of the three MLP training algorithms applied to C-band slot size classification. All evaluated algorithms achieved perfect classification accuracy (100%) across the training, validation and testing datasets, indicating that the C-band dataset is highly separable and can be effectively modelled using different MLP training strategies. Among the three algorithms, the Resilient Backpropagation (RBP) algorithm with four hidden neurons recorded the lowest mean squared error (MSE) value of 0.0278, indicating reduced prediction error and improved numerical stability compared to the Levenberg-Marquardt (LM) and Scaled-Conjugate Gradient (SCG) algorithms, which recorded MSE values of 0.0474 and 0.0987, respectively.

Table 4.46
Summary of Best Hidden Neuron Configurations for Each MLP Algorithm (C-Band)

Training Algorithm	**Hidden**	**Accuracy (%)**			**MSE Value**
		Training	**Validation**	**Testing**	
Levenberg Marquardt (LM)	**8**	100	**100**	**100**	0.0474
*Resilient Backpropagation (RB)	**4**	100	**100**	**100**	0.0278
Scaled-Conjugate Gradient (SCG)	**1**	100	**100**	**100**	0.0987

'Best hidden neuron

To further clarify class-wise behaviour, slot size-based classification performance for each algorithm is presented in Table 4.47, derived from the corresponding confusion matrices.

Table 4.47
Slot Size-Based Classification Performance (Recall) for C-Band using Different ANN Training Algorithms

Slot Size	LM (%)	**RBP** (%)	**SCG** (%)
Small	100	100	100
Medium	100	100	100
Big	100	100	100

Note: Slot-size-based performance is reported using recall (sensitivity), which quantifies the proportion of correctly classified samples for each slot size.

As shown in Table 4.47, all three ANN training algorithms achieved perfect recall across all slot size categories, confirming that the small, medium and big slot sizes are clearly separable in the C-band frequency range. This consistent class-wise performance further demonstrates the robustness of the ANN-based classifiers for C-band slot size identification. While all algorithms performed equally well in terms of classification accuracy, the lower MSE obtained using the RBP algorithm suggests a more efficient learning process and improved numerical stability for this dataset.

4.4.3.5 Comprehensive Performance Evaluation of the ANN Classifiers for C-Band

Table 4.48 and Figure 4.44 present a comparative evaluation of the ANN classifiers based on overall accuracy, precision, sensitivity and specificity for C-band slot size classification. All three MLP training algorithms: Levenberg-Marquardt (LM), Resilient Backpropagation (RBP) and Scaled-Conjugate Gradient (SCG) achieved 100% across all evaluation metrics, indicating excellent and equivalent classification capability for the C-band dataset.

Table 4.48
Performance Evaluation of MLP Algorithms for C-Band

Training Algorithm	Hidden Neuron	Accuracy (%)	Precision (%)	Sensitivity (%)	Specificity (%)
Levenberg Marquardt (LM)	8	100	100	100	100
*Resilient Backpropagation (RB)	4	100	100	100	100
Scaled-Conjugate Gradient (SCG)	1	100	100	100	100

*all algorithms achieved perfect classification performance, the RBP recorded the lowest MSE (0.0278)

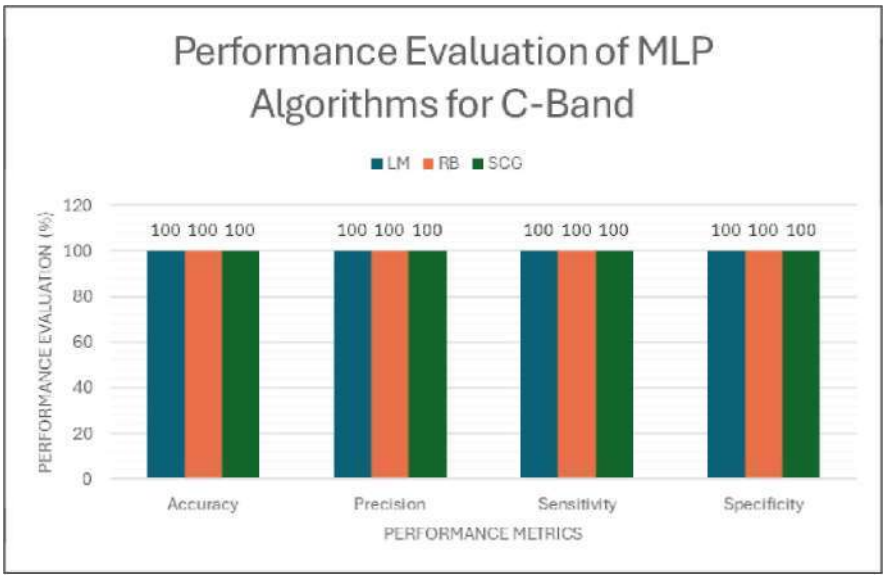

Figure 4.44 Comparative Performance Evaluation of MLP Algorithms for C-Band

Figure 4.44 illustrates the comparative performance of the MLP algorithms for the C-band, further confirming that all classifiers exhibit identical overall classification effectiveness. These results demonstrate that the C-band slot size classification problem is highly separable, enabling all three ANN training algorithms to learn the underlying decision boundaries effectively. Although classification performance is equivalent across algorithms in terms of accuracy and class-wise discrimination, differences in MSE values indicates variations in convergence efficiency. In particular, the RBP algorithm achieved the lowest MSE, suggesting more efficient learning and improved numerically stability for the C-band dataset.

4.4.4 ANN-Based Classification Results for X-Band

Following the preprocessing stage, the dataset for the X-band consisted of 593 data points, distributed into three single-slot size categories: small (194), medium (198), and big (201). The dataset was divided into training, validation, and testing subsets following the partitioning strategy described in Chapter 3. This section presents the classification performance of the ANN model for the X-band across different training algorithms.

4.4.4.1 Classification of X-band Using the Levenberg-Marquardt (LM) Algorithm

Table 4.49 presents the classification accuracy and mean squared error (MSE) obtained using the Levenberg-Marquardt (LM) algorithm for different hidden neuron configurations in the X-band classification task. Overall, the LM-based ANN demonstrates strong and consistent classification performance across the training, validation, and testing datasets. Training accuracy ranges from 88.9% to 100%. For validation set, the accuracy ranged from 85.4% to 100%, while testing accuracy ranged from 82% to 100%, indicating reliable generalization behaviour across configurations.

The optimal configuration was achieved with four hidden neurons, which produced perfect classification accuracy (100%) for training, validation and testing datasets while maintaining a low MSE value of 0.0498. This configuration was therefore selected for further detailed evaluation. These results highlight the effectiveness of the LM algorithm in modelling the nonlinear characteristics of the X-band absorption data and achieving precise slot size classification.

Table 4.49
Classification Accuracy and MSE Values for LM Algorithm (X-Band)

Hidden Neuron	Accuracy (%)			MSE Value
	Training	Validation	Testing	
1	100	100	100	0.1011
2	100	100	100	0.0899
3	100	100	100	0.0599
*4	100	100	100	0.0498

Hidden Neuron	Accuracy (%)			MSE Value
	Training	Validation	Testing	
5	90.4	85.4	89.9	0.0505
6	99.3	100	100	0.0431
7	88.9	92.1	82	0.0430
8	100	100	100	0.1086
9	100	100	100	0.0692
10	99	98.9	98.9	0.0487

*Best hidden neuron in LM

To further evaluate class-wise prediction behaviour, confusion matrix analysis was performed for the optimal LM configuration, as illustrated in Figure 4.45. The confusion matrices for the training, validation, testing and overall datasets show that all samples are correctly classified into their respective slot size categories (small, medium and big), with no misclassification observed. This confirms excellent class separability and robust learning behaviour of the LM based ANN classifier for X-band dataset.

Figure 4.45 Confusion Matrices for X-band Slot Size Classification Using the LM Algorithm: (a) Training, (b) Validation, (c) Testing, (d) Overall

Based on the confusion matrix results, class-specific performance metrics are computed and summarized in Table 4.50. The LM classifier achieves 100% precision, recall and F1-score for all three slot size classes, indicating balanced and unbiased classification performance across categories.

Table 4.50
Class-Wise Classification Performance Metrics for X-Band using the LM Algorithm (4 Hidden Neurons

Slot Size	**Precision (%)**	**Recall (%)**	**F1-Score (%)**
Small	100	100	100
Medium	100	100	100
Big	100	100	100

The overall classification performance of the LM-based classifier is summarized in Table 4.51. The model achieves 100% overall accuracy, sensitivity, specificity and precision, confirming its reliability and consistency for X-band slot size classification.

Table 4.51
Overall Classification Performance Metrics for X-Band using the LM Algorithm (4 Hidden Neurons)

Performance Metric	**Percentage (%)**
Accuracy	100
Sensitivity	100
Specificity	100
Precision	100

Note: Metrics are based on the best hidden neuron configuration (HN=4).

The training convergence behaviour of the LM-based ANN classifier is illustrated in Figure 4.46, which shows the training, validation and testing performance curves plotted against the number of epochs. The mean squared error decreases steadily during training and the validation curve closely follows the training trend, reaching the best validation performance at epoch 92. The absence of divergence between training and validation curves indicates stable learning behaviour and confirms that overfitting does not occur.

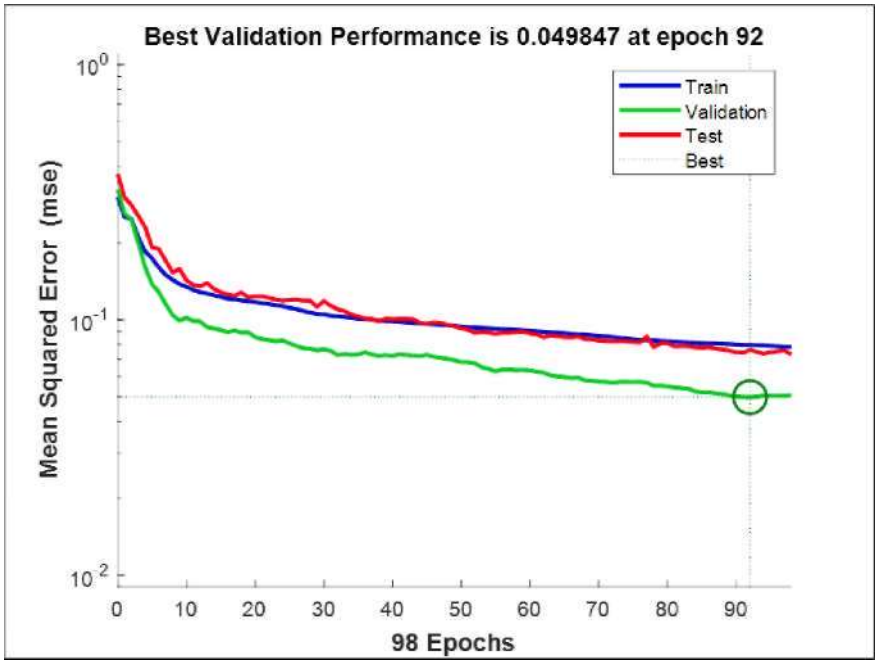

Figure 4.46 Training, Validation, and Testing Mean Squared Error (MSE) Versus Epochs For the LM-based ANN Classifier (X-band)

Overall, the LM algorithm demonstrates excellent classification performance for the X-band dataset. The combined analysis of confusion matrices, class specific performance metrics for the training convergence behaviour together with the lowest MSE value confirms that the LM-based ANN classifier provides an accurate, stable and well generalized solution for slot size classification in the X-band frequency range.

4.4.4.2 Classification of X-band Using the Resilient Backpropagation (RBP) Algorithm

Table 4.52 presents the classification results of the training, validation and testing datasets using the Resilient Backpropagation (RBP) algorithm for the X-band dataset under different hidden neuron configurations. Overall, the RBP-based ANN demonstrates strong and consistent classification capability across the training, validation and testing datasets. The training accuracy ranges from 86.7% to100%, validation accuracy varied from 95.5% to 100% and testing accuracy ranged from 82% to 100%, indicating reliable generalization behaviour across network configurations.

The optimal model configuration is obtained with five hidden neurons, achieving perfect classification accuracy (100%) for the training, validation and testing datasets while also recorded the lowest mean squared error (MSE) of 0.0275. This

configuration is therefore selected for detailed analysis, as it combines maximum classification accuracy with superior numerical stability. The results shows the effectiveness of the RBP algorithm in modelling the nonlinear absorption characteristics of the X-band dataset and accurately distinguishing slot size categories.

Table 4.52
Classification Accuracy and MSE Values for RBP Algorithm (X-Band)

Hidden Neuron	**Accuracy (%)**			**MSE Value**
	Training	**Validation**	**Testing**	
1	100	100	100	0.1011
2	100	100	100	0.0562
3	100	100	100	0.0506
4	100	100	100	0.0543
*5	100	100	100	0.0275
6	100	100	100	0.1348
7	86.7	95.5	82	0.0355
8	100	100	100	0.0936
9	95.4	95.5	96.6	0.0543
10	100	100	100	0.0533

*Best hidden neuron in RBP

To further examine class-wise prediction behaviour, confusion matrix analysis is performed for the optimal RBP configuration, as shown in Figure 4.47. The confusion matrices for the training, validation, testing and overall datasets exhibit perfectly diagonal structures, with all samples correctly classified into their respective slot size categories (small, medium, and big). The absence of misclassification confirms well-defined decision boundaries and robust learning behaviour of the RBP-based ANN classifier for the X-band dataset.

Figure 4.47 Confusion Matrices For X-band Slot Size Classification Using the RBP Algorithm: (a) Training, (b) Validation, (c) Testing, (d) Overall

Based on the confusion matrix results, class-specific performance metrics are computed and summarized in Table 4.53. The RBP classifier achieves 100% precision, recall and F1-score for all three slot size classes, indicating balanced and unbiased classification performance across categories.

Table 4.53
Class-Wise Classification Performance Metrics for X-Band using the RBP Algorithm (5 Hidden Neurons)

Slot Size	**Precision (%)**	**Recall (%)**	**F1-Score (%)**
Small	100	100	100
Medium	100	100	100
Big	100	100	100

While Table 4.53 presents the class-wise classification behaviour, the overall performance of the RBP-based classifier is summarized in Table 4.54. The model achieves 100% overall accuracy, sensitivity, specificity and precision, confirming its reliability and consistency for X-band slot size classification.

Table 4.54
Overall Classification Performance Metrics for X-Band using the RBP Algorithm (5 Hidden Neurons)

Performance Metric	Percentage (%)
Accuracy	100
Sensitivity	100
Specificity	100
Precision	100

Note: Metrics are based on the best hidden neuron configuration (HN=5).

The training convergence behaviour of the RBP-based ANN classifier is illustrated in Figure 4.48. The MSE decreases rapidly during the early training phase, indicating effective learning of class-discriminative features. As training progresses, the reduction in becomes more gradual and stabilizes toward later epochs. The validation curve closely follows the training trend without noticeable divergence, suggesting stable generalization perfromance and the absence of overfitting.

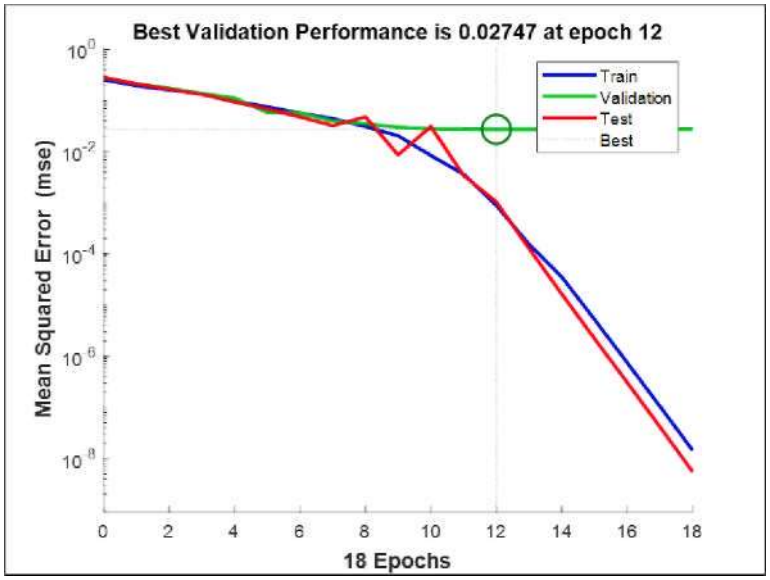

Figure 4.48 Training, Validation, and Testing Mean Squared Error (MSE) Versus Epochs For the RBP-based ANN Classifier (X-band)

Overall, the RBP algorithm demonstrates excellent classification performance for the X-band dataset. The combined analysis of classification accuracy, confusion matrices, class specific performance metrics and training convergence behaviour

confirms that the RBP-based ANN classifier provides an accurate, stable and well generalized solution for slot size classification for X-band slot size classification.

4.4.4.3 Classification of X-band Using the Scaled-Conjugate Gradient (SCG) Algorithm

Table 4.55 shows the classification results for training, validation and testing datasets using the Scaled-Conjugate Gradient (SCG) algorithm for different hidden neuron configurations in the X-band classification task. Overall, the SCG-based ANN demonstrates competitive classification performance, with training accuracy ranging from 83.6% to 100%, validation accuracy between 87.6% and100% and testing accuracy from 88.8% to 100%, indicating reliable generalization behaviour across different network configurations. The optimal configuration was achieved using three hidden neurons, which produced 100% classification accuracy for the training, validation, and testing datasets while exhibiting stable convergence behaviour with a mean squared error (MSE) value of 0.0625. This configuration was therefore selected for detailed evaluation.

Table 4.55
Classification Accuracy and MSE Values for SCG Algorithm (X-Band)

Hidden Neuron	**Accuracy (%)**			**MSE Value**
	Training	**Validation**	**Testing**	
1	100	100	100	0.1273
2	100	100	100	0.1311
*3	100	100	100	0.0625
4	84.8	87.6	93.3	0.0674
5	100	100	100	0.1161
6	100	100	100	0.1124
7	83.6	94.4	88.8	0.0599
8	100	100	100	0.1161
9	100	100	100	0.1011
10	95.2	97.8	97.8	0.0505

*Best hidden neuron in SCG

To examine class-wise prediction behaviour, confusion matrix analysis was performed for the optimal SCG configuration, as shown in Figure 4.49. The confusion matrices for the training, validation, testing and overall datasets show a perfectly diagonal structure, where all samples were correctly classified into their respective slot size categories (small, medium, and big), with no misclassification observed. This confirms excellent class separability for the X-band dataset using the SCG-based classifier.

Figure 4.49 Confusion Matrices For X-band Slot Size Classification Using the SCG Algorithm: (a) Training, (b) Validation, (c) Testing, (d) Overall

Based on the confusion matrix results, class-specific performance metrics are computed and summarized in Table 4.56. The SCG classifier achieves 100% precision, recall and F1-score for all three slot size classes, indicating balanced and unbiased classification performance across classes.

Table 4.56
Class-Wise Classification Performance Metrics for X-Band using the SCG Algorithm (3 Hidden Neuron)

Slot Size	Precision (%)	Recall (%)	F1-Score (%)
Small	100	100	100
Medium	100	100	100
Big	100	100	100

While Table 4.56 presents the class-wise classification behaviour, the overall performance of the SCG-based classifier is summarized in Table 4.57. The model achieves 100% overall accuracy, sensitivity, specificity and precision, confirming its reliability and consistency for X-band slot size classification.

Table 4.57
Overall Classification Performance Metrics for X-Band using the SCG Algorithm (3 Hidden Neurons)

Performance Metric	Percentage (%)
Accuracy	100
Sensitivity	100
Specificity	100
Precision	100

Note: Metrics are based on the best hidden neuron configuration (HN=3).

The training convergence behaviour of the SCG-based ANN classifier is illustrated in Figure 4.50, which presents the training, validation, and testing mean squared error (MSE) curves plotted against the number of epochs. The MSE decreases progressively during the training, and the validation curve closely follows the training trend without significant divergence. The best validation performance is achieved at approximately epoch 19, after which the curves stabilize, suggesting that overfitting does not occur.

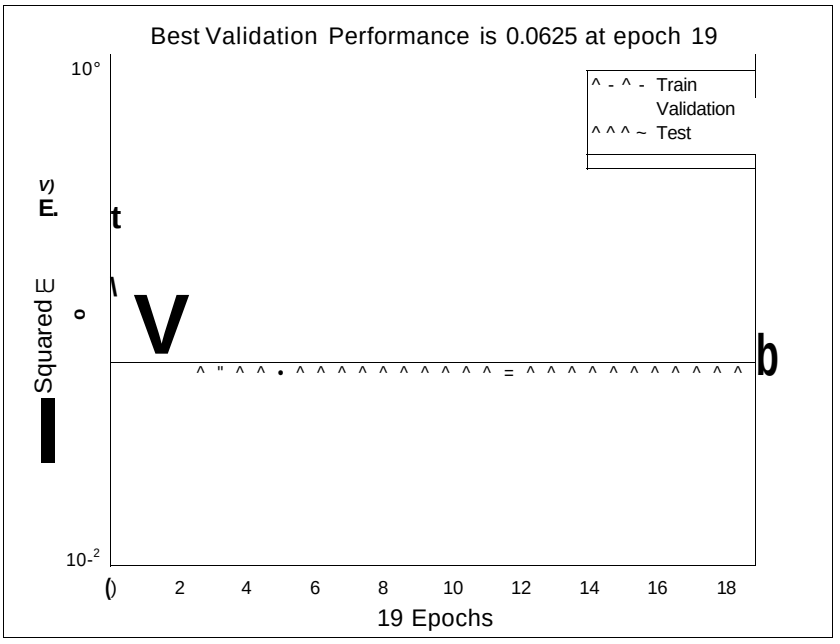

Figure 4.50 Training, Validation, and Testing Mean Squared Error (MSE) Versus Epochs For the SCG-based ANN Classifier (X-band)

Overall, the SCG algorithm demonstrates excellent classification performance for the X-band dataset. The combined analysis of classification accuracy, confusion matrices, class specific performance metrics and training convergence behaviour confirms that the SCG-based ANN classifier also provides an accurate, stable and well generalized solution for slot size classification in the X-band frequency range.

*4.4.4.4 Comparison **of the MLP Algorithms for X-Band***

Table 4.58 summarizes the optimal configurations and overall classification performance of the three MLP training algorithms applied to X-band slot size classification. All evaluated algorithms achieved perfect classification accuracy (100%) across the training, validation and testing datasets, indicating that the X-band dataset is highly separable and can be effectively modelled using different MLP training strategies. Among the three algorithms, the Resilient Backpropagation (RBP) algorithm with five hidden neurons recorded the lowest mean squared error (MSE) value of 0.0275, indicating reduced prediction error and improved numerical stability compared to the Levenberg-Marquardt (LM) and Scaled-Conjugate Gradient (SCG) algorithms, which recorded MSE values of 0.0498 and 0.0625, respectively.

Table 4.58
Summary of Best Hidden Neuron Configurations for Each MLP Algorithm (X-Band)

Training Algorithm	Hidden Neuron	Accuracy (%)			MSE Value
		Training	Validation	Testing	
Levenberg Marquardt (LM)	4	100	100	100	0.0498
*Resilient Backpropagation (RB)	5	100	100	100	0.0275
Scaled-Conjugate Gradient (SCG)	3	100	100	100	0.0625

*Best hidden neuron

To further clarify class-wise behaviour, slot size-based classification performance for each algorithm is presented in Table 4.59, derived from the corresponding confusion matrices.

Table 4.59
Slot Size-Based Classification Performance (Recall) for X-Band using Different ANN Training Algorithms

Slot Size	LM (%)	RBP (%)	SCG (%)
Small	100	100	100
Medium	100	100	100
Big	100	100	100

Note: Slot-size-based performance is reported using recall (sensitivity), which quantifies the proportion of correctly classified samples for each slot size.

As shown in Table 4.59, all three ANN training algorithms achieved perfect recall across all slot size categories, confirming that the small, medium and big slot sizes are clearly separable in the X-band frequency range. This consistent class-wise performance further demonstrates the robustness of the ANN-based classifiers for X-band slot size identification. While all algorithms performed equally well in terms of classification accuracy, the lower MSE obtained using the RBP algorithm suggests a more efficient learning process and superior numerical stability for this dataset.

4.4.4.5 Performance Evaluation of the MLP Algorithms for X-Band

Table 4.60 and Figure 4.51 present a comparative evaluation of the ANN classifiers based on overall accuracy, precision, sensitivity and specificity for X-band slot size classification. All three MLP training algorithms: Levenberg-Marquardt (LM), Resilient Backpropagation (RBP) and Scaled-Conjugate Gradient (SCG) achieved 100% across all evaluation metrics, indicating excellent and equivalent classification capability for the X-band dataset.

Table 4.60
Performance Evaluation of MLP Algorithms for X-Band

Training Algorithm	**Hidden Neuron**	**Accuracy (%)**	**Precision (%)**	**Sensitivity (%)**	**Specificity (%)**
Levenberg Marquardt (LM)	4	100	100	100	100
*Resilient Backpropagation (RB)	5	100	100	100	100
Scaled-Conjugate Gradient (SCG)	3	100	100	100	100

*all algorithms achieved perfect classification performance, RBP recorded the lowest MSE (0.0275)

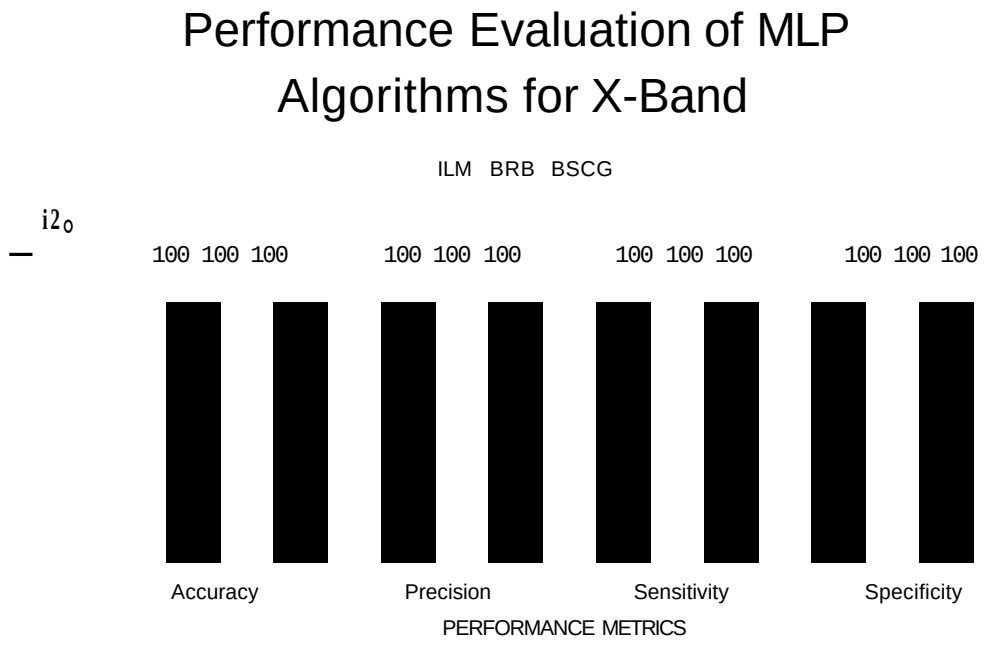

Figure 4.51 Comparative Performance Evaluation of MLP Algorithms for X-Band

Figure 4.51 illustrates the comparative performance of the MLP algorithms for the X-band, further confirming that all classifiers exhibit identical overall classification effectiveness. These results demonstrate that the X-band slot size classification problem is highly separable, enabling all three ANN training algorithms to learn the underlying decision boundaries effectively. Although classification performance is equivalent across algorithms in terms of accuracy and class-wise discrimination, differences in MSE values indicates variations in convergence efficiency. In particular, the RBP algorithm achieved the lowest MSE, suggesting more efficient learning and improved numerically stability for the X-band dataset.

4.5 Summary

This chapter presented a comprehensive analysis of Artificial Neural Networks (ANN) techniques for modelling and classifying the absorption performance of eco-friendly microwave absorbers. A total of 1206 experimental absorption measurements were initially collected and subjected to systematic data pre-processing. Outlier detection using boxplot analysis and Min-Max normalization resulted in a refined dataset of 1156 high-quality samples, covering three absorber geometries (small, medium, and big slots) across four frequency bands (L, S, C, and X).

To address the first research objective, regression analysis was conducted to investigate the relationship between frequency, slot size, and absorption performance. Linear regression was employed as a baseline model and exhibited limited predictive capability due to the nonlinear nature of the dataset. In contrast, ANN-based regression models demonstrated improved performance, confirming the suitability of ANN architectures for capturing complex nonlinear absorption behaviour. This regression analysis served to validate the modelling approach and provided insight into the underlying data characteristics rather than acting as an input stage for the classification task.

The second research objective, which focused on slot-size classification, was achieved through a detailed comparison of ANN classifiers trained using Levenberg-Marquardt (LM), Resilient Backpropagation (RBP) and Scaled Conjugate Gradient (SCG) algorithms. Classification performance was systematically evaluated using accuracy, precision, sensitivity, specificity, and mean squared error (MSE) across all frequency bands. For the L-band dataset, the LM algorithm achieved the best

performance with perfect classification accuracy and the lowest MSE. For the S-band, C-band, and X-band datasets, all three algorithms attained 100% classification accuracy; however, the RBP algorithm consistently recorded the lowest MSE values, indicating superior convergence efficiency and numerical stability.

Notably, Classification performance was systematically evaluated using accuracy, precision, sensitivity, specificity, and mean squared error (MSE) across all frequency bands. For the L-band dataset, the LM algorithm achieved the best performance with perfect classification accuracy and the lowest MSE. For the S-band, C-band, and X-band datasets, all three algorithms attained 100% classification accuracy; however, the RBP algorithm consistently recorded the lowest MSE values, indicating superior convergence efficiency and numerical stability.

Overall, these results of this chapter confirm that all research objectives were successfully achieved. The integration of rigorous data pre-processing with ANN-based regression and classification models provides a reliable and effective framework for analysing eco-friendly microwave absorbers across multiband frequencies. The consistently high classification performance demonstrates the potential of the proposed approach for practical RF applications, particularly in the development of sustainable and high-performance microwave absorbing materials.

CHAPTER 5
CONCLUSION AND RECOMMENDATION FOR FUTURE WORK

5.1 Conclusions

This study has successfully achieved its research objectives by establishing a unified Artificial Neural Network (ANN)-based modelling framework for predicting and classifying the absorption performance of eco-friendly microwave absorbers. The work addresses the inherent complexity and nonlinearity of electromagnetic absorption behaviour through a structured, data-driven methodology that integrates data pre-processing, regression modelling, and classification analysis.

A robust dataset comprising 1206 experimental measurements was systematically refined to 1156 high-quality samples using boxplot-based outlier removal and Min-Max normalization. This ensured reliable model training and evaluation across three slot sizes (small, medium, and big) and four microwave frequency bands (L, S, C, and X). This preprocessing stage directly supported the first research objective by improving data consistency and modelling reliability.

To evaluate predictive capability, linear regression and ANN-based regression were comparatively assessed. Linear regression exhibited limited performance, particularly in the L and C bands, confirming its inadequacy for modelling complex absorption behaviour. In contrast, ANN-based regression models demonstrated excellent predictive accuracy across all slot sizes, with strong correlations between predicted and measured values and consistently low validation errors. These findings confirm the effectiveness of ANN regression in capturing nonlinear absorption trends, thereby fulfilling the second research objective.

Building upon the regression outcomes, ANN-based classification models were implemented using Levenberg-Marquardt (LM), Resilient Backpropagation (RBP), and Scaled Conjugate Gradient (SCG) algorithms. All models achieved high classification accuracy; however, the RBP algorithm consistently demonstrated superior convergence behaviour and lower error across most frequency bands, particularly in the S, C, and X-bands. This validates the third research objective by identifying an optimal ANN configuration for multiband absorber classification.

The key contribution of this research lies in the novel integration of ANN-based regression and classification within a single modelling framework for eco-friendly microwave absorbers, an area that remains underexplored in existing literature. Unlike conventional studies that focus solely on material characterization or single-task prediction, this work introduces a comprehensive and scalable approach that enhances both predictive accuracy and interpretability across multiband frequencies.

In conclusion, the findings demonstrate that ANN-based modelling especially using RBP algorithm provides a reliable and efficient tool for characterizing the absorption performance of sustainable microwave absorbers. The proposed framework offers significant scientific value by supporting AI-driven material analysis and establishes a foundation for future research in intelligent electromagnetic absorber design and performance evaluation.

5.2 Recommendations for Future Work

While this study successfully demonstrated the effectiveness of ANN models for classifying eco-friendly microwave absorbers, several promising directions emerge for extending this research. First, the parameter space may be expanded beyond single-slot size absorber configurations to include additional critical variables such as material composition ratios, multilayer thickness variations and alternative geometric structures like fractal or honeycomb designs. Incorporating these factors through advanced manufacturing techniques could yield more comprehensive design guidelines while maintaining the sustainability focus.

The modelling approach itself could benefit from deeper feature integration, including the fusion of multiple data sources or multi-objective modelling through next-generation machine learning techniques. Particularly valuable would-be developing hybrid or ensemble approaches such as combining ANN with decision trees, support vector machines or optimization algorithms may further improve accuracy and robustness.

Experimental validation represents another crucial frontier. Future work should progress beyond simulation to include fabricated prototype testing in controlled anechoic chambers, with particular focus on the excellent S-band configurations identified in this study. For practical deployment, implementing these models in real-

time adaptive systems using FPGA hardware could enable dynamic tuning of absorbers in operational 5G environments.

Finally, the sustainability dimension should be further developed through comprehensive lifecycle analyses quantifying the carbon footprint reduction and cost savings compared to conventional absorbers. Complementary studies could map agricultural waste supply chains to assess scalability for industrial production. Together, these advancements would transform the current predictive framework into a complete platform for sustainable EMI solution development, aligning with global initiatives for greener wireless infrastructure while addressing both technical and environmental challenges in the field.

REFERENCES

[1] A. H. Hassan Nornikman, Mohd Fareq Bin Abd Malek, Ping Jack Soh, Azremi Abdullah Al-Hadi, Fwen Hoon Wee, "Parametric Study of Pyramidal Microwave Absorber Using Rice Husk," *Prog. Electromagn. Res.,* vol. 104, pp. 145-166, 2010, doi: 10.2528/PIER10041003.

[2] A. Arya and G. V. V. Sharma, "Prediction of material composition for microwave absorption through mathematical modelling," *J. Phys. Commun.,* vol. 5, no. 12, 2021, doi: 10.1088/2399-6528/ac37a7.

[3] D. Zhang *etal,* "The simulation design of microwave absorption performance for the multi-layered carbon-based nanocomposites using intelligent optimization algorithm," *Nanomaterials,* vol. 11, no. 8, 2021, doi: 10.3390/nanol 1081951.

[4] H. Mouna, V. Mekaladevi, and M. Nirmala Devi, "Design of microwave absorbers using improvised particle swarm optimization algorithm," *J. Microwaves, Optoelectron. Electromagn. Appl,* vol. 17, no. 2, pp. 188-200, 2018, doi: 10.1590/2179-10742018vl7i2836.

[5] M. Najim, S. Puthucheri, V. Agarwala, and D. Singh, "ANN-Based Two-Layer Absorber Design Using Fe-Al Hybrid Nano-Composites for Broad Bandwidth Microwave Absorption," *IEEE Trans. Magn.,* vol. 52, no. 12, pp. 1-8, 2016, doi: 10.1109/TMAG.2016.2598530.

[6] H. I. On, L. Jeong, M. Jung, D. J. Kang, J. H. Park, and H. J. Lee, "Optimal design of microwave absorber using novel variational autoencoder from a latent space search strategy," *Mater. Des.,* vol. 212, p. 110266, 2021, doi: 10.1016/j.matdes.2021.110266.

[7] E. M. Tentzeris, R. L. Robertson, J. F. Harvey, and L. P. B. Katehi, "PML absorbing boundary conditions for the characterization of open microwave circuit components using multiresolution time-domain techniques (MRTD)," *IEEE Trans. Antennas Propag.,* vol. 47, no. 11, pp. 1709-1715, 1999, doi: 10.1109/8.814951.

[8] G. Erboz, "How To Define Industry 4.0: Main Pillars Of Industry 4.0," *Manag Trends Dev. Enterp. Glob. Era,* no. November, pp. 761-767, 2017, [Online]. Available: https://www.researchgate.net/publication/326557388

[9] M. Gundall *et al,* "5G as Enabler for Industrie 4.0 Use Cases: Challenges and

Concepts," *IEEE Int. Conf. Enterg. Technol. Fact. Autom. ETFA*, vol. 2018-Septe, pp. 1401-1408, 2018, doi: 10.1109/ETFA.2018.8502649.

[10] A. B. Miller *et ah*, "Risks to Health and Well-Being From Radio-Frequency Radiation Emitted by Cell Phones and Other Wireless Devices," *Front Public Heal*, vol. 7, no. 223, 2019, doi: 10.3389/fpubh.2019.00223.

[11] R. Jan and G.M. Amanbaeva, "Electromagnetic Waves and Human health," *EurasianMedical Journal*, no. 1, Oct. 2020.

[12] F. Ozdemir and A. Kargi, "Electromagnetic Waves and Human Health," in *Electromagnetic Waves*, InTech, 2011, pp. 473-492.

[13] N. H. Narudin *et ah*, "The study of innovative anti-microwave brick walls by using POFA as partial cement replacement," *Mater. Today Proc*, vol. 48, pp. 1947-1952, 2021, doi: 10.1016/j.matpr.2021.11.149.

[14] L. M. Kasim *et ah*, "A Study of Electromagnetic Absorption Performance of Modern Biomass Wall Tile," *Int. J. Electr. Electron. Eng. Telecommun.*, vol. 9, no. 6, pp. 429-433, 2020, doi: 10.18178/IJEETC.9.6.429-433.

[15] N. M. Noor *et ah*, "Innovative Kenaf-Brick Composite for Effective Microwave Absorption," *14th IEEE Int. Conf. Control Syst. Comput. Eng. ICCSCE 2024 - Proc*, pp. 271-275, 2024, doi: 10.1109/ICCSCE61582.2024.10696576.

[16] A. Ahmad, H. Bin Abdullah, L. M. Kasim, N. A. Ismail, N. M. Noor, and N. M. Kasim, "A study of carbon coated flat stick bamboo microwave absorber performance," *Int. J. Electr. Electron. Eng. Telecommun.*, vol. 9, no. 5, pp. 331-336, 2020, doi: 10.18178/ijeetc.9.5.331-336.

[17] N. Ismail, M. H. F. Rahiman, M. N. Taib, N. A. M. Ali, M. Jamil, and S. N. Tajuddin, "Application of ANN in agarwood oil grade classification," *Proc. - 2014 IEEE 10th Int. Colloq. Signal Process. Its Appl. CSPA 2014*, pp. 216-220, 2014, doi: 10.1109/CSPA.2014.6805751.

[18] J. Kabuba, "Comparison between Neural Network Technique and Mathematical Modelling of Steam Extraction of Essential Oil," in *Proc. 9th Int. Conf. Advances in Science, Engineering, Technology & Waste Management (ASETWM-17)*, Paris, France, Nov. 27-28, 2017, doi: 10.17758/eares.eapl 117055.

[19] K. Pimparkar, R. Lulla, P. Rathod, V. Anirudh, and S. G. Dedgaonkar, "Document Management using Artificial Neural Network," *Proc. 4th Int. Conf. Commun. Electron. Syst. ICCES 2019*, no. Icces, pp. 897-900, 2019, doi: 10.1109/ICCES45898.2019.9002062.

[20] M. Agatonovic, Z. Marinkovic, and V. Markovic, "Modeling of microwave pyramidal absorbers using artificial neural networks," *2011 19th Telecommun. Forum, TELFOR 2011 - Proc. Pap.*, pp. 1012-1015, 2011, doi: 10.1109/TELFOR.2011.6143719.

[21] A. Arya and G. V. V Sharma, "Prototype for a Hybrid AI and ML based Model for efficient prediction of a Microwave Absorber," *IV.INTERNATIONAL ICONTECH Symp. Innov. Surv. Posit. Sci.*, 2021.

[22] M. I. Fazin, "Rectangular Slot Array On Biomass Hollow Pyramidal Microwave Absorber," PhD Dissertation, College of Engineering, Universiti Teknologi MARA, 2022.

[23] M. Fathi, S. Azis, I. Ismail, and F. Diana, "A review on electromagnetic microwave absorption properties : their materials and performance," *J. Mater. Res. TechnoL*, vol. 20, pp. 2188-2220, 2022, doi: 10.1016/j.jmrt.2022.07.140.

[24] A. Hasnain, B. M. Hafiz, M. I. Imran, A. A. Takiyuddin, A. Rusnani, and O. M. Khusairi, "Development of an Economic and Effective Microwave Absorber," in *2007 Asia-Pasific Conference on Applied Electromagnetics Proceedings*, 2007, pp. 1-5.

[25] H. Abdullah *et ah*, "Development of an Indigenous Microwave Absorber," *J. Telecommun. Electron. Comput. Eng.*, vol. 1, no. 1, pp. 17-24, 2009.

[26] H. Nornikman, P. J. Soh, A. A. Al-Hadi, and N. R. M. Husna, "Parametric Study of a Pyramidal Microwave Absorber Design," in *Conference: Antennas and Propagation*, 2008.

[27] C. L. Holloway *et ah*, "Comparison of Electromagnetic Absorber Used in Anechoic and Semi-Anechoic Chambers for Emissions and Immunity Testing of Digital Devices," *IEEE Trans. Electromagn. Compat*, vol. 39, no. 1, pp. 33-47, 1997.

[28] W. H. Emerson, "Electromagnetic Wave Absorbers and Anechoic Chambers Through the Years," *IEEE Trans. Electromagn. Compat*, no. 4, 1973.

[29] H. Nornikman, P. J. Soh, A. A. H. Azremi, F. H. Wee, and M. F. Malek, "Investigation of an Agricultural Waste as an Alternative Material for Microwave Absorbers," *PIERS ONLINE*, vol. 5, pp. 3-7, 2009.

[30] R. Kaur, G. D. Aul, and V. Chawla, "Improved Reflection Loss Performance of Dried Banana Leaves Pyramidal Microwave Absorbers by Coal for Application in Anechoic Chambers," *Prog. Electromagn. Res. M*, vol. 43, no. September, pp.

157-164,2015.

[31] N. S. Rosli *etal,* "Pyramidal microwave absorbers: leveraging ceramic materials for improved electromagnetic interference shielding," *Int. J. Electr. Comput. Eng., vol* 15, no. 1, pp. 435-447, 2025, doi: 10.11591/ijece.vl5il.pp435-447.

[32] H. Sun *et al,* "Broadband and High-Efficiency Microwave Absorbers Based on Pyramid Structure," *ACS Appl. Mater. Interfaces,* vol. 14, no. 46, pp. 52182-52192, 2022, doi: 10.1021/acsami.2cl6166.

[33] M. I. Fazin *et al,* "Absorption Performance of Biomass Hollow Pyramidal Microwave Absorber Using Multi-Slot Array Technique," *Indones. J. Electr. Eng. Comput. Set,* vol. 26, no. 2, p. 895, 2022, doi: 10.11591/ijeecs.v26.i2.pp895-902.

[3 4] ETS-Lindgren, *HP High Power Microwave Absorber,* datasheet, ET S-Lindgren, Cedar Park, TX, USA, Apr. 2018.

[35] TDK Corporation, *Radio Wave Absorbers for Microwave Anechoic Chambers (ISMaterial),* product datasheet, TDK Corp., Tokyo, Japan, Nov. 2023.

[36] E&C Anechoic Chambers nv, *WAVASORB® VHP: Advanced Broadband Pyramidal Absorber,* product datasheet, Westerlo, Belgium, Mar. 2024.

[37] H. N. Zhang, Z. F. Zhang, Y. Du, W. Kong, Y. Xiao, and Z. Q. Fang, "Design of multilayer wideband microwave absorbers using improved grey wolf optimizer," *Applied Computational Electromagnetics Society Journal,* vol. 39, no. 1, 2024, doi: 10.13052/2023.aces.j.380913.

[38] A. E. Assal, H. Breiss, R. Benzerga, and A. Sharaiha, "Design and Optimization of Ultra-Wideband Planar Multilayer Absorber Based on Long-Carbon Fiber-Loaded Composites," *J.Mater. Sci.,* vol. 56, no. 35, pp. 19484-19500,2021, doi: 10.1007/sl0853-021-06453-5.

[39] K. Li, X. Zhang, X. Hou, and P. Zhang, "Analysis and design of multilayer Jaumann absorbers," *ICMTCE2011 - Proc. 2011 IEEE Int. Conf. Microw. Technol Comput. Electromagn.,* pp. 81-84, 2011, doi: 10.1109/ICMTCE.2011.5915168.

[40] N. K. Uluaydin, S. S. Seker, O. Cerezci, and A. Y. Citkaya, "Economic anechoic chamber materials with polyester acoustic sponge matrix," *Proc. 2015 Int. Conf. Electromagn. Adv. Appl. ICEAA 2015,* pp. 1292-1295, 2015, doi: 10.1109/ICEAA.2015.7297325.

[41] S. Emc, "Pyramidal hybrid microwave absorber," product datasheet, S. EMC,

2019.

[42] M. I. Fazin *et al,* "Absorption performance of biomass hollow pyramidal microwave absorber using multi-slot array technique," *Indones. J. Electr. Eng. Comput. Set,* vol. 26, no. 2, pp. 895-902, 2022, doi: 10.11591/ijeecs.v26.i2.pp895-902.

[43] M. I. Fazin, H. A. Idris, M. F. Asmadi, A. R. Razali, N. M. Noor, and L. M. Kasim, "The Performance of Hollow Pyramidal Microwave Absorber Using Different Slot Size," *Solid State Phenom.,* vol. 344, pp. 103-108, 2023, doi: 10.4028/p-9cdm8n.

[44] M. Izzati *et al,* "Effect of Slot Array at Different Angles towards the Performance of Hollow Pyramidal Microwave Absorber," *Int. J. Emerg. Trends Eng. Res.,* vol. 8, no. 9, pp. 6306-6312, 2020, doi: 10.30534/ijeter/2020/224892020.

[45] H. A. Idris *et al,* "Slot Radial Array Design on Hollow Pyramidal Microwave Absorber," *Appl. Meek Mater.,* vol. 850, pp. 77-81, 2016, doi: 10.4028/www.scientific.net/amm.850.77.

[46] B. Li, B. Mao, T. He, H. Huang, and X. Wang, "Preparation and Microwave Absorption Properties of Double-Layer Hollow Reticulated SiC Foam," *Acs Appl. Electron. Mater.,* vol. 1, no. 10, pp. 2140-2149, 2019, doi: 10.1021/acsaelm.9b00510.

[47] P. Liu, S. Gao, G. Zhang, Y. Huang, W. You, and R. Che, "Hollow Engineering to Co@N-Doped Carbon Nanocages via Synergistic Protecting-Etching Strategy for Ultrahigh Microwave Absorption," *Adv. Funct. Mater.,* vol. 31, no. 27, p. 2102812, Jul. 2021, doi: https://doi.org/10.1002/adfm.202102812.

[48] and M. S. M. M. N. Iqbal, M. F. Malek, Y. S. Lee, L. Zahid, "study of the anechoic performance of rice husk-based, geometrically tapered, hollow absorbers," *Int. J. Antennas Propag,* vol. 2014, no. 2, pp. 1-9, 2014, doi: 10.1155/2014/498767.

[49] N. Mohamad Noor *et al.,* "The Impact Study of Anti-Radiation Biomass Material on Partition Wall Absorption Performance," *ESTEEM Acad. J.,* vol. 19, no. September, pp. 75-85, 2023, doi: 10.24191/esteem.vl9iseptember.23003.

[50] L. M. Kasim *et al,* "Microwave Absorption Performance of Multilayer Anti-Radiation Bricks for Sustainable Construction Materials," *14th IEEE Int. Conf. Control Syst. Comput. Eng. ICCSCE 2024 - Proc,* pp. 299-303, 2024, doi:

10.1109/ICCSCE61582.2024.10696070.

[51] L. Guo *et al*, "Constructing Stacked Structure of S-Doped Carbon Layer-Encapsulated M0O2 NPs With Dominated Dielectric Loss for Microwave Absorption," *Acs Sustain. Chem. Eng.*, vol. 7, no. 24, pp. 19546-19555, 2019, doi: 10.1021/acssuschemeng.9b04628.

[52] M. Mahmoodi, B. Aslibeiki, R. Peymanfar, and H. Naghshara, "Oleaster Seed-Derived Activated Carbon/Ferrite Nanocomposite for Microwave Absorption in the X-Band Range," *Front. Mater.*, vol. 9, 2022, doi: 10.3389/fmats.2022.1088196.

[53] M. F. Asmadi *et al*, "The Optimal Performance of a Geopolymer Hollow Pyramidal Microwave Absorber with Triangular Slotted," *Solid State Phenom.*, vol. 344, pp. 97-102, 2023, doi: 10.4028/p-belmea.

[54] B. Vagananthan, Y. S. Lee, K. Y. You, H.-S. Gan, and F. H. Wee, "Investigate the Effect of Dielectric Properties on Microwave Absorption of Pyramidal Microwave Absorber," *J. Microwaves Optoelectron. Electromagn. Appl*, vol. 21, no. 2, pp. 328-336, 2022, doi: 10.1590/2179-10742022v21i2257631.

[55] S. K. Singh, H. Prakash, M. J. Akhtar, and K. K. Kar, "Lightweight and High-Performance Microwave Absorbing Heteroatom-Doped Carbon Derived From Chicken Feather Fibers," *Acs Sustain. Chem. Eng.*, vol. 6, no. 4, pp. 5381-5393, 2018, doi: 10.1021/acssuschemeng.8b00183.

[56] IEEE Standard 1128-1998, *IEEE Recommended Practice for RF Absorber Evaluation in the Range of 30MHz to 5 GHz*, IEEE, New York, NY, USA, 1998.

[57] H. Abdullah *et al*, "Improvement study of the reflectivity for hollow pyramidal shape absorbers," *ISIEA 2014 - 2014IEEE Symp. Ind. Electron. Appl*, pp. 81-85, 2017, doi: 10.1109/ISIEA.2014.8049876.

[58] M. I. Fazin, A. Hasnain, A. R. Razali, M. N. Taib, and N. M. Noor, "Effect of Slot Array at Different Angles Towards the Performance of Hollow Pyramidal Microwave Absorber," *Int. J. Emerg. Trends Eng. Res.*, vol. 8, no. 9, pp. 6306-6312, 2020, doi: 10.30534/ijeter/2020/224892020.

[59] Y. S. Lee *et al*, "Enhanced Microwave Absorption of Rice Husk-based Pyramidal Microwave Absorber With Different Lossy Base Layer," *let Microwaves Antennas Propag.*, vol. 14, no. 3, pp. 215-222, 2020, doi: 10.1049/iet-map.2019.0571.

[60] B. Zhao *et al*, "Preparation of Honeycomb Sn02 Foams and Configuration-

Dependent Microwave Absorption Features," *ACS Appl. Mater. Interfaces,* vol. 7, no. 47, pp. 26217-26225, 2015, doi: 10.1021/acsami.5b08383.

[61] L. Wang *et al,* "The Effect of ZnCb Activation on Microwave Absorbing Performance in Walnut Shell-Derived Nano-Porous Carbon," *RSC Adv.,* vol. 9, no. 17, pp. 9718-9728, 2019, doi: 10.1039/c8ra09932d.

[62] S. Sharma, S. R. Parne, S. S. S. Panda, and S. Gandi, "Progress in microwave absorbing materials: A critical review," *Adv. Colloid Interface Sci.,* vol. 327, no. February, p. 103143, 2024, doi: 10.1016/j.cis.2024.103143.

[63] X. Luo, "A Comparison of Three Estimation Methods in Linear Regression Analysis," in *Proc. Int. Conf. Mechatronics, Manufacturing and Industrial Technology Applications,* 2016, doi: 10.2991/icmmita-16.2016.92.

[64] K. Qu, "Research on Linear Regression Algorithm," *Matec Web Conf,* vol. 395, p. 1046, 2024, doi: 10.1051/matecconf/202439501046.

[65] T. Gopalakrishnan, R. Choudhary, and S. Prasad, "Prediction of Sales Value in online shopping using Linear Regression," *2018 4th Int. Conf. Comput. Commun. Autom.,* pp. 1-6, 2018.

[66] K. Lee *etal.,* "Comparison and Analysis of Linear Regression & Artificial Neural Network," *Int. J. Appl. Eng. Res.,* vol. 12, no. 20, pp. 9820-9825, 2017.

[67] S. Sanyal, S. K. Biswas, D. Das, M. Chakraborty, and B. Purkayastha, "Boston House Price Prediction Using Regression Models," *2022 2nd Int. Conf. Intell. Techno!., pp.* 1-6, 2022, doi: 10.1109/CONIT55038.2022.9848309.

[68] M. S. Acharya, "A Comparison of Regression Models for Prediction of Graduate Admissions," *2019 Int. Conf. Comput. Intell. Data Sci.,* pp. 1-5, 2019.

[69] D. O. Sahin, S. Akleylek, and E. Kilic, "LinRegDroid : Detection of Android Malware Using Multiple Linear Regression Models-Based Classifiers," *IEEE Trans. Neural Networks Learn. Syst.,* vol. 31, no. 9, pp. 3269-3279, 2022.

[70] B. Warner and M. Misra, "Understanding Neural Networks as Statistical Tools," *Am. Stat.,* vol. 50, no. 4, pp. 284-293, 1996.

[71] S. Sonoda, Y. Takahashi, K. Kawagishi, N. Nishida, S. Wakao, and A. S. M. Regression, "Application of Stepwise Multiple Regression to Design Optimization of Electric Machine," *IEEE Trans. Magn.,* vol. 43, no. 4, pp. 1609-1612,2007.

[72] S. Shi, W. Zhe, W. Fei, and A. S. Duration, "Estimation of Solar Irradiation Based on Multiple Stepwise Regression," *2011 IEEE PES Innov. Smart Grid*

Technol,pp. 1-4, 2011, doi: 10.1109/ISGT-Asia.2011.6167101.

[73] M. Noryani, S. Mohd, M. Taha, M. Yusoff, M. Zuhri, and E. Syams, "Material selection of natural fibre using a stepwise regression model with error analysis," *J. Mater. Res. Technol,* vol. 8, no. 3, pp. 2865-2879, 2019, doi: 10.1016/j.jmrt.2019.02.019.

[74] M. Wang, J. Wright, A. Brownlee, and R. Buswell, "A comparison of approaches to stepwise regression on variables sensitivities in building simulation and analysis," *Energy Build.*, vol. 127, no. 313-326, 2016.

[75] M. Fraszczyk, "Expert-in-the-loop Stepwise Regression and its Application in Air Pollution Modeling," *2022 IEEE 11th Int. Conf. Intell. Syst.,* pp. 1-7, 2022, doi: 10.1109/IS57118.2022.10019609.

[76] P. Jain *et al,* "Machine Learning Techniques for Predicting Metamaterial Microwave Absorption Performance: A Comparison," *IEEE Access,* vol. 11, pp. 128774-128783, 2023, doi: 10.1109/ACCESS.2023.3332731.

[77] A. K. Jain, J. Mao, and K. M. Mohiuddin, "Artificial Neural Networks: A Tutorial," *Computer,* vol. 29, no. 3, pp. 31-44, 1996.

[78] N. Mohamad *et al,* "Comparison between Levenberg-Marquardt and Scaled Conjugate Gradient Training Algorithms for Breast Cancer Diagnosis using MLP," *2010 6th Int. Colloq. Signal Process, its Appl,* pp. 1-7, 2010, doi: 10.1109/CSPA.2010.5545325.

[79] M. Islam, G. Chen, and S. Jin, "An Overview of Neural Network," *Am. J. Neural Networks Appl,* vol. 5, no. 1, p. 7, 2019, doi: 10.11648/j.ajnna.20190501.12.

[80] J. T. Wei, Z. Zhang, S. D. Barnhill, K. R. Madyastha, H. Zhang, and J. E. Oesterling, "Understanding artificial neural networks and exploring their potential applications for the practicing urologist," *Urology,* vol. 52, no. 2, pp. 161-172, 1998, doi: https://doi.org/10.1016/S0090-4295(98)00181-2.

[81] W. Gerstner and W. M. T. A.-T. T.- Kistler, "Spiking neuron models : single neurons, populations, plasticity." Cambridge University Press, Cambridge, U.K., 2002. doi: LK -https://worldcat.org/title/57417395.

[82] Y. Yu, K. Adu, N. Tashi, P. Anokye, X. Wang, and M. A. Ayidzoe, "RMAF: Relu-Memristor-Like Activation Function for Deep Learning," *Ieee Access,* vol. 8, pp. 72727-72741, 2020, doi: 10.1109/access.2020.2987829.

[83] F. Godin, J. Degrave, J. Dambre, and W. De Neve, "Dual Rectified Linear Units (DReLUs): A Replacement for Tanh Activation Functions in Quasi-Recurrent

Neural Networks," *Pattern Recognit. Lett,* vol. 116, pp. 8-14, 2018, doi: 10.1016/j.patrec.2018.09.006.

[84] A. D. Jagtap, K. Kawaguchi, and G. E. Karniadakis, "Adaptive Activation Functions Accelerate Convergence in Deep and Physics-Informed Neural Networks," *J. Comput. Phys.,* vol. 404, p. 109136, 2020, doi: 10.1016/j.jcp.2019.109136.

[85] H. Wang and S. Smys, "Overview of Configuring Adaptive Activation Functions for Deep Neural Networks - A Comparative Study," *J. Ubiquitous Comput. Commun. Technol.,* vol. 3, no. 1, pp. 10-22, 2021, doi: 10.36548/jucct.2021.1.002.

[86] Q. Zheng, D. Tan, and F. Wang, "Improved Convolutional Neural Network Based on Fast Exponentially Linear Unit Activation Function," *Ieee Access,* vol. 7, pp. 151359-151367, 2019, doi: 10.1109/access.2019.2948112.

[87] M. Y. Javed, I. A. Khurshid, A. B. Asghar, S. T. H. Rizvi, S. Kamal, and K. Ej smont, "An Efficient Estimation of Wind Turbine Output Power Using Neural Networks," *Energies,* vol. 15, no. 14, p. 5210, 2022, doi: 10.3390/enl5145210.

[88] S.-Y. Hwang and J.-J. Kim, "A Universal Activation Function for Deep Learning," *Comput. Mater. Contin.,* vol. 75, no. 2, pp. 3553-3569, 2023, doi: 10.32604/cmc.2023.037028.

[89] A. A. Alkhouly, A. Mohammed, and H. A. Hefny, "Improving the Performance of Deep Neural Networks Using Two Proposed Activation Functions," *Ieee Access,* vol. 9, pp. 82249-82271, 2021, doi: 10.1109/access.2021.3085855.

[90] Y. Li, C. Fan, Y. Li, Q. Wu, and Y. Ming, "Improving Deep Neural Network With Multiple Parametric Exponential Linear Units," *Neurocomputing,* vol. 301, pp. 11-24, 2018, doi: 10.1016/j.neucom.2018.01.084.

[91] T. Szandala, "Review and Comparison of Commonly Used Activation Functions for Deep Neural Networks," in *Artificial Intelligence and Soft Computing,* Springer, 2020, doi: 10.1007/978-981-15-5495-711.

[92] S. Kihcarslan, K. Adem, and M. Celik, "An Overview of the Activation Functions Used in Deep Learning Algorithms," *J. New Results Sci.,* vol. 10, no. 3, pp. 75-88, 2021, doi: 10.54187/jnrs.l011739.

[93] M. Martinez-Gost, A. I. Perez-Neira, and M. A. Lagunas, "ENN: A Neural Network With DCT Adaptive Activation Functions," *IEEE J. Sel. Top. Signal Process.,* vol. 18, no. 2, pp. 232-241, 2024, doi: 10.1109/jstsp.2024.3361154.

[94] A. D. Jagtap, Y. Shin, K. Kawaguchi, and G. E. Karniadakis, "Deep Kronecker Neural Networks: A General Framework for Neural Networks With Adaptive Activation Functions," *arXiv preprint*, 2021, doi: 10.48550/arxiv.2105.09513.

[95] V. Kunc and J. Klema, "On Transformative Adaptive Activation Functions in Neural Networks for Gene Expression Inference," *PLoS One*, vol. 16, no. 1, p. e0243915, 2021, doi: 10.1371/journal.pone.0243915.

[96] S. A. Ebiaredoh-Mienye, E. Esenogho, and T. G. Swart, "Integrating Enhanced Sparse Autoencoder-Based Artificial Neural Network Technique and Softmax Regression for Medical Diagnosis," *Electronics*, vol. 9, no. 11, p. 1963, 2020, doi: 10.3390/electronics9111963.

[97] A. Meilan-Vila, M. Francisco-Fernandez, R. M. Crujeiras, and A. Panzera, "Nonparametric Regression Estimation for Circular Data," *Proceedings*, vol. 21, no. 2, p. 27, 2019, doi: 10.3390/proceedings2019021027.

[98] I. Kalogridis and S. Van Aelst, "Robust Functional Regression Based on Principal Components," *J. Multivar. Anal*, vol. 173, pp. 393-415, 2019, doi: 10.1016/j.jmva.2019.04.003.

[99] X. Sun, P. Du, X. Wang, and P. Ma, "Optimal Penalized Function-on-Function Regression Under a Reproducing Kernel Hilbert Space Framework," *J. Am. Stat. Assoc*, vol. 113, no. 524, pp. 1601-1611, 2018, doi: 10.1080/01621459.2017.1356320.

[100] A. Fermanian, "Functional Linear Regression With Truncated Signatures," *arXiv preprint* ,2020, doi: 10.48550/arxiv.2006.08442.

[101] A. Rabiee Kenaree and S. Fatemi, "Application of Artificial Neural Network in Simulation of Supercritical Extraction of Valerenic Acid from Valeriana officinalis L.," *ISRN Chem. Eng.*, vol. 2012, Dec. 2012, doi: 10.5402/2012/572421.

[102] H. Demuth, Mark Beale, and M. Hagan, *Neural Network Toolbox™ User's Guide*, MathWorks Inc., Natick, MA, USA, 2014.

[103] D. Howard and B. Mark, "Neural Network Toolbox User's Guide," *The MathWorks*, p. 846, 2004.

[104] A. Hashemi Fath, F. Madanifar, and M. Abbasi, "Implementation of multilayer perceptron (MLP) and radial basis function (RBF) neural networks to predict solution gas-oil ratio of crude oil systems," *Petroleum*, vol. 6, no. 1, pp. 80-91, 2020, doi: 10.1016/j.petlm.2018.12.002.

[105] E.-H. A. Rady and A. S. Anwar, "Prediction of kidney disease stages using data mining algorithms," *Informatics Med. Unlocked*, vol. 15, p. 100178, 2019, doi: https://doi.Org/10.1016/j.imu.2019.100178.

[106] A. de Ramon-Fernandez, M. J. Salar-Garcia, D. R. Fernandez, J. Greenman, and I. Ieropoulos, "Evaluation of Artificial Neural Network Algorithms for Predicting the Effect of the Urine Flow Rate on the Power Performance of Microbial Fuel Cells," *Energy*, vol. 213, p. 118806, 2020, doi: 10.1016/j.energy.2020.118806.

[107] A. Moghadassi, S. M. Hosseini, F. Parvizian, I. Alhajri, and M. Talebbeigi, "Predicting the supercritical carbon dioxide extraction of oregano bract essential oil," *Songklanakarin J. Sci. Technol*, vol. 33, Sep. 2011.

[108] O. Kisi and E. Uncuoglu, "Comparison of three back-propagation training algorithms for two case studies," *Indian J. Eng. Mater. Sci.*, vol. 12, pp. 434-442,2005.

[109] N. Coskun and T. Yildirim, "The effects of training algorithms in MLP network on image classification," in *Proceedings of the International Joint Conference on Neural Networks, 2003.*, 2003, pp. 1223-1226 vol.2, doi: 10.1109/IJCNN.2003.1223867.

[110] H Z . Alemu, W. Wu, and J. Zhao, "Feedforward neural networks with a hidden layer regularization method," *Symmetry (Basel).*, vol. 10, no. 10, 2018, doi: 10.3390/syml0100525.

[Ill] F. S. Panchal and M. Panchal, "Reviews on Methods of Selecting Number of Hidden Nodes in Artificial Neural Network," *Int. J. Comput. Sci. Mob. Comput*, vol. 3, no. 11, pp. 455-464, 2014, [Online]. Available: www.ijcsmc.com

[112] Z. Qatawneh, M. Alshraideh, N. Almasri, L. Tahat, and A. Awidi, "Clinical Decision Support System for Venous Thromboembolism Risk Classification," *Appl. Comput. Informatics*, vol. 15, Sep. 2017, doi: 10.1016/j.aci.2017.09.003.

[113] K. Mansouri, F. Bahmanzadegan, and A. Ghaemi, "Evaluation of Hydrogen Production via Steam Reforming and Partial Oxidation of Dimethyl Ether Using Response Surface Methodology and Artificial Neural Network," *Sci. Rep.*, vol. 14, no. 1, 2024, doi: 10.1038/s41598-024-66402-5.

[114] S. M. Cabaneros, J. K. Calautit, and B. R. Hughes, "A Review of Artificial Neural Network Models for Ambient Air Pollution Prediction," *Environ. Model. Softw.*, vol. 119, pp. 285-304, 2019, doi: 10.1016/j.envsoft.2019.06.014.

[115] B. B. Bezabeh and A. D. Mengistu, "The Effects of Multiple Layers Feed-Forward Neural Network Transfer Function in Digital Based Ethiopian Soil Classification and Moisture Prediction," *Int. J. Electr. Comput. Eng.*, vol. 10, no. 4, p. 4073, 2020, doi: 10.11591/ijece.vl0i4.pp4073-4079.

[116] I. G. Kerdan and D. M. Galvez, "Artificial Neural Network Structure Optimisation for Accurately Prediction of Exergy, Comfort and Life Cycle Cost Performance of a Low Energy Building," *Appl. Energy*, vol. 280, p. 115862, 2020, doi: 10.1016/j.apenergy.2020.115862.

[117] N. S. A. Zubir *etal.*, "Analysis of algorithms variation in Multilayer Perceptron Neural Network for agarwood oil qualities classification," in *2017 IEEE 8th Control and System Graduate Research Colloquium (ICSGRC)*, 2017, pp. 122-126. doi: 10.1109/ICSGRC.2017.8070580.

[118] T. Vujicic, T. Matijevic, and Z. Sevarac, "Comparative Analysis of Methods for Determining Number of Hidden Neurons in Artificial Neural Network," *Cent. Eur. Conf. Inf. Intell. Syst.*, pp. 219-223, 2016.

[119] S. Syaharuddin, F. Fatmawati, and H. Suprajitno, "The Formula Study in Determining the Best Number of Neurons in Neural Network Backpropagation Architecture With Three Hidden Layers," *J. Resti (Rekayasa Sist. Dan Teknol. Informasi)*, vol. 6, no. 3, pp. 397-402, 2022, doi: 10.29207/resti.v6i3.4049.

[120] B. M. Hussein and S. M. Shareef, "An Empirical Study on the Correlation Between Early Stopping Patience and Epochs in Deep Learning," *Itm Web Conf.*, vol. 64, p. 1003, 2024, doi: 10.1051/itmconf/20246401003.

[121] H. Li, G K. Rajbahadur, D. Lin, C. Bezemer, and Z. M. Jiang, "Keeping Deep Learning Models in Check: A History-Based Approach to Mitigate Overfitting," *IeeeAccess,vol* 12, pp. 70676-70689,2024, doi: 10.1109/access.2024.3402543.

[122] T. Zoumpekas, M. Salamo, and A. Puig, "Effective Early Stopping Of Point Cloud Neural Networks," in *Proc. Int. Conf. Pattern Recognition Applications and Methods*, 2022, pp. 156-167, doi: 10.1007/978-3-031-13448-7_13.

[123] N. Shah and S. Jain, "Detection of Disease in Cotton Leaf using Artificial Neural Network," in *2019 Amity International Conference on Artificial Intelligence (AICAI)*, 2019, pp. 473-476. doi: 10.1109/AICAI.2019.8701311.

[124] C.-C. Peng, S.-H Wang, S.-J. Liu, Y.-K. Yang, and B.-H. Liao, "Artificial Neural Network Application to the Stroke Prediction," in *2020 IEEE 2nd Eurasia Conference on Biomedical Engineering, Healthcare and Sustainability*

(ECBIOS), 2020, pp. 130-133. doi: 10.1109/ECBIOS50299.2020.9203638.

[125] L. Hu, J. Zhang, Y. Xiang, and W. Wang, "Neural Networks-Based Aerodynamic Data Modeling: A Comprehensive Review," *Ieee Access*, vol. 8, pp. 90805-90823, 2020, doi: 10.1109/access.2020.2993562.

[126] P. Aghelpour and V. Varshavian, "Forecasting Different Types of Droughts Simultaneously Using Multivariate Standardized Precipitation Index (MSPI), MLP Neural Network, and Imperialistic Competitive Algorithm (ICA)," *Complexity*, vol. 2021, no. 1, 2021, doi: 10.1155/2021/6610228.

[127] M. Mustaqeem, S. Mustajab, and M. Alam, "A Hybrid Approach for Optimizing Software Defect Prediction Using A grey Wolf Optimization and Multilayer Perceptron," *Int. J. Intell. Comput. Cybern.*, vol. 17, no. 2, pp. 436-464, 2024, doi: 10.1108/ijicc-l 1-2023-0385.

[128] S. V. Raghav Dunga, Kumaran Rengaswamy, Jayaganthan Rengaswamy, Chitti Venkata Krishnamurthy, Ramanujam Sarathi, "Machine Learning-Based Design and Fabrication of Multilayered Microwave Absorber," *Polym. Adv. Technol*, vol. 36, no. 5, 2025, doi: https://doi.org/10.1002/pat.70222.

[129] X.-Y. Qi, L.-Y. Xiao, H. Lv, Y.-F. Liu, and W. Shao, "A machine learning-based inverse design method for frequency-selective surface microwave absorbers," *Eng. Appl. Artif. Intell*, vol. 160, p. 111842, 2025, doi: https://doi.Org/10.1016/j.engappai.2025.111842.

[130] Y. Benjamini, "Opening the Box of aBoxplot," *Am. Stat.*, vol. 42, no. 4, pp. 257-262, Jul. 1988, doi: 10.2307/2685133.

[131] A. Fitrianto, W. Z. A. Wan Muhamad, S. Kriswan, and B. Susetyo, "Comparing Outlier Detection Methods using Boxplot Generalized Extreme Studentized Deviate and Sequential Fences," *Acehlnt. J. Set Technol*, vol. 11, no. 1, pp. 38-45, 2022, doi: 10.13170/aijst.ll. 1.23809.

[132] Y. Jain, "Min Max Normalization Based Data Perturbation Method for Privacy Protection," *Int. J. Comput*, vol. 2, Jan. 2011, doi: 10.47893/IJCCT.2013.1201.

[133] A. Jain, K. Nandakumar, and A. Ross, "Score normalization in multimodal biometricsystems,"*Pattern Recognit*, vol. 38,no. 12,pp. 2270-2285,2005, doi: https://doi.Org/10.1016/j.patcog.2005.01.012.

[134] L. Al Shalabi and Z. Shaaban, "Normalization as a Preprocessing Engine for Data Mining and the Approach of Preference Matrix," *Proc. Int. Conf. Dependability Comput. Syst. DepCoS-RELCOMEX 2006*, pp. 207-214, 2006, doi:

10.1109/DEPCOS-RELCOMEX.2006.38.

[135] M. L. Walker, Y. H. Dovoedo, S. Chakraborti, and C. W. Hilton, "An Improved Boxplot for Univariate Data," *Am. Stat*, vol. 72, no. 4, pp. 348-353, Oct. 2018, doi: 10.1080/00031305.2018.1448891.

[136] K. Patil, N. K. Nagwani, and S. Tripathi, "A Parametric Study of Partitioning and Density Based Clustering Techniques for Boxplot Generation," in *2018 3rd International Conference for Convergence in Technology (I2CT)*, 2018, pp. 1-5. doi: 10.1109/I2CT.2018.8529468.

[137] B. I. Babura, M. B. Adam, A. R. Abdul Samad, A. Fitrianto, and B. Yusif, "Analysis and Assessment of Boxplot Characters for Extreme Data," *J. Phys. Conf Ser.*, vol. 1132, no. 1,2018, doi: 10.1088/1742-6596/1132/1/012078.

[138] D. C. Li, W. K. Huang, and Y. S. Lin, "New Product Short-Term Demands Forecasting with Boxplot-Based Fractional Grey Prediction Model," *Appl. Sci.*, vol. 12, no. 10, 2022, doi: 10.3390/appl2105131.

[139] J. Williams, R. R. Hill, J. J. Pignatiello Jr., and E. Chicken, "Wavelet analysis of variance box plot," *J. Appl. Stat.*, vol. 49, no. 14, pp. 3536-3563, Oct. 2022, doi: 10.1080/02664763.2021.1951685.

[140] A. H. 'Izzati H. Al-Hadi *etal*, "Boxplot analysis of 4 grade agarwood essential oil for various grades," *Indones. J. Electr. Eng. Comput. Sci.*, vol. 29, no. 1, pp. 238-244, 2023, doi: 10.11591/ijeecs.v29.il.pp238-244.

[141] M. Melo *etal*, "The impact of virtual reality and biological sex on the promotion of tourist destinations: effects on destination image, place attachment, and behavioural intention," *J. Hosp. Tour. Technol*, vol. 15, no. 1, pp. 18-36, 2024, doi: 10.1108/JHTT-01-2023-0015.

[142] D. A. Ayejoto, J. C. Agbasi, J. C. Egbueri, and S. I. Abba, "Evaluation of oral and dermal health risk exposures of contaminants in groundwater resources for nine age groups in two densely populated districts, Nigeria," *Heliyon*, vol. 9, no. 4, p. el5483, 2023, doi: 10.1016/j.heliyon.2023.el5483.

[143] D. Marczak, K. Lejcus, I. Lejcus, and J. Misiewicz, "Sustainable Innovation: Turning Waste Into Soil Additives," *Materials (Basel).*, vol. 16, no. 7, p. 2900, 2023, doi: 10.3390/mal6072900.

[144] A. I. S. Loureiro, C. P. Melo, and A. Bressane, "Descriptive Statistical Analysis of Noticed Green Areas Benefits for Human Health," *Research Square*, preprint, 2023, doi: 10.21203/rs.3.rs-2358836/vl.

[145] N. Wan Hisarudin Wan Abdullah *etal,* "Electromyography Indices of Handgrip Force With Swinging Motion," *J. Adv. Res. Appl. Sci. Eng. Technol.,* vol. 31, no. 3, pp. 126-136, 2023, doi: 10.37934/araset.31.3.126136.

[146] M. Nakao *etal,* "Empagliflozin Maintains Capillarization and Improves Cardiac Function in a Murine Model of Left Ventricular Pressure Overload," *Sci. Rep.,* vol. 11, no. 1,2021, doi: 10.1038/s41598-021-97787-2.

[147] W. Dai and M. G. Genton, "Functional Boxplots for Multivariate Curves," *Stat,* vol. 7, no. 1, 2018, doi: 10.1002/sta4.190.

[148] M. G. Genton and Y. Sun, "Functional Data Visualization," pp. 1-11, 2020, doi: 10.1002/9781118445112.stat08290.

[149] W. Dai and M. G. Genton, "Directional Outlyingness for Multivariate Functional Data," *Comput. Stat. Data Anal,* vol. 131, pp. 50-65, 2019, doi: 10.1016/j.csda.2018.03.017.

[150] W. Dai and M. G. Genton, "Multivariate Functional Data Visualization and Outlier Detection," *J. Comput. Graph. Stat,* vol. 27, no. 4, pp. 923-934, 2018, doi: 10.1080/10618600.2018.1473781.

[151] I. Martinez-Hernandez, M. G. Genton, and G. Gonzalez-Farias, "Robust Depth-Based Estimation of the Functional Autoregressive Model," *Comput. Stat. Data Anal,* vol. 131, pp. 66-79, 2019, doi: 10.1016/j.csda.2018.06.003.

[152] F. Wang *et al,* "6g-Enabled Short-Term Forecasting for Large-Scale Traffic Flow in Massive IoT Based on Time-Aware Locality-Sensitive Hashing," *Ieee Internet Things J.,* vol. 8, no. 7, pp. 5321-5331, 2021, doi: 10.1109/jiot.2020.3037669.

[153] M. Jaago *et al,* "Differential Patterns of Cross-Reactive Antibody Response Against SARS-CoV-2 Spike Protein Detected for Chronically 111 and Healthy COVID-19 Naive Individuals," *Sci. Rep.,* vol. 12, no. 1, 2022, doi: 10.1038/s41598-022-20849-6.

[154] S. Kandanaarachchi, M. A. Munoz, R. J. Hyndman, and K. Smith-Miles, "On Normalization and Algorithm Selection for Unsupervised Outlier Detection," *Data Min. Knowl Discov.,* vol. 34, no. 2, pp. 309-354, 2019, doi: 10.1007/sl0618-019-00661-z.

[155] H. Henderi, "Comparison of Min-Max Normalization and Z-Score Normalization in the K-Nearest Neighbor (kNN) Algorithm to Test the Accuracy of Types of Breast Cancer," *Ijiis Int. J. Informatics Inf. Syst,* vol. 4, no. 1, pp.

13-20, 2021, doi: 10.47738/ijiis.v4il.73.

[156] S. Songma, T. Sathuphan, and T. Pamutha, "Optimizing Intrusion Detection Systems in Three Phases on the CSE-CIC-IDS-2018 Dataset," *Computers,* vol. 12, no. 12, 2023, doi: 10.3390/computers 12120245.

[157] Sowndharya M, Duraisamy S, Pavithra M, "Predicting Groundwater Level using Temporal Attention Enhanced Graph Neural Network," *Tuijin Jishu/Journal Propuls. Technol,* vol. 44, no. 3, pp. 4571-4581, 2023, doi: 10.52783/tjjpt.v44.i3.2581.

[158] F. AKCAKOCA and H. APAYDIN, "Modelling of Bektas Creek Daily Streamflow with Generalized Regression Neural Network Method," *Int. J. Adv. Sci. Res. Eng.,* vol. 06, no. 02, pp. 97-103, 2020, doi: 10.31695/ijasre.2020.33717.

[159] K. Zou *et al,* "The Role of Artificial Neural Networks in Prediction of Severe Acute Pancreatitis Associated Acute Respiratory Distress Syndrome: A Retrospective Study," *Medicine (Baltimore).,* vol. 102, no. 29, p. e34399, 2023, doi: 10.1097/md.0000000000034399.

[160] W. Wei and X. Yang, "Comparison of Diagnosis Accuracy Between a Backpropagation Artificial Neural Network Model and Linear Regression in Digestive Disease Patients: An Empirical Research," *Comput. Math. Methods Med,* vol. 2021, pp. 1-10, 2021, doi: 10.1155/2021/6662779.

[161] G. Perchiazzi *et al,* "Imitating the Respiratory Activity of the Brain Stem by Using Artificial Neural Networks: Exploratory Study on an Animal Model of Lactic Acidosis and Proof of Concept," 2024, doi: 10.21203/rs.3.rs-4461706/vl.

[162] F. Akcakoca and H. Apaydin, "Modelling of Bektas Creek Daily Streamflow With Generalized Regression Neural Network Method," *Int. J. Adv. Sci. Res. Eng.,* vol. 06, no. 02, pp. 97-103, 2020, doi: 10.31695/ijasre.2020.33717.

[163] A. I. Arvanitidis, D. Bargiotas, A. Daskalopulu, V. Laitsos, andL. H. Tsoukalas, "Enhanced Short-Term Load Forecasting Using Artificial Neural Networks," *Energies,* vol. 14, no. 22, p. 7788, 2021, doi: 10.3390/enl4227788.

[164] K. Hu *et al,* "Application of Nonlinear Correction Algorithm in Near Infrared Spectra Analysis During on-Site Quick Detection," 2022, doi: 10.1117/12.2638467.

[165] J. Zou, Y. Han, and S. So, "Overview of Artificial Neural Networks," in *Neural Networks and Soft Computing,* Springer, 2008, pp. 14-22, doi: 10.1007/978-1-

60327-101-12.

[166] A. A. Pishro, S. Zhang, D. Huang, F. Xiong, W. Li, and Q. Yang, "Application of Artificial Neural Networks and Multiple Linear Regression on Local Bond Stress Equation of UHPC and Reinforcing Steel Bars," *Sci. Rep.*, vol. 11, no. 1, 2021, doi: 10.1038/s41598-021-94480-2.

[167] M. Fang, C. Poskanzer, and S. Anzellotti, "PyMVPD: A Toolbox for Multivariate Pattern Dependence," *Front. Neuroinform.*, vol. 16, 2022, doi: 10.3389/fninf.2022.835772.

[168] H. Taherdoost, "Deep Learning and Neural Networks: Decision-Making Implications," *Symmetry (Basel).*, vol. 15, no. 9, p. 1723, 2023, doi: 10.3390/syml5091723.

[169] X. Ying, "An Overview of Overfitting and its Solutions," *J. Phys. Conf. Ser.*, vol. 1168, no. 2, 2019, doi: 10.1088/1742-6596/1168/2/022022.

[170] P. Giudici, B. H. Misheva, and A. Spelta, "Network Based Scoring Models to Improve Credit Risk Management in Peer to Peer Lending Platforms," *Front. Artif. Intell*, vol. 2, 2019, doi: 10.3389/frai.2019.00003.

[171] F. Espinoza and M. A. C. Ygnacio, "Development of a Credit Risk Evaluation System Using Multilayer Neural Networks," *Mater. Sci. Eng. Int. J.*, vol. 8, no. 1, pp. 1-7, 2024, doi: 10.15406/mseij.2024.08.00228.

[172] S. Jiang, Y. Feng, X. Liao, and B. O. Onasanya, "Credit Card Fraud Recognition Based on Width and Depth Neural Networks," *Research Square*, preprint, 2023, doi: 10.21203/rs.3.rs-3378590/vl.

[173] G. Li, X. Wang, D. Bi, and J. Hou, "Risk Measurement of the Financial Credit Industry Driven by Data," *J. Glob. Inf. Manag.*, vol. 30, no. 11, pp. 1-20, 2022, doi: 10.4018/jgim.308806.

[174] I. Ercanli, "Innovative Deep Learning Artificial Intelligence Applications for Predicting Relationships Between Individual Tree Height and Diameter at Breast Height," *For. Ecosyst*, vol. 7, no. 1, 2020, doi: 10.1186/s40663-020-00226-3.

[175] M. Mandal and S. Bandyopadhyay, "Artificial Neural Network Approach to Predict the Lightfastness of Gravure Prints on the Plastic Film," *Color Res. Appl*, vol. 45, no. 4, pp. 686-698, 2020, doi: 10.1002/col.22504.

[176] H. MolaAbasi, M. Saberian, A. Kordnaeij, J. Omer, J. Li, and P. Kharazmi, "Predicting the Stress-Strain Behaviour of Zeolite-Cemented Sand Based on the Unconfmed Compression Test Using GMDH Type Neural Network," *J. Adhes.*

Sci. Technol., vol. 33, no. 9, pp. 945-962, 2019, doi: 10.1080/01694243.2019.1571659.

[177] S. K. S. C. Hidayati, P. B. G. P. Raharja, I. N. G. A. M. Wardhiana, and S. Klemm, "Optimizing Segmentation and Purchase Forecasting in Credit Card Transactions: A PSO-enhanced K-Means and ANN Approach," *J. Inf. Eng. Educ. Technol*, vol. 7, no. 2, pp. 59-65, 2023, doi: 10.26740/jieet.v7n2.p59-65.

[178] R. Krishnan, C. V Krishnaveni, and A. V. K. Prasad, "Telecom Churn Prediction Using Machine Learning," *World J. Adv. Eng. Technol. Set*, vol. 7, no. 2, pp. 87-96, 2022, doi: 10.30574/wjaets.2022.7.2.0130.

[179] L. T. Khrais and O. S. Shidwan, "The Role of Neural Network for Estimating Real Estate Prices Value in Post COVID-19: A Case of the Middle East Market," *Int. J. Electr. Comput. Eng.*, vol. 13, no. 4, p. 4516, 2023, doi: 10.11591/ijece.vl3i4.pp4516-4525.

[180] M. Najim, S. Puthucheri, V. Agarwala, and D. Singh, "ANN-Based Two-Layer Absorber Design Using Fe-Al Hybrid Nano-Composites for Broad Bandwidth Microwave Absorption," *IEEE Trans. Magn.*, vol. 52, no. 12, 2016, doi: 10.1109/TMAG.2016.2598530.

[181] H. Yu and M. Bogdan, "Levenberg-Marquardt Training 12.1," in *Neural Network Toolbox™ User's Guide*, Math Works Inc., Natick, MA, USA, 2010, pp. 1-16.

[182] Z. Min, L. Xiao, L. Cao, and H. Yan, "Application of the neural network in diagnosis of breast cancer based on levenberg-marquardt algorithm," in *2017 International Conference on Security, Pattern Analysis, and Cybernetics (SPAC)*, 2017, pp. 268-272. doi: 10.1109/SPAC.2017.8304288.

[183] T. Jia-li, L. Yi-jun, and W. Fang-sheng, "Levenberg-Marquardt neural network for gear fault diagnosis," in *2010 International Conference on Networking and Digital Society*, 2010, pp. 134-137. doi: 10.1109/ICNDS.2010.5479613.

[184] M. Miaoli, W. Xiaolong, and H. Honggui, "Accelerated Levenberg-Marquardt Algorithm for Radial Basis Function Neural Network," in *2020 Chinese Automation Congress (CAC)*, 2020, pp. 6804-6809. doi: 10.1109/CAC51589.2020.9327740.

[185] I. D. Sabukunze, Y. Alvinika, B. J. Waworuntu, and P. Mudjihartono, "Prediction of Students' GPA Using Levenberg-Marquardt Backpropagation Algorithm," in *2021 6th International Conference for Convergence in*

Technology (I2CT), 2021, pp. 1-5. doi: 10.1109/I2CT51068.2021.9418184.

[186] S. Basterrech, S. Mohammed, G. Rubino, and M. Soliman, "Levenberg—Marquardt Training Algorithms for Random Neural Networks," *Comput. J.*, vol. 54, no. 1, pp. 125-135, 2011, doi: 10.1093/comjnl/bxpl01.

[187] D. O. Anggriawan, A. L. Satriawan, I. Sudiharto, E. Wahjono, E. Prasetyono, and A. Tjahjono, "Levenberg Marquardt Backpropagation Neural Network for Harmonic Detection," in *2018 International Electronics Symposium on Engineering Technology and Applications (IES-ETA),* 2018, pp. 129-132. doi: 10.1109/ELECSYM.2018.8615531.

[188] P. Sehgal, "Comparative Study of GD , LM and SCG Method of Neural Network for Thyroid Disease Diagnosis," *Int. J. Appl. Res.,* vol. 1, pp. 34-39, 2015.

[189] S. Alice Saji and B. Dr. K, "Performance analysis of training algorithms of multilayer perceptrons in diabetes prediction," in *2015 International Conference on Advances in Computer Engineering and Applications (ICACEA),* Mar. 2015, pp. 201-206. doi: 10.1109/ICACEA.2015.7164695.

[190] D. Wang, X. Shuai, X. Hu, and L. Zhu, "Research on Computer Network Security Evaluation Method Based on Levenberg-Marquardt Algorithms," in *2019 International Conference on Communications, Information System and Computer Engineering (CISCE),* 2019, pp. 399-402. doi: 10.1109/CISCE.2019.00094.

[191] A. Salemdawod and Z. Asian, "Water and air quality in modern farms using neural network," in *2017 International Conference on Engineering and Technology (ICET),* 2017, pp. 1-4. doi: 10.1109/ICEngTechnol.2017.8308190.

[192] A. A. Bataineh and D. Kaur, "A Comparative Study of Different Curve Fitting Algorithms in Artificial Neural Network using Housing Dataset," in *NAECON 2018 - IEEE National Aerospace and Electronics Conference,* 2018, pp. 174-178. doi: 10.1109/NAECON.2018.8556738.

[193] M. Riedmiller and H. Braun, "A direct adaptive method for faster backpropagation learning: the RPROP algorithm," in *IEEE International Conference on Neural Networks,* 1993, pp. 586-591 vol.1, doi: 10.1109/ICNN. 1993.298623.

[194] B. Sartono, "Comparison of Backpropagation and Resilient Backpropagation Algorithms in Non-Invasive Blood Glucose Measuring Device," *International Journal of Electrical and Computer Engineering,* vol. 8, no. 1, pp. 153-157,

2017.

[195] W. Saputra, A. P. Windarto, and A. Wanto, "Analysis of the Resilient Method in Training and Accuracy in the Backpropagation Method," *Ijics (International J. Informatics Comput. Sci,* vol. 5, no. 1, p. 52, 2021, doi: 10.30865/ijics.v5il.2922.

[196] J. Kim *et al,* "On-Chip Trainable Hardware-Based Deep Q-Networks Approximating a Backpropagation Algorithm," *Neural Comput. Appl,* vol. 33, no. 15, pp. 9391-9402, 2021, doi: 10.1007/s00521-021-05699-z.

[197] S. A. Etemad and A. Arya, "3D Human Action Recognition and Style Transformation Using Resilient Backpropagation Neural Networks," in *Proc. Int. Conf. Intelligent Computing andIntelligent Systems*, 2009, pp. 296-301, doi: 10.1109/icicisys.2009.5357690.

[198] L. R. Reddy, P. Patel, and S. K. Rajendra, "Utilization of Resilient Back Propagation Algorithm and Discrete Wavelet Transform for the Differential Protection of Three Phase Power Transformer," in *2020 21st National Power Systems Conference (NPSC),* 2020, pp. 1-6. doi: 10.1109/NPSC49263.2020.9331861.

[199] X. Li, M. P. Wu, X. F. He, and K. D. Zhang, "The Training Method of General Regression Neural Network for GDOP Approximation," *Appl. Mech. Mater.,* vol. 278-280, pp. 1265-1270, 2013, doi: 10.4028/www.scientific.net/amm.278-280.1265.

[200] E. Benes, D. Bajusz, A. Gere, M. Fodor, and A. Racz, "Comprehensive chemometric classification of snack products based on their near infrared spectra," *LWT,* vol. 133, p. 110130, 2020, doi: https://doi.Org/10.1016/j.lwt.2020.110130.

[201] V. C. Liyanaarachchi, G. K. S. H. Nishshanka, P. H. V. Nimarshana, T. U. Ariyadasa, and R. A. Attalage, "Development of an artificial neural network model to simulate the growth of microalga Chlorella vulgaris incorporating the effect of micronutrients," *J. Biotechnol.,* vol. 312, pp. 44-55, 2020, doi: https://doi.Org/10.1016/j.jbiotec.2020.02.010.

[202] A. Christofer, C. Kusuma, V. Pribadi, and W. Budiharto, "The Notation Scanner Systems Using Resilient Backpropagation Method," *Procedia Comput. Sci.,* vol. 59, pp. 98-105, 2015, doi: https://doi.Org/10.1016/j.procs.2015.07.342.

[203] M. F. Miller, "A scaled conjugate gradient algorithm for fast supervised

learning," *Neural Networks*, vol. 6, no. 4, pp. 525-533, 1993, doi: https://doi.org/10.1016/S0893-6080(05)80056-5.

[204] B. Ceti§li and A. Barkana, "Speeding Up the Scaled Conjugate Gradient Algorithm and Its Application in Neuro-Fuzzy Classifier Training," *Soft Comput*, vol. 14, no. 4, pp. 365-378, 2009, doi: 10.1007/s00500-009-0410-8.

[205] P. Upadhyay, A. Pandita, and N. Joshi, "Scaled Conjugate Gradient Backpropagation based SLA Violation Prediction in Cloud Computing," in *2019 International Conference on Computational Intelligence and Knowledge Economy (ICCIKE)*, Dec. 2019, pp. 203-208. doi: 10.1109/ICCIKE47802.2019.9004240.

[206] A. F. M. Amidon, S. M. H. M. Huzir, Z. M. Yusoff, N. Ismail, and M. N. Taib, "The Significance of Artificial Intelligent Technique in Classifying Various Grades of Agarwood Oil," *Indones. J. Electr. Eng. Comput. Set*, vol. 29, no. 1, p. 261, 2022, doi: 10.11591/ijeecs.v29.il.pp261-269.

[207] A. Zabidi, L. Y. Khuan, W. Mansor, I. M. Yassin, and R. Sahak, "Detection of infant hypothyroidism with mel frequency cepstrum analysis and multi-layer perceptron classification," in *2010 6th International Colloquium on Signal Processing & its Applications*, IEEE, May 2010, pp. 1-5. doi: 10.1109/CSPA.2010.5545331.

[208] S. Masood, M. Doja, and P. Chandra, "Analysis of Weight Initialization Routines for Scaled Conjugate Gradient Training Algorithm," in *2016 Second International Conference on Computational Intelligence & Communication Technology (CICT)*, Feb. 2016, pp. 533-538. doi: 10.1109/CICT.2016.111.

[209] Jyoti and A. K. Rawat, "Scale conjugate gradient based learning applied to handwritten digit classification," in *2017 Conference on Information and Communication Technology (CICT)*, 2017, pp. 1-6. doi: 10.1109/INFOCOMTECH.2017.8340583.

[210] N. Aburaed, S. Atalla, H. Mukhtar, M. Al-Saad, and W. Mansoor, "Scaled Conjugate Gradient Neural Network for Optimizing Indoor Positioning System," in *2019 International Symposium on Networks, Computers and Communications* (XWCQ, 2019, pp. 1-4. doi: 10.1109/ISNCC.2019.8909147.

[211] C. B. Khadse, M. A. Chaudhari, and V. B. Borghate, "Comparison of seven backpropagation algorithms for three phase power quality assessment," in *TENCON2017 - 2017 IEEE Region 10 Conference*, 2017, pp. 2548-2553. doi:

10.1109/TENCON.2017.8228291.

[212] M. Borole and S. R. Kolhe, "Statistical Feature Based Digital Camera Identification," in *2020 2nd International Conference on Advances in Computing, Communication Control and Networking (ICACCCN)*, 2020, pp. 1019-1023. doi: 10.1109/ICACCCN51052.2020.9362844.

[213] C. F. Rodriguez-Hernandez, M. Musso, E. Kyndt, and E. Cascallar, "Artificial neural networks in academic performance prediction: Systematic implementation and predictor evaluation," *Comput. Educ. Artif. Intell*, vol. 2, p. 100018, 2021, doi: https://doi.Org/10.1016/j.caeai.2021.100018.

[214] K. Riehl, M. Neunteufel, and M. Hemberg, "Hierarchical Confusion Matrix for Classification Performance Evaluation," *J. R Stat. Soc. Ser. C (Applied Stat.*, vol. 72, no. 5, pp. 1394-1412, 2023, doi: 10.1093/jrsssc/qlad057.

[215] G. Canbek, "BenchMetrics Prob: Benchmarking of Probabilistic Error/Loss Performance Evaluation Instruments for Binary-Classification Problems," *Research Square*, preprint, 2022, doi: 10.21203/rs.3.rs-1356087/vl.

[216] S. Sathyanarayanan, "Confusion Matrix-Based Performance Evaluation Metrics," *Asian Journal of Business Research*, vol. 27, no. 4(S), pp. 4023-4031, 2024, doi: 10.53555/ajbr.v27i4s.4345.

[217] A. H. Saputro and C. Aprichilia, "Classification System of Honey Floral Origin based on Visual Near-Infrared Imaging," in *2019 International Conference on Sustainable Information Engineering and Technology (SIET)*, 2019, pp. 125—129. doi: 10.1109/SIET48054.2019.8986024.

[218] H. Yang, "Prediction and Analysis of Blood Glucose Levels Based on Tabnet," *Sci. J. Techno!.*, vol. 5, no. 7, pp. 45-54, 2023, doi: 10.54691/sjt.v5i7.5288.

[219] J. F. Mas and J. J. Flores, "The application of artificial neural networks to the analysis of remotely sensed data," *Int. J. Remote Sens.*, vol. 29, no. 3, pp. 617-663, 2008, doi: 10.1080/01431160701352154.

[220] F. T. Liu, K. M. Ting, and Z.-H. Zhou, "Isolation Forest," in *2008 Eighth IEEE International Conference on Data Mining*, 2008, pp. 413-422. doi: 10.1109/ICDM.2008.17.

[221] O. A. Montesinos Lopez, A. Montesinos Lopez, and J. Crossa, "Fundamentals of Artificial Neural Networks and Deep Learning BT - Multivariate Statistical Machine Learning Methods for Genomic Prediction," O. A. Montesinos Lopez, A. Montesinos Lopez, and J. Crossa, Eds., Cham: Springer International

Publishing, 2022, pp. 379-425. doi: 10.1007/978-3-030-89010-0_10.

[222] B. G. Kermani, S. S. Schiffman, and H. T. Nagle, "Performance of the Levenberg-Marquardt neural network training method in electronic nose applications," *Sensors Actuators B Chem.*, vol. 110, no. 1, pp. 13-22, 2005, doi: https://doi.Org/10.1016/j.snb.2005.01.008.

[223] S. Hudnurkar and N. Rayavarapu, "Binary classification of rainfall time-series using machine learning algorithms," *Int. J. Electr. Comput. Eng.*, vol. 12, no. 2, pp. 1945-1954, 2022, doi: 10.11591/ijece.vl2i2.ppl945-1954.

[224] Q. Gu, L. Zhu, and Z. Cai, "Evaluation Measures of the Classification Performance of Imbalanced Data Sets BT - Computational Intelligence and Intelligent Systems," Z. Cai, Z. Li, Z. Kang, and Y. Liu, Eds., Berlin, Heidelberg: Springer Berlin Heidelberg, 2009, pp. 461-471.

[225] S. Jain, E. Kotsampasakou, and G. F. Ecker, "Comparing the performance of meta-classifiers—a case study on selected imbalanced data sets relevant for prediction of liver toxicity," *J. Comput. Aided. Mol. Des., vol.* 32, no. 5, pp. 583-590, 2018, doi: 10.1007/sl0822-018-0116-z.

APPENDICES

APPENDIX 1

Original experimental Absorption Performance Data of Eco-Friendly Hollow Pyramidal Microwave Absorbers - Small Size

Table A.l: Original Experimental Absorption Performance Data of Eco-Friendly Hollow Pyramidal Microwave Absorber in the L-Band (Small Size)

No. of Experimental Data Points	Frequency (GHz)	Absorption (dB)
1	1.000	-3.7689
2	1.035	-3.5248
3	1.070	-3.2916
4	1.105	-3.3273
5	1.140	-3.3498
6	1.175	-3.3585
7	1.210	-3.352
8	1.245	-3.3294
9	1.280	-3.2900
10	1.315	-3.2338
11	1.350	-3.1624
12	1.385	-3.0773
13	1.420	-2.9804
14	1.455	-2.8733
15	1.490	-2.7578
16	1.525	-2.6358
17	1.560	-2.5094
18	1.595	-2.3807
19	1.630	-2.2514
20	1.665	-2.2839
21	1.700	-2.4625
22	1.735	-2.6372
23	1.770	-2.8066
24	1.805	-2.9681
25	1.840	-3.1181
26	1.875	-3.2525
27	1.910	-3.3677
28	1.945	-3.4601
29	1.980	-3.5269

Table A.2: Original Experimental Absorption Performance Data of Eco-Friendly Hollow Pyramidal Microwave Absorber in the S-Band (Small Size)

No. of Experimental Data Points	Frequency (GHz)	Absorption (dB)
1	2.015	-3.5662
2	2.050	-3.5773
3	2.085	-3.5607
4	2.120	-3.5184
5	2.155	-3.4536
6	2.190	-3.3703
7	2.225	-3.2732
8	2.260	-3.1676
9	2.295	-3.0587
10	2.330	-2.9514
11	2.365	-2.8498
12	2.400	-2.7878
13	2.435	-2.9461
14	2.470	-3.1115
15	2.505	-3.2842
16	2.540	-3.4639
17	2.575	-3.6504
18	2.610	-3.8432
19	2.645	-4.0417
20	2.680	-4.2451
21	2.715	-4.4522
22	2.750	-4.6612
23	2.785	-4.8702
24	2.820	-5.0767
25	2.855	-5.2781
26	2.890	-5.4718
27	2.925	-5.6555
28	2.960	-5.8271
29	2.995	-5.9847
30	3.030	-6.1262
31	3.065	-6.2497
32	3.100	-6.3535
33	3.135	-6.4363
34	3.170	-6.4965
35	3.205	-6.5323
36	3.240	-6.5489
37	3.275	-6.8234

(Continued)

38	3.310	-7.1370
39	3.345	-7.4415
40	3.380	-7.7341
41	3.415	-8.1338
42	3.450	-8.5335
43	3.485	-8.9310
44	3.520	-9.3236
45	3.555	-9.7095
46	3.590	-10.0860
47	3.625	-10.7635
48	3.660	-11.8315
49	3.695	-13.1138
50	3.730	-14.6378
51	3.765	-16.3758
52	3.800	-18.0941
53	3.835	-19.0936
54	3.870	-18.6086
55	3.905	-17.0070
56	3.940	-15.1505
57	3.975	-13.4470

Table A.3: Original Experimental Absorption Performance Data of Eco-Friendly Hollow Pyramidal Microwave Absorber in the C-Band (Small Size)

No. of Experimental Data Points	Frequency (GHz)	Absorption (dB)
1	4.010	-12.3765
2	4.045	-12.2781
3	4.080	-12.1398
4	4.115	-11.9694
5	4.150	-11.7752
6	4.185	-11.6400
7	4.220	-11.5527
8	4.255	-11.4143
9	4.290	-11.2240
10	4.325	-10.9841
11	4.360	-11.1553
12	4.395	-11.8097
13	4.430	-12.4712
14	4.465	-13.1369
15	4.500	-13.8043
16	4.535	-14.4741
17	4.570	-15.1517
18	4.605	-15.8454
19	4.640	-16.5670
20	4.675	-17.3302
21	4.710	-18.1548
22	4.745	-19.0670
23	4.780	-20.1013
24	4.815	-21.2990
25	4.850	-22.7138
26	4.885	-24.4203
27	4.920	-26.5310
28	4.955	-29.2110
29	4.990	-32.5765
30	5.025	-35.6472
31	5.060	-34.8828
32	5.095	-31.8421
33	5.130	-29.2357
34	5.165	-27.2941
35	5.200	-26.3733
36	5.235	-26.1019
37	5.270	-29.6660

(Continued)

38	5.305	-35.1463
39	5.340	-44.6295
40	5.375	-40.1122
41	5.410	-34.4304
42	5.445	-31.3845
43	5.480	-29.4423
44	5.515	-28.0609
45	5.550	-26.9815
46	5.585	-26.0575
47	5.620	-25.1956
48	5.655	-24.3380
49	5.690	-23.4565
50	5.725	-22.5432
51	5.760	-22.1984
52	5.795	-22.0352
53	5.830	-22.1958
54	5.865	-22.4420
55	5.900	-22.3452
56	5.935	-21.8983
57	5.970	-21.1744
58	6.005	-20.2816
59	6.040	-19.3175
60	6.075	-18.6727
61	6.110	-18.1537
62	6.145	-18.3609
63	6.180	-19.1443
64	6.215	-20.0008
65	6.250	-20.9501
66	6.285	-22.0113
67	6.320	-23.2040
68	6.355	-24.5421
69	6.390	-26.0310
70	6.425	-27.6536
71	6.460	-29.3448
72	6.495	-30.9742
73	6.530	-32.3563
74	6.565	-33.3886
75	6.600	-34.1777
76	6.635	-35.0340
77	6.670	-36.3912
78	6.705	-38.9219
79	6.740	-44.4324

(Continued)

80	6.775	-50.1436
81	6.810	-38.6302
82	6.845	-32.7291
83	6.880	-28.7832
84	6.915	-40.8398
85	6.950	-32.6649
86	6.985	-25.4005
87	7.020	-21.4012
88	7.055	-19.3235
89	7.090	-21.2460
90	7.125	-23.5659
91	7.160	-26.0282
92	7.195	-27.3266
93	7.230	-26.1232
94	7.265	-28.1074
95	7.300	-32.3936
96	7.335	-31.4112
97	7.370	-27.2970
98	7.405	-24.1731
99	7.440	-21.9311
100	7.475	-20.2661
101	7.510	-19.9230
102	7.545	-20.0870
103	7.580	-20.2214
104	7.615	-20.3508
105	7.650	-20.4953
106	7.685	-20.6697
107	7.720	-20.8853
108	7.755	-21.1488
109	7.790	-21.4676
110	7.825	-21.8429
111	7.860	-22.2729
112	7.895	-22.7584
113	7.930	-23.2970
114	7.965	-23.8891

Table A.4: Original Experimental Absorption Performance Data of Eco-Friendly Hollow Pyramidal Microwave Absorber in the X-Band (Small Size)

No. of Experimental Data Points	Frequency (GHz)	Absorption (dB)
1	8.000	-24.5328
2	8.000	-15.5662
3	8.020	-15.4480
4	8.040	-15.3062
5	8.060	-15.1400
6	8.080	-14.9498
7	8.100	-14.7355
8	8.120	-14.4986
9	8.140	-14.2414
10	8.160	-13.9667
11	8.180	-13.9602
12	8.200	-14.3126
13	8.220	-14.6900
14	8.240	-15.0865
15	8.260	-15.4935
16	8.280	-15.8985
17	8.300	-16.2849
18	8.320	-16.6339
19	8.340	-16.9256
20	8.360	-17.1413
21	8.380	-17.2668
22	8.400	-17.2950
23	8.420	-17.2270
24	8.440	-17.0731
25	8.460	-16.8488
26	8.480	-16.7318
27	8.500	-16.8393
28	8.520	-17.1112
29	8.540	-17.7800
30	8.560	-18.3511
31	8.580	-18.7700
32	8.600	-18.9985
33	8.620	-19.0366
34	8.640	-18.9144
35	8.660	-18.6813
36	8.680	-18.3881
37	8.700	-18.0793

(Continued)

38	8.720	-17.7814
39	8.740	-17.5122
40	8.760	-17.2848
41	8.780	-17.1012
42	8.800	-16.9608
43	8.820	-16.8611
44	8.840	-16.7964
45	8.860	-16.7565
46	8.880	-16.7288
47	8.900	-16.7028
48	8.920	-16.6638
49	8.940	-16.6019
50	8.960	-16.5115
51	8.980	-16.3927
52	9.000	-16.2531
53	9.020	-16.2952
54	9.040	-16.7099
55	9.060	-17.1497
56	9.080	-17.6143
57	9.100	-18.1029
58	9.120	-18.6123
59	9.140	-19.1349
60	9.160	-19.6568
61	9.180	-20.1553
62	9.200	-20.5941
63	9.220	-20.9261
64	9.240	-21.0995
65	9.260	-21.0740
66	9.280	-20.8381
67	9.300	-20.4161
68	9.320	-20.8083
69	9.340	-21.1200
70	9.360	-21.2709
71	9.380	-21.2499
72	9.400	-21.0666
73	9.420	-20.7388
74	9.440	-20.2919
75	9.460	-19.7552
76	9.480	-19.1585
77	9.500	-18.9675
78	9.520	-19.1644
79	9.540	-19.3669

(Continued)

80	9.560	-19.6602
81	9.580	-20.1104
82	9.600	-20.3656
83	9.620	-20.3665
84	9.640	-20.1133
85	9.660	-19.9410
86	9.680	-20.1826
87	9.700	-20.9212
88	9.720	-21.6952
89	9.740	-22.5137
90	9.760	-23.3867
91	9.780	-24.3232
92	9.800	-25.3264
93	9.820	-26.3892
94	9.840	-27.4773
95	9.860	-28.5058
96	9.880	-29.3089
97	9.900	-29.6637
98	9.920	-29.4220
99	9.940	-28.6475
100	9.960	-27.5554
101	9.980	-26.3483
102	10.000	-25.1463
103	10.020	-24.0074
104	10.040	-24.2721
105	10.060	-26.0500
106	10.080	-28.1473
107	10.100	-30.5229
108	10.120	-32.6635
109	10.140	-33.1287
110	10.160	-31.5092
111	10.180	-29.2675
112	10.200	-27.2138
113	10.220	-25.4754
114	10.240	-24.0094
115	10.260	-22.7566
116	10.280	-21.6692
117	10.300	-20.7093
118	10.320	-19.8497
119	10.340	-19.0709
120	10.360	-19.6728
121	10.380	-20.6104

(Continued)

122	10.400	-21.7314
123	10.420	-23.0944
124	10.440	-24.7909
125	10.460	-26.9768
126	10.480	-29.9327
127	10.500	-34.1038
128	10.520	-38.0330
129	10.540	-34.6574
130	10.560	-30.2097
131	10.580	-27.0163
132	10.600	-26.6307
133	10.620	-27.1499
134	10.640	-26.8656
135	10.660	-27.0877
136	10.680	-29.6915
137	10.700	-32.2769
138	10.720	-33.3461
139	10.740	-31.9986
140	10.760	-37.0938
141	10.780	-40.8714
142	10.800	-35.1663
143	10.820	-30.7696
144	10.840	-27.8347
145	10.860	-25.7072
146	10.880	-24.0763
147	10.900	-22.7803
148	10.920	-21.7245
149	10.940	-20.8489
150	10.960	-20.1975
151	10.980	-19.6993
152	11.000	-19.2087
153	11.020	-18.7251
154	11.040	-18.6252
155	11.060	-18.5065
156	11.080	-17.9811
157	11.100	-17.8213
158	11.120	-18.5880
159	11.140	-19.6129
160	11.160	-21.4902
161	11.180	-24.4693
162	11.200	-24.7371
163	11.220	-27.6226

(Continued)

164	11.240	-31.8677
165	11.260	-38.9198
166	11.280	-37.5219
167	11.300	-30.7936
168	11.320	-26.6475
169	11.340	-23.7294
170	11.360	-21.4936
171	11.380	-20.7133
172	11.400	-21.1018
173	11.420	-21.3945
174	11.440	-21.5748
175	11.460	-21.6363
176	11.480	-21.5793
177	11.500	-21.4178
178	11.520	-21.1747
179	11.540	-20.8762
180	11.560	-20.5480
181	11.580	-20.2132
182	11.600	-20.3950
183	11.620	-21.4603
184	11.640	-22.7114
185	11.660	-24.1991
186	11.680	-26.0060
187	11.700	-28.2586
188	11.720	-31.1416
189	11.740	-34.7198
190	11.760	-37.1839
191	11.780	-35.0383
192	11.800	-31.6756
193	11.820	-28.9862
194	11.840	-26.9225
195	11.860	-27.0326
196	11.880	-27.7213
197	11.900	-28.0641
198	11.920	-28.9651
199	11.940	-29.8733
200	11.960	-30.4313
201	11.980	-30.5337
202	12.000	-30.1731

APPENDIX 2

Original experimental Absorption Performance Data of Eco-Friendly Hollow Pyramidal Microwave Absorbers - Medium Size

Table B.l: Original Experimental Absorption Performance Data of Eco-Friendly Hollow Pyramidal Microwave Absorber in the L-Band (Medium Size)

No. of Experimental Data Points	Frequency (GHz)	Absorption (dB)
1	1.000	-2.4619
2	1.035	-2.2892
3	1.070	-2.1234
4	1.105	-1.9632
5	1.140	-1.8080
6	1.175	-1.6621
7	1.210	-1.5284
8	1.245	-1.4061
9	1.280	-1.2951
10	1.315	-1.1969
11	1.350	-1.1120
12	1.385	-1.0379
13	1.420	-0.9728
14	1.455	-0.9164
15	1.490	-0.8676
16	1.525	-0.8503
17	1.560	-0.8498
18	1.595	-0.8565
19	1.630	-0.8699
20	1.665	-0.8898
21	1.700	-0.9165
22	1.735	-0.9507
23	1.770	-0.9929
24	1.805	-1.0430
25	1.840	-1.1005
26	1.875	-1.1649
27	1.910	-1.2349
28	1.945	-1.3089
29	1.980	-1.3851

Table B.2: Original Experimental Absorption Performance Data of Eco-Friendly Hollow Pyramidal Microwave Absorber in the S-Band (Medium Size)

No. of Experimental Data Points	Frequency (GHz)	Absorption (dB)
1	2.015	-1.4618
2	2.050	-1.5370
3	2.085	-1.6089
4	2.120	-1.6760
5	2.155	-1.7375
6	2.190	-1.7927
7	2.225	-1.8418
8	2.260	-1.8854
9	2.295	-1.9241
10	2.330	-1.9590
11	2.365	-1.9914
12	2.400	-2.0611
13	2.435	-2.1378
14	2.470	-2.2191
15	2.505	-2.3067
16	2.540	-2.4012
17	2.575	-2.5026
18	2.610	-2.6109
19	2.645	-2.7257
20	2.680	-2.8464
21	2.715	-2.9715
22	2.750	-3.0995
23	2.785	-3.2284
24	2.820	-3.3565
25	2.855	-3.4810
26	2.890	-3.5996
27	2.925	-3.7109
28	2.960	-3.8132
29	2.995	-3.9049
30	3.030	-3.9860
31	3.065	-4.1682
32	3.100	-4.3460
33	3.135	-4.5177
34	3.170	-4.6817
35	3.205	-4.8370
36	3.240	-4.9822
37	3.275	-5.1156

(Continued)

38	3.310	-5.2351
39	3.345	-5.3389
40	3.380	-5.4248
41	3.415	-5.4895
42	3.450	-5.5300
43	3.485	-5.5434
44	3.520	-5.5271
45	3.555	-5.4799
46	3.590	-5.4023
47	3.625	-5.2973
48	3.660	-5.1705
49	3.695	-5.0283
50	3.730	-4.8780
51	3.765	-4.7270
52	3.800	-4.5816
53	3.835	-4.4463
54	3.870	-4.3243
55	3.905	-4.2170
56	3.940	-4.1247
57	3.975	-4.1400

Table B.3: Original Experimental Absorption Performance Data of Eco-Friendly Hollow Pyramidal Microwave Absorber in the C-Band (Medium Size)

No. of Experimental Data Points	Frequency (GHz)	Absorption (dB)
1	4.010	-4.2258
2	4.045	-4.3151
3	4.080	-4.4083
4	4.115	-4.5064
5	4.150	-4.6108
6	4.185	-4.7234
7	4.220	-4.8461
8	4.255	-4.9810
9	4.290	-5.1306
10	4.325	-5.2971
11	4.360	-5.4825
12	4.395	-5.6886
13	4.430	-5.9165
14	4.465	-6.1675
15	4.500	-6.4418
16	4.535	-6.7393
17	4.570	-7.0595
18	4.605	-7.4015
19	4.640	-7.7639
20	4.675	-8.1444
21	4.710	-8.5407
22	4.745	-8.9497
23	4.780	-9.3676
24	4.815	-9.7898
25	4.850	-10.2108
26	4.885	-10.6245
27	4.920	-11.0235
28	4.955	-11.4001
29	4.990	-11.7457
30	5.025	-12.0521
31	5.060	-12.3111
32	5.095	-12.5154
33	5.130	-12.6597
34	5.165	-12.7404
35	5.200	-12.7563
36	5.235	-12.7088
37	5.270	-12.6012

(Continued)

38	5.305	-12.4384
39	5.340	-12.2264
40	5.375	-11.9719
41	5.410	-11.6818
42	5.445	-11.4391
43	5.480	-11.4815
44	5.515	-11.4816
45	5.550	-11.4419
46	5.585	-11.3667
47	5.620	-11.2614
48	5.655	-11.1323
49	5.690	-10.9859
50	5.725	-10.8278
51	5.760	-11.0686
52	5.795	-11.4130
53	5.830	-11.7588
54	5.865	-12.0920
55	5.900	-12.3917
56	5.935	-12.6316
57	5.970	-12.7815
58	6.005	-12.8127
59	6.040	-12.7064
60	6.075	-12.4617
61	6.110	-12.0965
62	6.145	-11.6415
63	6.180	-11.1324
64	6.215	-10.6028
65	6.250	-10.0806
66	6.285	-9.5854
67	6.320	-9.1301
68	6.355	-8.7226
69	6.390	-8.8294
70	6.425	-8.9485
71	6.460	-9.0712
72	6.495	-9.1970
73	6.530	-9.3256
74	6.565	-9.4582
75	6.600	-9.5960
76	6.635	-9.7410
77	6.670	-9.8954
78	6.705	-10.0612
79	6.740	-10.2400

(Continued)

80	6.775	-10.4333
81	6.810	-10.6425
82	6.845	-10.8680
83	6.880	-11.1098
84	6.915	-11.3676
85	6.950	-11.6405
86	6.985	-11.9275
87	7.020	-12.2818
88	7.055	-12.9493
89	7.090	-13.7019
90	7.125	-14.5468
91	7.160	-15.4890
92	7.195	-16.5288
93	7.230	-17.6543
94	7.265	-18.8277
95	7.300	-19.9648
96	7.335	-20.9179
97	7.370	-21.5012
98	7.405	-21.5891
99	7.440	-21.2203
100	7.475	-20.5610
101	7.510	-19.7811
102	7.545	-18.9915
103	7.580	-18.2484
104	7.615	-18.0583
105	7.650	-17.8733
106	7.685	-17.5483
107	7.720	-17.1188
108	7.755	-16.6233
109	7.790	-16.0961
110	7.825	-15.5629
111	7.860	-15.0406
112	7.895	-14.5403
113	7.930	-14.0738
114	7.965	-13.8720

Table B.4: Original Experimental Absorption Performance Data of Eco-Friendly Hollow Pyramidal Microwave Absorber in the X-Band (Medium Size)

No. of Experimental Data Points	Frequency (GHz)	Absorption (dB)
1	8.000	-13.6935
2	8.000	-10.5593
3	8.020	-10.4598
4	8.040	-10.3531
5	8.060	-10.2411
6	8.080	-10.1253
7	8.100	-10.0091
8	8.120	-9.8949
9	8.140	-9.7846
10	8.160	-9.6790
11	8.180	-9.5791
12	8.200	-9.4855
13	8.220	-9.4884
14	8.240	-9.6013
15	8.260	-9.7247
16	8.280	-9.8588
17	8.300	-10.0038
18	8.320	-10.1600
19	8.340	-10.3276
20	8.360	-10.5060
21	8.380	-10.6945
22	8.400	-10.8916
23	8.420	-11.0963
24	8.440	-11.3080
25	8.460	-11.5254
26	8.480	-11.7475
27	8.500	-11.9728
28	8.520	-12.1985
29	8.540	-12.4221
30	8.560	-12.6409
31	8.580	-12.8523
32	8.600	-13.0546
33	8.620	-13.2462
34	8.640	-13.4253
35	8.660	-13.5907
36	8.680	-13.7417
37	8.700	-13.8788

(Continued)

38	8.720	-14.0038
39	8.740	-14.1196
40	8.760	-14.2293
41	8.780	-14.3365
42	8.800	-14.4436
43	8.820	-14.5534
44	8.840	-14.6686
45	8.860	-14.7921
46	8.880	-14.9261
47	8.900	-15.0724
48	8.920	-15.2319
49	8.940	-15.4043
50	8.960	-15.5888
51	8.980	-15.7846
52	9.000	-15.9913
53	9.020	-16.2088
54	9.040	-16.4374
55	9.060	-16.6769
56	9.080	-16.9269
57	9.100	-17.1871
58	9.120	-17.4576
59	9.140	-17.7392
60	9.160	-18.0334
61	9.180	-18.3419
62	9.200	-18.6668
63	9.220	-19.0090
64	9.240	-19.3681
65	9.260	-19.7444
66	9.280	-20.1377
67	9.300	-20.5473
68	9.320	-20.9721
69	9.340	-21.4077
70	9.360	-21.8467
71	9.380	-22.2780
72	9.400	-22.6866
73	9.420	-23.0530
74	9.440	-23.9656
75	9.460	-25.2148
76	9.480	-26.4856
77	9.500	-27.6029
78	9.520	-28.2754
79	9.540	-28.2467

(Continued)

80	9.560	-27.5491
81	9.580	-26.4641
82	9.600	-25.2606
83	9.620	-24.0887
84	9.640	-23.0083
85	9.660	-22.0347
86	9.680	-21.2036
87	9.700	-20.8992
88	9.720	-20.6099
89	9.740	-20.3342
90	9.760	-20.0694
91	9.780	-19.8125
92	9.800	-19.5599
93	9.820	-19.3076
94	9.840	-19.0515
95	9.860	-18.7882
96	9.880	-18.5161
97	9.900	-18.2347
98	9.920	-17.9448
99	9.940	-17.6482
100	9.960	-17.3470
101	9.980	-17.0436
102	10.000	-16.7403
103	10.020	-16.4401
104	10.040	-16.1463
105	10.060	-15.8623
106	10.080	-15.5909
107	10.100	-15.3347
108	10.120	-15.0955
109	10.140	-14.8749
110	10.160	-14.6736
111	10.180	-14.4931
112	10.200	-14.3343
113	10.220	-14.1972
114	10.240	-14.0810
115	10.260	-13.9847
116	10.280	-13.9063
117	10.300	-13.8438
118	10.320	-13.7959
119	10.340	-13.7607
120	10.360	-13.7364
121	10.380	-13.7210

(Continued)

122	10.400	-13.7130
123	10.420	-13.7114
124	10.440	-13.7157
125	10.460	-13.7258
126	10.480	-13.7426
127	10.500	-13.7664
128	10.520	-13.7973
129	10.540	-13.8349
130	10.560	-13.8781
131	10.580	-13.9255
132	10.600	-13.9756
133	10.620	-14.0259
134	10.640	-14.0770
135	10.660	-14.2794
136	10.680	-14.4838
137	10.700	-14.6862
138	10.720	-14.8821
139	10.740	-15.0665
140	10.760	-15.2338
141	10.780	-15.3774
142	10.800	-15.7798
143	10.820	-16.4898
144	10.840	-17.2484
145	10.860	-18.0642
146	10.880	-18.9492
147	10.900	-19.9199
148	10.920	-20.9985
149	10.940	-22.2154
150	10.960	-23.6112
151	10.980	-25.2439
152	11.000	-27.1912
153	11.020	-29.5550
154	11.040	-32.3876
155	11.060	-35.1826
156	11.080	-35.7601
157	11.100	-33.5994
158	11.120	-31.0643
159	11.140	-28.9811
160	11.160	-27.3500
161	11.180	-26.0704
162	11.200	-25.0575
163	11.220	-24.2511

(Continued)

164	11.240	-23.6076
165	11.260	-23.0937
166	11.280	-23.3308
167	11.300	-23.6197
168	11.320	-23.6693
169	11.340	-23.4676
170	11.360	-23.0484
171	11.380	-22.4740
172	11.400	-21.8093
173	11.420	-21.3348
174	11.440	-21.2607
175	11.460	-21.2113
176	11.480	-21.1858
177	11.500	-21.1827
178	11.520	-21.1988
179	11.540	-21.2269
180	11.560	-21.2569
181	11.580	-21.2742
182	11.600	-21.2609
183	11.620	-21.1999
184	11.640	-21.0751
185	11.660	-20.8789
186	11.680	-20.6125
187	11.700	-20.2872
188	11.720	-19.9215
189	11.740	-19.5351
190	11.760	-19.1462
191	11.780	-18.7687
192	11.800	-19.1412
193	11.820	-19.8019
194	11.840	-20.3959
195	11.860	-20.9045
196	11.880	-21.3150
197	11.900	-21.6248
198	11.920	-21.8388
199	11.940	-21.9680
200	11.960	-22.0313
201	11.980	-22.0400
202	12.000	-22.0021

APPENDIX 3

Original experimental Absorption Performance Data of Eco-Friendly Hollow Pyramidal Microwave Absorbers - Big Size

Table C.l: Original Experimental Absorption Performance Data of Eco-Friendly Hollow Pyramidal Microwave Absorber in the L-Band (Big Size)

No. of Experimental Data Points	Frequency (GHz)	Absorption (dB)
1	1.000	-2.3881
2	1.035	-2.1938
3	1.070	-2.0047
4	1.105	-1.8212
5	1.140	-1.6437
6	1.175	-1.4993
7	1.210	-1.4086
8	1.245	-1.3295
9	1.280	-1.2630
10	1.315	-1.2103
11	1.350	-1.1716
12	1.385	-1.1459
13	1.420	-1.1320
14	1.455	-1.1285
15	1.490	-1.1337
16	1.525	-1.1454
17	1.560	-1.1614
18	1.595	-1.1805
19	1.630	-1.2013
20	1.665	-1.2225
21	1.700	-1.2432
22	1.735	-1.2635
23	1.770	-1.2830
24	1.805	-1.3014
25	1.840	-1.3183
26	1.875	-1.3335
27	1.910	-1.3465
28	1.945	-1.3569
29	1.980	-1.3641

Table C.2: Original Experimental Absorption Performance Data of Eco-Friendly Hollow Pyramidal Microwave Absorber in the S-Band (Big Size)

No. of Experimental Data Points	Frequency (GHz)	Absorption (dB)
1	2.015	-1.3681
2	2.05	-1.3686
3	2.085	-1.3758
4	2.12	-1.4075
5	2.155	-1.4323
6	2.19	-1.4826
7	2.225	-1.5279
8	2.26	-1.5687
9	2.295	-1.605
10	2.33	-1.6375
11	2.365	-1.6668
12	2.4	-1.6939
13	2.435	-1.72
14	2.47	-1.7457
15	2.505	-1.7725
16	2.54	-1.8013
17	2.575	-1.8329
18	2.61	-1.868
19	2.645	-1.907
20	2.68	-1.9503
21	2.715	-1.9979
22	2.75	-2.0495
23	2.785	-2.1044
24	2.82	-2.1617
25	2.855	-2.2199
26	2.89	-2.2774
27	2.925	-2.3328
28	2.96	-2.3845
29	2.995	-2.4309
30	3.03	-2.4706
31	3.065	-2.5028
32	3.1	-2.5267
33	3.135	-2.5412
34	3.17	-2.5759
35	3.205	-2.6585
36	3.24	-2.7431
37	3.275	-2.8285

(Continued)

38	3.31	-2.9131
39	3.345	-2.9949
40	3.38	-3.0723
41	3.415	-3.1428
42	3.45	-3.2045
43	3.485	-3.2558
44	3.52	-3.2955
45	3.555	-3.3233
46	3.59	-3.34
47	3.625	-3.3474
48	3.66	-3.3483
49	3.695	-3.3458
50	3.73	-3.3434
51	3.765	-3.3444
52	3.8	-3.3517
53	3.835	-3.3673
54	3.87	-3.3927
55	3.905	-3.4283
56	3.94	-3.4742
57	3.975	-3.5302

Table C.3: Original Experimental Absorption Performance Data of Eco-Friendly Hollow Pyramidal Microwave Absorber in the C-Band (Big Size)

No. of Experimental Data Points	Frequency (GHz)	Absorption (dB)
1	4.010	-3.5954
2	4.045	-3.6692
3	4.080	-3.7508
4	4.115	-3.9089
5	4.150	-4.1726
6	4.185	-4.4628
7	4.220	-4.7832
8	4.255	-5.1371
9	4.290	-5.5278
10	4.325	-5.9580
11	4.360	-6.4296
12	4.395	-6.9435
13	4.430	-7.4993
14	4.465	-8.0957
15	4.500	-8.7298
16	4.535	-9.3975
17	4.570	-10.0930
18	4.605	-10.8086
19	4.640	-11.5348
20	4.675	-12.2595
21	4.710	-12.9683
22	4.745	-13.6441
23	4.780	-14.2678
24	4.815	-14.8198
25	4.850	-15.2814
26	4.885	-15.6381
27	4.920	-15.8825
28	4.955	-16.0143
29	4.990	-16.0400
30	5.025	-15.9715
31	5.060	-15.8210
32	5.095	-15.6011
33	5.130	-15.3222
34	5.165	-14.9916
35	5.200	-15.0197
36	5.235	-15.2545
37	5.270	-15.3772

(Continued)

38	5.305	-15.3806
39	5.340	-15.2647
40	5.375	-15.0953
41	5.410	-14.9741
42	5.445	-14.7513
43	5.480	-14.4417
44	5.515	-14.0643
45	5.550	-13.6395
46	5.585	-13.1858
47	5.620	-12.7191
48	5.655	-12.2520
49	5.690	-11.7942
50	5.725	-11.3520
51	5.760	-10.9295
52	5.795	-10.5286
53	5.830	-10.1504
54	5.865	-9.7943
55	5.900	-9.4585
56	5.935	-9.1410
57	5.970	-8.8392
58	6.005	-8.5504
59	6.040	-8.2714
60	6.075	-7.9999
61	6.110	-7.7554
62	6.145	-7.7338
63	6.180	-7.7081
64	6.215	-7.6764
65	6.250	-7.6394
66	6.285	-7.5985
67	6.320	-7.5569
68	6.355	-7.5194
69	6.390	-7.4916
70	6.425	-7.4790
71	6.460	-7.4875
72	6.495	-7.5223
73	6.530	-7.5886
74	6.565	-7.6909
75	6.600	-7.8331
76	6.635	-8.0191
77	6.670	-8.2530
78	6.705	-8.5388
79	6.740	-8.8804

(Continued)

80	6.775	-9.2826
81	6.810	-9.7506
82	6.845	-10.2902
83	6.880	-10.9073
84	6.915	-11.6089
85	6.950	-12.4015
86	6.985	-13.2892
87	7.020	-14.2708
88	7.055	-15.3323
89	7.090	-16.4334
90	7.125	-17.4871
91	7.160	-18.3459
92	7.195	-18.8334
93	7.230	-18.8471
94	7.265	-18.4471
95	7.300	-19.5544
96	7.335	-21.2994
97	7.370	-23.2850
98	7.405	-25.4519
99	7.440	-27.2854
100	7.475	-27.4774
101	7.510	-25.7062
102	7.545	-23.3047
103	7.580	-21.0530
104	7.615	-19.1014
105	7.650	-17.4290
106	7.685	-15.9901
107	7.720	-14.7436
108	7.755	-13.7391
109	7.790	-13.6811
110	7.825	-13.6144
111	7.860	-13.5375
112	7.895	-13.4506
113	7.930	-13.3548
114	7.965	-13.2520

Table C.4: Original Experimental Absorption Performance Data of Eco-Friendly Hollow Pyramidal Microwave Absorber in the X-Band (Big Size)

No. of Experimental Data Points	Frequency (GHz)	Absorption (dB)
1	8.000	-13.1436
2	8.000	-11.4333
3	8.020	-11.2499
4	8.040	-11.0648
5	8.060	-10.8781
6	8.080	-10.6896
7	8.100	-10.5011
8	8.120	-10.3133
9	8.140	-10.1267
10	8.160	-9.9421
11	8.180	-9.7606
12	8.200	-9.5837
13	8.220	-9.4127
14	8.240	-9.4219
15	8.260	-9.4871
16	8.280	-9.5548
17	8.300	-9.6242
18	8.320	-9.6944
19	8.340	-9.7641
20	8.360	-9.8321
21	8.380	-9.8975
22	8.400	-9.9594
23	8.420	-10.0170
24	8.440	-10.0699
25	8.460	-10.1174
26	8.480	-10.1592
27	8.500	-10.1949
28	8.520	-10.2241
29	8.540	-10.2466
30	8.560	-10.2618
31	8.580	-10.2694
32	8.600	-10.2695
33	8.620	-10.2619
34	8.640	-10.2468
35	8.660	-10.2249
36	8.680	-10.1970
37	8.700	-10.1646

(Continued)

38	8.720	-10.1292
39	8.740	-10.0925
40	8.760	-10.0565
41	8.780	-10.0234
42	8.800	-9.9950
43	8.820	-9.9730
44	8.840	-9.9588
45	8.860	-9.9536
46	8.880	-9.9581
47	8.900	-9.9727
48	8.920	-9.9973
49	8.940	-10.0319
50	8.960	-10.0761
51	8.980	-10.1292
52	9.000	-10.1907
53	9.020	-10.2603
54	9.040	-10.3375
55	9.060	-10.4220
56	9.080	-10.5141
57	9.100	-10.6142
58	9.120	-10.7228
59	9.140	-10.8404
60	9.160	-10.9680
61	9.180	-11.1886
62	9.200	-11.4760
63	9.220	-11.7696
64	9.240	-12.0702
65	9.260	-12.3795
66	9.280	-12.6996
67	9.300	-13.0326
68	9.320	-13.3818
69	9.340	-13.7502
70	9.360	-14.1409
71	9.380	-14.5563
72	9.400	-14.9988
73	9.420	-15.4696
74	9.440	-15.9698
75	9.460	-16.4989
76	9.480	-17.0543
77	9.500	-17.6299
78	9.520	-18.2145
79	9.540	-18.7910

(Continued)

80	9.560	-19.3354
81	9.580	-19.8174
82	9.600	-20.2028
83	9.620	-20.4591
84	9.640	-20.5635
85	9.660	-20.5103
86	9.680	-20.3118
87	9.700	-19.9945
88	9.720	-19.5908
89	9.740	-19.1318
90	9.760	-18.6437
91	9.780	-18.1465
92	9.800	-17.6541
93	9.820	-17.1752
94	9.840	-16.7151
95	9.860	-16.2758
96	9.880	-15.8590
97	9.900	-15.4645
98	9.920	-15.0919
99	9.940	-14.7403
100	9.960	-14.4083
101	9.980	-14.0935
102	10.000	-13.7938
103	10.020	-13.7898
104	10.040	-14.0906
105	10.060	-14.3996
106	10.080	-14.7136
107	10.100	-15.0293
108	10.120	-15.3426
109	10.140	-15.6487
110	10.160	-15.9415
111	10.180	-16.2144
112	10.200	-16.4600
113	10.220	-16.6697
114	10.240	-16.8342
115	10.260	-16.9454
116	10.280	-16.9959
117	10.300	-16.9809
118	10.320	-16.8984
119	10.340	-16.7498
120	10.360	-16.5395
121	10.380	-16.2742

(Continued)

122	10.400	-15.9618
123	10.420	-15.6115
124	10.440	-15.2324
125	10.460	-14.8325
126	10.480	-14.4194
127	10.500	-13.9995
128	10.520	-13.7023
129	10.540	-13.4018
130	10.560	-13.0957
131	10.580	-12.7854
132	10.600	-12.4730
133	10.620	-12.1602
134	10.640	-11.8491
135	10.660	-11.5418
136	10.680	-11.2409
137	10.700	-10.9485
138	10.720	-10.6669
139	10.740	-10.4436
140	10.760	-10.3789
141	10.780	-10.3148
142	10.800	-10.2517
143	10.820	-10.1896
144	10.840	-10.1287
145	10.860	-10.0687
146	10.880	-10.0101
147	10.900	-9.9530
148	10.920	-9.8977
149	10.940	-9.8452
150	10.960	-9.7965
151	10.980	-9.7531
152	11.000	-9.7168
153	11.020	-9.6896
154	11.040	-9.6733
155	11.060	-9.6703
156	11.080	-9.6821
157	11.100	-9.7104
158	11.120	-9.7570
159	11.140	-9.8232
160	11.160	-9.9100
161	11.180	-10.0181
162	11.200	-10.1475
163	11.220	-10.2984

(Continued)

164	11.240	-10.4704
165	11.260	-10.6637
166	11.280	-10.8775
167	11.300	-11.1113
168	11.320	-11.3656
169	11.340	-11.6406
170	11.360	-11.9369
171	11.380	-12.2562
172	11.400	-12.6003
173	11.420	-12.9722
174	11.440	-13.3751
175	11.460	-13.8135
176	11.480	-14.2925
177	11.500	-14.8176
178	11.520	-15.3948
179	11.540	-16.0306
180	11.560	-16.8001
181	11.580	-17.6930
182	11.600	-18.7063
183	11.620	-19.8707
184	11.640	-21.2290
185	11.660	-22.8430
186	11.680	-24.8085
187	11.700	-27.2831
188	11.720	-30.5110
189	11.740	-34.5581
190	11.760	-36.4620
191	11.780	-33.1919
192	11.800	-29.7287
193	11.820	-27.1460
194	11.840	-25.1990
195	11.860	-23.6798
196	11.880	-22.4609
197	11.900	-21.4620
198	11.920	-20.6304
199	11.940	-19.9277
200	11.960	-19.3268
201	11.980	-18.8098
202	12.000	-18.3606

APPENDIX 4

MATLAB CODE FOR LINEAR REGRESSION

```
load('C:\Users\User\Desktop\training  matlab\thesis\NLBT.mat');

RandStream.setGlobalStream ...
(RandStream ('mt19937ar','seed',1));

x= NLBT(:,1);
y= NLBT(:,2);  %colum 2 sampai 3 adalah output
% Fit a linear regression model
mdl = fitlm(x, y, 'linear');
mdl.SSR
mdl.SST
mdl.SSE

% Display the regression results
disp('Linear Regression Model:')
disp(mdl)

% Plot the regression line
% plot (x, y_new, 'r','LineWidth', 2);
plot (mdl);
title('Linear Regression for L-Band: Frequency (GHz) vs Normalized Absorption');
xlabel('Frequency (GHz)');
ylabel('Normalized Absorption');
```

APPENDIX 5

MATLAB CODE FOR ANN REGRESSION

```
%% Load input-output data to the workspace

load('C:\Users\User\Desktop\training  matlab\RSSM1.mat');

rng(1); % Initializes the Mersenne Twister generator using a seed of 1, mt19937ar

inputs = SSM(:, 1)'; % Original frequency values (transpose for consistency)

outputs = SSM(:, 2)'; % Outputs (transpose for consistency)

%% Normalize both inputs and outputs

[inputs, inputSettings] = mapminmax(inputs);

[outputs, outputSettings] = mapminmax(outputs);

%% Create and configure the neural network

hiddenLayerSizes = [10, 20, 10]; % Simplified network structure

net = feedforwardnet(hiddenLayerSizes);

net.trainFcn = 'trainscg'; % Try Scaled Conjugate Gradient algorithm

net.performParam.regularization = 0.1; % Add regularization

net.trainParam.max_fail = 20; % Increase early stopping patience

net.trainParam.epochs = 1000; % Increase epochs for better convergence

net.trainParam.lr = 0.001; % Further lower learning rate

%% Cross-Validation

k = 5; % Number of folds

cvIndices = crossvalind('Kfold', length(inputs), k);
```

```
R_values = zeros(k, 1);

for i = 1:k

    testIdx = (cvIndices == i);

    trainIdx = ~testIdx;

    % Train the network

    [net, tr] = train(net, inputs(:, trainIdx), outputs(:, trainIdx));

    % Test the network

    testInputs = inputs(:, testIdx);

    testOutputs = outputs(:, testIdx);

    predictions = net(testInputs);

    % Calculate R-value

    R = corrcoef(testOutputs, predictions);

    R_values(i) = R(1, 2);

end

average_R = mean(R_values);

%% Train final model on all data

[net, tr] = train(net, inputs, outputs); % Train the network using all data

%% Test the trained network to make predictions on test data

predictions = net(inputs);
```

```
%% Denormalize predictions and actual values for comparison
outputs = mapminmax('reverse', outputs, outputSettings);
predictions = mapminmax('reverse', predictions, outputSettings);
%% Plotting the graph with lines using original frequency values
figure;
plot(inputs, outputs, 'b-', 'LineWidth', 0.5); % Actual outputs (blue line)
hold on;
plot(inputs, predictions, 'r--', 'LineWidth', 0.5); % Predictions (red dashed line)
xlabel('Frequency (GHz)');
ylabel('Absorption  Coefficient');
title('Improved ANN Predictions vs Actual Absorption');
legend('Actual Absorption', 'ANN Predictions', 'Location', 'best');
grid on;
```

AUTHOR'S PROFILE

Azizah binti Ahmad obtained her diploma and B.Eng. Hons in electrical and electronics engineering from Universiti Teknologi MARA in 2003 (UiTM Pulau Pinang) and 2006 (UiTM Shah Alam) respectively and M.Sc. in Electronic System Design Engineering from Universiti Sains Malaysia in 2008. In 2009, she joined the Faculty of Electrical Engineering, Universiti Teknologi MARA, Pulau Pinang as a lecturer and became a senior lecturer since 2016. She is currently persuing PhD degree in Electrical Engineering at Universiti Teknologi MARA, Shah Alam, Malaysia. Her current research interests include artificial intelligence, machine learning, and microwave absorbers.

LIST OF PUBLICATION:

A. REFEREED JOURNAL

[1] **Azizah Ahmad,** Mohd Nasir Taib, Hasnain Abdullah, Nurlaila Ismail, Ahmad Ihsan Mohd Yassin, Linda Mohd Kasim, Norhayati Mohd Noor, 'ANN Classification of S-Band Absorption Performance in Eco-Friendly Microwave Absorbers", in *International Journal of Electrical and Computer Engineering (IJECE),* 2025. scopus indexed. - PUBLISHED ON FEB2025.

[2] **Azizah Ahmad,** Mohd Nasir Taib, Hasnain Abdullah, Nurlaila Ismail, Ahmad Ihsan Mohd Yassin, Norhayati Mohd Noor , Linda Mohd Kasim, Shafaq Mardhiyana Mohamat Kasim, Nazirah Mohamat Kasim, Noor Azila Ismail, Yaakub Omar "Optimizing Absorption Performance of Eco-Friendly Microwave Absorbers Using Boxplot Analysis and Min-Max Normalization

Across Multiband Frequencies", *Bulletin of Electrical Engineering and Informatic.* - **scopus indexed.** - SUBMITTED ON 02 AUGUST 2025.

[3] Shafaq Mardhiyana Mohamat Kasim, Hasnain Abdullah, ***Azizah Ahmad,** Nazirah Mohamat Kasim, Ali Othman, Mohd Nasir Taib, Basharudin, Irsyad, "The Potential of Biomass as Anti-Microwave Material in Organic Cement Brick", *Jurnal Teknologi (Sciences & Engineering)*, 2025 - **scopus indexed.** - PUBLISHED ON 26 JUN 2025.

[4] Nur Shafikah Rosli, Hasnain Abdullah, Linda Mohd Kasim, Samihah Abdullah, Norhayati Mohamad Noor, Noor Azila Ismail, **Azizah Ahmad,** Shafaq Mardhiyana Mohamat Kasim, Mohd Nasir Taib, "Pyramidal Microwave Absorbers: Leveraging Ceramic Materials for Improved Electromagnetic Interference Shielding", *Int. J. Electr. Comput. Eng.*, vol. 15, no. 1, pp. 435-447, 2025, doi: 10.11591/ijece.vl5il.pp435-447. - **scopus indexed.** - PUBLISHED ON FEB2025.

[5] Linda Mohd Kasim, Hasnain Abdullah, Mohd Nasir Taib, Norhayati Mohamad Noor, **Azizah Ahmad,** Noor Azila Ismail, Nur Qaisarah Anuar, "Investigation of Electromagnetic Absorption Performance of Porous Cement Brick Microwave Absorber", in *International Journal of Electrical and Computer Engineering (IJECE),* 2025. - **scopus indexed.** - PUBLISHED ON 26 JUL 2025.

[6] Norhayati Mohamad Noor, Hasnain Abdullah@Idris, Mohd Nasir Taib, Nurin Sabihah Shamsul Bahari, Linda Mohd Kasim, **Azizah Ahmad,** Nazirah Mohamat Kasim, Noor Azila Ismail, "Enhance Microwave Absorption in Partition Walls using Rice Husk Biomass Composite", in *TELKOMNIKA (Telecommunication Computing Electronics and Control),* 2025 **-scopus indexed.** - PUBLISHED ON JUN 2025.

[7] Norhayati Mohamad Noor, Hasnain Abdullah@ Idris, Mohd Nasir Taib, Nabila Husna Mustapar, Linda Mohd Kasim, **Azizah Ahmad,** Nazirah Mohamat Kasim and Noor Azila Ismail "The Impact Study of Anti-Radiation Biomass Material on Partition Wall Absorption Performance," *ESTEEM Acad. J.*, vol. 19, no. September, pp. 75-85, 2023, doi: 10.24191/esteem.vl9iseptember.23003 - **MyCite indexed.** - PUBLISHED ON 2023.

[8] Linda Mohd Kasim, Hasnain Abdullah, Mohd Nasir Taib, Norhayati Mohamad Noor, **Azizah Ahmad,** Noor Azila Ismail, Nur Qaisarah Anuar, "Textured Surface Development of PET-POFA Anti-Microwave Bricks", in *International Journal of Nanoelectronics and Materials (IJNeaM)*, 2025 **-WoS indexed.** - ACCEPTED ON 20 MARCH 2025 .

B. REFEREED CONFERENCE PROCEEDINGS

[1] **Azizah Ahmad,** Mohd Nasir Taib, Hasnain Abdullah, Nurlaila Ismail, Ahmad Ihsan Mohd Yassin, Linda Mohd Kasim, Norhayati Mohd Noor,Nazirah Mohamat Kasim, Noor Azila Ismail, "A Novel Application of MLP Networks in Classifying L Band Eco-Friendly Microwave Absorbers", *14th IEEE Int. Conf. Control Syst. Comput. Eng. ICCSCE 2024 - Proc*, pp. 294-298, 2024, doi: 10.1109/ICCSCE61582.2024.10696895.- **scopus indexed.**-PUBLISHED ON 3rd OCT 2024.

[2] **Azizah Ahmad,** Mohd Nasir Taib, Hasnain Abdullah, Nurlaila Ismail, Ahmad Ihsan Mohd Yassin, Norhayati Mohd Noor, Linda Mohd Kasim, Nazirah Mohamat Kasim, Noor Azila Ismail, "A Comparative Analysis of Neural Network Regression Models for Medium Slot Eco-Friendly Microwave AbsorberPerformance Across Frequency Bands", *15th IEEE Int. Conf. Control Syst. Comput. Eng. ICCSCE 2025* - **scopus indexed.** - ACCEPTED ON 3rd August 2025.

[3] Norhayati Mohamad Noor, Hasnain Abdullah@Idris, Mohd Nasir Taib, Mas Izati Fazin, Mohamad Amirun Zafri, Nazirah Mohamat Kasim, **Azizah Ahmad,** Linda Mohd Kasim, Noor Azila Ismail, "Innovative Kenaf-Brick Composite for Effective Microwave Absorption", *14th IEEE Int. Conf. Control Syst. Comput. Eng. ICCSCE 2024 - Proc*, pp. 271-275, 2024, doi: 10.1109/ICCSCE61582.2024.10696576. - scopus indexed. - PUBLISHED ON 3rd OCT 2024.

[4] Linda Mohd Kasim, Hasnain Abdullah, Mohd Nasir Taib, **Azizah Ahmad,** Norhayati Mohamad Noor,Noor Azila Ismail, Nazirah Mohamat Kasim, Nurul Haida Hilmi, "Microwave Absorption Performance of Multilayer Anti-Radiation Bricks for Sustainable Construction Materials", *14th IEEE Int. Conf. Control Syst. Comput. Eng. ICCSCE 2024 - Proc*, pp. 299-303, 2024, doi:

10.1109/ICCSCE61582.2024.10696070. - **scopus indexed.**-PUBLISHED ON 3rd OCT 2024.

[5] Linda Mohd Kasim, Hasnain Abdullah, Mohd Nasir Taib, **Azizah Ahmad,** Norhayati Mohamad Noor,Noor Azila Ismail, Nazirah Mohamat Kasim, Nurul Haida Hilmi, "Enhanced Electromagnetic Wave Absorption in Plastic Composite Bricks with Hollow Pyramidal Surface Modification", *15th IEEE Int. Conf. Control Syst. Comput. Eng. ICCSCE 2025* - **scopus indexed.** - ACCEPTED ON 3rd August 2025.

[6] Norhayati Mohamad Noor, Hasnain Abdullah@Idris, Mohd Nasir Taib, Mas Izati Fazin, Mohamad Amirun Zafri, Nazirah Mohamat Kasim, **Azizah Ahmad,** Linda Mohd Kasim, Noor Azila Ismail, "Lightweight Partition Walls with Embedded Biomass-Based Microwave Absorbers", *15th IEEE Int. Conf. Control Syst. Comput. Eng. ICCSCE 2025* - **Scopus indexed.** - ACCEPTED ON 3rd August 2025.

B. GENERAL PUBLICATION

[1] Linda Binti Mohd. Kasim, Hasnain Bin Abdullah @ Idris, Mohd Nasir Bin Taib, Norhayati Bt Mohamad Noor, **Azizah Binti Ahmad,** "Plastic Biomass Composite Cement Brick Microwave Absorber (PBCA)", in *Penang International Invention, Innovation and Design (PUD 2023),* 25th Oct 2023 - elSBNNo: 978-967-26358-5-7.

[2] Norhayati Binti Mohamad Noor, Hasnain Bin Abdullah@Idris, Mohd Nasir Bin Taib, **Azizah Binti Ahmad,** Linda Binti Mohd Kasim, Nazirah Binti Mohamat Kasim, "Kenaf Composite Anti-Radiation Partition Wall", in *International Industrial Revolution 4.0 Exposition 2024 (IREx2024),* 21st Mei 2024 - elSBN No: 978-967-2948-71-1.

[3] Linda Mohd Kasim, Hasnain Abdullah@Idris, Mohd Nasir Taib, Norhayati Mohamad Noor, **Azizah Ahmad,** Noor Azila Ismail, "PET-POFA Composite Solid Cement Brick Microwave Absorber", in *International Industrial Revolution 4.0 Exposition 2024 (IREx2024),* 21st Mei 2024 - elSBN No: 978-967-2948-71-1.

[4] Syafaq,Hasnain Abdullah, Nazirah, Norhayati Mohamad Noor, **Azizah Ahmad,** Nur Ain, "The Geometrically Elegent Design of Hevea Brasiliensis-Based Biomass Lightweight Brick Walls for Radio Frequency Radiation

Absorption", in *International Industrial Revolution 4.0 Exposition 2024 (IREx2024)*, 21stMei 2024 - elSBNNo: 978-967-2948-71-1.

D. AWARDS

[1] **Azizah Ahmad,** Mohd Nasir Taib, Hasnain bin Abdullah, Nurlaila Ismail, Linda Mohd Kasim, "An Innovative Approach to ANN Classification Techniques for L-Band Absorption Performance in Biomass Microwave Absorbers" in *CREATIONS de UiTM: International Mega Innovation Carnival 2024* (CDU2024), 27th April 2024, Silver Award.

[2] Norhayati Mohamad Noor, Hasnain Abdullah@Idris, Mohd Nasir Taib, **Azizah Ahmad,** Linda Mohd Kasim, Nazirah Mohamat Kasim, "Kenaf Composite Anti-Radiation Partition Wall", in International Industrial Revolution 4.0 Exposition 2024 (TREx2024), 21st Mei 2024, Diamond & Gold Awards

[3] Linda Mohd Kasim, Hasnain Abdullah@Idris, Mohd Nasir Taib, Norhayati Mohamad Noor, **Azizah Ahmad,** Noor Azila Ismail, "PET-POFA Composite Solid Cement Brick Microwave Absorber", in International Industrial Revolution 4.0 Exposition 2024 (TREx2024), 21st Mei 2024, Gold Award.

[4] Syafaq,Hasnain Abdullah, Nazirah, Norhayati Mohamad Noor, **Azizah Ahmad,** Nur Ain, "The Geometrically Elegent Design of Hevea Brasiliensis-Based Biomass Lightweight Brick Walls for Radio Frequency Radiation Absorption", in International Industrial Revolution 4.0 Exposition 2024 (IREx2024), 21st Mei 2024, Gold Award.

[5] Linda Mohd Kasim, Hasnain Bin Abdullah@Idris, Mohd Nasir Bin Taib, Norhayati Mohamad Noor, **Azizah Ahmad,** "Plastic Biomass Composite Brick Microwave Absorber", in Penang International Invention, Innovation and Design (PIID)2023, Gold Awards.